

IMPROVING IMMUNOTHERAPY FOR BREAST CANCER PATIENTS



Leonie Voorwerk

Improving immunotherapy for breast cancer patients

Leonie Voorwerk

Cover design: Anastasia Gangaev
Lay-out and printing: Proefschriftmaken

ISBN: 978-94-6469-230-3

DOI: <https://doi.org/10.33540/1633>

The printing of this thesis was financially supported by the Oncology Graduate School Amsterdam (OGA) and the Netherlands Cancer Institute.

© 2023, Leonie Voorwerk, Amsterdam, the Netherlands.

All rights reserved. No part of this thesis may be reproduced, stored, or transmitted in any form by any means, without permission of the author.

Improving immunotherapy for breast cancer patients

Verbeteren van immuuntherapie voor borstkanker patiënten
(met een samenvatting in het Nederlands)

Proefschrift

ter verkrijging van de graad van doctor aan de
Universiteit Utrecht
op gezag van de
rector magnificus, prof.dr. H.R.B.M. Kummeling,
ingevolge het besluit van het college voor promoties
in het openbaar te verdedigen op

vrijdag 14 april 2023 des middags te 4.15 uur

door

Leonie Voorwerk

geboren op 18 mei 1991
te Purmerend

Promotor:

Prof. dr. S.C. Linn

Copromotoren:

Dr. M. Kok

Dr. H.M. Horlings

Beoordelingscommissie:

Prof. dr. E. van der Wall

Prof. dr. L. Meyaard

Prof. dr. J.E. van Rheeën

Prof. dr. M.K. Schmidt

Prof. dr. H.M. Verkooijen (voorzitter)

Het onderzoek in dit proefschrift werd (mede) mogelijk gemaakt met financiële steun van KWF Kankerbestrijding, de Nederlandse Organisatie voor Wetenschappelijk Onderzoek (NWO), Pink Ribbon, de Breast Cancer Research Foundation (BCRF) en het Hendrika Roet fonds.

Table of contents

Chapter 1	General introduction and outline of the thesis	7
Part I	Immunomodulatory strategies to improve responses to immune checkpoint blockade in metastatic breast cancer	23
Chapter 2	'IMpassionate conflicts' in immunotherapy trials for metastatic triple-negative breast cancer	25
Chapter 3	Immune induction strategies in metastatic triple-negative breast cancer to enhance the sensitivity to PD-1 blockade: the TONIC-trial	35
Chapter 4	IL-5-producing CD4+ T cells and eosinophils cooperate to enhance response to immune checkpoint blockade in breast cancer	79
Chapter 5	PD-L1 blockade in combination with carboplatin as immune induction in metastatic lobular breast cancer: the GELATO-trial	131
Part II	Identification and implementation of potential biomarkers for immunotherapy response in breast cancer	173
Chapter 6	Towards predictive biomarkers for immunotherapy response in breast cancer patients	175
Chapter 7	Application of a risk-management framework for integration of stromal tumor-infiltrating lymphocytes in clinical trials	195
Chapter 8	Immune landscape of breast tumors with low and intermediate estrogen receptor expression	213
Chapter 9	Discussion and future perspectives	239
Appendix	Nederlandse samenvatting	261
	List of publications	265
	Curriculum Vitae	268
	Acknowledgements/dankwoord	269



Chapter 1

General introduction and
outline of the thesis

Breast cancer is the most common cancer in women worldwide¹ and encompasses a heterogeneous disease². Besides the patient's clinical stage, assessment of tumor characteristics such as hormone receptor expression, molecular phenotype, histological subtype and immunological features of the tumor microenvironment are vital to assess prognosis and aid clinical decision making in breast cancer³.

Molecular subtypes of breast cancer

The expression of hormone receptors and amplification of Human Epidermal growth factor receptor 2 (HER2) are the main determinants of clinical behavior and molecular features of breast cancers. Expression of the Estrogen Receptor (ER) is common in approximately 70-80% of breast cancers³, and patients with ER-positive breast cancer have the best prognosis as compared to other subtypes⁴. The generally used cut-off for ER positivity is $\geq 1\%$, with some countries such as the Netherlands using $\geq 10\%$ ⁵, based on response to endocrine treatment^{6,7}. Breast cancers with ER expression usually express Progesterone Receptor (PR) as well⁷ and patients with breast tumors with negative or low PR expression have a worse prognosis as compared to patients with high PR expression⁸. Endocrine treatment remains the cornerstone of treatment of patients with early-stage and metastatic ER-positive breast cancer, with the addition of CDK4/6 inhibitors to palliative endocrine therapy being a major breakthrough in recent years⁹. Using molecular classification based on gene expression (PAM50^{10,11}), ER-positive breast cancers with low proliferation can most often be classified as luminal A and ER-positive breast cancers with a high proliferation rate are usually of the luminal B subtype³ (Figure 1). Approximately 10-20% of patients have HER2-positive breast cancer, with amplification of the *HER2* gene, which can be either ER-positive or negative¹². The HER2-positive subgroup can be treated with targeted agents and while the field of HER2-positive breast cancer is rapidly evolving¹³, this breast cancer subtype will not be covered in this thesis. Triple-negative breast cancer (TNBC) comprises approximately 10-20% of all breast tumors and is characterized by the lack of expression of estrogen receptor (ER), progesterone receptor (PR) and amplification of HER2^{14,15}. Until very recently, no targeted treatment options were available for patients with TNBC¹⁶, with TNBC patients having a median survival of only 12-18 months in the metastatic setting^{17,18}. In recent years, new treatment options emerged for TNBC, with the (upcoming) approval of the antibody-drug conjugates (ADC) sacituzumab govitecan¹⁹ and trastuzumab deruxtecan (with low HER2 expression)²⁰ for patients with metastatic TNBC and pembrolizumab (PD-1 blockade) plus chemotherapy for both patients with early-stage TNBC²¹ and with PD-L1 positive metastatic TNBC²². Additionally, for patients with a germline *BRCA* mutation, most common among patients with TNBC, the PARP inhibitor olaparib will soon be available in the adjuvant setting²³ and can already be used as palliative treatment²⁴. TNBCs are usually highly proliferative and basal-like, comprising the group with the most aggressive features¹⁶ (Figure 1).

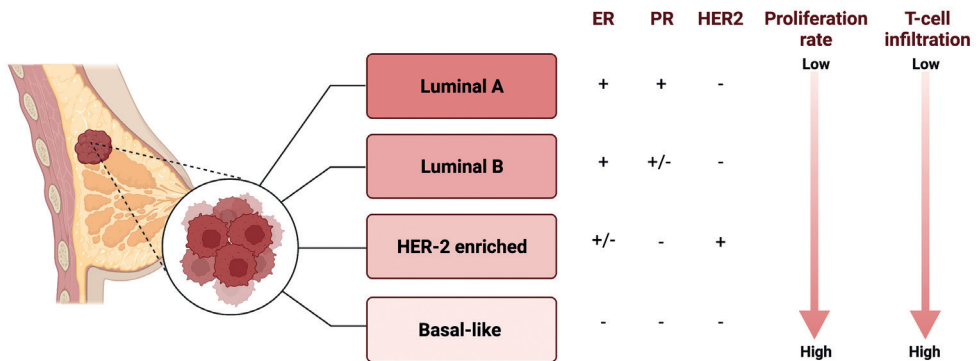


Figure 1: Relation of PAM50 molecular subtypes¹⁰ receptor expression^{25,26}, proliferation rate and T-cell infiltration^{27,28}. Figure created with Biorender.com

Histological subtypes of breast cancer

The tissue origin of the invasive breast tumor is also a major determinant of clinical behavior. The most common histological subtype is breast cancer of no special type (NST), which comprises approximately 70-75% of all breast tumors³. Invasive lobular breast cancer (ILC) is the most common special histological subtype²⁹, originates from the breast lobes and is common in 10-20% of all breast tumors^{30,31}. ILC has different molecular alterations compared to NST and is characterized by the loss of function of E-cadherin, causing its typical growth pattern and preferred metastatic spread to the bone and gastro-intestinal tract³¹⁻³³. A subset of ILCs can be characterized as immune-related with high lymphocytic infiltration and expression of immune-related genes³⁴⁻³⁶. Patients with metastatic ER-positive ILC have worse overall survival as compared to patients with metastatic ER-positive NST³⁷. The clinical features of ILC, such as the lack of measurable disease, makes this subtype challenging to study and ILC patients are therefore often underrepresented in clinical trials³⁸. ILC-specific clinical trials are ongoing³², and in **chapter 4** of this thesis, we report the results of the first ILC-specific clinical trial.

The immune system in breast cancer

In the past, breast cancer has been considered an immunologically cold cancer type with little immune cell infiltration. However, it has become clear that a subset of breast cancers is highly inflamed^{10,39-41} with complex crosstalk in the tumor microenvironment (TME) between myeloid cells, lymphoid cells, regulatory immune cells, tumor cells and cancer-associated fibroblasts (CAFs)^{42,43}. Immunosuppressive mechanisms hampering an effective immune response in cancer include the upregulation of immune checkpoints, such as programmed death-ligand 1 (PD-L1) and a shifted balance towards relatively high levels of tumor-infiltrating myeloid

cells and low levels of effector immune cells⁴⁴. Immune checkpoint blockade (ICB), in the form of PD-(L)1 inhibition, can interrupt the immunosuppressive interaction between PD-L1 expressing tumor cells or immune cells (primarily antigen-presenting cells) and PD-1 expressing T cells⁴⁵. For an effective reinvigorated immune response upon ICB, infiltration of CD8+ T cells in the TME is needed with intact interferon signaling and proper functioning antigen-presenting machinery in tumor cells⁴⁶. In breast cancer, immunosuppressive cells, such as tumor-associated macrophages, can negatively affect CD8+ T-cell infiltration and activation^{47,48}. Additionally, relatively low levels of tumor mutations are observed in breast cancer, limiting the number of neo-antigens arising from these mutations and thus potentially reducing the chances of an effective tumor- or neoantigen-specific CD8+ T-cell response^{49,50}.

As a read-out for the immune infiltrate in breast tumors, stromal tumor-infiltrating lymphocytes (sTILs) levels, comprising all T cells, B cells and plasma cells infiltrating the tumor-associated stroma, can be assessed⁵¹. Relatively high levels of sTILs are observed in patients with TNBC, as compared to the other breast cancer subtypes^{27,52,53} (Figure 1). In early-stage breast cancer, sTILs are positively associated with increased responses to neo-adjuvant chemotherapy and improved prognosis in TNBC^{27,54-57}. The same goes for CD8+ T-cells specifically, which are higher in TNBC as compared to ER-positive breast cancer with a positive correlation with prognosis in TNBC⁵⁸. In ER-positive breast cancer, the protective role of T-cell presence is less clear^{27,59}, but some reports have shown a positive association between sTILs and prognosis in highly proliferative/luminal B ER-positive breast cancer^{28,60}.

Less attention has been paid to immune cells circulating in the blood in breast cancer. It has been shown that breast cancer patients harbor higher levels of circulating myeloid-derived suppressor cells (MDSCs) and regulatory T cells in comparison to healthy women, but that these immune inhibitory cells decreased upon treatment response⁶¹. It has also been appreciated that intact systemic immune cell function is critical for ICB efficacy⁶². For example, it has been shown that an early increase in proliferating CD8+ T cells in melanoma⁶³, an increase in eosinophils in melanoma⁶⁴ or a decrease in the neutrophil-to-lymphocyte ratio in renal-cell carcinoma⁶⁵ are associated with response to ICB. In breast cancer, increases in circulating activated, proliferating CD8+ T cells upon ICB plus chemotherapy have been observed⁶⁶. The results of our study investigating the involvement of circulating immune cells in ICB response in breast cancer will be discussed in **Chapter 3** of this thesis.

Immune checkpoint blockade in breast cancer

As several translational studies have demonstrated extensive lymphocytic infiltration in primarily early-stage TNBC, ICB is unsurprisingly more effective in this breast cancer subtype. In early-stage breast cancer, high pathological complete response rates (pCR) have been observed to neoadjuvant chemotherapy plus ICB

(Table 1). In the KEYNOTE-522²¹, treatment with neo-adjuvant pembrolizumab plus ICB not only improved pCR rates but also improved event-free survival in early-stage TNBC⁶⁷, leading to FDA approval of this treatment regimen and thereby revolutionizing treatment for this historically difficult-to-treat breast cancer. Results of phase three trials of the addition of ICB to neo-adjuvant chemotherapy in high-risk ER-positive breast cancer (grade 3; NCT04109066, NCT03725059) have yet to be reported. Two phase II trials demonstrated promising activity in high-risk ER-positive breast cancer^{68,69} and it remains to be elucidated whether addition of ICB to neo-adjuvant treatment for ER-positive patients will prove to be a vital treatment option.

Table 1: Randomized phase II-III trials of neo-adjuvant ICB in early-stage TNBC and ER+ BC.

Nab-paclitaxel (Nab-P), paclitaxel (P), dd (dose-dense), anthracyclines (A), cyclophosphamide (C), carboplatin (Cp), pathological complete response (pCR), non-significant (ns)

	Subtype	Drug name	Chemo-therapy backbone	No. of patients	pCR rates
IMpassion031 ⁷⁰	TNBC	Atezolizumab	Nab-P + dd AC	333 (165 experimental vs. 169 placebo)	58% experimental vs. 41% placebo (p = 0.0044)
Keynote-522 ^{21,67}	TNBC	Pembrolizumab	P/Cp + AC	1174 (784 experimental vs. 390 placebo)	64.8% experimental vs 51.2% placebo (p < 0.001)
Gepar-Nuevo ⁷¹	TNBC	Durvalumab	Nab-P + dd AC	174 (88 experimental vs. 86 placebo)	53.4% experimental vs. 44.2% placebo (ns)
NeoTRIP ⁷²	TNBC	Atezolizumab	Cp + Nab-P	280 (138 experimental vs. 142 placebo)	48.6% experimental vs. 44.4% placebo (ns)
I-SPY2 ⁶⁹	TNBC ER+ (MammaPrint high)	Pembrolizumab	P + AC	TNBC: 28 (experimental) vs. 80 (control) ER+: 38 (experimental) vs. 92 (control)	TNBC: 60% (experimental) vs. 22% (control) ER+: 30% (experimental) vs. 13% (control)

In the palliative setting, ICB monotherapy is only effective in a subgroup of patients with ER-positive breast cancer or TNBC. The first single-arm phase I and II trials of ICB monotherapy in breast cancer reported objective response rates (ORR) of 3% to ICB monotherapy⁷³ and up to 12% in PD-L1 positive patients⁷⁴ in ER-positive breast cancer. Notably, two out of three responders in the latter trial had tumors with lobular histology⁷⁴. The SAFIR-02-BREAST-IMMUNO trial tested maintenance PD-1 blockade against chemotherapy in patients with metastatic HER2-negative breast cancer and reported a statistically significant hazard ratio (HR) for PFS of 2.08 in favor of chemotherapy in the ER-positive subgroup⁷⁵ (Table 2). Pembrolizumab in combination with eribulin induced responses in 27% of ER-positive breast cancer patients, while the ORR was 34% in patients treated with eribulin alone⁷⁶ (Table 2). These results indicate that ICB for patients with metastatic ER-positive breast cancer needs to be further improved by rational combinations to overcome intrinsic ICB resistance.

Table 2: Randomized phase II-III trials of ICB in metastatic ER+ breast cancer and TNBC. Hazard ratio (HR), progression-free survival (PFS), Confidence Interval (CI)

	Subtype	Drug	Chemotherapy backbone	No. of patients	HR (95% CI) PFS intention-to-treat population	HR (95% CI) PFS PD-L1 positive population
Pembrolizumab + eribulin ⁷⁶	ER+	Pembrolizumab	Eribulin	88 (44 experimental vs. 44 control)	0.80 (0.50-1.26)	0.84 (0.35-2.00)
SAFIRO2-BREAST-IMMUNO ⁷⁵	ER+, TNBC	Durvalumab maintenance	None (maintenance chemotherapy)	ER+: 110 TNBC: 82	ER+: 2.08 (1.28-3.40) TNBC: 0.87 (0.54 - 1.42)	0.75 (0.38-1.49)
KEYNOTE-119 ⁸¹	TNBC	Pembrolizumab	None (investigator's choice in control arm)	624 (312 experimental vs. 310 control)	0.97 (0.82-1.15)	0.78 (0.57-1.06)
IMpassion130 ^{82,84,85}	TNBC (first-line)	Atezolizumab	Nab-paclitaxel	902 (451 experimental vs. 451 placebo)	0.80 (0.69-0.92)	0.62 (0.49-0.78)
IMpassion131 ⁸³	TNBC (first-line)	Atezolizumab	Paclitaxel	651 (431 experimental vs. 220 placebo)	0.86 (0.70-1.05)	0.82 (0.60-1.12)
KEYNOTE-355 ²²	TNBC (first-line)	Pembrolizumab	Nab-paclitaxel, paclitaxel or carboplatin/gemcitabine	847 (566 experimental vs. 281 placebo)	0.82 (0.69-0.97)	0.65 (0.49-0.86)

In TNBC, the average ORRs for ICB monotherapy are slightly higher, with an ORR of 5-10% in unselected patients^{73,77,78} and 19-21% in PD-L1 positive patients in single-arm trials^{79,80}. In the TNBC subgroup of the SAFIRO2-BREAST-IMMUNO trial, a non-significant HR of 0.87 was observed in favor of maintenance durvalumab⁷⁵ (Table 2). In a phase III trial investigating ICB monotherapy in metastatic TNBC, an ORR of 10% was reported, but no difference in survival as compared to the control arm with investigator's choice chemotherapy⁸¹. While ICB monotherapy has proven insufficient to overcome immune evasion in most patients with TNBC, ICB in combination with chemotherapy is the first long-awaited new treatment option for patients with metastatic TNBC (Table 2). The IMpassion130⁸² demonstrated improved primary progression-free survival (PFS) in patients with PD-L1 positive tumors (SP142, $\geq 1\%$ immune cells) upon nab-paclitaxel and atezolizumab. However, the confirmatory IMpassion131 trial, with paclitaxel and atezolizumab, failed to demonstrate improved survival in this subgroup⁸³. Differences between the IMpassion trials will be further discussed in **chapter 2**. In contrast, the primary PFS analysis of the KEYNOTE-355 trial was positive for adding pembrolizumab to chemotherapy in the PD-L1 positive subgroup (22C3, combined positive score of $\geq 10\%$)²², leading to approval of ICB plus chemotherapy for first-line treatment of patients with PD-L1 positive metastatic TNBC. Although this is a massive milestone in the treatment for TNBC, much is unknown about the optimal chemotherapy backbone for ICB.

The immunomodulatory capacity of chemotherapy and irradiation

Besides its anti-tumorigenic effects, preclinical and translational studies have attributed several immunogenic properties to chemotherapy and irradiation⁸⁶. For example, fractionated irradiation can induce CD8+ T-cell priming via cGAS-STING signaling and increased type I interferons^{87,88}. Similarly, platinum agents, such as cisplatin or carboplatin, have also been shown to increase DNA damage, thereby increasing the amount of cytosolic DNA and consequently cGAS-STING signaling⁸⁹. Additionally, radiation and platinum can increase MHC class I expression, improving antigen presentation⁹⁰. Anthracyclines have been implicated in the induction of immunogenic cell death⁹¹ and a decrease in MDSCs⁹². (Low-dose) cyclophosphamide can reduce regulatory T cells and restore effector T-cell function⁹³. These studies underline the potential synergy between chemotherapy or irradiation with ICB, but in contrast, these treatment modalities can induce strong lymphopenia^{94,95}. Since these myelosuppressive effects seem to be dose-dependent, this raises the question whether short-term treatment with low-dose chemotherapy or irradiation can alter a favorable immune microenvironment to prime tumors for ICB.

Improving immunotherapy for breast cancer patients - thesis outline

As described in **Chapter 1**, treatment with ICB has found its place as standard-of-care for patients with TNBC. However, as highlighted, there is a lot to learn about the rational improvement of ICB for breast cancer patients. In the research described in this thesis, we aim: 1) to explore the use of short-term immune induction treatments to prime tumors for ICB response; 2) to dissect responses to ICB in breast cancer patients by comprehensive translational research of the TME and circulating immune cells; 3) to explore potential predictive features for ICB response in breast cancer; 4) to identify novel potential subgroups of breast cancer patients that might benefit from ICB.

Immunomodulatory strategies to improve responses to ICB in metastatic breast cancer

Leveraging the immunogenic effects of chemotherapy on immune cell functioning, in the first part of this thesis, we hypothesize that low-dose and short-term treatment with chemotherapy or radiation potentially primes the breast cancer TME to improve ICB response and we open avenues for novel immunomodulatory strategies.

We discuss the contradicting results of the landmark phase III trials IMpassion130 and IMpassion131, testing atezolizumab plus nab-paclitaxel or paclitaxel, respectively, in **Chapter 2** and place this in context with ongoing work on ICB in breast cancer.

Chapter 3 reports the clinical and translational results of the phase II multi-cohort TONIC trial's interim analysis. In this trial, 67 patients with metastatic TNBC were randomized to an immune induction treatment of two weeks: radiation

(3x8 Grey); oral cyclophosphamide; cisplatin; low-dose doxorubicin or a waiting period of two weeks, all followed by PD-1 blockade. Using clinical measurements and comprehensive immune profiling of the TME as an outcome, we describe the potential of short-term immune induction to improve response to PD-1 blockade in patients with metastatic TNBC.

With extensive translational studies of circulating immune cells and paired tumor biopsies of the patients treated with PD-1 blockade in the TONIC trial (**chapter 3**), we found that systemic and intratumoral eosinophils increased upon PD-1 blockade in responders, which was not seen in non-responders, as described in **chapter 4**. *In vivo* experiments demonstrated that eosinophils were essential for response to ICB. Our work provides the first hints towards a potential strategy to engage eosinophils for improved ICB responses in breast cancer.

Based on preclinical and translational research, there is a strong rationale for the clinical activity of platinum plus ICB in ILC patients. This was tested in the phase II, single-arm GELATO trial, of which the clinical and translational results are described in **chapter 5**. Here, 23 patients with metastatic ILC were treated with 12 cycles of weekly carboplatin as immune induction, combined with PD-L1 blockade from the third cycle of carboplatin onwards. We are the first to report the results of a clinical trial specifically for ILC and demonstrate the promising clinical activity of carboplatin plus PD-L1 blockade in patients with triple-negative ILC.

Identification and implementation of potential biomarkers for response to ICB in breast cancer

Proper selection of patients using clinical features or relevant biomarkers for ICB treatment response is needed to further improve personalized treatment for breast cancer patients. Therefore, the second part of this thesis focuses on exploring predictive biomarkers in ICB response in breast cancer and we demonstrate how such biomarkers can be implemented in clinical trials. **Chapter 6** gives a literature review of potential biomarkers for predicting response to ICB in breast cancer and beyond.

A biomarker should be easy-to-use, validated for its intended use and feasible to implement in clinical trials and daily practice⁹⁶. Since sTILs are a basic read-out for pre-existing anti-tumor immunity and international guidelines exist for the scoring sTILs in breast cancer⁵¹, we designed a framework for implementing sTILs as an inclusion criterium and stratification factor in clinical trials, as described in **chapter 7**. Here, we demonstrate our pipeline on how to obtain reliable sTIL scores within 72 hours after a biopsy and use sTILs as a stratification factor in the TONIC trial (**chapter 3**).

In **chapter 8**, we describe the identification of a potential new subgroup of breast cancer patients that might benefit from ICB. So far, most research in HER2-negative breast cancer has focused on comparing ER-positive and ER-negative breast cancer^{27,28}. Still, it is unclear whether immune characteristics of breast tumors

with low (1-9%) and intermediate ER-expression (10-50%) are similar to TNBC. In this chapter, we compare the immune landscape of HER2-negative breast tumors with low ER expression (1-9%), intermediate ER expression (10-50%) and high ER expression (51-99%) to breast tumors with negative (0%) or complete (100%) ER expression.

Finally, the results of this thesis are summarized and placed in the context of this rapidly evolving field in **chapter 9**. In this chapter, we highlight future perspectives of our work and focus on potential new research avenues.

References

1. Sung, H. *et al.* Global Cancer Statistics 2020: GLOBOCAN Estimates of Incidence and Mortality Worldwide for 36 Cancers in 185 Countries. *CA Cancer J Clin* **71** (3), 209-249, 2021.
2. Zardavas, D., Irtthum, A., Swanton, C. & Piccart, M. Clinical management of breast cancer heterogeneity. *Nature Reviews Clinical Oncology* **12** (7), 381-394, 2015.
3. Harbeck, N. *et al.* Breast cancer. *Nature Reviews Disease Primers* **5** (1), 66, 2019.
4. Blows, F. M. *et al.* Subtyping of breast cancer by immunohistochemistry to investigate a relationship between subtype and short and long term survival: a collaborative analysis of data for 10,159 cases from 12 studies. *PLoS Med* **7** (5), e1000279, 2010.
5. Specialisten, F. M. Richtlijndatabase Borstkanker. Consulted at 31-03-2022.
6. Allison, K. H. *et al.* Estrogen and Progesterone Receptor Testing in Breast Cancer: ASCO/CAP Guideline Update. *Journal of Clinical Oncology* **38** (12), 1346-1366, 2020.
7. Davies, C. *et al.* Relevance of breast cancer hormone receptors and other factors to the efficacy of adjuvant tamoxifen: patient-level meta-analysis of randomised trials. *Lancet (London, England)* **378** (9793), 771-784, 2011.
8. Purdie, C. A. *et al.* Progesterone receptor expression is an independent prognostic variable in early breast cancer: a population-based study. *British journal of cancer* **110** (3), 565-572, 2014.
9. Gao, J. J. *et al.* CDK4/6 inhibitor treatment for patients with hormone receptor-positive, HER2-negative, advanced or metastatic breast cancer: a US Food and Drug Administration pooled analysis. *The Lancet. Oncology* **21** (2), 250-260, 2020.
10. Perou, C. M. *et al.* Molecular portraits of human breast tumours. *Nature* **406** (6797), 747-752, 2000.
11. Sorlie, T. *et al.* Gene expression patterns of breast carcinomas distinguish tumor subclasses with clinical implications. *Proc Natl Acad Sci U S A* **98** (19), 10869-10874, 2001.
12. Dodson, A. *et al.* Breast cancer biomarkers in clinical testing: analysis of a UK national external quality assessment scheme for immunocytochemistry and in situ hybridisation database containing results from 199 300 patients. *J Pathol Clin Res* **4** (4), 262-273, 2018.
13. Loibl, S. & Gianni, L. HER2-positive breast cancer. *The Lancet* **389** (10087), 2415-2429, 2017.
14. van Maaren, M. C. *et al.* Ten-year recurrence rates for breast cancer subtypes in the Netherlands: A large population-based study. *Int J Cancer* **144** (2), 263-272, 2019.
15. Kohler, B. A. *et al.* Annual Report to the Nation on the Status of Cancer, 1975-2011, Featuring Incidence of Breast Cancer Subtypes by Race/Ethnicity, Poverty, and State. *J Natl Cancer Inst* **107** (6), djv048, 2015.
16. Bianchini, G., Balko, J. M., Mayer, I. A., Sanders, M. E. & Gianni, L. Triple-negative breast cancer: challenges and opportunities of a heterogeneous disease. *Nature reviews. Clinical oncology* **13** (11), 674-690, 2016.
17. Skinner, K. E., Haiderali, A., Huang, M. & Schwartzberg, L. S. Real-world effectiveness outcomes in patients diagnosed with metastatic triple-negative breast cancer. *Future oncology (London, England)* **17** (8), 931-941, 2021.
18. Kassam, F. *et al.* Survival outcomes for patients with metastatic triple-negative breast cancer: implications for clinical practice and trial design. *Clinical breast cancer* **9** (1), 29-33, 2009.
19. Bardia, A. *et al.* Sacituzumab Govitecan in Metastatic Triple-Negative Breast Cancer. *New England Journal of Medicine* **384** (16), 1529-1541, 2021.
20. Modi, S. *et al.* Trastuzumab Deruxtecan in Previously Treated HER2-Low Advanced Breast Cancer. *New England Journal of Medicine*, 2022.
21. Schmid, P. *et al.* Pembrolizumab for Early Triple-Negative Breast Cancer. *New England Journal of Medicine* **382** (9), 810-821, 2020.
22. Cortes, J. *et al.* Pembrolizumab plus chemotherapy versus placebo plus chemotherapy for previously untreated locally recurrent inoperable or metastatic triple-negative breast cancer (KEYNOTE-355): a randomised, placebo-controlled, double-blind, phase 3 clinical trial. *Lancet (London, England)* **396** (10265), 1817-1828, 2020.
23. Tutt, A. N. J. *et al.* Adjuvant Olaparib for Patients with BRCA1- or BRCA2-Mutated Breast Cancer. *New England Journal of Medicine* **384** (25), 2394-2405, 2021.
24. Robson, M. *et al.* Olaparib for Metastatic Breast Cancer in Patients with a Germline BRCA Mutation. *New England Journal of Medicine* **377** (6), 523-533, 2017.

25. Wang, L. *et al.* PAM50- and immunohistochemistry-based subtypes of breast cancer and their relationship with breast cancer mortality in a population-based study. *Breast Cancer* **28** (6), 1235-1242, 2021.
26. Kim, H. K. *et al.* Discordance of the PAM50 Intrinsic Subtypes Compared with Immunohistochemistry-Based Surrogate in Breast Cancer Patients: Potential Implication of Genomic Alterations of Discordance. *Cancer Res Treat* **51** (2), 737-747, 2019.
27. Denkert, C. *et al.* Tumour-infiltrating lymphocytes and prognosis in different subtypes of breast cancer: a pooled analysis of 3771 patients treated with neoadjuvant therapy. *The Lancet. Oncology* **19** (1), 40-50, 2018.
28. Hammerl, D. *et al.* Clonality, antigen recognition and suppression of CD8+ T cells differentially affect prognosis of breast cancer subtypes. *Clinical Cancer Research*, clincanres.0285.2019, 2019.
29. Lakhani, S. R., Ellis, I. O., Schnitt, S., Tan, P. H. & van de Vijver, M. WHO Classification of Tumours of the Breast. 2012.
30. Sledge, G. W., Chagpar, A. & Perou, C. Collective Wisdom: Lobular Carcinoma of the Breast. *American Society of Clinical Oncology Educational Book* (36), 18-21, 2016.
31. Arpino, G., Bardou, V. J., Clark, G. M. & Elledge, R. M. Infiltrating lobular carcinoma of the breast: tumor characteristics and clinical outcome. *Breast cancer research : BCR* **6** (3), R149-R156, 2004.
32. Van Baelen, K. *et al.* Current and future diagnostic and treatment strategies for patients with invasive lobular breast cancer. *Annals of Oncology*, 2022.
33. Pestalozzi, B. C. *et al.* Distinct clinical and prognostic features of infiltrating lobular carcinoma of the breast: combined results of 15 International Breast Cancer Study Group clinical trials. *Journal of clinical oncology : official journal of the American Society of Clinical Oncology* **26** (18), 3006-3014, 2008.
34. Michaut, M. *et al.* Integration of genomic, transcriptomic and proteomic data identifies two biologically distinct subtypes of invasive lobular breast cancer. *Sci Rep* **6**, 18517-18517, 2016.
35. Du, T. *et al.* Invasive lobular and ductal breast carcinoma differ in immune response, protein translation efficiency and metabolism. *Sci Rep* **8** (1), 7205, 2018.
36. Ciriello, G. *et al.* Comprehensive Molecular Portraits of Invasive Lobular Breast Cancer. *Cell* **163** (2), 506-519, 2015.
37. Dalenc, F. *et al.* Impact of lobular versus ductal histology on overall survival in metastatic breast cancer: a French retrospective multicentre cohort study. *European journal of cancer (Oxford, England : 1990)* **164**, 70-79, 2022.
38. Abel, M. K. *et al.* Decreased enrollment in breast cancer trials by histologic subtype: does invasive lobular carcinoma resist RECIST? *NPJ Breast Cancer* **7** (1), 139, 2021.
39. Desmedt, C. *et al.* Biological processes associated with breast cancer clinical outcome depend on the molecular subtypes. *Clinical cancer research : an official journal of the American Association for Cancer Research* **14** (16), 5158-5165, 2008.
40. Teschendorff, A. E., Miremadi, A., Pinder, S. E., Ellis, I. O. & Caldas, C. An immune response gene expression module identifies a good prognosis subtype in estrogen receptor negative breast cancer. *Genome Biol* **8** (8), R157, 2007.
41. Aaltomaa, S. *et al.* Lymphocyte infiltrates as a prognostic variable in female breast cancer. *European Journal of Cancer* **28** (4), 859-864, 1992.
42. Salemme, V., Centonze, G., Cavallo, F., Defilippi, P. & Conti, L. The Crosstalk Between Tumor Cells and the Immune Microenvironment in Breast Cancer: Implications for Immunotherapy. *Front Oncol* **11**, 610303, 2021.
43. Nederlof, I. *et al.* Spatial interplay of lymphocytes and fibroblasts in estrogen receptor-positive HER2-negative breast cancer. *NPJ Breast Cancer* **8** (1), 56, 2022.
44. Garner, H. & de Visser, K. E. Immune crosstalk in cancer progression and metastatic spread: a complex conversation. *Nature Reviews Immunology* **20** (8), 483-497, 2020.
45. Topalian, Suzanne L., Drake, Charles G. & Pardoll, Drew M. Immune Checkpoint Blockade: A Common Denominator Approach to Cancer Therapy. *Cancer cell* **27** (4), 450-461, 2015.
46. Kalbasi, A. & Ribas, A. Tumour-intrinsic resistance to immune checkpoint blockade. *Nature reviews. Immunology* **20** (1), 25-39, 2020.
47. Wagner, J. *et al.* A Single-Cell Atlas of the Tumor and Immune Ecosystem of Human Breast Cancer. *Cell* **177** (5), 1330-1345.e1318, 2019.
48. Zhang, Y. *et al.* Single-cell analyses reveal key immune cell subsets associated with response to PD-L1 blockade in triple-negative breast cancer. *Cancer cell* **39** (12), 1578-1593.e1578, 2021.

49. Alexandrov, L. B. *et al.* Signatures of mutational processes in human cancer. *Nature* **500** (7463), 415-421, 2013.
50. Schumacher, T. N. & Schreiber, R. D. Neoantigens in cancer immunotherapy. *Science* **348** (6230), 69-74, 2015.
51. Salgado, R. *et al.* The evaluation of tumor-infiltrating lymphocytes (TILs) in breast cancer: recommendations by an International TILs Working Group 2014. *Annals of Oncology* **26** (2), 259-271, 2015.
52. Loi, S. *et al.* Tumor infiltrating lymphocytes are prognostic in triple negative breast cancer and predictive for trastuzumab benefit in early breast cancer: results from the FinHER trial. *Annals of Oncology* **25** (8), 1544-1550, 2014.
53. Stanton, S. E., Adams, S. & Disis, M. L. Variation in the Incidence and Magnitude of Tumor-Infiltrating Lymphocytes in Breast Cancer Subtypes: A Systematic Review. *JAMA Oncol* **2** (10), 1354-1360, 2016.
54. Park, J. H. *et al.* Prognostic value of tumor-infiltrating lymphocytes in patients with early-stage triple-negative breast cancers (TNBC) who did not receive adjuvant chemotherapy. *Annals of Oncology*, 2019.
55. de Jong, V. M. T. *et al.* Prognostic Value of Stromal Tumor-Infiltrating Lymphocytes in Young, Node-Negative, Triple-Negative Breast Cancer Patients Who Did Not Receive (neo)Adjuvant Systemic Therapy. *Journal of Clinical Oncology*, JCO.21.01536, 2022.
56. Loi, S. *et al.* Tumor-Infiltrating Lymphocytes and Prognosis: A Pooled Individual Patient Analysis of Early-Stage Triple-Negative Breast Cancers. *Journal of clinical oncology : official journal of the American Society of Clinical Oncology* **37** (7), 559-569, 2019.
57. Adams, S. *et al.* Prognostic value of tumor-infiltrating lymphocytes in triple-negative breast cancers from two phase III randomized adjuvant breast cancer trials: ECOG 2197 and ECOG 1199. *Journal of clinical oncology : official journal of the American Society of Clinical Oncology* **32** (27), 2959-2966, 2014.
58. Mahmoud, S. M. A. *et al.* Tumor-Infiltrating CD8+ Lymphocytes Predict Clinical Outcome in Breast Cancer. *Journal of Clinical Oncology* **29** (15), 1949-1955, 2011.
59. Sobral-Leite, M. *et al.* Assessment of PD-L1 expression across breast cancer molecular subtypes, in relation to mutation rate, BRCA1-like status, tumor-infiltrating immune cells and survival. *Oncoimmunology*, 1-15, 2018.
60. Fujimoto, Y. *et al.* Prognostic significance of tumor-infiltrating lymphocytes may differ depending on Ki67 expression levels in estrogen receptor-positive/HER2-negative operated breast cancers. *Breast Cancer* **26** (6), 738-747, 2019.
61. Palazón-Carrión, N. *et al.* Circulating immune biomarkers in peripheral blood correlate with clinical outcomes in advanced breast cancer. *Sci Rep* **11** (1), 14426, 2021.
62. Hiam-Galvez, K. J., Allen, B. M. & Spitzer, M. H. Systemic immunity in cancer. *Nature Reviews Cancer* **21** (6), 345-359, 2021.
63. Huang, A. C. *et al.* A single dose of neoadjuvant PD-1 blockade predicts clinical outcomes in resectable melanoma. *Nat Med* **25** (3), 454-461, 2019.
64. Simon, S. C. S. *et al.* Eosinophil accumulation predicts response to melanoma treatment with immune checkpoint inhibitors. *Oncoimmunology* **9** (1), 1727116, 2020.
65. Lalani, A.-K. A. *et al.* Change in neutrophil-to-lymphocyte ratio (NLR) in response to immune checkpoint blockade for metastatic renal cell carcinoma. *Journal for ImmunoTherapy of Cancer* **6** (1), 5, 2018.
66. Adams, S. *et al.* Atezolizumab Plus nab-Paclitaxel in the Treatment of Metastatic Triple-Negative Breast Cancer With 2-Year Survival Follow-up: A Phase 1b Clinical Trial. *JAMA Oncol* **5** (3), 334-342, 2019.
67. Schmid, P. *et al.* Event-free Survival with Pembrolizumab in Early Triple-Negative Breast Cancer. *New England Journal of Medicine* **386** (6), 556-567, 2022.
68. Dieci, M. V. *et al.* Neoadjuvant Chemotherapy and Immunotherapy in Luminal B-like Breast Cancer: Results of the Phase II GIADA Trial. *Clinical Cancer Research* **28** (2), 308-317, 2022.
69. Nanda, R. *et al.* Effect of Pembrolizumab Plus Neoadjuvant Chemotherapy on Pathologic Complete Response in Women With Early-Stage Breast Cancer: An Analysis of the Ongoing Phase 2 Adaptively Randomized I-SPY2 Trial. *JAMA Oncology* **6** (5), 676-684, 2020.

70. Mittendorf, E. A. *et al.* Neoadjuvant atezolizumab in combination with sequential nab-paclitaxel and anthracycline-based chemotherapy versus placebo and chemotherapy in patients with early-stage triple-negative breast cancer (IMpassion031): a randomised, double-blind, phase 3 trial. *The Lancet* **396** (10257), 1090-1100, 2020.
71. Loibl, S. *et al.* A randomised phase II study investigating durvalumab in addition to an anthracycline taxane-based neoadjuvant therapy in early triple negative breast cancer - clinical results and biomarker analysis of GeparNuevo study. *Ann Oncol* **30**(8), 1279-1288, 2019.
72. Gianni, L. *et al.* Pathologic complete response (pCR) to neoadjuvant treatment with or without atezolizumab in triple-negative, early high-risk and locally advanced breast cancer: NeoTRIP Michelangelo randomized study. *Annals of Oncology* **33** (5), 534-543, 2022.
73. Dirix, L. Y. *et al.* Avelumab, an anti-PD-L1 antibody, in patients with locally advanced or metastatic breast cancer: a phase 1b JAVELIN Solid Tumor study. *Breast Cancer Res Treat* **167** (3), 671-686, 2018.
74. Rugo, H. S. *et al.* Safety and Antitumor Activity of Pembrolizumab in Patients with Estrogen Receptor-Positive/Human Epidermal Growth Factor Receptor 2-Negative Advanced Breast Cancer. *Clinical cancer research : an official journal of the American Association for Cancer Research* **24** (12), 2804-2811, 2018.
75. Bachelot, T. *et al.* Durvalumab compared to maintenance chemotherapy in metastatic breast cancer: the randomized phase II SAFIRO2-BREAST IMMUNO trial. *Nat Med* **27** (2), 250-255, 2021.
76. Tolaney, S. M. *et al.* Effect of Eribulin With or Without Pembrolizumab on Progression-Free Survival for Patients With Hormone Receptor-Positive, ERBB2-Negative Metastatic Breast Cancer: A Randomized Clinical Trial. *JAMA Oncology* **6** (10), 1598-1605, 2020.
77. Adams, S. *et al.* Pembrolizumab Monotherapy for Previously Treated Metastatic Triple-Negative Breast Cancer: Cohort A of the Phase 2 KEYNOTE-086 Study. *Annals of Oncology*, mdy517, 2018.
78. Emens, L. A. *et al.* Long-term Clinical Outcomes and Biomarker Analyses of Atezolizumab Therapy for Patients With Metastatic Triple-Negative Breast Cancer: A Phase 1 Study. *JAMA Oncol*, 2018.
79. Nanda, R. *et al.* Pembrolizumab in Patients With Advanced Triple-Negative Breast Cancer: Phase 1b KEYNOTE-012 Study. *Journal of clinical oncology : official journal of the American Society of Clinical Oncology* **34** (21), 2460-2467, 2016.
80. Adams, S. *et al.* Pembrolizumab Monotherapy for Previously Untreated, PD-L1-Positive, Metastatic Triple-Negative Breast Cancer: Cohort B of the Phase 2 KEYNOTE-086 Study. *Annals of Oncology*, 2018.
81. Winer, E. P. *et al.* Pembrolizumab versus investigator-choice chemotherapy for metastatic triple-negative breast cancer (KEYNOTE-119): a randomised, open-label, phase 3 trial. *The Lancet. Oncology* **22** (4), 499-511, 2021.
82. Schmid, P. *et al.* Atezolizumab and Nab-Paclitaxel in Advanced Triple-Negative Breast Cancer. *N Engl J Med*, 2018.
83. Miles, D. *et al.* Primary results from IMpassion131, a double-blind, placebo-controlled, randomised phase III trial of first-line paclitaxel with or without atezolizumab for unresectable locally advanced/metastatic triple-negative breast cancer. *Annals of Oncology* **32** (8), 994-1004, 2021.
84. Schmid, P. *et al.* Atezolizumab plus nab-paclitaxel as first-line treatment for unresectable, locally advanced or metastatic triple-negative breast cancer (IMpassion130): updated efficacy results from a randomised, double-blind, placebo-controlled, phase 3 trial. *The Lancet. Oncology* **21** (1), 44-59, 2020.
85. Emens, L. A. *et al.* First-line atezolizumab plus nab-paclitaxel for unresectable, locally advanced, or metastatic triple-negative breast cancer: IMpassion130 final overall survival analysis. *Annals of Oncology* **32** (8), 983-993, 2021.
86. Galluzzi, L., Humeau, J., Buqué, A., Zitvogel, L. & Kroemer, G. Immunostimulation with chemotherapy in the era of immune checkpoint inhibitors. *Nature Reviews Clinical Oncology* **17** (12), 725-741, 2020.
87. Demaria, S. *et al.* Ionizing radiation inhibition of distant untreated tumors (abscopal effect) is immune mediated. *International Journal of Radiation Oncology*Biophysics* **58** (3), 862-870, 2004.
88. Vanpouille-Box, C. *et al.* DNA exonuclease Trex1 regulates radiotherapy-induced tumour immunogenicity. *Nat Commun* **8**, 15618, 2017.
89. Schadt, L. *et al.* Cancer-Cell-Intrinsic cGAS Expression Mediates Tumor Immunogenicity. *Cell Rep* **29** (5), 1236-1248.e1237, 2019.
90. Wan, S. *et al.* Chemotherapeutics and radiation stimulate MHC class I expression through elevated interferon-beta signaling in breast cancer cells. *PLoS one* **7** (3), e32542, 2012.

91. Casares, N. *et al.* Caspase-dependent immunogenicity of doxorubicin-induced tumor cell death. *J Exp Med* **202** (12), 1691-1701, 2005.
92. Alizadeh, D. *et al.* Doxorubicin eliminates myeloid-derived suppressor cells and enhances the efficacy of adoptive T-cell transfer in breast cancer. *Cancer research* **74** (1), 104-118, 2014.
93. Scurr, M. *et al.* Low-Dose Cyclophosphamide Induces Antitumor T-Cell Responses, which Associate with Survival in Metastatic Colorectal Cancer. *Clinical cancer research : an official journal of the American Association for Cancer Research* **23** (22), 6771-6780, 2017.
94. Tolaney, S. M., Najita, J., Winer, E. P. & Burstein, H. J. Lymphopenia associated with adjuvant anthracycline/ taxane regimens. *Clinical breast cancer* **8** (4), 352-356, 2008.
95. Venkatesulu, B. P., Mallick, S., Lin, S. H. & Krishnan, S. A systematic review of the influence of radiation-induced lymphopenia on survival outcomes in solid tumors. *Critical reviews in oncology/ hematology* **123**, 42-51, 2018.
96. Hall, J. A., Salgado, R., Lively, T., Sweep, F. & Schuh, A. A risk-management approach for effective integration of biomarkers in clinical trials: perspectives of an NCI, NCRI, and EORTC working group. *The Lancet. Oncology* **15** (4), e184-193, 2014.

Part I

Immunomodulatory strategies
to improve responses to immune
checkpoint blockade in metastatic
breast cancer



Chapter 2

'IMpassionate conflicts' in
immunotherapy trials for metastatic
triple-negative breast cancer

- Editorial-

Leonie Voorwerk, Marleen Kok

Annals of Oncology, 2021;32 (8):947-949

Triple-negative breast cancer (TNBC) comprises a heterogeneous group of breast cancers, with an extremely poor prognosis in patients with metastatic disease. Important advancements are made in the treatment landscape for TNBC, with most notably the approval of first-line treatment with nanoparticle albumin-bound (nab)-paclitaxel and atezolizumab for patients with programmed death-ligand 1 (PD-L1) positive metastatic TNBC based on the IMpassion130 trial¹. More recently, the Food and Drug Administration granted accelerated approval to pembrolizumab in combination with chemotherapy for patients with metastatic TNBC with PD-L1 positive tumors (Combined Positive Score (CPS) ≥ 10) based on progression-free survival (PFS) data of the KEYNOTE-355 study². Since nab-paclitaxel is not as widely used as its solvent-based counterpart paclitaxel, the phase III IMpassion131 study evaluated atezolizumab in combination with paclitaxel. In this issue of the *Annals*, the final overall survival (OS) results of IMpassion130³ and primary PFS plus final OS results of IMpassion131 are presented⁴.

In IMpassion130, patients were randomized to nab-paclitaxel with either atezolizumab or placebo. As demonstrated previously, PFS was statistically significantly prolonged in both the intention-to-treat (ITT) population and the PD-L1 positive population ($\geq 1\%$ expression on immune cells in the tumor area) in the atezolizumab arm (Table 1)^{1,5}. As presented in this issue, final OS analysis shows no statistically significant difference between the arms in the ITT population. The trial had a hierarchical design for OS, meaning that OS in the PD-L1 positive population was not formally tested. However, an exploratory analysis in the PD-L1 positive population revealed a 7.5-months survival benefit with the addition of atezolizumab (Table 1)³. In IMpassion131, patients were randomized to paclitaxel with either atezolizumab or placebo. The primary endpoint of IMpassion131 was PFS in the PD-L1 positive population. Here, it is demonstrated that PFS is not statistically significantly different in the PD-L1 positive population when atezolizumab was added to paclitaxel. Exploratory analyses reveal that OS is also not statistically different in both the ITT and PD-L1 positive populations (Table 1)⁴.

Table 1: Overview of main efficacy results in IMpassion130 and IMpassion131.

Intention-to-treat population				
	IMpassion130 nP+A	IMpassion130 nP+Pla	IMpassion131 P+A	IMpassion131 P+P
Primary PFS analysis (median in months, 95% CI)	7.2 months (5.6-7.5)	5.5 months (5.3-5.6)	5.7 months (5.4-7.2)	5.6 months (5.4-6.5)
HR PFS (95% CI)	0.80 (0.69-0.92) <i>Coprimary endpoint</i>		0.86 (0.70-1.05) <i>Exploratory</i>	
Final OS (median in months, 95% CI)	21 months (19.0-23.4)	18.7 months (16.9-20.8)	19.2 months (16.6-22.1)	22.8 months (17.1-28.3)
HR OS (95% CI)	0.87 (0.75-1.02) <i>Coprimary endpoint</i>		1.12 (0.88-1.43) <i>Exploratory</i>	
PD-L1 positive population				
	IMpassion130 nP+A	IMpassion130 nP+P	IMpassion131 P+A	IMpassion131 P+P
Primary PFS analysis (median in months, 95% CI)	7.5 months (6.7-9.2)	5.0 months (3.8-5.6)	6.0 months (5.6-7.4)	5.7 months (5.4-7.2)
HR PFS (95% CI)	0.62 (0.49-0.78) <i>Coprimary endpoint</i>		0.82 (0.60-1.12) <i>Primary endpoint</i>	
Final OS (median in months, 95% CI)	25.4 months (19.6-30.7)	17.9 months (13.6-20.3)	22.1 months (19.2-30.5)	28.3 months (19.1-not estimable)
HR OS (95% CI)	0.67 (0.53-0.86) <i>Exploratory</i>		1.11 (0.76-1.64) <i>Exploratory</i>	

A, atezolizumab; CI, confidence interval; HR, hazard ratio; nP, nab-paclitaxel; OS, overall survival; P, paclitaxel; Pla, placebo; PFS, progression-free survival

Although confidence intervals between the main effect measures in IMpassion130 and IMpassion131 overlap (Table 1), several explanations for the differences in outcome between the IMpassion trials can be proposed. First, it is tempting to speculate on possible distinct immunogenic effects of nab-paclitaxel versus paclitaxel. For paclitaxel, it has been described that it can increase CD8+ T cell infiltration and MHC class I expression in ovarian cancer⁶ and nab-paclitaxel has been shown to reduce stromal density⁷. Both drugs can have an effect on the polarization of macrophages into a favorable M1-like phenotype via Toll-like receptor 4 (TLR4), but paclitaxel mainly exerts its effects via binding to TLR4 on macrophage membranes⁸, whereas nab-paclitaxel is internalized by macrophages potentially being more potent in inducing its effects on the macrophage phenotype⁹. However, since the pivotal KEYNOTE-522 trial in early breast cancer demonstrated improved pathological response rates upon addition of pembrolizumab to a paclitaxel-containing regimen¹⁰, it is unlikely that paclitaxel has a detrimental effect on anti-cancer T-cell responses. This is supported by the KEYNOTE-355 trial in which the nab-paclitaxel/pembrolizumab and paclitaxel/pembrolizumab arms seem to perform equally well in an exploratory analysis².

Second, an advantage of using nab-paclitaxel over paclitaxel is the avoidance of corticosteroids. As expected, steroids were widely used in IMpassion131⁴. Steroids have been proposed to have immunosuppressive capacities with dampening effects on effector immune cells, potentially hampering an effective immune response¹¹. However, it has been shown that the inferior outcome on PD1-blockade associated with steroids as co-medication is driven by a poor-prognosis subgroup of patients

who receive corticosteroids for palliative indications¹². Given that in IMpassion131 steroids were mainly used as prophylaxis for hypersensitivity reactions, together with efficacy data of both KEYNOTE-355 and KEYNOTE-522, it is not plausible that the difference in steroids alone explains the distinct results of IMpassion131 and IMpassion130.

Third, although at first glance the patient populations included in IMpassion130 and IMpassion131 appear similar, small differences in patient selection could influence the results, especially for treatment regimens such as immune checkpoint inhibitors (ICI), of which only a minority of patients benefit. While in both IMpassion130 and IMpassion131, patients were predominantly of Caucasian ethnicity (69% vs. 58% in the PD-L1 positive population), the proportion of patients of Asian origin differed (18% vs. 30% in the PD-L1 positive population). Tumor-host interactions are still an unexplored area of research and may partly explain the different outcome of IMpassion131 and IMpassion130. Also, in IMpassion131 more patients with only one to three metastatic sites were included (79% vs. 84% in the PD-L1 positive populations of IMpassion130 and IMpassion131, respectively). The latter might have contributed to the exceptionally good outcome of the placebo-paclitaxel arm in IMpassion131 with a median OS of 28.3 months in the PD-L1 positive population, while this was 17.9 months for the control arm in IMpassion130 (Table 1).

The recent translational analyses from IMpassion130, revealing that levels and patterns of tumor-infiltrating lymphocytes (TILs), CD8+ T-cell infiltration and the basal-like immune-activated (BLIA) molecular subtype were associated with a more pronounced benefit of atezolizumab, underscore the importance of extended molecular analyses^{13,14}. Performing the same analyses in IMpassion131 will not only provide a validation of these exploratory findings, but will contribute to a better understanding of seemingly conflicting trial results.

Where to go from here? Assuming that the follow-up results of KEYNOTE-355 will confirm the positioning of chemotherapy plus PD1-blockade as new first-line treatment for patients with metastatic TNBC, two developments could alter this standard within a couple of years. First, the IMpassion031, KEYNOTE-522 and GeparNuevo results indicate that anthracycline-taxane-based chemotherapy plus PD1-blockade could become the new standard for (high-risk) early TNBC^{10,15,16}. Subsequently, it is likely that the vast majority of tumors of relapsing patients will not be sensitive to PD1-blockade anymore, highlighting the need for strategies beyond conventional chemotherapy-PD1-blockade combinations. Early trials evaluating combinations of ICI (beyond PD1-blockade) or combinations with other immunomodulatory approaches such as oncolytic viruses, STING-agonists, IL2-based immunostimulations or anti-body drug conjugates have now shown promising results in TNBC¹⁷⁻²³. In addition, preliminary data of trials evaluating triplet therapy (chemotherapy, PD1-blockade and tyrosine kinase inhibitors (TKIs)) suggest impressive response rates when VEGF or AKT inhibitors are added to chemo-immunotherapy^{24,25}.

Additionally, with the growing body of evidence that TNBC is highly heterogeneous with regard to endogenous anti-cancer immune responses, it is time to design trials for specific subsets of TNBCs beyond PD-L1 expression. Selection based on low serum lactate dehydrogenase (LDH), TILs, CD8, BLIA molecular subtype, hypermutated phenotype or biomarkers related to the mechanism of action of a particular drug combination could help in bringing the right treatment to the right patients^{13,14,24,26,27}.

Although the exact reasons for discrepancies between the results of the IMpassion130 and IMpassion131 trials remain to be elucidated and the impressive OS benefit of 7.5 months upon atezolizumab addition in PD-L1 positive patients in IMpassion130 is based on an explorative analysis, these results should still be considered as a huge leap forward in the treatment of metastatic TNBC. Further research is needed to better identify long-term responders to ICI and to find the ideal chemotherapy or targeted treatment partner. The IMpassion130 and KEYNOTE-355 landmark trials, together with existing evidence from phase I/II trials, prelude a new era for a long-awaited new treatment option which induces durable responses in a substantial subset of advanced TNBC patients.

Funding: this work was supported by funding from the Hendrika Roet fund (no grant number applies). M.K. receives a research grant from the Dutch Cancer Society (Young Investigator Grant, 2020-1/12968).

Disclosure: M.K. reports funding to the institute from Bristol-Myers-Squib (BMS), Roche/Genentech, AstraZeneca and an advisory role for BMS, Roche, MSD and Daiichi Sankyo, outside the submitted work. L.V. has declared no conflicts of interests.

References

- Schmid P, Adams S, Rugo HS et al. Atezolizumab and Nab-Paclitaxel in Advanced Triple-Negative Breast Cancer. *N Engl J Med* **379**: 2108-2121, 2018 .
- Cortes J, Cescon DW, Rugo HS et al. Pembrolizumab plus chemotherapy versus placebo plus chemotherapy for previously untreated locally recurrent inoperable or metastatic triple-negative breast cancer (KEYNOTE-355): a randomised, placebo-controlled, double-blind, phase 3 clinical trial. *Lancet* **396**: 1817-1828, 2020.
- L. A. Emens SA, C. H. Barrios, V. Diéras, H. Iwata, S. Loi, H. S. Rugo, A. Schneeweiss, E. P. Winer, S. Patel, V. Henschel, A. Swat, M. Kaul, L. Molinero, S. Patel, S. Y. Chui, P. Schmid. First-Line Atezolizumab Plus Nab-Paclitaxel For Unresectable, Locally Advanced or Metastatic Triple-Negative Breast Cancer: IMpassion130 Final Overall Survival Analysis. *Annals of Oncology* 2021; **32**.
- D. Miles JG, F. André, D. Cameron, A. Schneeweiss, C. Barrios, B. Xu, A. Wardley, D. Kaen, L. Andrade, V. Semiglazov, M. Reinisch, S. Patel, M. Patre, L. Morales, S.L. Patel, M. Kaul, T. Barata & J. O’Shaughnessy. Primary results from IMpassion131, a double-blind placebo-controlled randomised phase III trial of first-line paclitaxel with or without atezolizumab for unresectable locally advanced/metastatic triple-negative breast cancer. *Annals of Oncology* 2021; **32**.
- Schmid P, Rugo HS, Adams S et al. Atezolizumab plus nab-paclitaxel as first-line treatment for unresectable, locally advanced or metastatic triple-negative breast cancer (IMpassion130): updated efficacy results from a randomised, double-blind, placebo-controlled, phase 3 trial. *Lancet Oncol* **21**: 44-59, 2020
- Peng J, Hamanishi J, Matsumura N et al. Chemotherapy Induces Programmed Cell Death-Ligand 1 Overexpression via the Nuclear Factor- κ B to Foster an Immunosuppressive Tumor Microenvironment in Ovarian Cancer. *Cancer Res* **75**: 5034-5045, 2015.
- Alvarez R, Musteanu M, Garcia-Garcia E et al. Stromal disrupting effects of nab-paclitaxel in pancreatic cancer. *Br J Cancer* **109**: 926-933, 2013
- Wanderley CW, Colón DF, Luiz JPM et al. Paclitaxel Reduces Tumor Growth by Reprogramming Tumor-Associated Macrophages to an M1 Profile in a TLR4-Dependent Manner. *Cancer Res* **78**: 5891-5900, 2018.
- Cullis J, Siolas D, Avanzi A, Barui S, Maitra A, Bar-Sagi D. Macropinocytosis of Nab-paclitaxel Drives Macrophage Activation in Pancreatic Cancer. *Cancer Immunol Res* **5**: 182-190, 2017
- Schmid P, Cortes J, Pusztai L et al. Pembrolizumab for Early Triple-Negative Breast Cancer. *New England Journal of Medicine* **382**: 810-821, 2020.
- Cain DW, Cidlowski JA. Immune regulation by glucocorticoids. *Nature Reviews Immunology* **17**: 233-247, 2017.
- Petrelli F, Signorelli D, Ghidini M et al. Association of Steroids use with Survival in Patients Treated with Immune Checkpoint Inhibitors: A Systematic Review and Meta-Analysis. *Cancers* **12**(3):546, 2020.
- Emens LA, Molinero L, Loi S et al. Atezolizumab and nab-Paclitaxel in Advanced Triple-Negative Breast Cancer: Biomarker Evaluation of the IMpassion130 Study. *Journal of the National Cancer Institute* 2021;djab004.
- Leisha A. Emens LDG, Peter Schmid, Hope S. Rugo, Sylvia Adams, Carlos H. Barrios, Andreas Schneeweiss, Veronique Dieras, Hiroji Iwata, Ching-Wei Chang, Hartmut Koeppen, Stephen Y. Chui, Sherene Loi, Luciana Molinero; . The tumor microenvironment (TME) and atezolizumab + nab-paclitaxel (A+nP) activity in metastatic triple-negative breast cancer (mTNBC): IMpassion130. *Journal of Clinical Oncology* **39**(suppl 15):1006, 2021.
- Mittendorf EA, Zhang H, Barrios CH et al. Neoadjuvant atezolizumab in combination with sequential nab-paclitaxel and anthracycline-based chemotherapy versus placebo and chemotherapy in patients with early-stage triple-negative breast cancer (IMpassion031): a randomised, double-blind, phase 3 trial. *The Lancet* **396**: 1090-1100, 2020.
- Loibl S, Untch M, Burchardi N et al. A randomised phase II study investigating durvalumab in addition to an anthracycline taxane-based neoadjuvant therapy in early triple negative breast cancer - clinical results and biomarker analysis of GeparNuevo study. *Ann Oncol* **30**(8): 1279-1288, 2019.
- Santa-Maria CA, Kato T, Park J-H et al. A pilot study of durvalumab and tremelimumab and immunogenomic dynamics in metastatic breast cancer. *Oncotarget* **9**:18985-18996, 2018.

18. Adams S, Othus M, Patel SP et al. Dual anti-CTLA-4 and anti-PD-1 blockade in metaplastic carcinoma of the breast: Dart (SWOG S1609, Cohort 36). *Journal of Clinical Oncology*. **38**(suppl 15):1073, 2020.
19. Manso L, Villagrasa P, Chic N et al. PS12-08: A window-of-opportunity study with atezolizumab and the oncolytic virus pelareorep in early breast cancer (REO-027, AWARE-1). *Cancer Research* **81**(4 supplement):PS12-08, 2021
20. Meric-Bernstam F, Sandhu SK, Hamid O et al. Phase Ib study of MIW815 (ADU-S100) in combination with spartalizumab (PDR001) in patients (pts) with advanced/metastatic solid tumors or lymphomas. *Journal of Clinical Oncology* **37**(suppl 15):2507, 2019
21. Uhlik MT, Bose N, Cox J et al. PD1-02: Response and clinical benefit assessment of the combination of the dectin-1 agonist imprime PGG and anti-PD-1 pembrolizumab in chemotherapy-resistant metastatic triple negative breast cancer (TNBC). *Cancer Research* **80**(4 supplement):PD1-02, 2020
22. Tolaney S, Baldini C, Spira A et al. A001 / Clinical activity of BEMPEG plus NIVO observed in metastatic TNBC: preliminary results from the TNBC cohort of the Ph1/2 PIVOT-02 study. 5th CRI-CIMT-EATI-AACR International Cancer Immunotherapy conference (CICON) 2019 2019.
23. Schmid P, Im S-A, Armstrong A et al. BEGONIA: Phase 1b/2 study of durvalumab (D) combinations in locally advanced/metastatic triple-negative breast cancer (TNBC)—Initial results from arm 1, d+paclitaxel (P), and arm 6, d+trastuzumab deruxtecan (T-DXd). *J Clin Oncol* **39** (suppl 15):1023, 2021
24. Chen L, Zhimin S, Wang Z et al. Combination of famitinib with camrelizumab plus nab-paclitaxel as first-line treatment for patients with immunomodulatory advanced triple-negative breast cancer (FUTURE-C-PLUS): A prospective, single-arm, phase 2 study. *J Clin Oncol* **39**(suppl 15):1007, 2021
25. Schmid P, Savas P, Espinosa E et al. PS12-28: Phase 1b study evaluating a triplet combination of ipatasertib (IPAT), atezolizumab, and a taxane as first-line therapy for locally advanced/metastatic triple-negative breast cancer (TNBC). *Cancer Research* **81**(4 supplement):PS12-28, 2021
26. Voorwerk L, Slagter M, Horlings HM et al. Immune induction strategies in metastatic triple-negative breast cancer to enhance the sensitivity to PD-1 blockade: the TONIC trial. *Nature Medicine* **25**: 920-928, 2019
27. Loi S, Adams S, Schmid P et al. LBA13 - Relationship between tumor infiltrating lymphocyte (TIL) levels and response to pembrolizumab (pembro) in metastatic triple-negative breast cancer (mTNBC): Results from KEYNOTE-086. *Ann Oncol* **28** (suppl_5): v608, 2017



Chapter 3

Immune induction strategies in metastatic triple-negative breast cancer to enhance the sensitivity to PD-1 blockade: the TONIC-trial

Leonie Voorwerk*, Maarten Slagter*, Hugo M. Horlings, Karolina Sikorska, Koen K. van de Vijver, Michiel de Maaker, Iris Nederlof, Roelof J. C. Kluin, Sarah Warren, SuFey Ong, Terry G. Wiersma, Nicola S. Russell, Ferry Lalezari, Philip C. Schouten, Noor A. M. Bakker, Steven L. C. Ketelaars, Dennis Peters, Charlotte A. H. Lange, Erik van Werkhoven, Harm van Tinteren, Ingrid A. M. Mandjes, Inge Kemper, Suzanne Onderwater, Myriam Chalabi, Sofie Wilgenhof, John B. A. G. Haanen, Roberto Salgado, Karin E. de Visser, Gabe S. Sonke, Lodewyk F. A. Wessels, Sabine C. Linn, Ton N. Schumacher, Christian U. Blank, Marleen Kok

*these authors contributed equally

Nature Medicine, 2019; 25 (6): 920-928

Abstract

The efficacy of programmed cell death protein 1 (PD-1) blockade in metastatic triple-negative breast cancer (TNBC) is low¹⁻⁵, highlighting a need for strategies that render the tumor microenvironment more sensitive to PD-1 blockade. Preclinical research has suggested immunomodulatory properties for chemotherapy and irradiation⁶⁻¹³. In the first stage of this adaptive, non-comparative phase 2 trial, 67 patients with metastatic TNBC were randomized to nivolumab (1) without induction or with 2-week low-dose induction, or with (2) irradiation (3 × 8 Gy), (3) cyclophosphamide, (4) cisplatin or (5) doxorubicin, all followed by nivolumab. In the overall cohort, the objective response rate (ORR; iRECIST¹⁴) was 20%. The majority of responses were observed in the cisplatin (ORR 23%) and doxorubicin (ORR 35%) cohorts. After doxorubicin and cisplatin induction, we detected an upregulation of immune-related genes involved in PD-1-PD-L1 (programmed death ligand 1) and T cell cytotoxicity pathways. This was further supported by enrichment among upregulated genes related to inflammation, JAK-STAT and TNF- α signaling after doxorubicin. Together, the clinical and translational data of this study indicate that short-term doxorubicin and cisplatin may induce a more favorable tumor microenvironment and increase the likelihood of response to PD-1 blockade in TNBC. These data warrant confirmation in TNBC and exploration of induction treatments prior to PD-1 blockade in other cancer types.

Triple-negative breast cancer (TNBC), characterized by estrogen receptor, progesterone receptor and HER2 negativity, comprises 10-20% of all breast cancers¹⁵. In patients with metastatic disease, tumors rapidly become resistant to chemotherapy, resulting in a median overall survival of only 8-13 months^{16,17}. Although durable responses to PD-1 and programmed death-ligand 1 (PD-1/PD-L1) blockade have been observed in TNBC, the fraction of patients with metastatic TNBC that benefit from PD-1/PD-L1 blockade is low, with response rates around 5%^{1,4}. Response rates seem to increase to 19-23% upon selection of patients with PD-L1-positive tumor microenvironments (TMEs)^{2,18}. However, the majority of patients with TNBC do not benefit from PD-1/PD-L1 blockade, highlighting the need for strategies that can alter the immune-suppressive TME and increase sensitivity to PD-1/PD-L1 blockade.

Preclinical and clinical studies have shown that low-dose chemotherapy or irradiation may be utilized to stimulate anticancer immune responses. For example, irradiation has been shown to induce type I interferons via the stimulator of interferon genes (STING) pathway and consequently enhance T cell priming^{6,7}. Some studies have demonstrated that cyclophosphamide can deplete regulatory T cells and could restore effector functions of T cells and natural killer cells⁸. In addition, cisplatin has been shown to upregulate major histocompatibility complex class I expression and directly stimulate T cell function^{9,10}. Finally, doxorubicin has been associated with myeloid-derived suppressor cell (MDSC) depletion¹¹, an increase in the level of type I interferons¹² and induction of immunogenic cell death¹³.

Here, we present a phase 2 trial in which we dissect the immunomodulatory effects of hypofractionated irradiation and low-dose cyclophosphamide, cisplatin and doxorubicin in patients with TNBC, with the hypothesis that these treatments may be utilized as priming strategies to improve the efficacy of PD-1/PD-L1 blockade. This multi-cohort TONIC trial evaluates the efficacy of nivolumab after short-term induction with low-dose chemotherapy, irradiation or no induction. A 'pick-the-winner' strategy, taking into account clinical responses and translational findings, was used with a Simon's two-stage design¹⁹ to decide which cohorts would be expanded.

In the TONIC trial (NCT02499367), patients were randomized to one of four different induction treatments, consisting of irradiation to a single lesion, low-dose cyclophosphamide, cisplatin or doxorubicin, or a 2-week waiting period (Figure 1a). Biopsies from metastatic lesions were taken at baseline (biopsy one), after induction (biopsy two) and after three cycles of nivolumab (biopsy three). Seventy patients were randomized between September 2015 and October 2017. Accrual continued until a minimum of ten patients who received at least one cycle of nivolumab and from whom we could acquire high-quality paired biopsies were included for each cohort, resulting in a slightly uneven number of patients across cohorts (Extended Data Figure 1). At data cut-off, the median follow-up was 19.9 months. Characteristics were as expected for advanced TNBC (Table 1) and balanced

between cohorts, with a relatively high proportion of patients in the doxorubicin and control cohorts receiving their first-line treatment in this trial (Supplementary Table 1). Sixty-six patients were available for efficacy analysis (Supplementary Table 2). All patients had received previous chemotherapy in the (neo-)adjuvant and/or the metastatic setting. Patients with *de novo* stage IV disease ($n = 8$ out of 66) were pretreated with palliative chemotherapy before entering the TONIC trial.

Table 1. Baseline characteristics of the intention-to-treat population.

Total population (n = 70)	No. of patients	Percentage
Median age, years (range)	51 (29-70)	
WHO performance status, n (%)		
0	41	59%
1	29	41%
Germline BRCA1/2, n (%)		
Mutation	6	9%
Wildtype	50	71%
Unknown	14	20%
Location of metastasis, n (%)		
Lymph node only	6	9%
Visceral metastasis	50	71%
Other metastasis	14	20%
Number of previous therapies for metastatic disease, n (%)		
0	17	24%
1	34	49%
2-3	19	27%
Previous neoadjuvant or adjuvant therapy, n (%)	59	84%
Previous chemotherapy exposure, n (%)		
Taxane	64	91%
Anthracycline	60	86%
Platinum	42	60%
Capecitabine	34	49%
Disease Free Interval (DFI), n (%)		
<i>De novo</i> metastatic disease	9	13%
DFI \leq 12 months	23	33%
DFI $>$ 12 months	38	54%
LDH level, n (%)		
\leq ULN	39	56%
\leq 2x ULN	31	44%
PD-L1 expression on tumor cells, n (%)		
Not available	5	7%
\geq 1% on tumor cells	44	63%
\geq 5% on tumor cells	23	33%
PD-L1 expression on immune cells, n (%)		
Not available	5	7%
\geq 1% on immune cells	60	86%
\geq 5% on immune cells	47	67%

Clinical baseline characteristics of all allocated patients. PD-L1 immunohistochemistry was performed using the DAKO 22C3 clone.

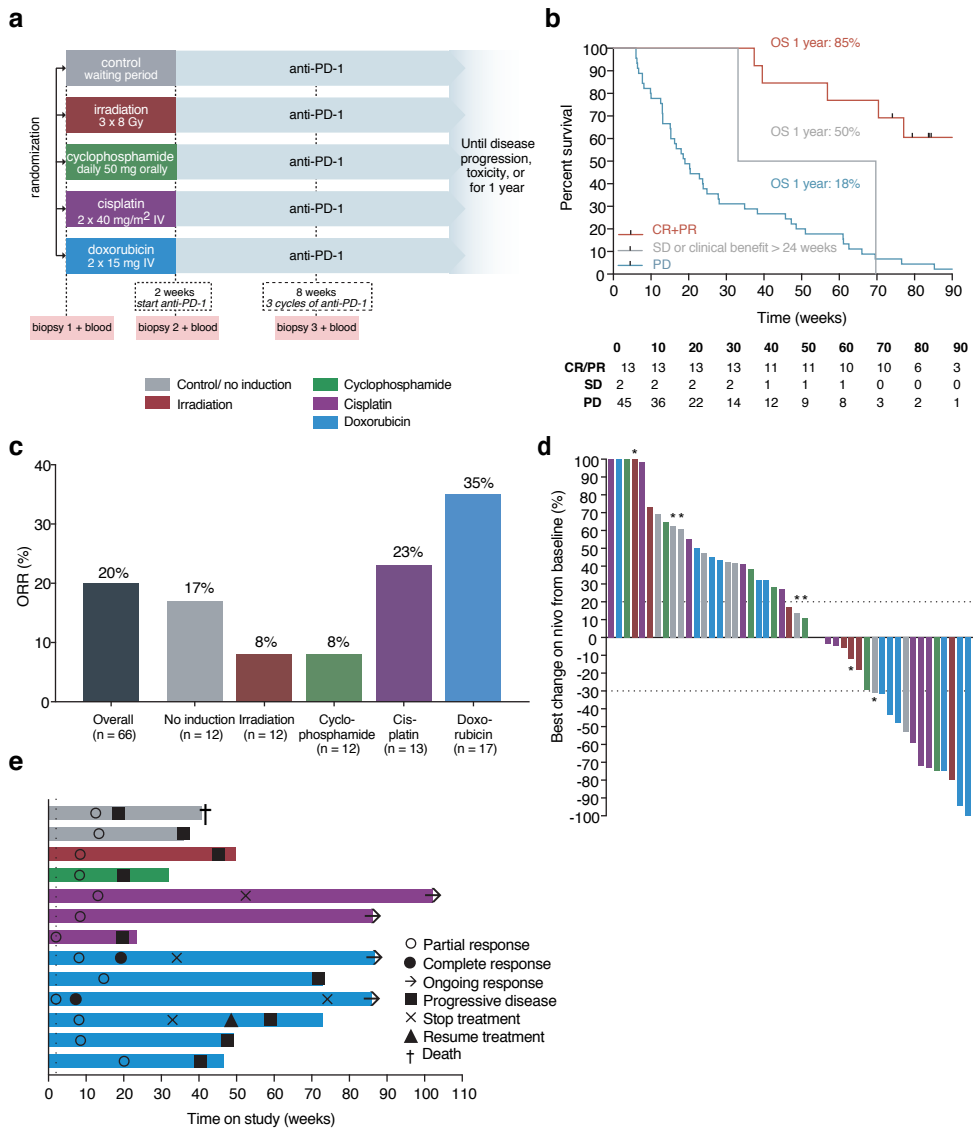


Figure 1. Anti-tumor activity of nivolumab after immune induction in the per protocol population. (a) Design of the TONIC trial. Patients were randomized to 1 of 4 cohorts with induction treatments or no induction, all followed by nivolumab (3 mg per kg every 2 weeks). Biopsies and blood samples were taken at baseline (biopsy one), on post-induction treatment (biopsy two) and on nivolumab (after three cycles of nivolumab; biopsy three). i.v., intravenous. (b) Overall survival (OS) by response. Kaplan-Meier curves of overall survival by best overall response were calculated. All 67 patients of the per protocol population were included, but 7 patients were deceased within 6 weeks after nivolumab initiation, and their data are not displayed (that is, a landmark was used at 6 weeks). The stable disease (SD) group includes a patient with stable disease, as defined by RECIST, for 26 weeks and a patient with non-evaluable disease but clinical benefit for 26 weeks. PD, progressive disease. (c) ORR per cohort as the percentage of total patients per cohort (iRECIST, investigator determined). ORR comprises all PRs and CRs. (d) Waterfall plot. Best radiological response of target lesions during nivolumab treatment compared to baseline. Eleven patients with clinical evidence of disease progression did not have a follow-up CT scan after nivolumab initiation, and nine patients had non-measurable disease. Depicted is the largest change in the sum of target lesions, in comparison to baseline or the post-induction CT scan (changes compared to the post-induction scan are indicated by asterisks; $n = 7$). Bar colors

reflect the induction treatment shown in a. The y axis was cut-off at 100% for illustration purposes. Dotted black lines indicate the response as described by RECIST1.1. (e) Swimmers plot. Duration of response of patients with PR or CR according to iRECIST. Progressive disease was assessed according to iRECIST; the first date of progressive disease is depicted in case of confirmation on a subsequent CT scan. Only two patients had a PR after induction treatment, with one prolongation after nivolumab treatment. One patient with a microsatellite instable tumor, pretreated with cisplatin, ended treatment after 1 year and has had an ongoing remission for 102 weeks. One patient with a CR stopped treatment after 17 nivolumab cycles due to a grade 2 pneumonitis and has had an ongoing CR for 86 weeks; another patient with a CR stopped treatment due to a grade 2 gastritis after 38 cycles of nivolumab and has had an ongoing CR for 86 weeks. The vertical dotted line marks the 2-week induction period.

Nivolumab after induction was not associated with any previously unreported toxicity. Induction treatment-related adverse events (AEs) of any grade occurred in 19 patients (28%, with 3% grade 3) and immune-related AEs of grades 3-5 occurred in 13 patients (19%; Supplementary Tables 3 and 4). Two patients with evidence of progression died on study.

Median progression-free survival (PFS) for all patients was 1.9 months (Supplementary Table 5). We observed an objective response rate (ORR) to nivolumab of 20% (13 out of 66 patients; iRECIST¹⁴), with two complete responses (CRs; 3%) and 11 partial responses (PRs; 17%) (Supplementary Table 5). The median duration of response according to iRECIST was 9 months (95% CI: 4.7 not reached). At data lock, four patients were still on study: one patient was still receiving nivolumab with an ongoing response, and three patients were in remission after stopping nivolumab.

We explored the potential predictive value of clinical characteristics and baseline aspects of the TME and peripheral blood. Patients with a disease-free interval (DFI) of 1 year or shorter had lower response rates ($P = 0.02$; Extended Data Figure 2a). The ORR for patients treated in the first line was 33%, while the ORR was 16% in patients treated in the second or later lines ($P = 0.15$; Extended Data Figure 2a). We observed significantly higher levels of stromal tumor-infiltrating lymphocytes (sTILs) and higher levels of CD8 and PD-L1 on immune cells in responders than in non-responders (Figure 2a,b and Extended Data Figures 2a,b and 3). Furthermore, we observed significantly lower cancer antigen 15-3 (CA 15-3) and carcinoembryonic antigen (CEA) levels in responders (Figure 2c and Extended Data Figure 2a,d). CA 15-3 showed a moderate correlation with the number of metastatic sites (Extended Data Figure 2e). In a multivariate analysis, CA 15-3 remained associated with response after adjustment for sTILs and lines of treatment (odds ratio: 0.69; $P = 0.05$) but not after adjustment for number of metastatic sites (odds ratio: 0.72; $P = 0.08$). No significant correlation with response was observed for lactate dehydrogenase (LDH), C-reactive protein, neutrophils, lymphocytes, neutrophil-to-lymphocyte ratio, eosinophils or serum levels of 12 CD8 T cell and natural-killer-cell-related cytokines (Extended Data Figures 2f-k and 4). In addition, we observed higher gene signature scores for T helper 1 cells, B cells and neutrophils in responders than in non-responders (Figure 2d), using the NanoString IO 360 Panel. Higher T cell receptor (TCR) clonality, more T cells and a larger TCR repertoire diversity (the number of unique intratumoral T cell clones) were observed in responders than in non-responders, both intratumoral and in the blood (Extended Data Figure 2l-q), however these associations were not statistically significant.

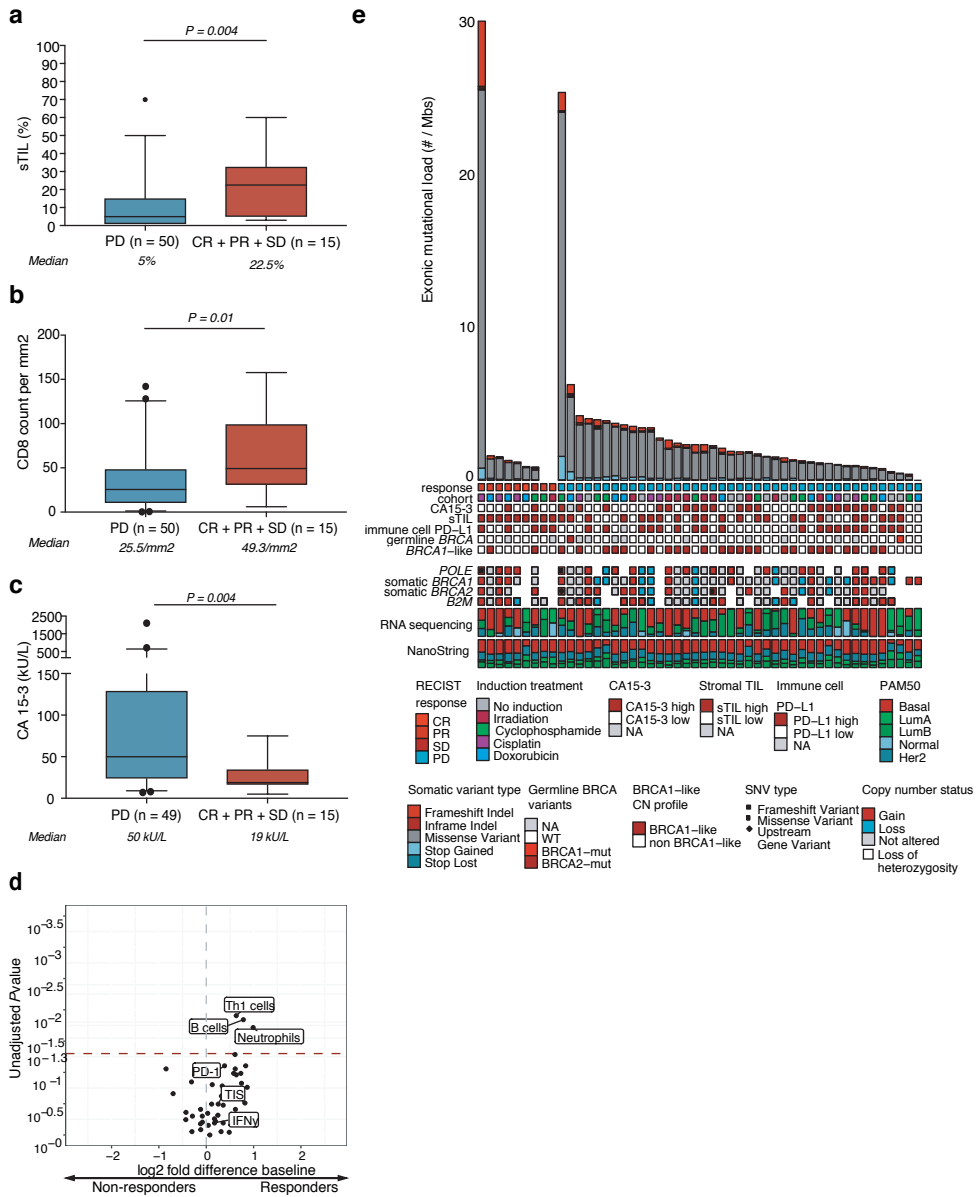


Figure 2. Intratumoral and systemic baseline parameters associated with response. (a) Baseline sTILs determined according to guidelines of the TIL working group on a H&E staining of tumor biopsies. The median value is displayed for patients with or without clinical benefit; the median in the overall cohort was 5%. Boxplots represent the median and 25th and 75th percentiles, and the vertical bars span the 5th to the 95th percentiles. Statistical significance was tested with a two-tailed Mann-Whitney *U*-test (unadjusted *P* value). (b) Baseline CD8 cell count per mm² in tumor biopsies. The median value is displayed for patients with or without clinical benefit; the median in the overall cohort was 30 cells per mm². Boxplots represent the median and 25th and 75th percentiles, and the vertical bars span the 5th to the 95th percentiles. Statistical significance was tested with a two-tailed Mann-Whitney *U*-test (unadjusted *P* value). (c) Baseline serum levels of CA 15-3. CA 15-3 was measured according to local guidelines. The median value is displayed for patients with or without clinical benefit; the median in the overall cohort was 35 kU l⁻¹ (which is

1× ULN). Boxplots represent the median and 25th and 75th percentiles, and the vertical bars span the 5th to the 95th percentiles. Statistical significance was tested with a two-tailed Mann-Whitney *U*-test (unadjusted *P* value). (d) Volcano plot of baseline gene expression signatures assessed with the NanoString IO 360 panel of 770 genes. Displayed is the log₂ fold difference of the median gene expression signature score between non-responders and responders (all patients with clinical benefit). Statistical significance is observed for signatures above the red dashed line (two-sided Wilcoxon signed-rank test; unadjusted *P* value of 0.05). Every dot represents one gene expression signature, as previously determined by Ayers et al.²² and Danaher et al.^{23,26}. The gray dashed line indicates no difference in gene expression. IFN-γ, interferon-γ; T_H1, T helper 1; TIS, tumor inflammation signature. (e) Mutational load, germline (according to routine clinical diagnostics) and somatic *BRCA* variants, *BRCA1*-like copy number (CN) profiles, copy number or mutation status of *POLE*, *BRCA1*, *BRCA2* and *B2M*, and PAM50 subtype assessed by RNA sequencing and NanoString are depicted. Data were available for 50 patients, samples were taken at baseline before study treatment. NA, not available; SNV, single-nucleotide variant; WT, wild type; LumA, Luminal A; LumB, Luminal B.

We found no association between mutational load or predicted neo-epitopes and response (Figure 2e and Extended Data Figure 2r,s). Two patients with exceptionally high mutational loads had somatic mutations in *POLE*. One of those cases was also identified as microsatellite instable and had a durable response²⁰. No mutations in *B2M* were observed at baseline. We found no associations between response and *BRCA1/2* mutations (Figure 2e), but we did observe *BRCA1*-like genomic copy number profiles to be negatively associated with response (Figure 2e and Extended Data Figure 2a). Molecular subtypes according to PAM50²¹ were not associated with response.

Most clinical responses occurred during nivolumab, with two patients having the onset of response during the induction period (Extended Data Figure 5a,b). Most responses were observed in the doxorubicin cohort (ORR: 35%; 95% CI: 14.2-61.7%), followed by cisplatin (ORR: 23%; 95% CI: 5-53.8%; Figure 1c,d). In the no induction treatment cohort, two patients experienced a PR (ORR: 17%; 95% CI: 2.1-48.4%); in the irradiation and cyclophosphamide cohorts, only one patient had a PR (ORR: 8%; 95% CI: 0.2-38.5%). When restricting analysis to non-first-line patients, the doxorubicin, cisplatin and no induction cohorts still showed numerically higher ORRs than the irradiation and cyclophosphamide cohorts (Extended Data Figure 5c). According to the Simon's two-stage design²², discontinuation of a cohort was required if fewer than three out of ten patients had no progressive disease after 12 weeks (Extended Data Figure 5e-g). According to iRECIST (Extended Data Figure 5e,f), only the doxorubicin cohort was allowed to continue.

The main objective of the TONIC trial was to explore whether induction treatment can induce a more inflamed TME. To determine the desired state of inflammation, we first studied the ongoing anti-cancer immune response in biopsy three of responders compared to biopsy three from non-responders. On nivolumab, we observed higher TCR clonality (*P* = 0.009) and increased T cell infiltration (*P* = 0.004; Figure 3a,d). Although T cell repertoire clonality appeared more strongly increased in the cisplatin and doxorubicin cohorts after nivolumab treatment (biopsy three versus biopsy one) than in the control cohort (Figure 3c), such inter-cohort differences were not observed directly after induction (biopsy two versus biopsy one; Figure 3b). In addition, we observed a trend in increased T cell infiltration after induction with cisplatin and doxorubicin (biopsy two versus biopsy one; Figure 3e), which

became more pronounced after nivolumab treatment (biopsy three versus biopsy one; Figure 3f). Finally, increases in the number of unique intratumoral T cell clones (TCR diversity) were significantly higher on nivolumab in the doxorubicin cohort than in the control cohort (Extended Data Figure 6). We observed higher TIL (H&E) and CD8 counts (immunohistochemistry) in on-nivolumab biopsies of responders than in non-responders (Extended Data Figure 7a,b). Comparing post-induction and baseline, we observed a trend towards increased TIL and CD8 counts in all cohorts except for the irradiation cohort (Extended Data Figure 7c,d) and non-significant increases in TIL and CD8 counts after nivolumab treatment in the doxorubicin cohort. We observed no changes in stromal CD4 or FOXP3 expression after induction. A non-significant increase in CD4 expression in the doxorubicin cohort was observed (Extended Data Figure 7e,f).

Next, we evaluated treatment-induced changes in the expression of immune-related genes (NanoString IO 360 Panel)^{22,23}. On nivolumab (biopsy three), several gene signatures associated with inflammation were significantly higher for responders than for non-responders (Figure 3g). Following cisplatin and doxorubicin treatments, most of these inflammation-related signatures (Figure 3g) showed a trend towards upregulation, but after irradiation or a 2-week waiting period these signatures tended to get downregulated (biopsy two versus biopsy one; Figure 3h). Upregulation of inflammation-related signatures in the cisplatin and doxorubicin cohorts was even more pronounced after nivolumab treatment (biopsy three versus biopsy one; Figure 3i). Using a Bayesian model, we estimated the effect sizes of the four induction treatments on immune-related gene signatures (Figure 3g). We observed that the effect sizes of cisplatin and doxorubicin equaled or exceeded changes in the no induction cohort with 98.0% and 85.2% probability, respectively (Extended Data Figure 8b). After correction for baseline gene expression, clinical response to nivolumab, lines of palliative treatment and lymph node only metastasis, probabilities of 92.1% and 80.7% (Extended Data Figure 8g,h), respectively, were obtained. Subsequently, a gene set enrichment analysis (GSEA) on 50 hallmark gene sets²⁴ on RNA sequencing data demonstrated an enrichment of eight immune-related gene sets among upregulated genes (biopsy two versus biopsy one) after doxorubicin treatment (six out of eight gene sets passed multiple testing correction) and after cisplatin treatment (zero out of eight passed multiple testing correction). After irradiation and cyclophosphamide treatments, the majority of these gene sets showed a non-significant enrichment among downregulated genes. By contrast, only 7 out of 42 non-immune-related hallmark gene sets were enriched among upregulated genes after doxorubicin. In addition, we tested previously established gene signatures related to myeloid cells^{23,25,26} and CD4 T cells²⁷. Three (out of four) myeloid-related signatures showed upregulation after induction and/or on nivolumab treatment (Extended Data Figure 9a,b). Furthermore, we evaluated two MDSC-related signatures²⁵ and two CD4 T cell signatures²⁷ in a separate GSEA and observed all to be enriched among upregulated genes after doxorubicin and cisplatin (false discovery rate ≤ 0.25 ; Extended Data Figure 9c).

Wallis test for all groups. Patients with clinical benefit are highlighted with a red dot. The dotted black line indicates no change. (d) Percentage of tumor-infiltrating T cells (TCR sequencing) on nivolumab treatment. The percentage of T cells of total nucleated cells, as assessed by TCR sequencing is depicted. Boxplots represent the median, 25th and 75th percentiles and the vertical bars span the 5th to the 95th percentiles. Statistical significance was tested with a two-tailed Mann-Whitney *U*-test (unadjusted *P* value). (e) FC in the percentage of tumor-infiltrating T cells (TCR sequencing) after induction treatment versus baseline (biopsy two versus biopsy one). The percentage of T cells over nucleated cells is depicted. The boxes in the boxplots represent the median and interquartile ranges and the whiskers represent the full range. Statistical significance was tested with a Kruskal-Wallis test for all groups. Patients with clinical benefit are highlighted with a red dot. The dotted black line indicates no change. (f) FC in the percentage of tumor-infiltrating T cells (TCR sequencing) on nivolumab treatment versus baseline (biopsy three versus biopsy one). The percentage of T cells over nucleated cells is depicted. The boxes in the boxplots represent the median and interquartile ranges and the whiskers represent the full range. Statistical significance was tested with a Kruskal-Wallis test for all groups. Patients with clinical benefit are highlighted with a red dot. The dotted black line indicates no change. (g) Volcano plot of previously established gene expression signatures^{22,23,26}, assessed with the NanoString IO 360 panel of 770 genes. The \log_2 fold difference of the median gene expression per signature between non-responders and patients with clinical benefit in biopsies taken after three cycles of nivolumab (biopsy three) is displayed. Statistical significance is observed for signatures above the red dashed line (two-sided Wilcoxon signed-rank test; unadjusted *P* value of 0.05). Each dot represents one of the previously established gene expression signatures by NanoString^{22,23,26}. The gray dashed line indicates no difference in gene expression. MMR, DNA mismatch repair. (h) Heatmap of post-induction FCs in gene expression signatures (NanoString; significantly upregulated during an active ongoing response on nivolumab, determined in g) in post-induction samples (biopsy two) compared to baseline (biopsy one). Depicted is the \log_2 FC in median gene expression of paired biopsies. Statistical significance (two-sided Wilcoxon signed-rank test) is highlighted with a black dot. (i) Heatmap of on-nivolumab FCs in gene expression signatures (NanoString; significantly upregulated during an active ongoing response on nivolumab, determined in g) in samples taken on nivolumab (biopsy three) compared to baseline (biopsy one). Depicted is the \log_2 FC in median gene expression of paired biopsies. Statistical significance (two-sided Wilcoxon signed-rank test) is highlighted with a black dot. (j) Gene set enrichment analysis of 50 hallmark gene sets²⁴, performed on whole-transcriptome RNA sequencing of pre-induction and post-induction samples (biopsy 2 compared to biopsy 1). Cells are colored according to normalized enrichment scores, and Benjamini-Hochberg (FDR) corrected *P* values equaling or below 0.25 are highlighted with black dots. Immune-related gene sets are highlighted in bold font. DN, downregulated; IL-6, interleukin-6; JAK, Janus kinase; mTOR, mechanistic target of rapamycin; mTORC1, mTOR complex 1; NF- κ B, nuclear factor- κ B; PI3K, phosphatidylinositol-3-OH kinase; STAT3, signal transducer and activator of transcription 3; TGF- β , transforming growth factor- β ; TNF- α , tumor necrosis factor- α ; UP, upregulated.

To our knowledge, TONIC is the first trial to evaluate the concept of TME modulation using chemotherapy or irradiation prior to PD-1/PD-L1 blockade. Our data provide substantial evidence that induction with cisplatin or doxorubicin can prime tumors for response to anti-PD-1, based on high response rates to anti-PD-1 and upregulation of immune-related gene sets. Finally, we observed trends towards increased T cell infiltration and TCR diversity in the doxorubicin cohort. On the basis of the Simon's two-stage design, the doxorubicin cohort is currently expanded in stage II of the trial (Extended Data Figure 5h). We note that this trial was not designed nor powered for direct comparison of response rates between arms and, as such, the data cannot be used as conclusive evidence for the inferiority of other induction treatments.

The majority of clinical trials that evaluate immune checkpoint blockade (ICB) in combination with chemotherapy simply combine PD-1/PD-L1 blockade with standard chemotherapy^{5,28}, which was shown to lead to increased survival for patients with PD-L1-positive TNBC⁵. By contrast, the sequential administration of chemotherapy or irradiation in the TONIC trial allowed us to test whether conventional treatments can turn 'cold' into 'hot' tumors. To the best of our knowledge, strong preclinical or clinical data that assess whether the sequential use of chemotherapy or irradiation is better than concomitant use are still lacking. Arguments in favor of

the latter are the relatively long time to response to PD-1/PD-L1 blockade during which chemotherapy can provide early tumor control and the potential synergy between PD-1/PD-L1 blockade and chemotherapy. Conversely, the short-term use of chemotherapy reduces toxicity substantially while potentially still effectuating the immunomodulation associated with cytostatic agents. Interestingly, the first results of the GeparNuevo trial, evaluating anti-PD-L1 added to chemotherapy in primary TNBC, suggested that induction with anti-PD-L1 increased responses in primary TNBC²⁹. Of note, our analyses of sequential on-treatment biopsies revealed that the immunomodulatory effects induced by three cycles of anti-PD-1 were substantially larger than the changes observed after 2 weeks of induction, arguing for an earlier start of ICB. Recent work has demonstrated that high response rates are observed upon ICB in the neoadjuvant setting in melanoma and non-small-cell lung cancer^{30,31}, supporting the notion that primary tumors may be more sensitive to immune control than metastases. Given this, it would be interesting to apply the design of TONIC to the neoadjuvant setting.

We found that nivolumab in patients with metastatic TNBC resulted in an ORR of 20%. This ORR is higher than in other studies in this patient population that show an ORR of only 5-10%^{1,3,4}. This may be due to the priming strategy that was used in our trial, but patient selection may also have contributed, for example, as, in contrast to some previous studies^{3,4}, we excluded patients with high serum levels of LDH. Importantly, we confirm that patients with a short DFI (<1 year) had a low likelihood (<5%) of response to ICB even when the LDH level is <2× upper limit normal (ULN), as previously reported¹⁸. In contrast to data for melanoma and non-small-cell lung cancer^{32,33}, the tumor mutational burden did not correlate with response in our series, in line with previous work^{34,35}. Although this lack of correlation may simply be explained by small sample sizes, it is interesting to consider that the tumor mutational burden might not be a determinant of response in relatively ‘cold’ tumors, such as breast cancer, in which copy number aberrations are more prevalent. This is supported by the significant association that we observed between *BRCA1*-like copy number profiles and non-response to anti-PD-1 and in line with previous studies in melanoma suggesting that copy number aberration burden is negatively associated with anti-PD-1 response^{36,37}.

We observed a significant correlation between PD-L1 on immune cells and nivolumab benefit (Extended Data Figures 2a,b and 3e,f), in line with several studies in TNBC³⁻⁵. Of note, the prevalence of PD-L1-positive tumors is somewhat higher in our study than in other studies^{2,18}, with 86% of patients expressing PD-L1 on immune cells (assessed using the 22C3 clone). Using the SP142 clone and by scoring of immune cells, Schmid et al.⁵ reported 41% PD-L1-positive tumors in the first-line setting, whereas Emens et al.³ reported 81% PD-L1 positivity in heavily pretreated patients. Studies in non-small-cell lung cancer³⁸ and bladder cancer³⁹ have shown that the 22C3 clone yields higher proportions of PD-L1 positivity than the SP142 assay.

Although the TONIC trial design allowed relatively quick prioritization of treatments, there are several limitations to address. First, the TONIC trial was designed as a

non-comparative trial with relatively small numbers. Although we only included patients with TNBC, this population is still quite heterogeneous in terms of previous treatments and metastatic patterns. Second, no stratification was applied in the first stage of the trial. Consequently, the cohorts were not perfectly balanced for several characteristics, such as the location of metastases and the number of previous palliative treatments. Third, we required a short period of preferential recruitment to the doxorubicin arm ($n = 17$) to obtain at least ten good-quality paired biopsies. As such, we cannot exclude that low-dose doxorubicin might also have a direct anti-tumor effect. Finally, according to the very stringent decision rules (requiring a success rate of at least 30%) that we set before the start of the trial (2014) without knowing that the ORR to PD-1/PD-L1 blockade would be only 5-10%^{1,3,4}, doxorubicin was picked as a winner only when the iRECIST criteria (ORR 35%) were applied, but not according to RECIST1.1⁴⁰ (Extended Data Figure 5e-g).

In summary, induction treatment with short-term chemotherapy or irradiation followed by nivolumab is feasible and leads to clinical benefit in a substantial subset of patients, with higher than expected response rates and durable responses. Priming with doxorubicin or cisplatin seems to induce a more favorable TME and was associated with a higher likelihood of response to nivolumab in this study. Next to the ongoing validation in stage II of this TONIC trial, which incorporates a nivolumab monotherapy cohort and a doxorubicin followed by nivolumab cohort (Extended Data Figure 5h), independent validation of our findings is required. In addition, the design of this study may serve as a template for other signal-finding combination immunotherapy studies in breast cancer and beyond.

Methods

Study design

The TONIC trial (full title: adaptive phase 2 randomized non-comparative trial of nivolumab after induction treatment in triple-negative breast cancer patients; NCT02499367) is a single center, non-blinded, randomized, non-comparative phase II study designed to evaluate the feasibility and efficacy of nivolumab after a 2-week induction treatment with chemotherapy or irradiation in patients with metastatic TNBC. The first stage of the trial consisted of five cohorts (four with induction treatment before nivolumab, one with a 2-week waiting period), all with a Simon's two-stage design¹⁹. For the second stage, the number of arms is reduced based on the results obtained in the first stage, according to the 'pick-the-winner' principle, considering clinical as well as translational end points. The trial was conducted in accordance with the protocol, Good Clinical Practice standards and the Declaration of Helsinki. The full protocol, including two amendments, and the informed consent form were approved by the institution's medical-ethical committee. All patients provided written informed consent before enrollment. This investigator-initiated trial was designed by the Netherlands Cancer Institute (NKI). Funding was provided by Bristol-Myers-Squibb (BMS) through the International Immuno-Oncology Network (II-ON) and by the Dutch Cancer Society (NKI2015-7710)

with the NCI being the sponsor. Translational research was funded by Pink Ribbon (NKI2016-8214), the Breast Cancer Research Foundation (BCRF-17-188) and BMS/II-ON. The study protocol was written during the ECCO-AACR-ESMO-EORTC course 'Methods in Clinical Cancer Research' Flims, 2014.

Patients

Key inclusion criteria included: 18 years of age or older; metastatic or incurable locally advanced TNBC with confirmation of estrogen receptor and HER2 negativity (ER < 10% and HER2 0, 1 or 2 in the absence of amplification as determined by in situ hybridization) on a biopsy of a metastatic lesion or recurrence in the breast; a WHO (World Health Organization) performance status of 0 or 1; measurable or evaluable disease according to RECIST1.1⁴⁰; and a maximum of three previous lines of palliative systemic treatment. Key exclusion criteria included: a LDH level above 500 U l⁻¹ (>2× ULN); symptomatic brain metastasis (treated and stable brain metastasis were allowed); previous therapy with ICB; and active autoimmune disease or chronic infections. Patients were not selected based on PD-L1 expression and had to have an accessible lesion for sequential biopsies and a different lesion accessible for irradiation. Full eligibility criteria are listed in the Supplementary Note (online version of this article). At the start of the trial, PD-L1 was assessed using immunohistochemistry and was used for stratification of the first 17 patients. For logistical reasons and an unacceptable waiting time for patients due to this PD-L1 analysis, this stratification procedure was stopped.

Procedures

Before the start of the induction treatment (biopsy one), before the start of nivolumab (biopsy two) and after 6 weeks of nivolumab (biopsy three), a biopsy was taken from a metastatic lesion, preferably the same lesion throughout the study. In the case of irradiation as induction treatment, a biopsy was taken from a non-irradiated lesion. When a good-quality baseline biopsy (at least 100 invasive tumor cells) of a metastatic lesion or recurrence in the breast was obtained, subjects were randomly allocated to 1 of 4 induction treatments. Induction treatments consisted of irradiation of 1 metastatic lesion (3 fractions of 8 Gy within 10 weekdays after randomization), cyclophosphamide (50 mg orally daily for 2 weeks), cisplatin (40 mg per m² intravenously weekly for 2 weeks) or doxorubicin (15 mg intravenously weekly for 2 weeks). A fifth control cohort was subjected to a 2-week waiting period. The irradiation was delivered to an accessible lesion, which was defined as a metastatic, preferably visceral, otherwise lymph node or bone, lesion at a distant location from the biopsy site. The radiation technique depended on the metastasis site (Supplementary Table 6). In general, the lesion was expanded with a 5-mm margin to acquire a planning target volume. Tumor coverage was assessed by the volume of the planning target volume receiving 95% of the prescribed dose. All patients underwent a second biopsy, after which nivolumab (3 mg per kg intravenously every 2 weeks) was given until disease progression according to iRECIST¹⁴ or until unacceptable toxicity. Accrual to a cohort was continued until ten patients were included who received at least one cycle of nivolumab, and for whom we were able to obtain a good-quality biopsy at baseline and after

induction treatment. Twelve patients were allocated to the control or no induction cohort, 12 to the irradiation cohort, 13 to the cyclophosphamide cohort, 13 to the cisplatin cohort and 17 to the doxorubicin cohort. Clinically stable patients with radiographic evidence of progressive disease according to RECIST1.1 were permitted to continue nivolumab treatment until radiographic confirmation of progressive disease on a second CT scan. When patients had an ongoing response after 12 months of treatment, nivolumab was allowed to be discontinued and reintroduced when progressive disease occurred. Dose modification for nivolumab was not permitted, but dose interruptions were allowed in case of (or suspicion of) toxicity. Safety was assessed every 2 weeks and included monitoring of AEs by clinical laboratory assessments and physical examinations. AEs were classified and graded per National Cancer Institute's Common Terminology Criteria for Adverse Events (NCI-CTCAE), v4.03. Serious AEs were collected up to 30 d after the last nivolumab administration. Imaging was performed after the 2-week induction treatment period and thereafter every 6 weeks until 6 months, after which imaging was performed every 8 weeks. Best overall response, duration of response and the date of progression were assessed according to RECIST1.1 and iRECIST, investigator assessed. An independent radiologist with extensive experience with response assessment in patients treated with ICB reviewed the scans of the responding cases.

End points

The primary end point of the study was PFS, assessed from randomization (PFS1) to tumor progression or death from any cause as defined by RECIST1.1. Secondary end points of the study were ORR, defined as the percentage of patients with a best overall response of CR or PR according to RECIST1.1 and iRECIST; clinical benefit rate, defined as the percentage of patients with a best overall response of CR, PR and stable disease for 24 weeks, according to RECIST1.1 and iRECIST; PFS1 as defined by iRECIST; PFS, assessed from nivolumab treatment initiation (PFS2) to tumor progression or death from any cause as defined by RECIST1.1 and iRECIST; overall survival, defined as the time from nivolumab initiation to death from any cause; and the percentage of patients with toxicity according to NCI-CTCAE v4.03 and immune-related toxicity. Translational objectives included: the effects of the induction treatments on the anticancer immune response evaluated using immune-related gene expression signatures; T cell influx determined using H&E and immunohistochemistry and TCR sequencing; and the exploration of putative predictive biomarkers.

Statistical analysis

For patients with metastatic TNBC, no first-line 'standard' therapies have been defined. Frequently used anticancer agents are capecitabine or taxanes. The median PFS with these therapies typically lies between 4-6 months. No 'standard' second-line therapy exists for patients with TNBC, but carboplatin (\pm gemcitabine), vinorelbine, capecitabine and taxanes are often used. On the basis of four phase 2 trials in TNBC allowing one or two previous lines of chemotherapy, a median PFS between 2 and 4 months was anticipated⁴¹⁻⁴⁴. Thus, the investigators considered a proportion of >30% of the patients having a PFS of at least 12 weeks as potentially

interesting. The null hypothesis that the true PFS rate as a binary end point at 12 weeks is 30% was tested against an alternative of 50%. A Simon two-stage minimax design with a one-sided alpha of 15% and 85% power was also optimal with respect to the expected sample size. A sample size of ten evaluable patients in the first stage required early discontinuation of a particular treatment cohort if less than three out of ten patients were free of progression and alive at 12 weeks. Because the number of patients in each cohort is larger than ten (due to the collection of ten paired biopsies), the decision about discontinuation of a cohort was based on the first ten patients. A patient was considered evaluable when at least one cycle of nivolumab was administered and both the baseline biopsy (biopsy one) and the post-induction biopsy (biopsy two) were available for immunohistochemistry. PFS and OS were assessed in all patients who received at least one dose of nivolumab (per protocol population). The safety population consisted of all patients who started their allocated treatment. PFS, OS, duration of response and median follow-up were calculated from the date of randomization and estimated using the Kaplan-Meier method. The duration of response was calculated from the first date of response to the date of progression. Median time to response was calculated as the time between randomization and the first measured objective response in responding cases. The DFI was defined as the time between the diagnosis of the primary tumor or locoregional recurrence and the date of diagnosis of metastatic disease. Patients with *de novo* metastatic disease at diagnosis were excluded from the exploratory analysis testing the association between DFI and ORR. A binary logistic regression analysis was performed to assess the effect of CA 15-3 (per 10 units) on response after correction for possible confounding factors (one model corrected for the number of metastatic sites and another model corrected for TIL and previous lines of treatment). As the number of metastatic sites and CA 15-3 were correlated (Spearman's ρ : 0.46; $P = 0.0001$), we tested for multicollinearity and found a variance inflation factor of 1.02, indicating no multicollinearity. The number of metastatic sites (1-2 versus 3 or more sites) and the number of previous lines of treatment (0 versus 1-3 lines) were included as categorical variables with the lowest category as a reference. Two-sided non-parametric tests were used for all analyses of the translational data: that is, the Mann-Whitney U-test was used for independent observations and the Wilcoxon's signed-rank test was used for paired observations. The data cut-off date for all analyses was 1 December 2018. Microsoft Excel v16.13.1, GraphPad Prism v7.0, IBM SPSS Statistics 23, SAS v9.4 and R v3.3.2⁴⁵ were used for statistical analyses. Reported P values are unadjusted, unless stated otherwise.

Peripheral blood parameters

Baseline neutrophil, lymphocyte and eosinophil counts and LDH and C-reactive protein levels were measured according to local guidelines as part of routine diagnostics. The neutrophil-to-lymphocyte ratio was calculated as the ratio of neutrophils over lymphocytes. Baseline cytokine levels were assessed in the serum by BioLegend's LEGENDplex bead-based cytokine assay (human CD8/natural killer cell panel; lot no. 740267) according to the manufacturer's instructions.

TILs and immunohistochemistry

Formalin-fixed paraffin-embedded tissue sections were used for H&E stainings, and for CD8 (C8/144B, DAKO), PD-L1 (22C3, DAKO), CD4 (SP35, CellMarque) and FOXP3 (236A/E7, Abcam) immunohistochemistry. Immunohistochemistry of samples was performed on a BenchMark Ultra autostainer (Ventana Medical Systems). Paraffin sections of 3 μm were deparaffinized in the instrument with EZ prep solution (Ventana Medical Systems). Heat-induced antigen retrieval was carried out using Cell Conditioning 1 (Ventana Medical Systems) for 48 min at 95 °C. Slides were counterstained with Hematoxylin and Bluing Reagent (Ventana Medical Systems). CD4 (red) and FOXP3 (DAB) were double stained. FOXP3 was detected in the first sequence (1:200 dilution, 2 h at room temperature). Bound antibody was detected using the OptiView DAB Detection Kit (Ventana Medical Systems). In the second sequence of the double-staining procedure, CD4 was detected (1:200 dilution, 1 h at room temperature) with an additional amplification step (Ventana Medical Systems). CD4 was visualized using the UltraView Universal Alkaline Phosphatase Red Detection Kit (Ventana Medical Systems). Slides were scanned at Aperio ScanScope and uploaded on Slide Score (www.slidescore.com). Two pathologists independently evaluated the stainings digitally. The absolute CD8 count was scored manually by one pathologist. The percentage of tumor cells and sTILs was assessed by pathologists trained for TIL assessment on H&E-stained slides according to an accepted international standard from the International Immuno-Oncology Biomarker Working Group (see www.tilsinbreastcancer.org for all guidelines on TIL assessment in solid tumors). CD8 staining was assessed on all intratumoral and stromal immune cells, whereas PD-L1 staining was assessed on both tumor cells and infiltrating immune cells separately. CD4 and FOXP3 were assessed as the percentage of the total stromal area by two pathologists.

DNA and RNA sequencing

DNA and RNA was isolated from freshly frozen sections of tissue biopsies containing at least 30% tumor cells, using the Qiagen AllPrep DNA/RNA/miRNA Universal Kit. Genomic DNA from peripheral blood cells was isolated using the QIASymphony DSP circulating DNA kit. For exome sequencing, DNA was fragmented to 200-300-bp fragments by Covaris shearing, after which library preparation was performed using the KAPA HTP DNA Library Kit, according to the manufacturer's instructions. Exome enrichment was performed using the IDT Human Exome V1.0 Kit according to the manufacturer's instructions. Resultant libraries were sequenced with 100-bp paired-end reads on a HiSeq2500 in high-output mode using V2 chemistry (Illumina), and median sequencing depths of 146 (range: 122-217) for tumor samples and 64.7 (range: 44.6-83.2) for germline DNA samples were obtained. Raw reads were aligned to GRCh38 using the Burrows-Wheeler Aligner (bwa), followed by marking of duplicate reads by Picard MarkDuplicates. Subsequently, base quality scores were recalibrated using GATK BaseRecalibrator, and single-nucleotide variants and indels (insertions or deletions) were called using GATK MuTect⁴⁶. Variants were filtered using MuTect TLOD and NLOD with thresholds of 40 and 10, respectively, and were required to have passed all other MuTect tests (FILTER field equals 'PASS'). Variants were subsequently annotated using SnpEff

4.3t (build 2017-110-24 10:18) and variants were classified according to their most severe effect in the case of effects on multiple transcripts. Non-synonymous, exonic mutational load in coding genes was determined by summation of coding single-nucleotide variants and indels, specifically variants annotated as one of the following classes: conservative in-frame deletion, disruptive in-frame deletion, disruptive in-frame insertion, frameshift variant, missense variant, protein-protein contact, start lost, stop gained, stop lost, stop-retained variant and structural interaction variant. Copy number aberrations, discretized to integer allele-specific copy number estimates, along with purity and ploidy estimates, were obtained using the R package Sequenza (version 2.1.2)⁴⁷ with default settings. Genomic segments were identified as having undergone loss of heterozygosity if any allele (that is, the minor allele) had a copy number estimate of 0. Candidate tumor-specific neo-epitopes were determined and annotated using an in-house epitope prediction pipeline, which uses a random forest model to score the probability of surface expression of candidate neo-epitopes based on the major prerequisites for (neo-)antigen presentation: RNA expression level (Salmon version 0.9.1)⁴⁸, proteasomal processing (NetChop version 3.1)^{49,50} and human leukocyte antigen binding (netMHCpan version 4)⁵¹. Candidate neo-epitopes that have a model prediction score lower than 0.02 are filtered out. The input variants used for the neo-epitope prediction pipeline were filtered using the default MuTect TLOD and NLOD thresholds and were required to have passed all other MuTect tests (FILTER field equals 'PASS'). Whole exome sequencing of tumor and germline DNA isolated from peripheral blood was available for 50 patients at baseline.

To obtain RNA sequencing data, strand-specific libraries were generated using the TruSeq Stranded mRNA sample preparation kit (Illumina) according to the manufacturer's instructions. The 3' end-adenylated and adapter-ligated RNA was amplified by 12 cycles of PCR. The libraries were analyzed on a 2100 Bioanalyzer using a 7500 chip (Agilent), diluted and pooled equimolar into a multiplex sequencing pool and stored at -20 °C. Resultant libraries were sequenced with 65-bp single-end reads on a HiSeq2500 in high-output mode using V4 chemistry (Illumina). Gene-specific read counts for the Ensembl version 86 build of the human transcriptome on reference genome GRCh38 were obtained by running Salmon (version 0.11.0)⁴⁸ directly on the FASTQ files using default settings, after which transcript specific read counts were collapsed to gene expression read counts using the R Bioconductor package tximport, version 1.4.0. Read counts were subsequently trimmed mean of M values (TMM)-normalized using the edgeR Bioconductor package, version 3.18.1^{52,53}. RNA sequencing data were obtained for 53 patients at baseline and 44 patients post-induction.

NanoString gene expression analysis

mRNA expression was measured with the nCounter technology, provided by NanoString Technologies. nCounter uses probes with barcodes attached to DNA oligonucleotides that directly bind to RNA. Preparation and analyses were performed according to the manufacturer's protocol using The PanCancer IO 360 gene expression panel that includes 770 genes (for research use only and not for use

in diagnostic procedures). Signatures were defined as described previously^{22,23,26}. Normalization was performed by correcting for the expression of technical controls and 30 housekeeping genes included in the panel. A PAM50 spike-in panel of 30 genes was used to determine PAM50 subtypes. nCounter gene expression data were obtained for 51 patients at baseline, 45 patients post-induction and 30 patients on nivolumab.

TCR sequencing

The ImmunoSEQ Assay (Adaptive Biotechnologies) covering the CDR3 region of the human TCR β - chain was performed on DNA isolated from baseline, post-induction and on-nivolumab tumor samples. For a subset of patients, DNA was isolated from peripheral blood mononuclear cells with the Qiagen DNeasy Blood & Tissue Kit. Extracted genomic DNA was amplified in a bias-controlled multiplex PCR, followed by high-throughput sequencing. Sequences were collapsed and filtered to identify and quantitate the absolute abundance of unique TCR- β CDR3 region for further analysis. TCR sequencing data of tumor-infiltrating T cells were obtained for 48 patients at baseline, 43 patients post-induction and 29 patients on nivolumab. TCR sequencing data of peripheral blood T cells were obtained for 20 patients at baseline, post-induction and on nivolumab. The following T cell repertoire summary statistics were extracted from the Adaptive ImmunoSeq Analyzer: clonality, number of unique clones (repertoire diversity), as estimated by the Efron-Thisted estimator⁵⁴, and T cell infiltration, as measured by the fraction of T cells over nucleated cells.

Gene Set Enrichment Analysis on RNA sequencing data

To analyze which cellular processes were most strongly affected by the four induction treatments, a GSEA⁵⁵ was performed on the 50 hallmark gene sets²⁴ and separately on 4 MDSC-associated²⁵ and CD4 T cell-associated²⁷ gene sets using the flexgsea-r R package (<https://github.com/NKI-CCB/flexgsea-r>) on the TMM-normalized read counts as detailed above. Having defined a custom gene-ranking function, genes were ranked according to the P values of a pairwise Wilcoxon rank-sum test, as implemented by the `wilcox.test()` function in R. Specifically, the following gene-ranking value was used: $r(g) = \text{sign}(FC_g)(1-P_g)$, in which the sign function returns either 1 or -1 depending on the sign of its operand, FC_g reflects the median fold change (FC) between the two compared time points and P_g represents the P value of the Wilcoxon rank-sum test. During permutation steps ($n = 1,000$), samples from both time points were assigned randomly to time point and patient combinations.

PAM50 subtyping on RNA sequencing data

PAM50 subtyping was done on TMM-normalized RNA sequencing data using the `genefu` package in R, version 2.11.2⁵⁶.

Bayesian hierarchical modelling of gene expression FCs

We noticed differences between the induction treatments in the FCs between the baseline and post-induction or on nivolumab timepoints of the 12 NanoString

gene set scores, related to inflammation and T-cell activation. Thus, we wanted to quantify to what degree induction cohorts were enriched for high or low FCs. As the gene expression scores for these gene sets were highly correlated, we first summarized them by taking the median (which we refer to as the ‘inflammation score’) per patient and time point. We then modelled the FCs in inflammation scores over time between the baseline (biopsy one) and post-induction (biopsy two) time points using a hierarchical Bayesian regression model. This model regularizes the effects ascribed to the induction treatments by partially pooling effects across induction arms, which increases inferential robustness. Specifically, the means of observed FCs for each induction treatment, μ_{arm} , were assumed to originate from a normal distribution, $N(\mu, \sigma_{arm})$, for which both the mean (μ) and the standard deviation (σ_{arm}) parameters were estimated using scaled Student’s t -distributions ($t(\text{d.f.}, m, s)$) as their priors, where d.f. denotes the degrees of freedom of the Student’s t -distributions, m represents the location of the mode and s represents the scaling to be applied to the data beforehand. We employed d.f. = 3, $m = 0$ and $s = 10$, throughout, to get weakly informative priors centered at 0. Next, the observed FCs were modelled as generated by induction arm-specific normal distributions with mean μ_{arm} and standard deviation σ_{FC} , the latter of which is shared between induction arms (variation in observed FCs within arms appeared equal). Combined, this gives the following set of expressions (as graphically represented in Extended Data Figure 8a):

$$\begin{aligned}\mu &\sim t(3, 0, 10) \\ \sigma_{arm} &\sim t(3, 0, 10) \\ \mu_{arm} &\sim N(\mu, \sigma_{arm}) \\ \mu_{FC} &= \mu_{arm} \\ \sigma_{FC} &\sim t(3, 0, 10) \\ FC &\sim N(\mu_{FC}, \sigma_{FC})\end{aligned}$$

In which μ_{FC} , the expected FC for an individual observation, equals μ_{arm} in this basic version of the model, but will shortly be augmented with additional co-variates. After fitting the model, we normalized the μ_{arm} -estimates of the induction treatments to that of the no induction cohort by computing and reporting the pairwise fold differences in μ_{arm} compared to μ_{arm} of the no induction cohort (Extended Data Figure 8b). Obtained results were robust to varying d.f. for both σ_{arm} and σ_{FC} between 1 and 6 (data not shown).

As we noticed the inflammation score at baseline (S_{BL}) to negatively associate with the observed inflammation score FCs (Extended Data Figure 8c), we also investigated an extension of this model in which S_{BL} influences the observed FC in a global, arm-unspecific manner by augmenting μ_{FC} :

$$\begin{aligned}b &\sim t(3, 0, 10) \\ \mu_{FC} &= \mu_{arm} + b S_{BL}\end{aligned}$$

where all statistical definitions of the previous model, except for the superseded μ_{FC} , still apply. Second, we tested whether describing the effect of having a clinical

response to nivolumab would abrogate the intercohort differences, as we did observe higher FCs in responding patients when comparing on-nivolumab (biopsy three) and baseline (biopsy one) time points, which is not surprising considering the way these gene sets were selected (Figure 3g). Similarly to the previous expansion of μ_{FC} with $b S_{BL}$, we thus augmented μ_{FC} with rR , in which r describes the effect attributed to having a clinical response (modeled as $r \sim t(3, 0, 10)$) and R is an indicator variable for clinical response to nivolumab (Extended Data Figure 8d). Third, we were interested in testing whether having previous treatment for metastatic disease before enrollment in the TONIC trial affected the observed upregulation. This was motivated by the fact that we observed a trend towards a higher clinical response rate in patients with no previous lines of treatment than in patients with one or more lines of previous treatment (Extended Data Figure 5c). Thus, we further expanded the expression for μ_{FC} with lL , in which l describes the effect attributed to having multiple treatment lines (prioritized as $l \sim t(3, 0, 10)$) and L is an indicator variable representing whether palliative treatment was administered (Extended Data Figure 8e). Finally, we also tested the relationship between having metastases restricted to the lymph nodes as opposed to other organs (Extended Data Figure 8f), expanding the expression for μ_{FC} with nN , in which n describes the effect attributed to having metastases restricted to lymph nodes (prioritized as $n \sim t(3, 0, 10)$) and N is an indicator variable for having lymph node-restricted metastases.

Testing various combinations of the four extra covariates described in the previous paragraph revealed that the inclusion of extra covariates minimally influenced the coefficients assigned to other covariates (Extended Data Figure 8h). The exception to this is r , which was reduced by about fourfold with the inclusion of other covariates. The full model, including all of the extra covariates, shows that the baseline inflammation score (S_{BL}) and lymph node-restricted metastases were most strongly associated with FCs in the inflammation score, besides the differential FCs apparently induced by the tested induction treatments.

These models were evaluated using the probabilistic programming language Stan⁵⁷, interfaced in R using the R package rstan (version 2.17.3). Ten chains of no-U-turn-sampler Markov chain Monte Carlo (MCMC) simulations were run for 100,000 iterations, of which 25,000 served as warm-up iterations. Sampling convergence was sufficient for all models as Rhat values were all 1. Inter-arm comparisons between μ_{arm} and $\mu_{arm'}$ were performed by extracting parameter values from non-warm-up MCMC iterations (using `rstan::extract`) for both arms and computing the proportion of iterations for which μ_{arm} equaled or exceeded $\mu_{arm'}$. The stan program is available on request.

BRCA1-like classification based on copy number profiles

A *BRCA1* classifier originally had been trained using the nearest shrunken centroids algorithm on bacterial artificial chromosome (BAC) array comparative genomic hybridization data⁵⁸. Data from platforms of higher resolution can be used to obtain reliable *BRCA1*-like classification⁵⁹. In this study, GC-content-corrected allele

imbalance log ratios, to be used for downstream copy number estimates, were obtained from whole-exome sequencing data using the Sequenza R package⁴⁷. To apply the *BRCA1*-like classifier, these estimates had to be preprocessed to comply with the format of the original training set. LiftOver was used to map the genomic locations from GRCh38 to hg19, the reference genome on which the *BRCA1*-like classifier was validated. Average log ratios for each of the original 3,277 BAC-array segments were computed by averaging the binned log ratios within 500 kb upstream and downstream of the central genomic position of the BAC clone. Missing values due to a lack of coverage were subsequently replaced using linear interpolation between adjacent features on the same chromosome. On average, 487 probes were estimated per sample, of which on average 372 had directly surrounding probes available for interpolation. The mean and maximum genomic distances between estimated and nearest measured segments were 2 Mb (2 segments) and 7 Mb (7 segments), respectively. The distribution of resulting whole-exome sequencing (WES)-derived segment log ratios differed in the mean from that of previously obtained BAC-derived segment log ratios of patients with TNBC⁶⁰. To correct the WES segments, we first fitted a linear model (iteratively reweighted least squares) between the sorted segment-wise averages of the WES and BAC segments. The WES data were then corrected using the following expression $f_c = \alpha + \beta f_o$, in which f_o and f_c represent the original and corrected segments, respectively, and α (0.16) and β (0.97) represent the fitted parameters. This yielded highly similar distributions between the newly obtained WES-derived and original BAC-derived log ratio estimates (Pearson's $r^2 = 0.96$), but the former remained slightly right skewed. Finally, the WES data were classified with the established nearest shrunken centroid classifier, using a previously established value of at least 0.63 to be classified as *BRCA1*-like (as used in earlier work⁶⁰; <http://ccb.nki.nl/software/nkibrca/>).

Reporting summary

Further information on research design is available in the Nature Research Reporting Summary linked to this article.

Data availability

DNA and RNA sequencing data have been deposited in the European Genome-phenome Archive (EGA) under accession number EGAS0001003535 and will be made available from the corresponding author on reasonable request. Data requests will be reviewed by the institutional review board of the NKI and applying researchers will need to sign a data access agreement with the NKI after approval. The TCR sequencing data are available from Adaptive Biotechnologies, but restrictions apply to their availability. However, data are available from the corresponding author on reasonable request and with permission of Adaptive Biotechnologies.

Acknowledgements

We thank the patients and their families for participating in the study. We thank J. Foekema, M. Holtkamp, M. Delfos, J. van Zyl-de Jong and K. Kersten for their support in the care for patients. We thank S. Vanhoutvin for legal support. We thank the Core Facility of Molecular Pathology & Biobanking for their support in processing of samples. In addition, we acknowledge the Genomics Core Facility for their support regarding sequencing. We acknowledge J. Lips from Adaptive Biotechnologies for his support. We thank the scientific administration department, in particular L. Ruiters, for data management/monitoring. The Clinical Chemistry Department is thanked for their support in blood withdrawals. We thank H. Garner, M. van der Heijden and J. Stouthard for critical reading of the manuscript. We acknowledge D. Cullen, A. Evans, D. Zardavas and D. Feltquate of Bristol-Myers Squibb (BMS) for scientific input. We thank BMS/II-ON and the Dutch Cancer Society (NKI2015-7710, 10653 ALPE) for funding the study and a fellowship to M.K. (NKI2015-7542). Pink Ribbon (NKI2016-8214), the Breast Cancer Research Foundation (BCRF-17-188) and BMS/II-ON are thanked for the funding of the translational research. R.S. is supported by a grant from the Breast Cancer Research Foundation (BCRF-17-194).

Author contributions

L.V. coordinated trial procedures, analyzed and interpreted clinical and translational data and wrote the manuscript with M.S., T.N.S., C.U.B. and M.K. M.S. performed and interpreted the bioinformatic analyses. H.M.H., K.K.v.d.V. and R.S. performed the histological scoring. K.S. performed the statistical analysis on the clinical data. M.d.M. was responsible for DNA and RNA isolations. I.N. provided input during work discussions. R.J.C.K. processed the raw DNA and RNA sequencing data. S. Warren and S. Ong were responsible for the NanoString nCounter assay experiments and analyses. T.G.W. and N.S.R. were responsible for initial screening and the patients treated with irradiation. F.L. revised the CT scans. P.C.S. adapted the *BRCA1*-like classifier and applied it to our data set. N.A.M.B. and L.V. performed and analyzed the cytokine assays. S.L.C.K. performed the prediction of neo-epitopes. D.P. was responsible for the double staining of CD4 and FOXP3. C.A.H.L. performed the majority of biopsies and assessment of the CT scans. E.v.W. and H.v.T. were involved in the statistical design. I.A.M.M. was the clinical projects manager involved in the trial. I.K. and S. Onderwater. were responsible for patient care. M.C., S. Wilgenhof, G.S.S., S.C.L. and M.K. included patients in the trial and were responsible for patient care. J.B.A.G.H. advised on the trial design. K.E.d.V. gave critical input and supervised the cytokine assays. L.F.A.W. supervised the bioinformatics analyses. G.S.S., S.C.L., C.U.B., T.N.S. and M.K. designed the trial. C.U.B., T.N.S. and M.K. made the experimental plan of investigation. All authors edited and approved the manuscript.

Competing interests

L.V., M.S., H.M.H., K.S., K.K.v.d.V., M.d.M., I.N., R.J.C.K., T.G.W., N.S.R., F.L., N.A.M.B., S.L.C.K., D.P., C.A.H.L., E.v.W., H.v.T., I.A.M.M., I.K., S. Onderwater and S. Wilgenhof declare no competing interests. S.Warren reports employment and stockholdership of NanoString Technologies, an advisory role for Roche and being a former employee of Oncofactor Corp., outside the submitted work. S. Ong reports employment and stockholdership of NanoString Technologies. P.C.S. has a close relative employed by AstraZeneca. M.C. reports funding to the institute from BMS and Roche/Genentech, outside the submitted work. J.B.A.G.H. reports financial compensation to the NKI for advisory roles from Amgen, AZ, BMS, Bayer, MSD, Celsius Therapeutics, Gadeta, Immunocore, Seattle Genetics, Merck Serono, Sanofi, Roche, Neon therapeutics, Pfizer and Ipsen and NKI, and received grants from BMS, MSD, Novartis and Neon therapeutics, outside the submitted work. R.S. reports research funding from Merck, Roche and Puma, as well as travel funds from AstraZeneca, Roche, Merck and an advisory role for BMS, outside the scope of this work. K.E.d.V. reports research funding from Roche, outside the scope of this work. G.S.S. reports funding to the institute from AstraZeneca, Merck Sharp & Dohme, Novartis and Roche, outside the submitted work. L.F.A.W. reports receiving a commercial research grant from Genmab. S.C.L. reports funding to the institute from Agendia, Amgen, AstraZeneca, BMS, Eurocept, Roche/Genentech, Tesaro and an advisory role for AstraZeneca, Bayer and IBM, outside the submitted work. T.N.S. is a consultant for Adaptive Biotechnologies, AIMM Therapeutics, Allogene Therapeutics, Amgen, Merus, Neon Therapeutics, Scenic Biotech; received grant or research support from Merck, BMS and Merck KGaA; is a stockholder in AIMM Therapeutics, Allogene Therapeutics, Neon Therapeutics and Neogene Therapeutics, all outside the submitted work. C.U.B. reports personal fees for advisory roles for MSD, BMS, Roche, GSK, Novartis, Pfizer, Lilly, Pierre Fabre and GenMab and grants from BMS, Novartis and NanoString, outside the submitted work. M.K. reports funding and a speaker's fee to the institute from BMS and Roche and an unpaid advisory role for BMS, outside the submitted work.

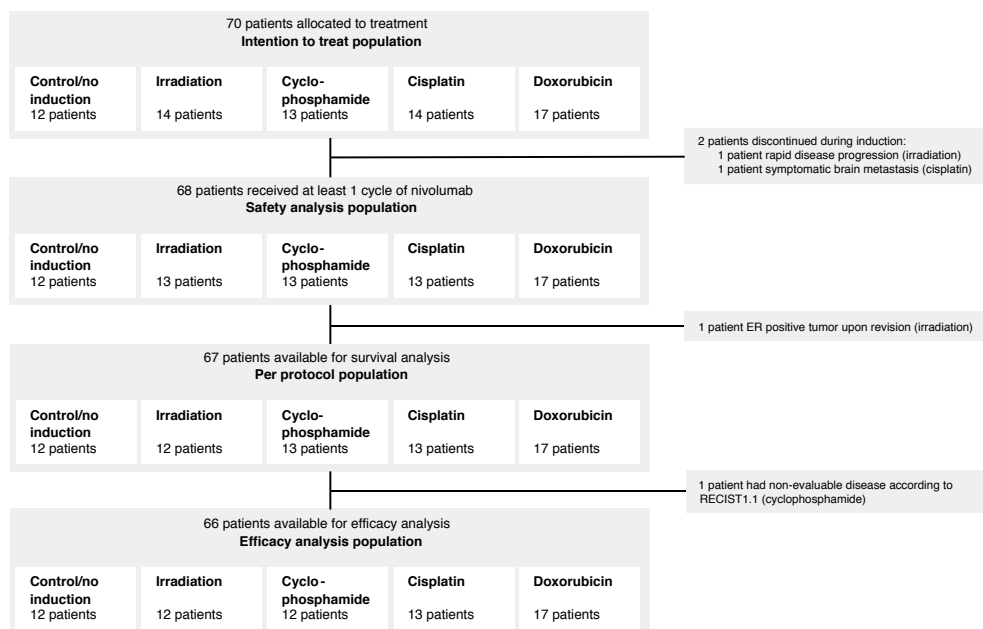
References

1. Adams, S., et al. Pembrolizumab Monotherapy for Previously Treated Metastatic Triple-Negative Breast Cancer: Cohort A of the Phase 2 KEYNOTE-086 Study. *Annals of Oncology*, mdy517 (2018).
2. Nanda, R., et al. Pembrolizumab in Patients With Advanced Triple-Negative Breast Cancer: Phase Ib KEYNOTE-012 Study. *Journal of Clinical Oncology* 34, 2460-2467 (2016).
3. Emens, L.A., et al. Long-term Clinical Outcomes and Biomarker Analyses of Atezolizumab Therapy for Patients With Metastatic Triple-Negative Breast Cancer: A Phase 1 Study. *JAMA oncology* 5, 74-82 (2018).
4. Dirix, L.Y., et al. Avelumab, an anti-PD-L1 antibody, in patients with locally advanced or metastatic breast cancer: a phase 1b JAVELIN Solid Tumor study. *Breast cancer research and treatment* 167, 671-686 (2018).
5. Schmid, P., et al. Atezolizumab and Nab-Paclitaxel in Advanced Triple-Negative Breast Cancer. *The New England Journal of Medicine* 380, 987-988 (2018).
6. Demaria, S., et al. Ionizing radiation inhibition of distant untreated tumors (abscopal effect) is immune mediated. *International Journal of Radiation Oncology*Biophysics* 58, 862-870 (2004).
7. Vanpouille-Box, C., et al. DNA exonuclease Trex1 regulates radiotherapy-induced tumour immunogenicity. *Nature communications* 8, 15618 (2017).
8. Scurr, M., et al. Low-Dose Cyclophosphamide Induces Antitumor T-Cell Responses, which Associate with Survival in Metastatic Colorectal Cancer. *Clinical cancer research* 23, 6771-6780 (2017).
9. de Biasi, A.R., Villena-Vargas, J. & Adusumilli, P.S. Cisplatin-induced antitumor immunomodulation: a review of preclinical and clinical evidence. *Clinical cancer research* 20, 5384-5391 (2014).
10. Wan, S., et al. Chemotherapeutics and radiation stimulate MHC class I expression through elevated interferon-beta signaling in breast cancer cells. *PLoS one* 7, e32542 (2012).
11. Alizadeh, D., et al. Doxorubicin eliminates myeloid-derived suppressor cells and enhances the efficacy of adoptive T-cell transfer in breast cancer. *Cancer Research* 74, 104-118 (2014).
12. Sistigu, A., et al. Cancer cell-autonomous contribution of type I interferon signaling to the efficacy of chemotherapy. *Nature medicine* 20, 1301-1309 (2014).
13. Casares, N., et al. Caspase-dependent immunogenicity of doxorubicin-induced tumor cell death. *The Journal of experimental medicine* 202, 1691-1701 (2005).
14. Seymour, L., et al. iRECIST: guidelines for response criteria for use in trials testing immunotherapeutics. *The Lancet Oncology* 18, e143-e152 (2017).
15. O'Brien, K.M., et al. Intrinsic breast tumor subtypes, race, and long-term survival in the Carolina Breast Cancer Study. *Clinical cancer research* 16, 6100-6110 (2010).
16. den Brok, W.D., et al. Survival with metastatic breast cancer based on initial presentation, *de novo* versus relapsed. *Breast cancer research and treatment* 161, 549-556 (2017).
17. Kassam, F., et al. Survival outcomes for patients with metastatic triple-negative breast cancer: implications for clinical practice and trial design. *Clinical breast cancer* 9, 29-33 (2009).
18. Adams, S., et al. Title: Pembrolizumab Monotherapy for Previously Untreated, PD-L1-Positive, Metastatic Triple-Negative Breast Cancer: Cohort B of the Phase 2 KEYNOTE-086 Study. *Annals of Oncology* mdy518 (2018).
19. Simon, R. Optimal two-stage designs for phase II clinical trials. *Controlled clinical trials* 10, 1-10 (1989).
20. Kok, M., et al. Profound Immunotherapy Response in Mismatch Repair-Deficient Breast Cancer. *JCO Precision Oncology* 1, 1-3 (2017).
21. Sørlie, T., et al. Gene expression patterns of breast carcinomas distinguish tumor subclasses with clinical implications. *Proceedings of the National Academy of Sciences of the United States of America* 98, 10869-10874 (2001).
22. Ayers, M., et al. IFN-gamma-related mRNA profile predicts clinical response to PD-1 blockade. *Journal of Clinical Investigation* 127, 2930-2940 (2017).
23. Danaher, P., et al. Gene expression markers of Tumor Infiltrating Leukocytes. *Journal for immunotherapy of cancer* 5, 18 (2017).
24. Liberzon, A., et al. The Molecular Signatures Database (MSigDB) hallmark gene set collection. *Cell systems* 1, 417-425 (2015).
25. Bezzi, M., et al. Diverse genetic-driven immune landscapes dictate tumor progression through distinct mechanisms. *Nature medicine* 24, 165-175 (2018).

26. DanaHER, P., Warren, S. & Cesano, A. Development of gene expression signatures characterizing the tumor-immune interaction. *Journal of Clinical Oncology* 36, 205 (2018).
27. Gu-Trantien, C., et al. CD4+ follicular helper T cell infiltration predicts breast cancer survival. *Journal of Clinical Investigation* 123, 2873-2892 (2013).
28. Adams, S., Diamond, J.R., Hamilton, E. & et al. Atezolizumab plus nab-paclitaxel in the treatment of metastatic triple-negative breast cancer with 2-year survival follow-up: A phase 1b clinical trial. *JAMA oncology* 5, 334-342 (2019).
29. Loibl, S., et al. Randomized phase II neoadjuvant study (GeparNuevo) to investigate the addition of durvalumab to a taxane-anthracycline containing chemotherapy in triple negative breast cancer (TNBC). *Journal of Clinical Oncology* 36, 104 (2018).
30. Blank, C.U., et al. Neoadjuvant versus adjuvant ipilimumab plus nivolumab in macroscopic stage III melanoma. *Nature medicine* 24, 1655-1661 (2018).
31. Forde, P.M., et al. Neoadjuvant PD-1 Blockade in Resectable Lung Cancer. *The New England Journal of Medicine* 378, 1976-1986 (2018).
32. Rizvi, N.A., et al. Mutational landscape determines sensitivity to PD-1 blockade in non-small cell lung cancer. *Science* 348, 124-128 (2015).
33. Van Allen, E.M., et al. Genomic correlates of response to CTLA-4 blockade in metastatic melanoma. *Science* 350, 207-211 (2015).
34. Samstein, R.M., et al. Tumor mutational load predicts survival after immunotherapy across multiple cancer types. *Nature genetics* 51, 202-206 (2019).
35. Molinero, L., et al. Abstract SABCS 2017 P2-09-13: Molecular characterization of tumors from metastatic TNBC patients treated with atezolizumab (atezo). 78, P2-09-13 (2018).
36. Davoli, T., Uno, H., Wooten, E.C. & Elledge, S.J. Tumor aneuploidy correlates with markers of immune evasion and with reduced response to immunotherapy. *Science* 355 eaaf8399 (2017).
37. Roh, W., et al. Integrated molecular analysis of tumor biopsies on sequential CTLA-4 and PD-1 blockade reveals markers of response and resistance. *Science translational medicine* 9 eaah3560 (2017).
38. Rimm, D.L., et al. A Prospective, Multi-institutional, Pathologist-Based Assessment of 4 Immunohistochemistry Assays for PD-L1 Expression in Non-Small Cell Lung Cancer. *JAMA oncology* 3, 1051-1058 (2017).
39. Zavalishina, L., et al. RUSSCO-RSP comparative study of immunohistochemistry diagnostic assays for PD-L1 expression in urothelial bladder cancer. *Virchows Archiv* 473, 719-724 (2018).
40. Eisenhauer, E.A., et al. New response evaluation criteria in solid tumours: revised RECIST guideline (version 1.1). *European journal of cancer* 45, 228-247 (2009).
41. Baselga, J., et al. Randomized phase II study of the anti-epidermal growth factor receptor monoclonal antibody cetuximab with cisplatin versus cisplatin alone in patients with metastatic triple-negative breast cancer. *Journal of Clinical Oncology* 31, 2586-2592 (2013).
42. Singh, J., et al. Phase 2 trial of everolimus and carboplatin combination in patients with triple negative metastatic breast cancer. *Breast cancer research* 16, R32 (2014).
43. O'Shaughnessy, J., et al. Iniparib plus chemotherapy in metastatic triple-negative breast cancer. *The New England Journal of Medicine* 364, 205-214 (2011).
44. Carey, L.A., et al. TBCRC 001: randomized phase II study of cetuximab in combination with carboplatin in stage IV triple-negative breast cancer. *Journal of Clinical Oncology* 30, 2615-2623 (2012).
45. R Core Team R: a language and environment for statistical computing v3.3.2 (2018).
46. Cibulskis, K., et al. Sensitive detection of somatic point mutations in impure and heterogeneous cancer samples. *Nature Biotechnology* 31, 213-219 (2013).
47. Favero, F., et al. Sequenza: allele-specific copy number and mutation profiles from tumor sequencing data. *Annals of Oncology* 26, 64-70 (2015).
48. Love, M.I., Hogenesch, J.B. & Irizarry, R.A. Modeling of RNA-seq fragment sequence bias reduces systematic errors in transcript abundance estimation. *Nature Biotechnology* 34, 1287-1291 (2016).
49. Nielsen, M., Lundegaard, C., Lund, O. & Kesmir, C. The role of the proteasome in generating cytotoxic T-cell epitopes: insights obtained from improved predictions of proteasomal cleavage. *Immunogenetics* 57, 33-41 (2005).
50. Kesmir, C., Nussbaum, A.K., Schild, H., Detours, V. & Brunak, S. Prediction of proteasome cleavage motifs by neural networks. *Protein engineering* 15, 287-296 (2002).

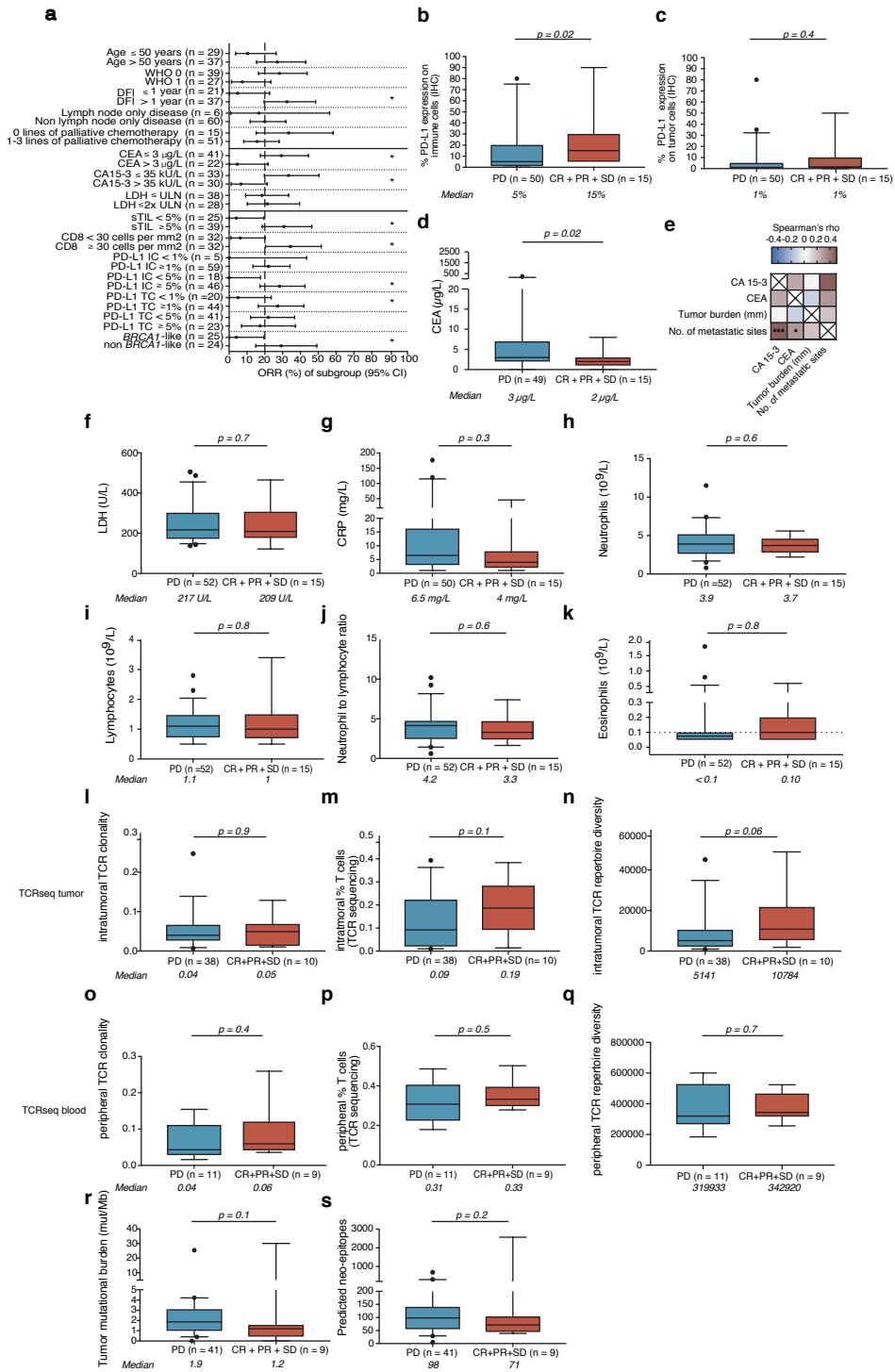
51. Jurtz, V., et al. NetMHCpan-4.0: Improved Peptide-MHC Class I Interaction Predictions Integrating Eluted Ligand and Peptide Binding Affinity Data. *Journal of immunology* 199, 3360-3368 (2017).
52. Robinson, M.D., McCarthy, D.J. & Smyth, G.K. edgeR: a Bioconductor package for differential expression analysis of digital gene expression data. *Bioinformatics* 26, 139-140 (2010).
53. McCarthy, D.J., Chen, Y. & Smyth, G.K. Differential expression analysis of multifactor RNA-Seq experiments with respect to biological variation. *Nucleic acids research* 40, 4288-4297 (2012).
54. Efron, B. & Thisted, R. Estimating the number of unseen species: How many words did Shakespeare know? *Biometrika* 63, 435-447 (1976).
55. Subramanian, A., et al. Gene set enrichment analysis: a knowledge-based approach for interpreting genome-wide expression profiles. *Proc. Natl Acad. Sci. USA* 102, 15545-15550 (2005).
56. Gendoo, D.M., et al. Genefu: an R/Bioconductor package for computation of gene expression-based signatures in breast cancer. *Bioinformatics* 32, 1097-1099 (2016).
57. Carpenter, B., et al. Stan: A Probabilistic Programming Language. *J. Stat. Softw* 76, 1-32 (2017).
58. Joosse, S.A., et al. Prediction of BRCA1-association in hereditary non-BRCA1/2 breast carcinomas with array-CGH. *Breast cancer research and treatment* 116, 479-489 (2009).
59. Schouten, P.C., et al. Robust BRCA1-like classification of copy number profiles of samples repeated across different datasets and platforms. *Molecular oncology* 9, 1274-1286 (2015).
60. Vollebergh, M.A., et al. An aCGH classifier derived from BRCA1-mutated breast cancer and benefit of high-dose platinum-based chemotherapy in HER2-negative breast cancer patients. *Annals of Oncology* 22, 1561-1570 (2011).

Extended data figures

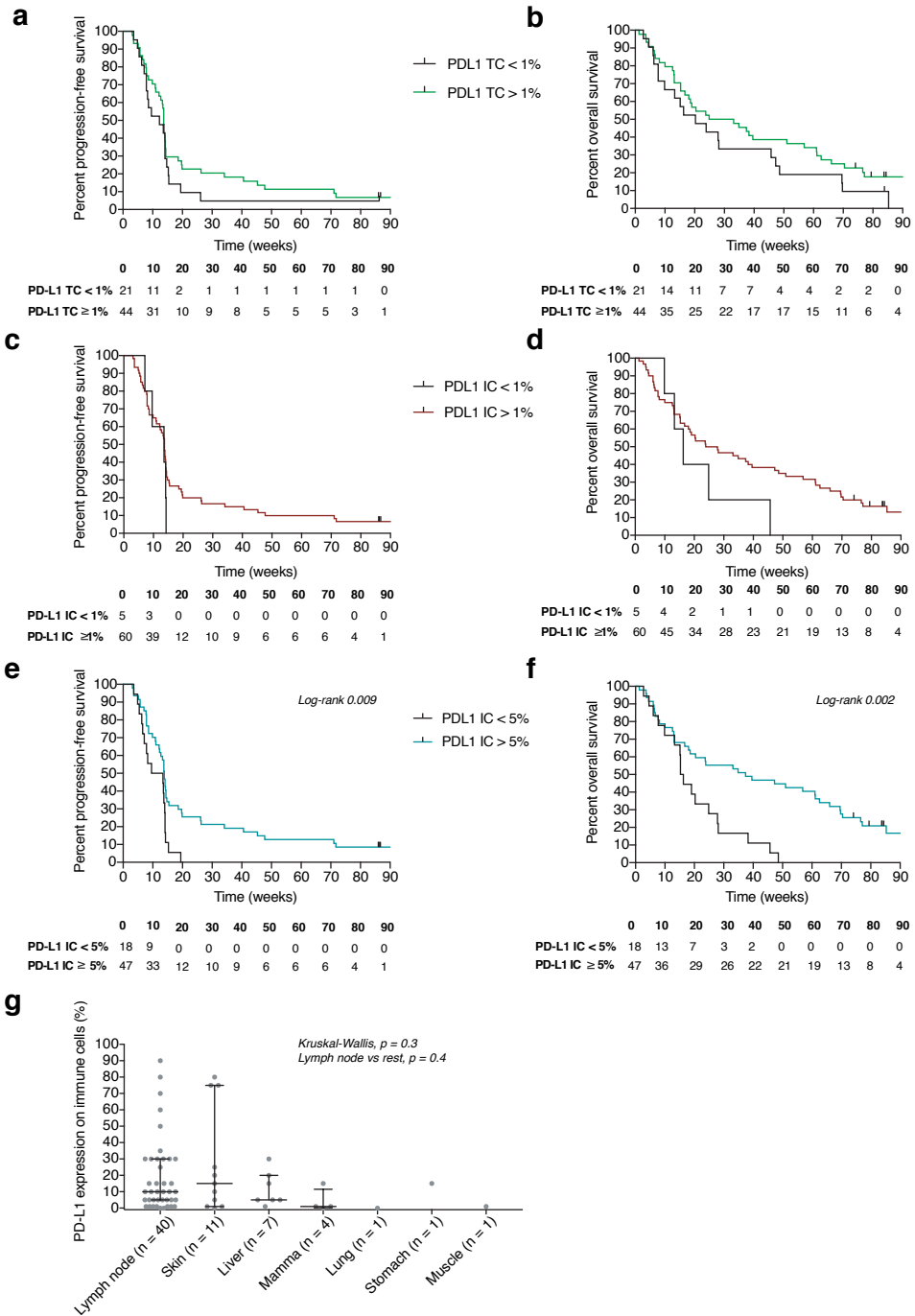


Extended Data Figure 1. CONSORT diagram. Flowchart for the allocation of subjects enrolled in the trial.

Extended Data Figure 2 (opposite). Clinical and other baseline parameters associated with response. Boxplots represent the median, 25th and 75th percentiles and the vertical bars span the 5th and 95th percentiles. Statistical significance was tested with a two-tailed Mann-Whitney *U*-test (unadjusted *P* values). Boxplots represent the median, 25th and 75th percentiles and the vertical bars span the 5th and 95th percentiles. Statistical significance was tested with a two-tailed Mann-Whitney *U*-test (unadjusted *P* values). (a) ORR per subgroup. Depicted is the ORR (CR + PR of $n = 66$) per subgroup. Cut-offs are set at the median for carcinoembryonic antigen (CEA), CA 15-3, sTIL and CD8. Statistical significance was determined by a two-sided Fisher's exact test. * $P < 0.05$. WHO, WHO performance status. †Patients with de novo metastatic disease at diagnosis were excluded ($n = 8$). (b) PD-L1 expression on immune cells. (c) PD-L1 expression on tumor cells. (d) Serum levels of CEA. (e) Correlation of CA 15-3 and CEA with tumor burden and the number of metastatic sites. Spearman correlation coefficients are depicted. Tumor burden was measured as the sum of all target lesions in millimeters; * $P < 0.05$; *** $P < 0.001$. (f) LDH levels. (g) C-reactive protein (CRP) levels. (h) Neutrophil counts. (i) Lymphocyte counts. (j) Neutrophil-to-lymphocyte ratio (NLR). (k) Eosinophil counts. The dashed line indicates the detection limit. (l) Intratumoral TCR clonality. (m) Percentage of intratumoral T cells by TCR sequencing. (n) Intratumoral TCR repertoire diversity. (o) TCR clonality in the peripheral blood. (p) Percentage of T cells by TCR sequencing in the peripheral blood. (q) TCR repertoire diversity in the peripheral blood. (r) Non-synonymous tumor mutational burden (TMB). (s) Predicted neo-epitopes.

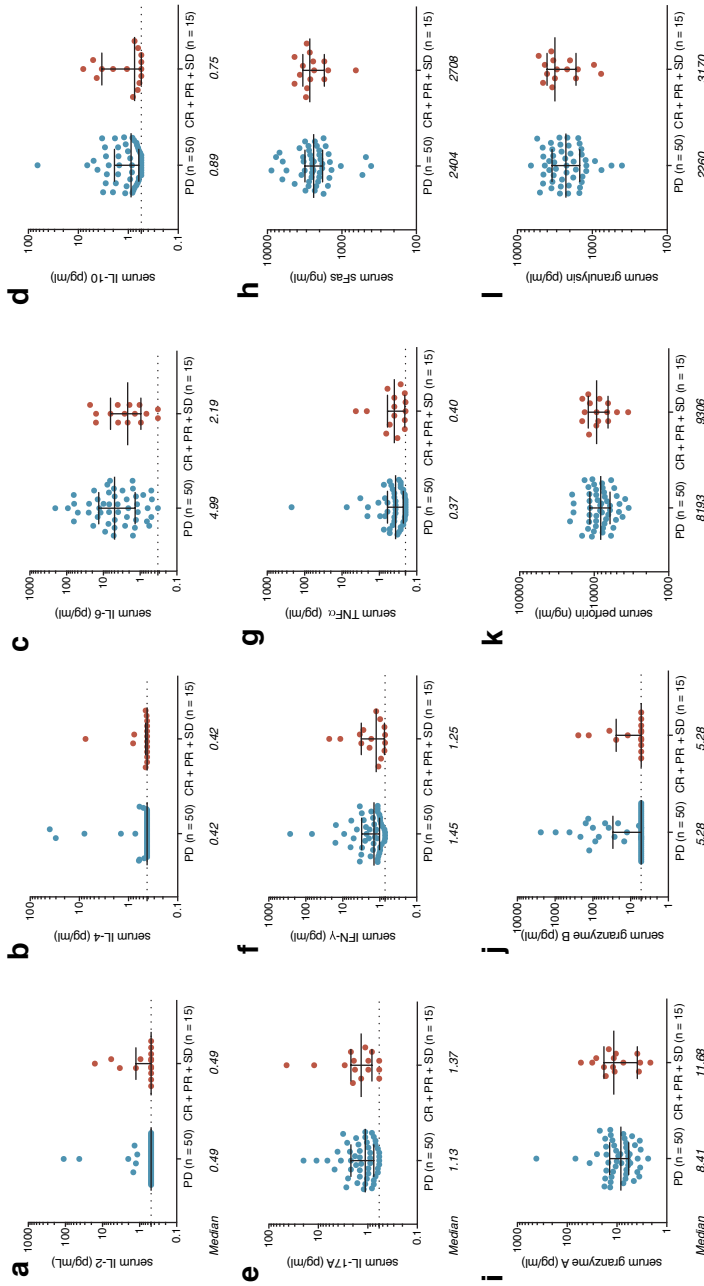


Extended Data Figure 2. Clinical and other baseline parameters associated with response.

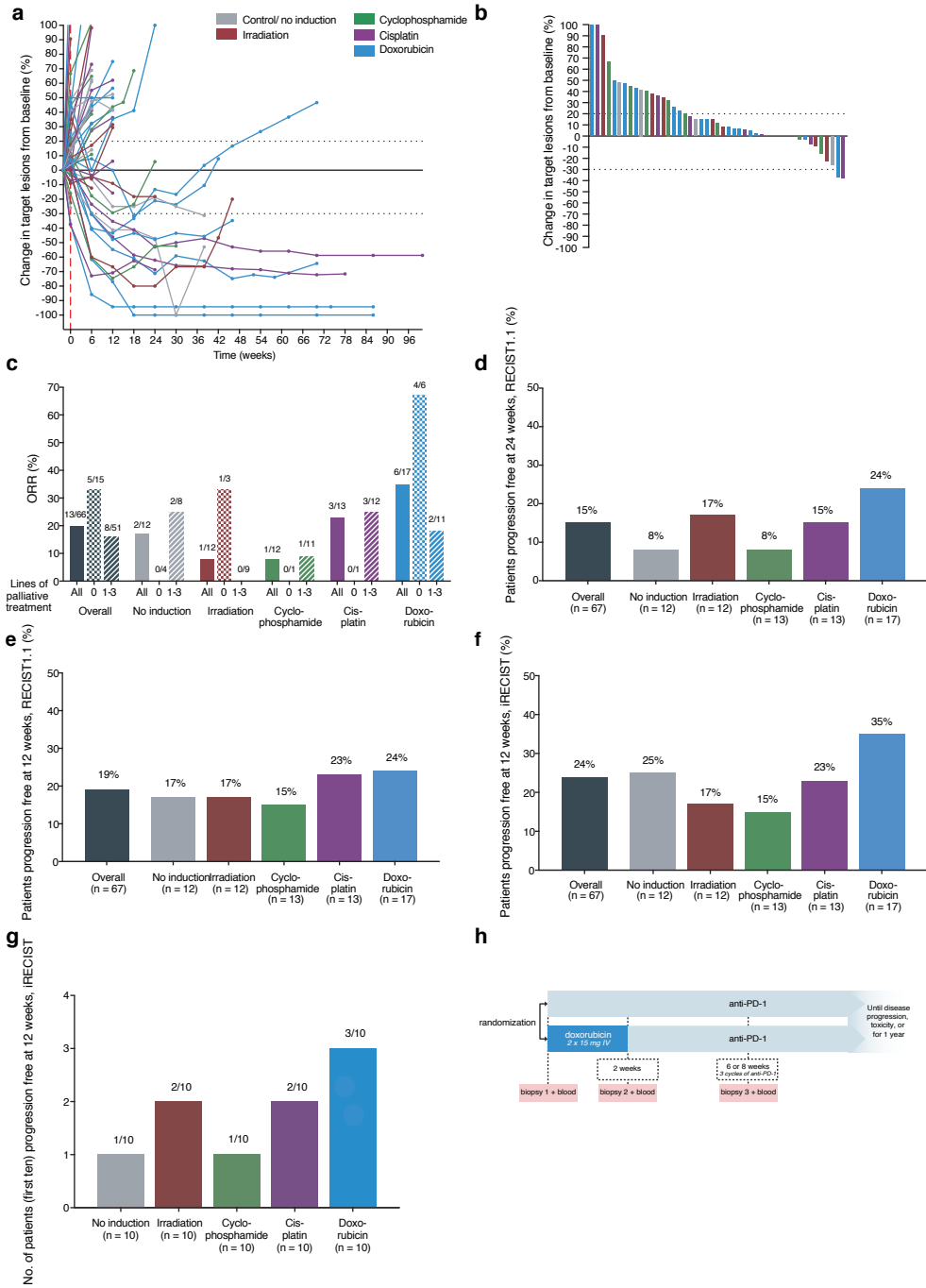


Extended Data Figure 3. Baseline PD-L1 expression.

Extended Data Figure 3 (opposite). Baseline PD-L1 expression. (a) PFS and PD-L1 expression on tumor cells. The Kaplan-Meier curve displays the proportion of patients free of progression, stratified by PD-L1 expression on tumor cells. A cut-off of 1% is used. The table lists the number of patients at risk. (b) Overall survival and PD-L1 expression on tumor cells. The Kaplan-Meier curve displays overall survival, stratified by PD-L1 expression on tumor cells. A cut-off of 1% is used. (c) PFS and PD-L1 expression on tumor-infiltrating immune cells. The Kaplan-Meier curve displays the proportion of patients free of progression, stratified by PD-L1 expression on tumor-infiltrating immune cells. A cut-off of 1% is used. (d) Overall survival and PD-L1 expression on tumor-infiltrating immune cells. The Kaplan-Meier curve displays overall survival, stratified by PD-L1 expression on tumor-infiltrating immune cells. A cut-off of 1% is used. (e) PFS and PD-L1 expression on tumor-infiltrating immune cells. The Kaplan-Meier curve displays the proportion of patients free of progression, stratified by PD-L1 expression on tumor-infiltrating immune cells. A cut-off of 5% is used. (f) Overall survival and PD-L1 expression on tumor-infiltrating immune cells. The Kaplan-Meier curve displays overall survival, stratified by PD-L1 expression on tumor-infiltrating immune cells. A cut-off of 5% is used. (g) PD-L1 expression on tumor-infiltrating immune cells and site of metastasis. PD-L1 expression per biopsy site at baseline is shown. Dots reflect the medians and whiskers reflect the interquartile ranges. IC, tumor-infiltrating immune cells; TC, tumor cells.

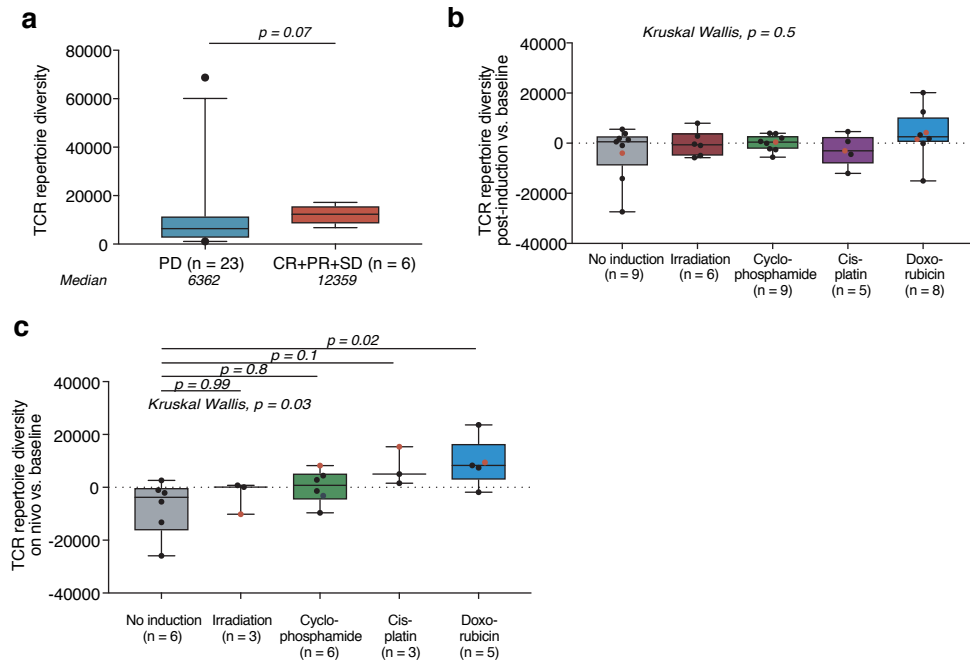


Extended Data Figure 4. Baseline serum cytokine levels. Cytokine levels were determined by a validated bead-based assay. Dots and whiskers represent medians and interquartile ranges, respectively. The dashed lines indicate the detection limit. (a) IL-2 levels were detectable in 5 patients with clinical benefit and 11 patients with progressive disease. (b) IL-4 levels were detectable in 5 patients with clinical benefit and 11 patients with progressive disease. (c) IL-6 levels were detectable in 13 patients with clinical benefit and 49 patients with progressive disease. (d) IL-10 levels were detectable in 11 patients with clinical benefit and 41 patients with progressive disease. (e) IL-17A levels were detectable in 12 patients with clinical benefit and 46 patients with progressive disease. (f) IFN- γ levels were detectable in 13 patients with clinical benefit and 47 patients with progressive disease. (g) TNF- α levels were detectable in 11 patients with clinical benefit and 45 patients with progressive disease. (h) Soluble Fas (sFas) levels were detectable in all tested patients. (i) Granzyme A levels. Granzyme A levels were detectable in all tested patients. (j) Granzyme B levels were detectable in 5 patients with clinical benefit and 17 patients with progressive disease. (k) Perforin levels. Perforin levels were detectable in all tested patients. (l) Granulysin levels. Granulysin levels were detectable in all tested patients.

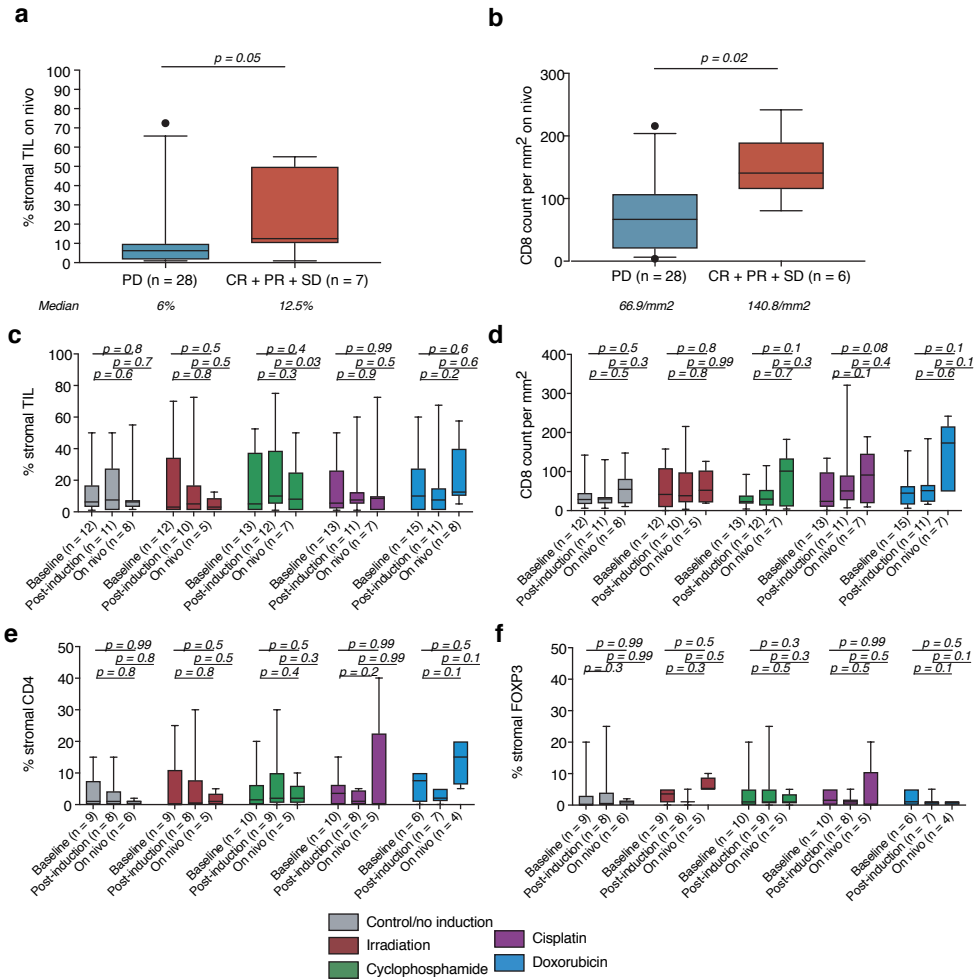


Extended Data Figure 5. Anti-tumor activity of nivolumab. (a) Changes in target lesions over time, reflecting the depth and duration of response. Every line represents one patient, and every dot is one time point. The colors reflect induction treatment. The y axis was cut-off at 100% for illustration purposes. Dotted black lines indicate the response as described by RECIST1.1. (b) Waterfall plot depicting the change in target lesions from baseline to post-induction. Every bar represents one patient and the colors correspond to induction treatment. The y axis was cut-off at 100%

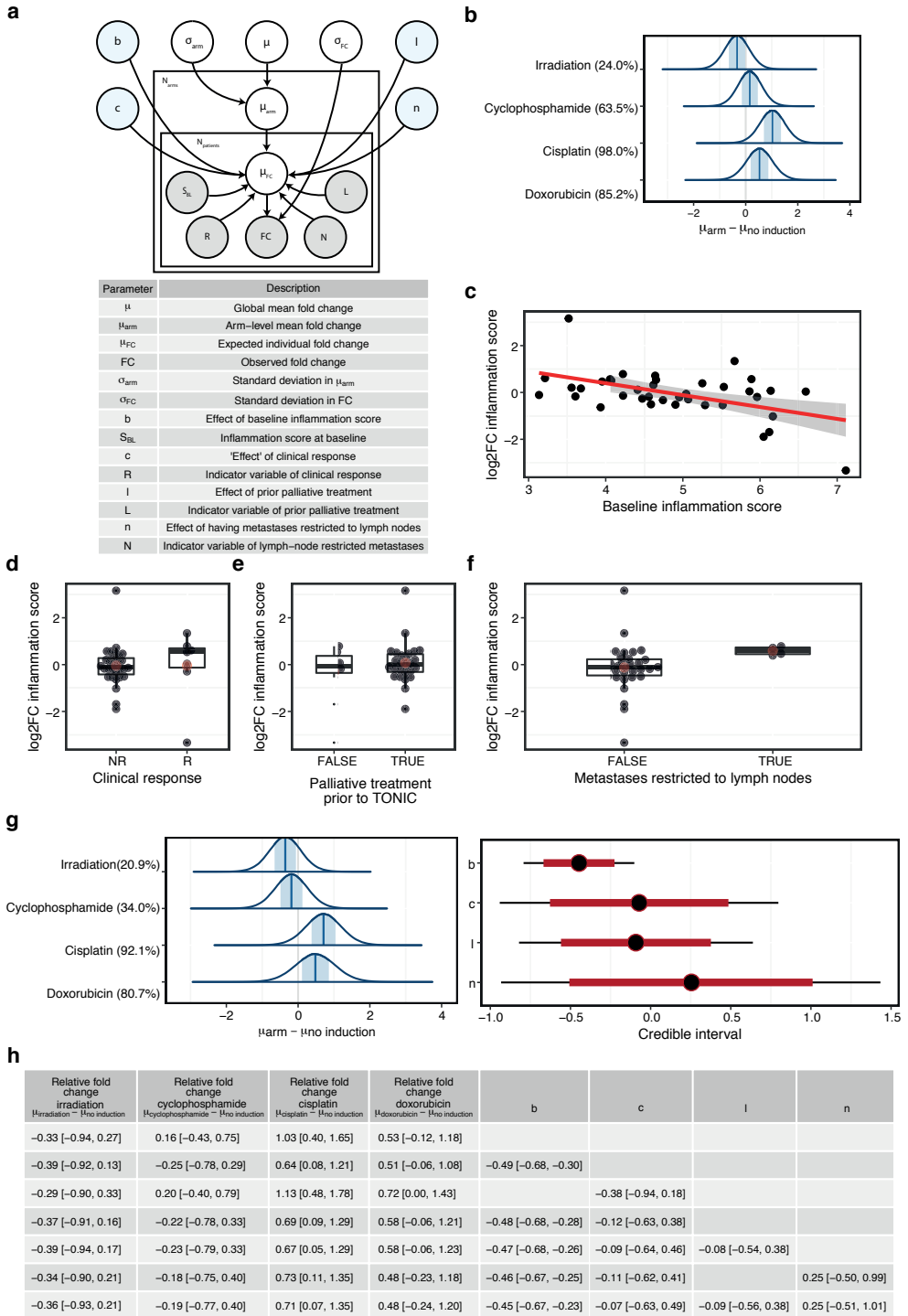
for illustration purposes. Dotted black lines indicate the response as described by RECIST1.1. (c) ORR per cohort and according to lines of palliative treatment. The bars with no pattern depict the overall response rate in all patients, the bars with a dotted pattern depict the overall response rate in first-line-treated patients and the bars with a lined pattern depict the overall response rate in the second-to-fourth-line-treated patients. The numbers above the bars reflect the number of responding patients (CR + PR) over the total number of patients in that subgroup. (d) Proportion of patients free of progression at 24 weeks. Measured from randomization according to RECIST1.1 (primary end point). (e) Proportion of patients free of progression at 12 weeks. Measured from nivolumab initiation (including response evaluation performed at 14 weeks from randomization) according to RECIST1.1. (f) Proportion of patients free of progression at 12 weeks. Measured from nivolumab initiation (including response evaluation performed at 14 weeks from randomization) according to iRECIST. (g) Number of patients free of progression at 12 weeks in the first 10 included patients. Measured from nivolumab initiation (including response evaluation performed at 14 weeks from randomization) according to iRECIST. (h) Trial design of TONIC stage 2. Patients are randomized between (1) induction treatment of 2 weeks with doxorubicin followed by anti-PD-1 or (2) start with anti-PD-1 without induction treatment..



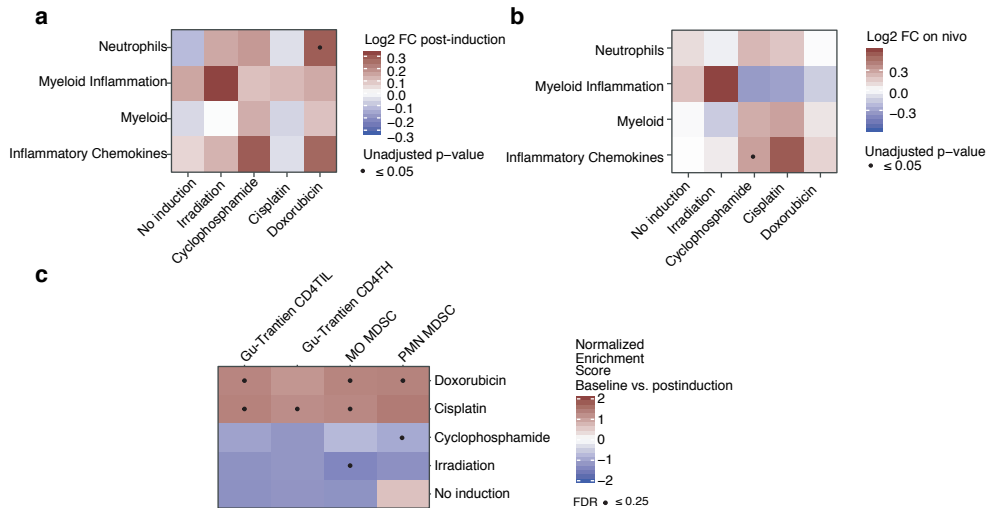
Extended Data Figure 6. TCR repertoire diversity during an ongoing anticancer response on nivolumab and changes observed after induction treatments. (a) TCR repertoire diversity on nivolumab treatment (biopsy three). TCR repertoire size was estimated using the Efron-Thisted method⁵⁴ and represents the number of unique intratumoral clones. The boxes in boxplots represent the median and interquartile ranges and the whiskers represent the 5th and 95th percentiles. (b) Fold change (FC) in the number of unique intratumoral TCR clones (TCR repertoire diversity) after induction treatment versus baseline (biopsy two versus biopsy one). Every dot represents one patient. Patients with clinical benefit are highlighted with a red dot. The dotted black line indicates no change. TCR repertoire size was estimated using the Efron-Thisted method⁵⁴. The boxes in the boxplots represent the median and interquartile ranges and the whiskers represent the full range. Statistical significance was tested with a Kruskal-Wallis test for all groups. (c) FC in the number of unique intratumoral TCR clones (TCR repertoire diversity) after nivolumab treatment versus baseline (biopsy three versus biopsy one). Every dot represents one patient. Patients with clinical benefit are highlighted with a red dot. The dotted black line indicates no change. TCR repertoire size was computed using the Efron-Thisted method⁵⁴. The boxes in the boxplots represent the median and interquartile ranges and the whiskers represent the full range. Statistical significance was tested with a Kruskal-Wallis test for all groups followed by Dunn's tests between the induction treatment groups and the control group (P values are adjusted).



Extended Data Figure 7. Histological characteristics of tumors during an ongoing anticancer response on nivolumab and changes observed after induction treatments. (a) sTILs in on-nivolumab biopsies (biopsy three), as determined according to guidelines of the TIL working group on a H&E staining. The boxes in the boxplots represent the median and interquartile ranges, and the whiskers represent the 5th and 95th percentiles. Statistical significance was tested with a two-tailed Mann-Whitney *U*-test (unadjusted *P* value). (b) CD8 cell count per mm² in on-nivolumab biopsies (biopsy three). The boxes in the boxplots represent medians with interquartile ranges, and the whiskers span the 5th to 95th percentiles. Statistical significance was tested with a two-tailed Mann-Whitney *U*-test (unadjusted *P* value). (c) sTILs per cohort. The boxes in the boxplots represent medians with interquartile ranges, and the whiskers span the 5th to 95th percentiles. Statistical significance was tested on paired biopsies with the Wilcoxon signed-rank test (two-tailed and unadjusted *P* value). (d) CD8 cell count per mm² per cohort. The boxes in the boxplots represent medians with interquartile ranges, and the whiskers span the 5th to 95th percentiles. Statistical significance was tested on paired biopsies with the Wilcoxon signed-rank test (two-tailed and unadjusted *P* value). (e) Stromal CD4 per cohort. The percentage of CD4 of the total stromal area was assessed. The boxes in the boxplots represent medians with interquartile ranges, and the whiskers span the 5th to 95th percentiles. Statistical significance was tested on paired biopsies with the Wilcoxon signed-rank test (two-tailed and unadjusted *P* value). (f) Stromal FOXP3 per cohort. The percentage of FOXP3 of the total stromal area was assessed. The boxes in the boxplots represent medians with interquartile ranges, and the whiskers span the 5th to 95th percentiles. Statistical significance was tested on paired biopsies with the Wilcoxon signed-rank test (two-tailed and unadjusted *P* value).



Extended Data Figure 8. (opposite) Bayesian hierarchical regression analysis of inflammation-related gene set FCs to investigate differences in upregulation between induction arms. (a) Plate model representation of the hierarchical model describing the FCs between baseline and post-induction. White-colored variables are inferred from the data using the model, and blue-colored variables are incorporated in extensions of the basic model. The boxes reflect repetition of the variables, $N_{\text{arms}} = 5$ and N_{patients} varies between arms. Data were available for 38 patients. (b) Distributions of posterior parameter estimates for the basic hierarchical regression model. The percentages in the vertical labels represent probabilities of exceeding the control arm (the proportion of the distribution above zero). (c) Effect of the baseline inflammation score on the observed FC in the inflammation score. Shown in red is the conditional mean (linear regression) with the 95% confidence interval shaded gray. The intercept of this line is not explicitly included in the model as it is already implicitly modelled by the μ . (d) Association between clinical response and the observed FC in the inflammation score. Red dots indicate the means. The boxes in the boxplots represent medians and interquartile ranges, and the whiskers span 1.5 times the interquartile range. (e) Association between previous lines of palliative treatment and the observed FC in the inflammation score. Boxplots are as in d. (f) Association between lymph node-only metastasis and the observed FC in the inflammation score. Boxplots are as in d. (g) Distributions of posterior parameter estimates for the full hierarchical regression model including all considered covariates. Format as in b. The points indicate the medians, the red lines indicate the 10-90% percentiles and the black lines indicate the 2.5-97.5% percentiles. (h) Robustness of coefficients with inclusion of extra covariates. Shown are the medians of the posterior parameter distributions with the 10th and 90th percentiles for 7 different models, including and excluding combinations of the non-induction arm covariates.



Extended Data Figure 9. Treatment-induced changes in myeloid cell-related and CD4 cell-related gene signatures. (a) Heatmap of post-induction FCs in gene expression signatures^{23,26} (NanoString gene expression data) in post-induction samples (biopsy two) compared to baseline (biopsy one). Depicted is the \log_2 FC in the median gene expression of paired biopsies. Statistical significance (two-sided Wilcoxon signed-rank test; unadjusted P value) is highlighted with a black dot. (b) Heatmap of on-nivolumab FCs in gene expression signatures^{23,26} (NanoString gene expression data) in samples taken on nivolumab (biopsy three) compared to baseline (biopsy one). Depicted is the \log_2 FC in the median gene expression of paired biopsies. Statistical significance (two-sided Wilcoxon signed-rank test; unadjusted P value) is highlighted with a black dot. (c) GSEA of selected gene sets related to myeloid cells and CD4 T cells^{25,27}, performed on whole-transcriptome RNA sequencing of pre-induction and post-induction samples (biopsy two compared to biopsy one). Cells are colored according to normalized enrichment scores, and Benjamini-Hochberg (false discovery rate (FDR))-corrected P values equaling or below 0.25 are highlighted with black dots. CD4FH, follicular helper CD4 T cells; CD4TIL, tumor-infiltrating CD4 T cells; MO MDSC, monocytic MDSC; PMN MDSC, polymorphonuclear MDSC.

Supplementary Table 1. Baseline characteristics of the intention-to-treat population per cohort. Clinical baseline characteristics of all allocated patients separated by induction treatment cohort (n = 70).

	Cohort 1, Control/no induction (n = 12)	Cohort 2, Irradiation (n = 14)	Cohort 3, Cyclophosphamide (n = 13)	Cohort 4, Cisplatin (n = 14)	Cohort 5, Doxorubicin (n = 17)
Median age, years (range)	53 (33-69)	47 (33-68)	51 (35-68)	53 (41-70)	46 (29-68)
Female, n (%)	12 (100)	14 (100)	13 (100)	14 (100)	17 (100)
WHO performance status, n (%)					
0	7 (58)	6 (43)	6 (46)	8 (57)	14 (82)
1	5 (42)	8 (57)	7 (54)	6 (43)	3 (18)
gBRCA1/2, n (%)					
Mutation	3 (25)	0 (0)	0 (0)	1 (7)	2 (12)
Wildtype	7 (58)	12 (86)	11 (85)	8 (57)	12 (71)
Unknown	2 (17)	2 (14)	2 (15)	5 (36)	3 (18)
Location of metastasis, n (%)					
Lymph node only	1 (8)	1 (7)	0 (0)	0 (0)	4 (24)
Visceral metastasis	7 (58)	12 (86)	11 (85)	10 (71)	10 (59)
Other metastasis	4 (33)	1 (7)	2 (15)	4 (29)	3 (18)
No. of prior therapies for metastatic disease, n (%)					
0	4 (33)	4 (29)	2 (15)	1 (7)	6 (35)
1	6 (50)	7 (50)	6 (46)	7 (50)	8 (47)
2-3	2 (17)	3 (21)	5 (38)	6 (43)	3 (18)
Previous neoadjuvant or adjuvant therapy, n (%)	11 (92)	13 (93)	11 (85)	10 (71)	14 (82)
Previous chemotherapy exposure, n (%)					
Taxane	11 (92)	13 (92)	12 (93)	12 (86)	16 (94)
Anthracycline	11 (92)	14 (100)	11 (85)	10 (71)	14 (82)
Platinum	12 (100)	7 (50)	5 (38)	8 (57)	10 (59)
Capecitabine	6 (50)	6 (43)	8 (62)	8 (57)	6 (35)
Disease free interval, n (%)					
<i>De novo</i> metastatic disease	1 (8)	1 (7)	2 (15)	3 (21)	2 (12)
Disease free interval ≤ 12 months	4 (33)	8 (57)	5 (38)	2 (14)	4 (24)
Disease free interval > 12 months	7 (58)	5 (36)	6 (46)	9 (64)	11 (65)
LDH level, n (%)					
≤ ULN	7 (58)	7 (50)	8 (62)	6 (43)	11 (65)
≤ 2x ULN	5 (42)	7 (50)	5 (38)	8 (57)	6 (35)
Stromal tumor infiltrating lymphocytes, n (%)					
Not available	0 (0)	2 (14)	0 (0)	1 (7)	2 (12)
< 5%	4 (33)	7 (50)	4 (31)	4 (29)	6 (35)
≥ 5%	8 (67)	5 (36)	9 (69)	9 (64)	9 (53)
PD-L1 expression on tumor cells, n (%)					
Not available	0 (0)	2 (14)	1 (8)	1 (7)	1 (6)
≥ 1% on tumor cells	8 (67)	10 (71)	9 (69)	8 (57)	9 (53)
≥ 5% on tumor cells	3 (25)	7 (50)	5 (38)	4 (29)	4 (24)
PD-L1 expression on immune cells, n (%)					
Not available	0 (0)	2 (14)	1 (8)	1 (7)	1 (6)
≥ 1% on immune cells	11 (92)	10 (71)	12 (92)	12 (86)	15 (88)
≥ 5% on immune cells	9 (75)	8 (57)	8 (62)	11 (79)	11 (65)
No. of nivolumab cycles, median (range)	5 (2-20)	2 (0-24)	5 (1-16)	6 (0-42)	6 (1-37)

Supplementary Table 2. Baseline characteristics of the efficacy analysis population. Clinical baseline characteristics of the patients included in the efficacy analysis (n = 66).

Efficacy analysis population (n = 66)	No. of patients	Percentage
Median age, years (range)		51 (29-70)
WHO performance status, n (%)		
0	39	59%
1	27	41%
gBRCA1/2, n (%)		
Mutation	6	9%
Wildtype	47	71%
Unknown	13	20%
Location of metastasis, n (%)		
Lymph node only	6	9%
Visceral metastasis	47	71%
Other metastasis	13	20%
No. of prior therapies for metastatic disease, n (%)		
0	15	23%
1	33	50%
2-3	18	27%
Previous neoadjuvant or adjuvant therapy, n (%)	56	85%
Previous chemotherapy exposure, n (%)		
Taxane	60	91%
Anthracycline	56	85%
Platinum	38	58%
Capecitabine	33	50%
Disease Free Interval, n (%)		
<i>De novo</i> metastatic disease	8	12%
Disease Free Interval ≤ 12 months	21	32%
Disease Free Interval > 12 months	37	56%
LDH level, n (%)		
≤ ULN	38	58%
≤ 2x ULN	28	42%
PD-L1 expression on tumor cells, n (%)		
Not available	2	3%
≥ 1% on tumor cells	41	62%
≥ 5% on tumor cells	23	35%
PD-L1 expression on immune cells, n (%)		
Not available	2	3%
≥ 1% on immune cells	59	89%
≥ 5% on immune cells	46	70%

Supplementary Table 3. Maximum grade of nivolumab or induction treatment-related adverse events. Maximum grade of treatment-related adverse event, separated by induction treatment cohort. Denoted are the maximum grade adverse events during nivolumab treatment and during induction treatment.

	Any grade, n (%)	Grade 3, n (%)	Grade 4, n (%)	Grade 5, n (%)
Induction related (n = 68)	19 (28)	2 (3)	0	0
Control/no induction (n = 12)	1 (8)	0	0	0
Irradiation (n = 13)	3 (23)	0	0	0
Cyclophosphamide (n = 13)	3 (23)	1 (8)	0	0
Cisplatin (n = 13)	8 (62)	1 (8)	0	0
Doxorubicin (n = 17)	4 (24)	0	0	0
Nivolumab related (n = 68)	55 (81)	9 (13)	2 (3)	2 (3) ¹
Control/no induction (n = 12)	9 (75)	2 (17)	0	1 (8)
Irradiation (n = 13)	10 (77)	3 (23)	0	1 (8)
Cyclophosphamide (n = 13)	13 (100)	2 (15)	2 (15)	0
Cisplatin (n = 13)	11 (85)	2 (15)	0	0
Doxorubicin (n = 17)	12 (71)	0	0	0

¹Two patients with clear evidence of progression died on study. One patient died from bacterial peritonitis probably due to progressive intestinal metastasis. One patient with progressive pleural fluid and lymphangitic carcinomatosis died from acute respiratory insufficiency not otherwise specified while being hospitalized.

Supplementary Table 4. Nivolumab related adverse events. Nivolumab related adverse events of any grade, occurring in at least 5% of patients, and all grade 3-5 adverse events, all immune-related adverse events and immune-related events of special interest.

N = 68	Any grade, no. (%)	Grade 3, no. (%)	Grade 4, no. (%)	Grade 5, no. (%)
Fatigue	16 (24)	0	0	0
Alanine aminotransferase increased	13 (19)	0	0	0
Aspartate aminotransferase increased	13 (19)	1 (1)	0	0
Hypothyroidism	12 (18)	0	0	0
Diarrhea	9 (13)	0	0	0
Dyspnea ¹	8 (12)	2 (3)	0	0
Gamma-glutamyltransferase increased	8 (12)	2 (3)	1 (1)	0
Alkaline phosphatase increased	7 (10)	1 (1)	0	0
Infusion related reaction	7 (10)	0	0	0
Fever	6 (9)	0	0	0
Flu like symptoms	5 (7)	0	0	0
Pain	5 (7)	0	0	0
Serum amylase increased	4 (6)	0	1 (1)	0
Hyperthyroidism	4 (6)	0	0	0
Sarcoidosis	4 (6)	1 (1)	0	0
Lipase increased	3 (4)	1 (1)	0	0
Anemia	2 (3)	1 (1)	0	0
Abdominal infection	1 (1)	0	0	1 (1)
Anorexia	1 (1)	1 (1)	0	0
Febrile neutropenia	1 (1)	1 (1)	0	0
Hypertension	1 (1)	1 (1)	0	0
Hyponatremia	1 (1)	1 (1)	0	0
Respiratory insufficiency	1 (1)	0	0	1 (1)
Syncope	1 (1)	1 (1)	0	0
Immune-related colitis	1 (1)	0	0	0
Immune-related gastritis	1 (1)	0	0	0
Immune-related pneumonitis	1 (1)	0	0	0

¹One patient had lymphangitic carcinomatosis in which an immune-related component could not be excluded.

Supplementary Table 5. Efficacy of nivolumab in the efficacy analysis population. Efficacy analysis was performed using the efficacy analysis population (n = 66) as determined by iRECIST. Complete and partial responses had to be confirmed on at least one subsequent CT scan. 1 patient was non-evaluable according to RECIST1.1 but had clinical benefit for more than 24 weeks. Progression-free survival was calculated in the per protocol population (n = 67) from randomization to date of progression according to RECIST1.1 or iRECIST. Eleven patients had unequivocal clinical progression before the first response evaluation. Duration of response was assessed using Kaplan Meier curves, with censoring of ongoing responses, and calculated from time of first PR or CR until progression according to iRECIST.

Objective response rate iRECIST, n, % (95% CI)	13	20% (11-31)
Clinical benefit rate iRECIST, n, % (95% CI)	14	21% (12-33)
Best overall response iRECIST, n (%)		
Complete response	2	3%
Partial response	11	17%
Stable disease > 24 weeks	1	2%
Non-evaluable, n (%)	1	2%
Median progression-free survival RECIST1.1, months (95% CI)	1.9 (1.8-2.0)	
Median progression-free survival iRECIST, months (95% CI)	1.9 (1.8-3.2)	
Duration of response, months (95% CI)	9.0 (4.7 - NR)	

Supplementary Table 6. Characteristics of irradiation cohort. The irradiated lesions per patient, volume and dose of the irradiation, radiation technique and response of both the irradiated lesions and the other lesions (abscopal effect) after irradiation and the best response on nivolumab are depicted. In the rightmost column, the absolute change in stromal tumor-infiltrating lymphocytes (TIL) after irradiation is depicted for a biopsy from a non-irradiated lesion. Gy: Gray; CTV: clinical target volume; PTV: planning target volume; VMAT: volumetric modulated arc therapy; 3D-CRT: conventional radiotherapy with anterior-posterior fields or tangential fields; 3D-IMRT: intensity modulated radiotherapy.

Patent ID	Irradiated lesion	Dose	Volume (mL)	Volume type	Radiation technique	Response irradiated lesion after irradiation	Response non-irradiated lesions after irradiation	Best response irradiated lesion after nivolumab	Best overall response non-irradiated lesions after nivolumab	Absolute change in TIL after irradiation in biopsied lesion (non-irradiated)
Pat_5	Lymph nodes left mediastinum	3 x 8 Gy	32.643	PTV	VMAT	Non-CR/non- PD	SD	Non-CR/non- PD	PR	-12.5%
Pat_7	Breast right	3 x 8 Gy	401.136	PTV	3D-CRT	Non-CR/non- PD	SD	Non-CR/non- PD	PD	+2%
Pat_9	Lymph nodes neck left	3 x 8 Gy	43.317	PTV	3D-IMRT	Non-CR/non- PD	Non-CR/non- PD	NA	PD (clinical)	-4.5%
Pat_17	Lymph nodes axilla left	3 x 8 Gy	45.2	PTV	VMAT	Non-CR/non- PD	SD	Non-CR/non- PD	PD	NA
Pat_28	Hip right	3 x 8 Gy	235.6	CTV	3D-CRT	Non-CR/non- PD	PD	NA	PD (clinical)	+4%
Pat_37	Lymph nodes supraclavicular right	3 x 8 Gy	12.2	CTV	3D-CRT	Non-CR/non- PD	SD	Non-CR/non- PD	SD > 24 weeks	+7%
Pat_38	Right breast	3 x 8 Gy	635.86	CTV	3D-CRT	PD	PD	PR	PD	-2%
Pat_47	Axilla right	3 x 8 Gy	56.997	PTV	3D-IMRT	Non-CR/non- PD	SD	NA	PD (clinical)	-32.5%
Pat_53	Lymph nodes neck right	3 x 8 Gy	35.64	PTV	VMAT	Non-CR/non- PD	PD	NA (not imaged)	PD	-2%
Pat_60	Liver segment 6/7	3 x 8 Gy	129.64	PTV	VMAT	PD	PD	PD	PD	+2.5%
Pat_67	Lung middle lobe	3 x 8 Gy	38.628	PTV	VMAT	PD	PD	NA	PD (clinical)	NA
Pat_68	Sternum	3 x 8 Gy	64.38	PTV	VMAT	Non-CR/non- PD	SD	Non-CR/non- PD	PD	+4%



Chapter 4

IL-5-producing CD4+ T cells and eosinophils cooperate to enhance response to immune checkpoint blockade in breast cancer

Olga S. Blomberg*, Lorenzo Spagnuolo*, Hannah Garner*, **Leonie Voorwerk***, Olga I. Isaeva**, Ewald van Dyk**, Noor A.M. Bakker**, Myriam Chalabi, Chris Klaver, Maxime Duijst, Kelly Kersten, Marieke Brüggemann, Dorien Pastoors, Cheei-Sing Hau, Kim Vrijland, Elisabeth A.M. Raeven, Daphne Kaldenbach, Kevin Kos, Inna S. Afonina, Paulien Kaptein, Louisa Hoes, Willemijn S.M.E. Theelen, Paul Baas, Emile E. Voest, Rudi Beyaert, Daniela S. Thommen, Lodewyk F.A. Wessels, Karin E. de Visser***, Marleen Kok***

*These authors contributed equally

** These authors contributed equally

*** These authors contributed equally, co-corresponding authors

Summary

Immune checkpoint blockade (ICB) has heralded a new era in cancer therapy. Research into the mechanisms underlying response to ICB has predominantly focused on T cells, however effective immune responses require tightly regulated crosstalk between innate and adaptive immune cells. Here, we combine unbiased analysis of blood and tumors from metastatic breast cancer patients treated with ICB with mechanistic studies in mouse models of breast cancer. We observed an increase in systemic and intratumoral eosinophils in patients and mice responding to ICB treatment. Mechanistically, we demonstrate that ICB increased IL-5 production by CD4⁺ T cells, stimulating elevated eosinophil production from the bone marrow, leading to systemic eosinophil expansion. Additional induction of IL-33 by ICB-cisplatin combination or recombinant IL-33 promoted intratumoral eosinophil infiltration and eosinophil-dependent CD8⁺ T-cell activation to enhance ICB response. This work demonstrates the critical role of eosinophils in ICB response and provides proof-of-principle for eosinophil engagement to enhance ICB efficacy.

Introduction

Immune checkpoint blockade (ICB) has emerged in the last decade as an effective strategy for the treatment of multiple cancer types. However, in metastatic breast cancer, durable responses are only seen in approximately 5% of the patients and are mainly limited to triple-negative breast cancer (TNBC)^{1,2}. Whilst response rates can be increased by selecting patients with PD-L1-positive tumors or by combining ICB with chemotherapy^{3,4}, most breast cancer patients do not benefit from ICB. A better understanding of the mechanisms that underlie response to ICB in patients is crucial for the rational design of novel immunomodulatory strategies.

Research into the mechanisms of response to ICB has predominantly focused on T cells, however, an effective immune response requires tightly regulated crosstalk between adaptive and innate immune cells⁵. One innate immune cell type gaining increasing attention in the context of anti-tumor immunity is the eosinophil^{6,7}. Eosinophils are bone marrow-derived granulocytes involved in tissue homeostasis and repair, parasite clearance and the pathophysiology of various diseases, including allergic asthma and autoimmunity⁸. In the context of cancer, opposing functions of eosinophils have been reported depending on cancer type and disease stage⁹⁻¹⁸. Recently, eosinophils have emerged as unexpected players in an effective response to ICB. Increased eosinophil levels during ICB treatment have been correlated with response to PD-1, PD-L1 or CTLA-4 targeting antibodies in patients with metastatic melanoma¹⁹⁻²¹, non-small cell lung cancer (NSCLC)^{22,23} and renal cell carcinoma (RCC)²⁴. Whether eosinophils are associated with response to ICB in patients with less immunogenic cancer types, such as breast cancer, remains to be elucidated. Moreover, it is critical to assess whether eosinophils merely serve as a biomarker or are causally involved in ICB response. Preclinical studies point towards a functional involvement of eosinophils in anti-tumor immunity¹¹⁻¹⁴ and eosinophils were also recently reported to promote intratumoral vessel normalization and anti-tumor immunity upon CTLA-4 blockade²⁵. Nonetheless, the role of eosinophils in ICB response remains poorly understood. Furthermore, the mechanisms leading to eosinophil accumulation and recruitment to the tumor upon ICB are still unknown. Addressing these outstanding questions may yield novel insights into the role of eosinophils in ICB response and more importantly, how to therapeutically exploit them.

In this study, we perform parallel unbiased analyses of the systemic immune landscape upon ICB in patients with metastatic TNBC and in spontaneous mouse models of primary and metastatic breast cancer (Figure 1A), which mimic the poorly immunogenic and highly immunosuppressive characteristics of human breast cancer^{26,27}. We show that ICB response in metastatic TNBC patients and preclinical breast cancer models is associated with systemic and intratumoral eosinophil expansion which in turn correlates with increased intratumoral CD8⁺ T-cell activation. Performing in-depth mechanistic studies *in vivo*, we uncover a critical role for eosinophils in ICB response and decipher which systemic factors are inducing eosinophil expansion and tumor infiltration. We validated our preclinical

findings in patients with metastatic TNBC and provide evidence of how eosinophils can be engaged to enhance ICB efficacy.

Results

Comprehensive unbiased analysis of blood reveals an increase in circulating eosinophils in patients responding to ICB

To assess response-related changes in the systemic immune landscape of patients with metastatic breast cancer, we set up an immunomonitoring pipeline of fresh blood by high-dimensional flow cytometry (Figure 1A). We profiled patients with metastatic TNBC treated with anti-PD-1 (nivolumab) enrolled in a phase II clinical trial (TONIC-trial, n=111, Figure S1A-B; characteristics in Supplementary Table 1 and 2)²⁸. Patients were treated with nivolumab alone or with nivolumab following a two-week induction period with either low dose chemotherapy, irradiation or a two-week waiting period (Figure S1A). Blood samples were analyzed by flow cytometry at baseline (before induction treatment), after induction treatment (pre-nivo) and after three cycles of nivolumab (on-nivo). Extensive analysis of either baseline, pre-nivo or on-nivo samples did not reveal predictive immune cell populations that could distinguish responders from non-responders (Figure S1C-E). However, when analyzing the dynamics of immune cell populations induced upon ICB treatment by comparing baseline to on-nivo, we identified three differentially regulated immune cell populations associated with response: CD1c⁺ dendritic cells (DCs), regulatory T cells (T_{regs}) and eosinophils (Figure 1B & S1F). We observed a decrease in CD1c⁺ DCs in non-responding patients (Figure S2A). In contrast, eosinophils and T_{regs} were increased upon ICB treatment specifically in responders (Figure 1C & S2B-C). The same three populations emerged when we compared the pre-nivo (post-induction) to on-nivo timepoints, indicating that the induction treatments did not significantly change the dynamics of these immune populations (Figure S2D-F). In light of recent reports of systemic eosinophil expansion correlating with ICB response in several tumor types¹⁹⁻²⁴, we further investigated the increase in eosinophils associated with response to ICB.

To validate our results in a technically independent manner we evaluated circulating eosinophil counts using routine hemocytometer analysis (Figure S1B for sample overlap with flow cytometry samples). We confirmed the significant increase in circulating eosinophils in responders on-nivo, both compared to baseline and pre-nivo (Figure 1D & S2G-H). Importantly, patients with increased circulating eosinophils upon treatment had longer progression-free survival (Figure 1E & S2I) and overall survival (Figure 1F & S2J), underscoring the clinical relevance of an eosinophil increase in ICB response.

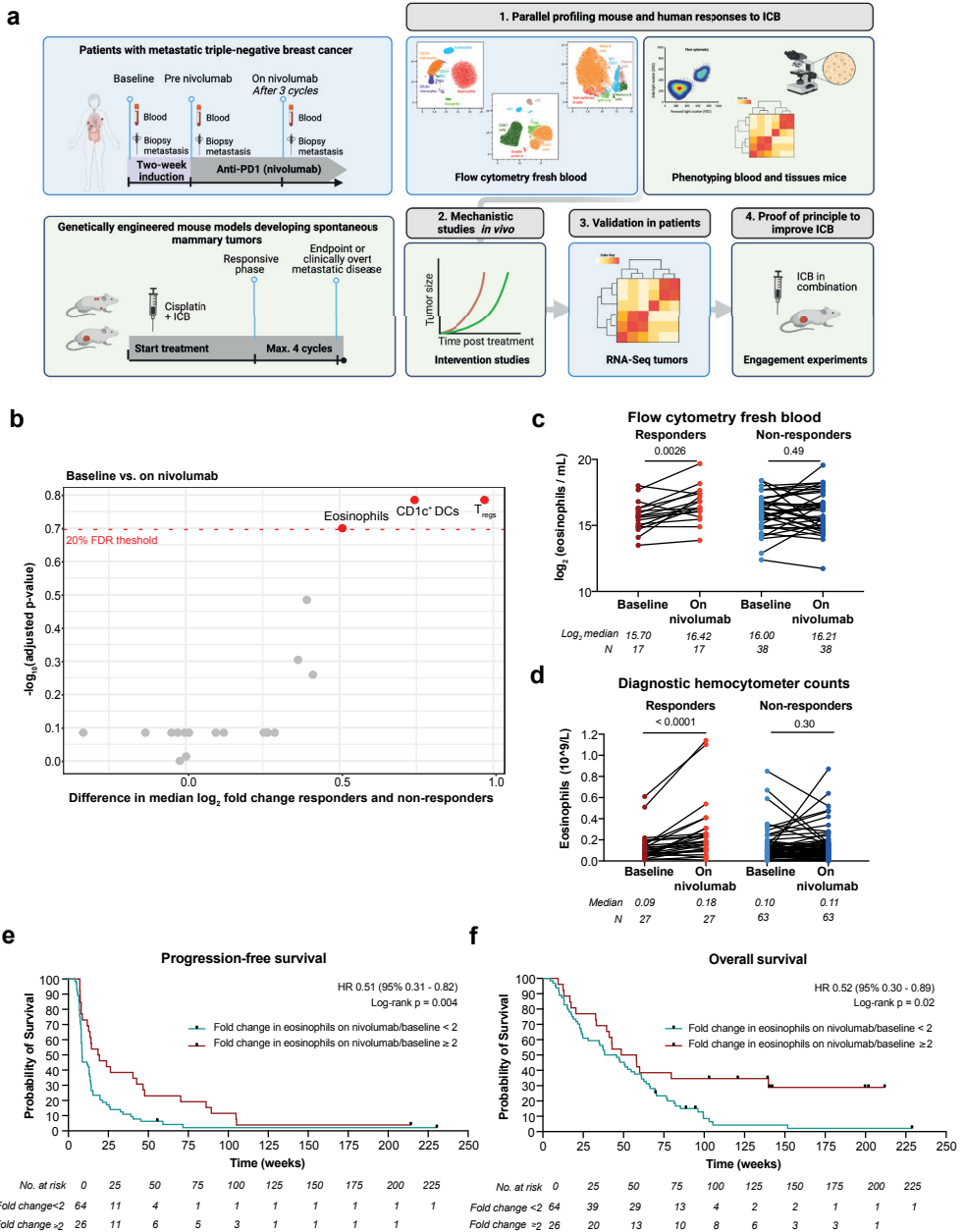


Figure 1. ICB response in metastatic TNBC patients is associated with systemic eosinophil expansion. (a) Schematic overview of study design. Created with Biorender.com. (b) Volcano plot depicting the difference in the median log₂ fold change from baseline to on-nivo between responding and non-responding patients with metastatic TNBC (TONIC-trial, NCT02499367) and adjusted p-values for systemic immune cell populations (cells/ml) analyzed by flow cytometry. (c) Paired flow cytometry analysis of circulating eosinophils (log₂ transformed cells/ml) comparing baseline to on-nivo in responders and non-responders. (d) Paired hemocytometer analysis of circulating eosinophils comparing baseline to on-nivo in responders and non-responders. Statistics for (c) and (d) by Wilcoxon Signed-Rank. (e-f) Kaplan-Meier curve of progression-free survival (e) or overall survival (f) of patients according to the fold change in eosinophils (baseline to on nivo) lower than 2 or equal to/higher than 2. Statistics with log-rank and univariate hazard ratios by Cox regression (fold change lower than 2 as reference category).

To evaluate whether increased eosinophils during ICB response extend beyond breast cancer, NSCLC^{22,23}, RCC²⁴ and melanoma¹⁹⁻²¹, we investigated eosinophil counts in patients treated with ICB in other phase II clinical trials in the Netherlands Cancer Institute. Comparing patients responding to ICB with non-responders, we observed a significantly higher fold change in circulating eosinophils in patients with advanced NSCLC (Figure S3A,B; PEMBRO-RT trial)²⁹ and in patients with early stage mismatch repair-proficient (pMMR) colon cancer (CC) (Figure S3C,D; NICHE-trial)³⁰. In contrast, no statistically significant difference in paired eosinophil counts could be seen upon ICB in patients with mismatch repair-deficient (dMMR) cancers (Figure S3E,G; NICHE-trial and dMMR cohort DRUP-trial)^{30,31}, suggesting that an eosinophil increase might be less relevant in highly immunogenic tumors. In summary, we demonstrate that eosinophils accumulate systemically upon ICB response in three independent cohorts of patients with metastatic TNBC, metastatic NSCLC or early-stage pMMR CC, emphasizing that systemic eosinophil expansion is a common feature of ICB response across multiple cancer types.

Increase of intratumoral eosinophil-related gene expression correlates with response to ICB and increased CD8⁺ T-cell signatures

To assess whether eosinophils accumulate intratumorally upon ICB, we evaluated the expression of *SIGLEC8* in paired metastases obtained at baseline and during nivolumab treatment of TNBC patients (TONIC-trial, NanoString IO360 panel, sample availability Figure S1B). *SIGLEC8* is a marker expressed at high levels on human eosinophils and mast cells and to a lower degree on basophils³². We detected a statistically significant increase in *SIGLEC8* upon ICB in tumors from responders but not in non-responding tumors (Figure 2A). To complement this analysis, we applied an eosinophil signature containing genes highly expressed by eosinophils to the RNA-sequencing dataset (Supplementary Table 3). Intratumoral expression of these genes increased upon ICB treatment in responders but not in non-responders (Figure 2B). Using this signature, we assessed whether elevation in intratumoral eosinophils is accompanied by an intratumoral increase in (activated) CD8⁺ T cells, as has been shown for metastatic melanoma¹⁹. We applied a widely used T-cell inflamed gene signature³³, an IFN γ signature³³ and a newly devised structural CD8⁺ T-cell gene signature consisting of genes related to the CD8⁺ T-cell receptor complex (Supplementary Table 3). We observed a significant correlation between increased expression upon ICB of eosinophil-related genes and all three T cell-related gene signatures in metastatic lesions of responders, and not in non-responders (Figure 2C-H). Together, our results indicate that response to ICB is not only associated with an increase in circulating eosinophils but also accompanied by an increase of eosinophil-related genes in the tumor microenvironment. This increase in eosinophil-related genes is correlated with an increase in CD8⁺ T-cell related genes, suggesting a potential connection between eosinophils and CD8⁺ T-cell activation during an effective ICB response.

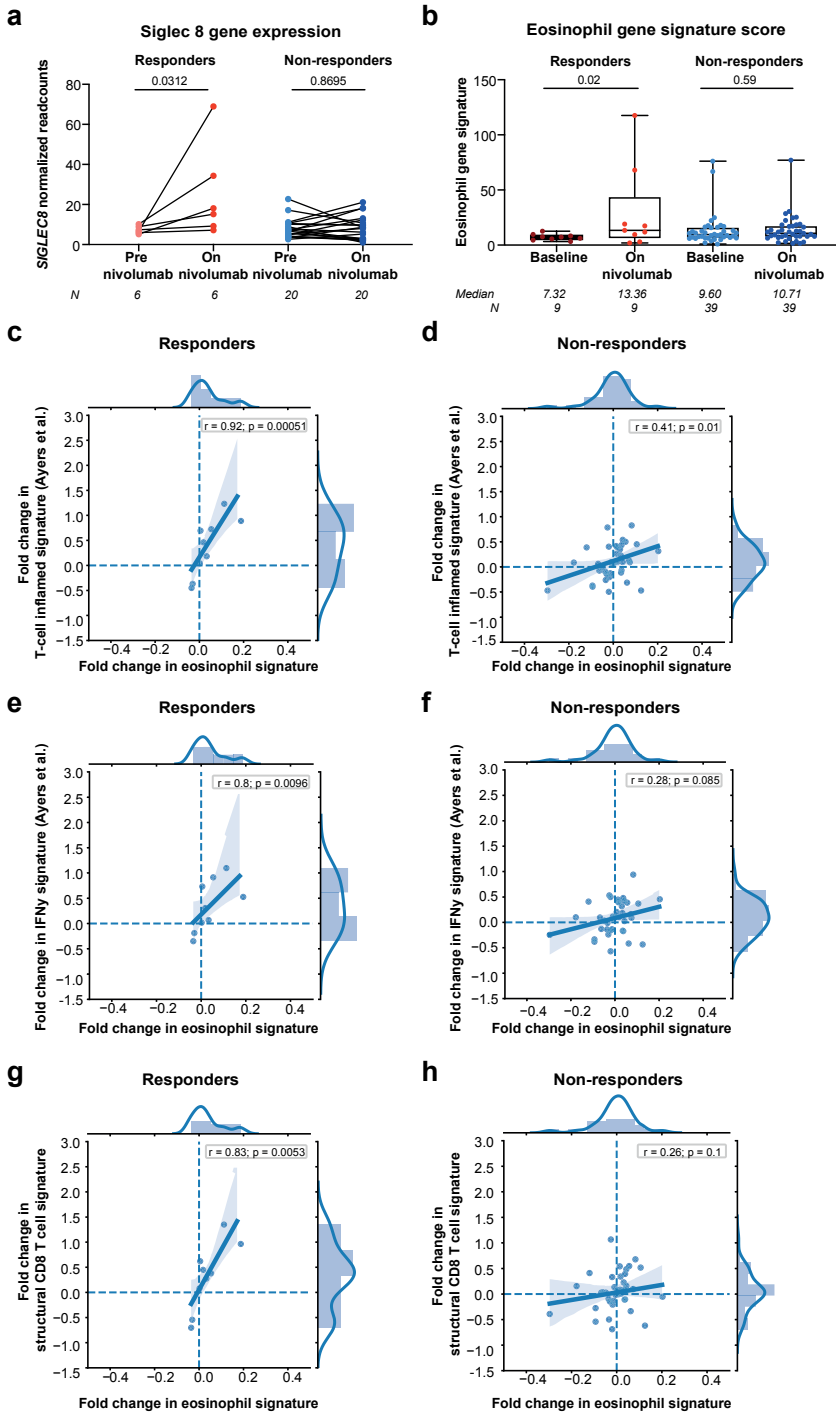


Figure 2. ICB response in TNBC patients is associated with increased intratumoral eosinophil-related gene expression. (a) Paired intratumoral *SIGLEC8* normalized read counts from NanoString IO360 gene expression analysis from pre-nivo and on-nivo biopsies. Wilcoxon Signed-Rank test. (b) Mean of normalized expression values of eosinophil signature genes (Supplementary Table 3) from paired biopsies of metastases as assessed by RNA-sequencing analysis.

Boxplots with median and IQR, whiskers with full range. Wilcoxon Signed-Rank test. (c-h) Correlation between the fold change (baseline to on nivo) in an eosinophil gene signature (described in b) and the fold change (baseline to on nivo) in a T-cell inflamed gene signature (expanded immune gene signature of Ayers *et al.*³³ (c,d), a structural CD8⁺ T cell gene signature (Supplementary Table 3) (e,f), or an IFN γ gene signature³³ (g,h) in responders (left) and non-responders (right). Lines with colored field represent the regression line with 95% confidence interval, including histogram and kernel density estimates. Statistics by Spearman's correlation coefficient.

ICB synergizes with cisplatin and induces eosinophil accumulation in spontaneous primary and metastatic breast cancer models

Our clinical observations raise the question whether eosinophil expansion is a bystander effect of ICB response, or whether eosinophils are functionally involved. To probe the causality between eosinophil dynamics and outcome after ICB in breast cancer, we made use of the transgenic *Keratin14-cre;Cdh1^{Fl/F};Trp53^{Fl/F}* (KEP) mouse model for *de novo* mammary tumorigenesis³⁴ (Figure 3A) and the KEP-based mastectomy model for spontaneous multi-organ metastatic disease³⁵ (Figure 3E & S4A,B). Despite expression of PD-1 and CTLA-4 on tumor-infiltrating T cells, KEP mice bearing established mammary tumors did not respond to blockade of PD-1 and CTLA-4 (referred to as ICB; Figure 3B). Similarly, metastasis-bearing mice did not respond to ICB alone (Figure 3F), recapitulating the poor response to ICB observed in metastatic breast cancer patients. Platinum-based drugs synergize with ICB in preclinical mouse models^{36,37} due to their beneficial immunomodulatory effects^{38,39}, which is in line with improved response rates when ICB is combined with chemotherapy in metastatic TNBC patients^{3,4}. While combining cisplatin with either anti-PD-1 or anti-CTLA-4 was insufficient to improve the survival benefit provided by cisplatin (Figure S4C), the combination of cisplatin with anti-PD-1 and anti-CTLA-4 (CIS + ICB) resulted in extension of survival of KEP mice (Figure 3B) and led to durable responses in mice bearing established metastases (Figure 3F). The therapeutic synergy between cisplatin and ICB was characterized by a systemic increase in effector CD44⁺ CD62L⁻ T cells and increased expression of activation markers and cytokines, such as IFN γ and TNF α by both CD4⁺ and CD8⁺ T cells (Figure S4D,E). Depletion of CD8⁺ T cells abrogated the synergistic effect observed upon combined ICB and cisplatin in mammary tumor-bearing KEP mice (Figure 3B), confirming a critical role of CD8⁺ T cells as effector cells in ICB-cisplatin combination therapy.

In addition to an increase in activated T cells, in-depth profiling of the immune landscape in primary tumors, metastases, and blood by flow cytometry of both mouse models revealed that only eosinophils consistently increased in frequency upon combined ICB and cisplatin (Figure 3C,D & 3G,H). Whilst ICB induced accumulation of eosinophils in the circulation (Figure 3C & 3G), increased eosinophil infiltration in primary tumors and metastatic lesions was only observed when ICB was combined with cisplatin (Figure 3D & 3H). In addition, we observed an increase in eosinophils in the tumor-draining lymph node (TDLN) and spleen of KEP mice treated with cisplatin and ICB (Figure S4F). Immunohistochemical staining for Major Basic Protein (MBP), a granular protein specifically expressed by eosinophils, confirmed that the increase in eosinophils in primary KEP tumors was only achieved upon ICB-cisplatin combination therapy (Figure S4G).

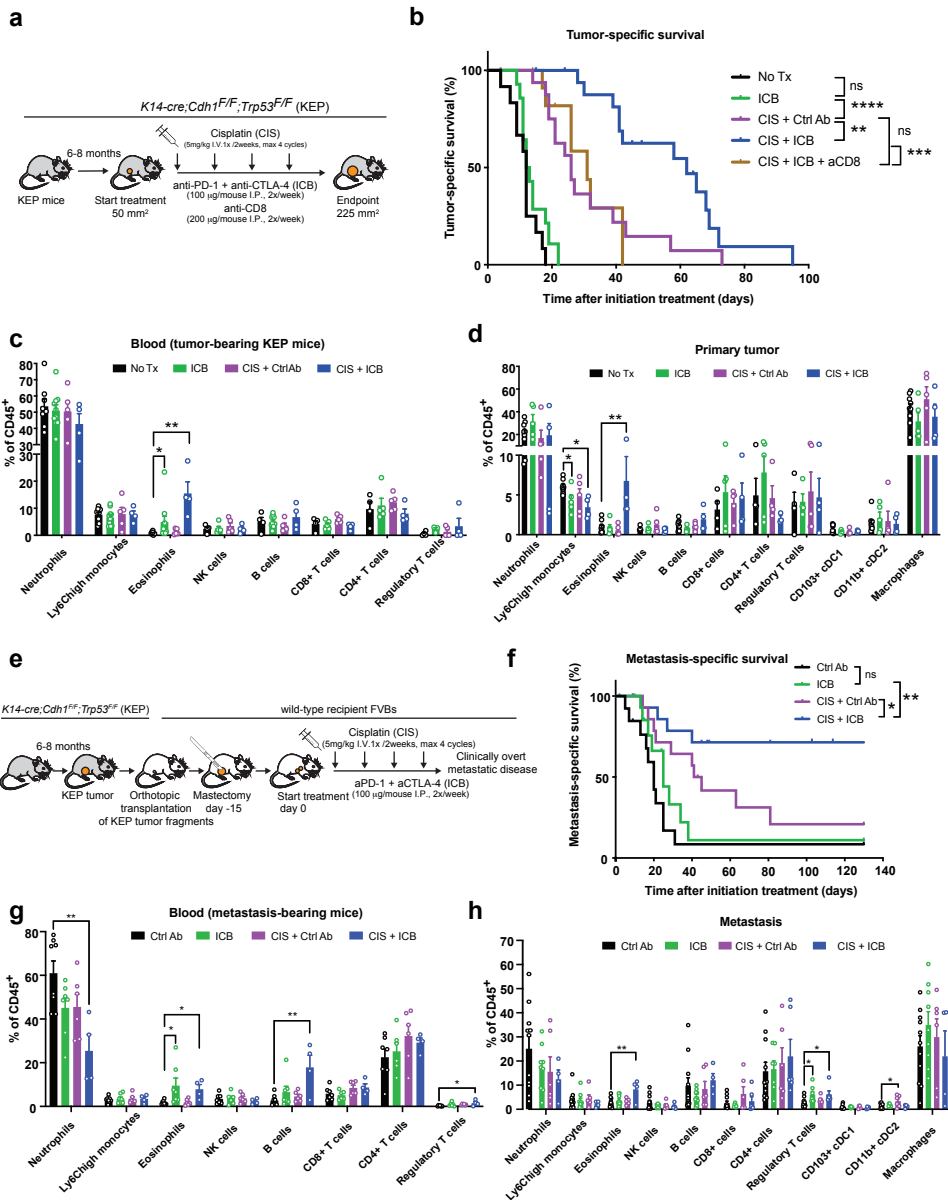


Figure 3. ICB synergizes with cisplatin and induces eosinophil expansion in preclinical mouse models. (a) Experimental set-up of transgenic KEP model and treatment scheme. (b) Kaplan-Meier survival curves of KEP mice treated as indicated (untreated, No Tx, n=12; ICB, n=14, 1 censored; CIS + Ctrl Ab, n=17, 2 censored; CIS + ICB, n=18, 5 censored; CIS + ICB + anti-CD8, n=12, 4 censored). Tumor-related endpoint was defined as cumulative tumor burden of 225mm². (c-d) Frequency of indicated immune cell populations in the blood (c) and primary tumor (d) of KEP mice at tumor-related endpoint as determined by flow cytometry. Eosinophils were defined as CD11b⁺ Ly6G^{low} SiglecF⁺ SSC^{high} in blood and CD11b⁺ Ly6G^{low} SiglecF⁺ F4/80^{int} in tumor. (e) Experimental set-up of KEP-based metastasis model and treatment scheme. (f) Kaplan-Meier survival curves of metastasis-bearing mice treated as indicated (control antibody, Ctrl Ab, n=13, 1 censored; ICB, n=15, 5 censored; CIS + Ctrl Ab, n=15, 3 censored; CIS + ICB, n=16, 7 censored). Metastasis-related endpoint was defined as mice displaying signs of distress caused by metastatic disease (respiratory distress) or when lymph node metastasis reached the size of 225mm². (g-h) Frequency of indicated immune cell

populations in the blood (g) or metastasis (h) of mice at metastasis-related endpoint as determined by flow cytometry. Censored events are mice sacrificed for weight loss (b & f) or local recurrence of the mastectomized tumor (f). All data are mean \pm S.E.M.. For immune cell analyses: 1-way ANOVA or Kruskal-Wallis followed by Dunnett's or Dunn's multiple comparisons test, comparing each group against control-treated mice. For survival analyses: Log-rank (Mantel Cox) test. * $p < 0.05$, ** $p < 0.01$, *** $p < 0.001$, **** $p < 0.0001$

To evaluate whether the treatment with cisplatin and ICB also influences the phenotype of eosinophils, we performed RNA-sequencing on eosinophils sorted from blood of metastasis-bearing mice during the responsive phase of therapy, namely 21 days after initiation of treatment. We observed 858 differentially expressed genes (fold change ≥ 1 and p -value ≤ 0.05) of which 498 were upregulated and 360 downregulated in eosinophils of ICB-cisplatin combination-treated mice compared to eosinophils of control antibody-treated mice (Figure S4H). Gene-set enrichment analysis identified IFN γ response as the top hit among the immune-related pathways enriched in eosinophils upon ICB-cisplatin combination (Figure S4I-J). Other immune-related pathways included TGF β signaling, TNF α signaling via NF- κ B, IL6-JAK-STAT3 signaling, and inflammatory response (Figure S4I). Moreover, we observed enrichment of oxidative phosphorylation pathway in eosinophils from control antibody-treated mice compared to combination-treated mice (Figure S4K). These observations indicate that, in ICB-cisplatin treated mice, eosinophils are not only increased in number, but also phenotypically altered. Collectively, these data demonstrate that ICB synergizes with cisplatin resulting in improved survival and is associated with systemic and intratumoral expansion of eosinophils, in line with our clinical observations.

Eosinophil depletion abrogates CD8⁺ T-cell activation and ICB response

To elucidate whether eosinophilia induced by ICB-cisplatin combination therapy is critical for the observed therapeutic benefit, we depleted eosinophils with an antibody targeting SiglecF, a commonly used strategy that induces apoptosis in eosinophils^{11,12,25,40,41}. Anti-SiglecF treatment effectively depleted eosinophils without altering other immune cells including neutrophils (Figure S5A-C). In line with literature⁴², we observed a subset of SiglecF⁺ neutrophils in our tumor models (5-20% of intratumoral neutrophils, data not shown). However, the expression levels of SiglecF on these neutrophils was lower than on eosinophils (Figure S5D). To exclude the possibility that anti-SiglecF treatment depletes SiglecF⁺ neutrophils, we quantified Ly6G⁺ (neutrophils) and MBP⁺ (eosinophils) cells by immunohistochemical staining. The total number of neutrophils was unaffected by anti-SiglecF treatment, whereas eosinophils were effectively depleted (Figure S5E,F). Importantly, eosinophils were also effectively depleted during anti-SiglecF treatment in combination with cisplatin +/- ICB (Figure 4A & S5G).

The administration of anti-SiglecF alone did not affect KEP tumor growth (Figure S5H). Strikingly, depletion of eosinophils abrogated the synergistic effect observed between cisplatin and ICB, both in terms of primary tumor outgrowth and survival, while depletion of eosinophils had no effect on therapeutic benefit of cisplatin alone (Figure 4B-D). Similarly, depletion of eosinophils completely abrogated the synergistic effect of ICB-cisplatin combination in mice with metastatic breast

cancer but had no effect on the efficacy of cisplatin alone (Figure 4E). These findings reveal a causal role for eosinophils in the synergistic effect of ICB and cisplatin combination therapy, both in primary and metastatic breast cancer models.

Because the synergistic effect of ICB and cisplatin is dependent on both CD8⁺ T cells and eosinophils, we hypothesized that eosinophils play a role in inducing intratumoral CD8⁺ T-cell infiltration or activation. It has been previously shown that eosinophils can promote T-cell activation and recruitment into tumors^{11,13,18,25,40}, and we observed an association between intratumoral eosinophils and CD8⁺ T cells in responding patients with advanced breast cancer (Fig 2C-H). To test this hypothesis, we analyzed the immune landscape of KEP mammary tumors during the responsive phase of therapy. Immunohistochemical staining of CD8 in primary tumors demonstrated that CD8 counts were increased upon treatment with cisplatin compared to control antibody but did not further increase upon addition of ICB. Importantly, CD8 counts were not dependent on the presence of eosinophils (Figure 4F). Instead, depletion of eosinophils completely reverted the increased activation state of intratumoral CD8⁺ T cells induced by ICB-cisplatin combination, most notably in terms of CD44 expression and IFN γ production (Figure 4G,H). These data demonstrate that eosinophils are essential for increased intratumoral CD8⁺ T-cell activation during ICB and cisplatin combination therapy.

Additionally, CD4 and FOXP3 cell counts were increased upon cisplatin treatment compared to control during the responsive phase of therapy, but did not change further when cisplatin was combined with ICB and was independent of eosinophil presence (Figure S5I,J). While combined ICB and cisplatin also increased the intratumoral frequency of effector CD44⁺ CD4⁺ T cells, this was independent of eosinophils (Figure S5K-N), demonstrating that eosinophils specifically affect intratumoral CD8⁺ T-cell activation. Interestingly, we also observed a higher frequency of CD44⁺ and IFN γ ⁺ CD8⁺ T cells in the TDLN upon cisplatin and ICB combination that was abrogated upon eosinophil depletion (Figure S5O). In contrast, the frequency of CD44⁺ CD4⁺ T cells or CD44⁺ T_{regs} in TDLN was not increased by the combination treatment nor affected by eosinophil depletion (Figure S5P,Q). Collectively, these observations show that eosinophils are critical for the therapeutic action of ICB in combination with cisplatin, by facilitating CD8⁺ T-cell activation in the tumor and TDLN.

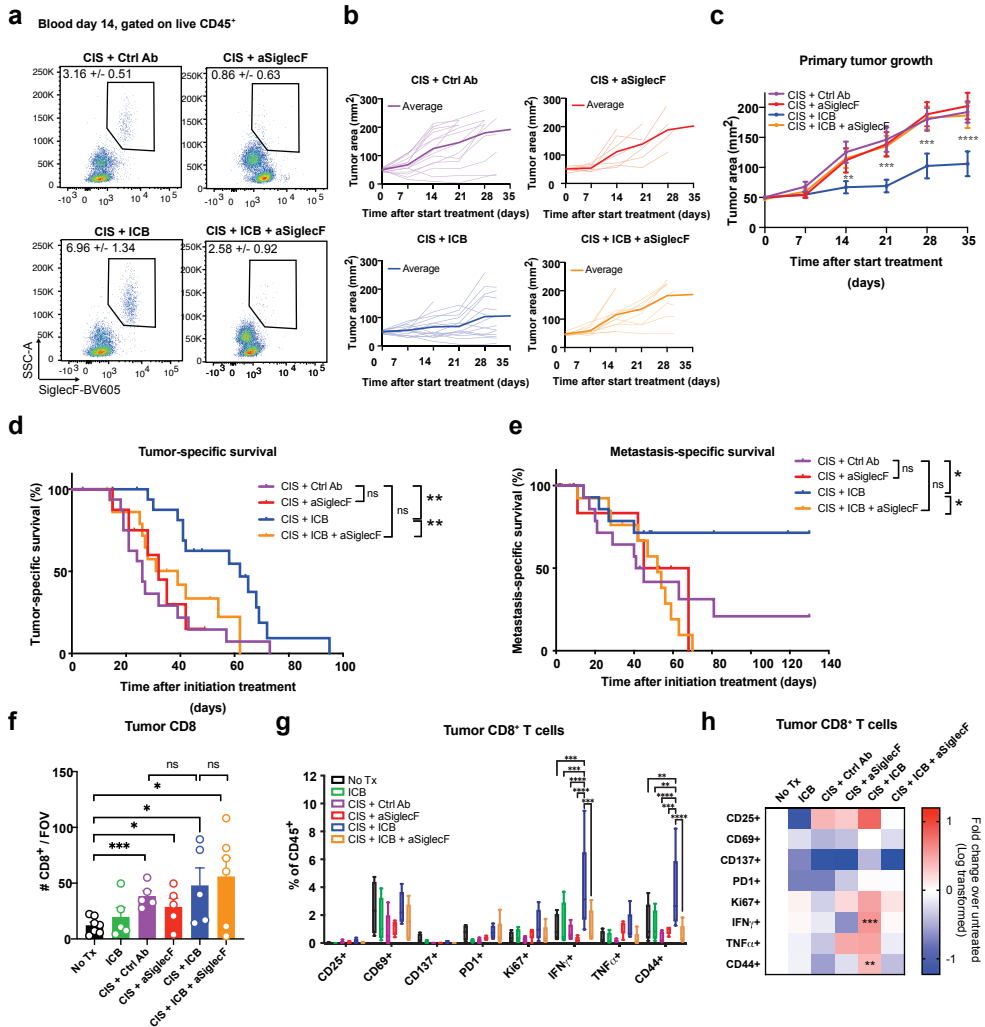


Figure 4. Eosinophils are critical for ICB-cisplatin response via CD8⁺ T-cell activation. (a) Representative dot plots showing eosinophil levels in blood of KEP mice 14 days after start of indicated treatments. Mean frequency of eosinophils as percentage of CD45⁺ cells \pm S.E.M. is displayed. (b) Individual (light) and average (dark) tumor growth curves of KEP mice treated as indicated. (c) Average growth curve \pm S.E.M. of the indicated aforementioned treatment groups. 2-way ANOVA followed by Dunnett’s multiple comparisons test. (d) Kaplan-Meier survival curves of KEP mice treated as indicated (CIS + Ctrl Ab, same curve as in Figure 3b); CIS + anti-SiglecF, n=8, 2 censored; CIS + ICB, same curve as in Figure 3B; CIS + ICB + anti-SiglecF, n=18, 5 censored). Log-rank (Mantel-Cox) test. (e) Kaplan-Meier survival curves showing metastasis-related survival of mice treated as indicated (CIS + Ctrl Ab, same curve as in Figure 3E; CIS + anti-SiglecF, n=6, 2 censored, CIS + ICB, same curve as in Figure 3F; CIS + ICB + anti-SiglecF, n=19, 7 censored). Log-rank (Mantel-Cox) test. (f) Number of tumor-infiltrating CD8⁺ cells quantified by IHC (n=5-7 mice per group, average of 5-9 high power microscopic fields per mouse). KEP mice were treated as described in Figure 3A and analyzed 21 days after start of treatment or when tumors reached an area of 225 mm². Mean \pm S.E.M. Student’s t-test. (g) Frequency of CD8⁺ T cells in the primary tumor expressing the indicated activation markers upon different treatments, determined by flow cytometry (n=4-5). Boxes represent median and interquartile range; whiskers represent full range. 2-way ANOVA followed by Tukey’s multiple comparison test. (h) Data of (g) was normalized to the frequency observed in control mice. Log transformed data is presented. ns, not significant, *p<0.05, **p<0.01, ***p<0.001, ****p<0.0001.

IL-5 is required for ICB-induced eosinophil accumulation and therapeutic benefit

To investigate how ICB mediates the systemic eosinophil increase, we analyzed mice bearing established metastases at different timepoints during the metastatic cascade and treatment. We observed that the eosinophil frequency in the blood was increased after 7 days of ICB treatment and was maintained at high levels until at least 21 days of ICB treatment (Figure S6A). Concomitantly, we observed an increase in eosinophils in the bone marrow (Figure 5A) and an increase of Lin⁻Sca1⁺CD34⁺cKit^{int}CD125⁺Gr1⁻ cells, which have been previously described as eosinophil progenitor cells (Figure 5B & S6B)⁴³. Furthermore, both immature (cKit^{int}CCR3^{low}) and fully mature (cKit⁺CCR3⁺) eosinophils increased in the bone marrow upon ICB treatment (Figure 5C-E). All other analyzed hematopoietic progenitor and immune cell populations in the bone marrow remained unaffected (Figure S6C). Altogether, these observations suggest that the systemic increase of eosinophils induced by ICB is caused by increased eosinophil production in the bone marrow.

To assess which systemic factors induced by ICB could promote eosinophil production in the bone marrow, followed by systemic eosinophil accumulation, we measured the expression of a panel of cytokines in the plasma of metastatic mice. Strikingly, the only cytokine which was significantly increased upon ICB treatment was IL-5 (Figure 5F & S6D), which is a major regulator of eosinophil biology⁴⁴. To investigate whether ICB treatment in human tumors induces IL-5 upregulation, we made use of the patient-derived tumor fragment (PDTF) platform⁴⁵. This platform allows interrogation of the early immunological response of human tumor tissues upon *ex vivo* ICB treatment (aPD1 and combined aPD1 + aCTLA4). Importantly, the observed *ex vivo* response (defined as previously described^{45,46}) correlates with the clinical response of the patient⁴⁵. We assessed the protein levels of IL-5 upon *ex vivo* ICB stimulation in tumors of patients with different types of tumors. We observed an increase in IL-5 expression specifically in tumors that showed an immunological response to *ex vivo* ICB treatment (PDTF-R) as compared to non-responding tumors (PDTF-NR), both upon anti-PD1 alone and upon combined anti-PD1/anti-CTLA4 treatment (Figure 5G), demonstrating that IL-5 can be induced in human tumors by ICB.

To assess whether IL-5 drives eosinophil expansion upon ICB treatment in metastasis-bearing mice, we blocked IL-5 using a neutralizing antibody. Indeed, the number of eosinophils in bone marrow, blood, and (pre-)metastatic lungs was drastically reduced (Figure 5H-J). Importantly, ICB did not promote an eosinophil increase after IL-5 blockade in any of the organs analyzed, indicating that ICB-induced eosinophils are IL-5 dependent. In line with our observations in metastasis-bearing mice, serum IL-5 levels were similarly increased in tumor-bearing KEP mice during the responsive phase of CIS + ICB therapy (Figure 5K). To assess the functional relevance of IL-5 for the therapeutic benefit observed upon CIS + ICB, we treated KEP mice with IL-5 targeting antibody and monitored tumor-related survival. Eosinophil levels were reduced upon IL-5 blockade both systemically and intratumorally (Figure 5L,M), without effecting other myeloid cells (Figure S6E,F). Importantly, anti-IL-5 treatment abolished the therapeutic benefit induced by CIS + ICB (Figure 5N), phenocopying the effect of anti-SiglecF-induced eosinophil

depletion (Figure 4D). Collectively, these findings demonstrate that IL-5 is a key driver of eosinophil accumulation and therapeutic benefit of CIS + ICB therapy.

IL-5 producing CD4⁺ T cells drive eosinophil production in the bone marrow and their systemic expansion upon ICB

IL-5 can be produced by various cell types, principally CD4⁺ T cells, type 2 innate lymphoid cells (ILC2) and other non-lymphoid innate immune cells, such as mast cells and eosinophils⁴⁴. To evaluate whether adaptive or innate immune cells are needed to induce eosinophils upon ICB, we treated KEP tumor-bearing wild-type and *Rag-1*-deficient mice, which lack mature B and T cells but retain ILC2s and myeloid cells, with ICB or control antibody. Importantly, ICB failed to induce an increase in eosinophils in tumor-bearing *Rag-1*-deficient mice (Figure 5O), indicating that adaptive immune cells trigger eosinophil expansion upon ICB. Based on these findings, we hypothesized that CD4⁺ T cells are the main source of IL-5 upon ICB, and thus cause eosinophilia. Indeed, we observed increased expression of IL-5 mRNA in circulating CD4⁺CD25⁻ T cells upon ICB treatment in mice with metastatic disease (Figure 5P). To establish a mechanistic link between CD4⁺ T cells and eosinophils, we depleted CD4⁺ T cells by treating metastasis-bearing mice with anti-CD4 during ICB treatment (Figure S6G) and measured IL-5 and eosinophil levels. Depletion of CD4⁺ T cells reduced plasma IL-5 levels and the number of eosinophils in bone marrow and blood (Figure 5Q,R), suggesting a role for CD4⁺ T cells in eosinophil homeostasis. Importantly, in the absence of CD4⁺ T cells, there is reduced induction of IL-5 by ICB (Figure 5Q). Of note, CD4⁺ T cell-depleted mice still display a slight but significant increase of IL-5 in the serum upon ICB treatment when compared to control antibody treated CD4⁺ T cell depleted mice (Figure 5Q). Since the efficiency of the CD4⁺ cell depletion is high at the timepoint analyzed (Figure S6G), we speculate that other sources of IL-5, such as ILC2s, mast cells and eosinophils themselves, may produce the residual IL-5 we observe. Importantly, in line with the reduced induction of IL-5 upon ICB in the absence of CD4⁺ T cells, systemic eosinophil numbers do not increase upon ICB in CD4⁺ T cell depleted mice (Figure 5R & S6H). In addition to mature bone marrow eosinophils, the frequency of Lin⁻Sca1⁻CD34⁺cKit^{Int}CD125⁺Gr1⁻ eosinophil progenitors in the bone marrow did not increase upon ICB treatment after CD4⁺ T cell-depletion (Figure S6I). These data demonstrate that CD4⁺ T cells are required for the ICB-induced increase in systemic IL-5 levels, eosinophil production in the bone marrow and systemic eosinophil accumulation. Importantly, CD4⁺ T-cell depletion also reduced the number of circulating eosinophils in metastasis-bearing mice treated with ICB and cisplatin (Figure S6J), confirming that CD4⁺ T cells are required for eosinophil increase not only upon ICB treatment alone, but also during combined ICB and cisplatin treatment. To exclude the potential contribution of T_{regs} in ICB-induced eosinophilia, we used KEP tumor-bearing *Foxp3^{DTR-GFP}* mice allowing specific depletion of FOXP3 expressing T_{reg} cells (Figure S6K,L)⁴⁷. Upon T_{reg} depletion, blood eosinophil numbers during ICB were further increased compared to T_{reg} proficient mice (Figure S6M), indicating that T_{regs} do not facilitate ICB-induced eosinophil expansion, but hamper ICB-induced eosinophilia.

To address whether CD4⁺ T cells are a source of IL-5 in TNBC patients, we utilized peripheral blood mononuclear cells (PBMCs) isolated from patients treated in the control arm of the TONIC trial at baseline and after one cycle of nivolumab and performed RT-qPCR for IL-5 mRNA in sorted CD4⁺ T cells. In 5 out of 6 patients, we observed an increase in IL-5 transcript in CD4⁺ T cells at the on-nivolumab timepoint compared to baseline (Figure 5S). To further demonstrate that CD4⁺ T cells produce IL-5 protein in response to nivolumab, we stimulated PBMCs from TNBC patients (TONIC-trial) with nivolumab for 48 hours and analyzed intracellular IL-5 in CD4⁺ T cells by flow cytometry. These data show a statistically significant fold change in IL-5⁺ CD4⁺ T cells upon nivolumab stimulation (Figure 5T), demonstrating that aPD-1 induces IL-5 expression in circulating CD4⁺ T cells of TNBC patients. Collectively, our data demonstrate that IL-5 producing CD4⁺ T cells drive eosinophil expansion upon ICB.

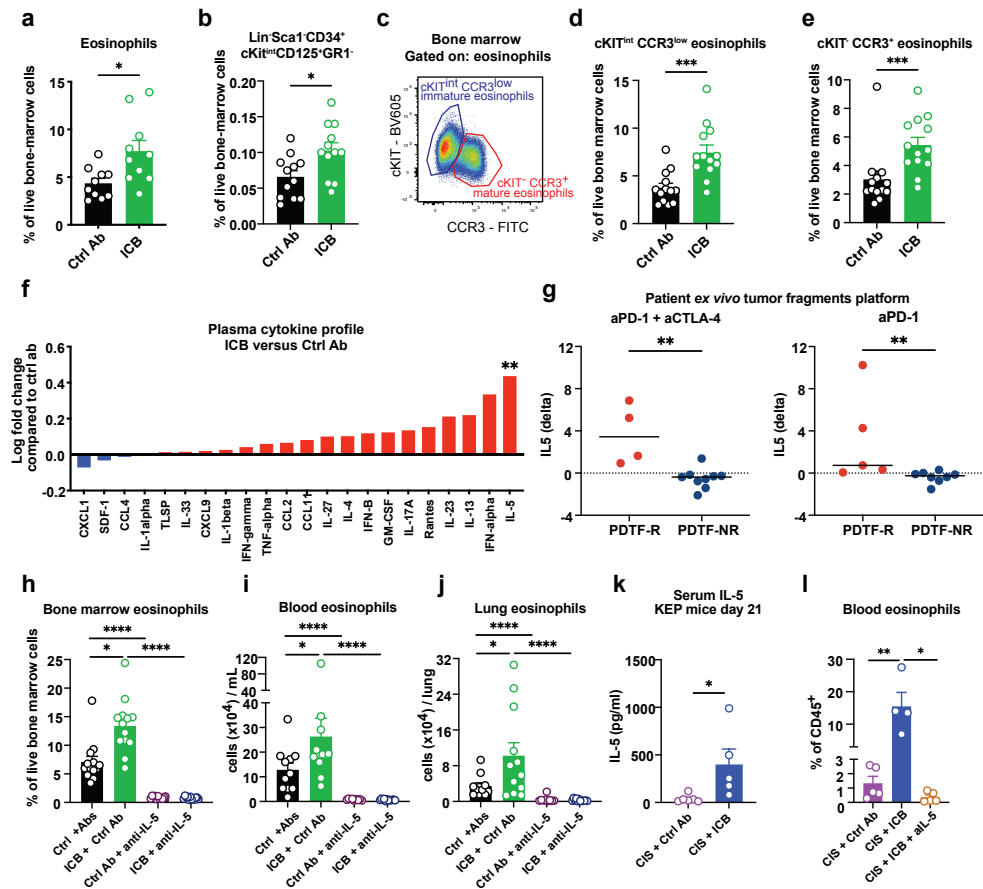


Figure 5. (continued on next page) CD4⁺ T cell-derived IL-5 is required for ICB-induced eosinophil expansion and therapeutic benefit.

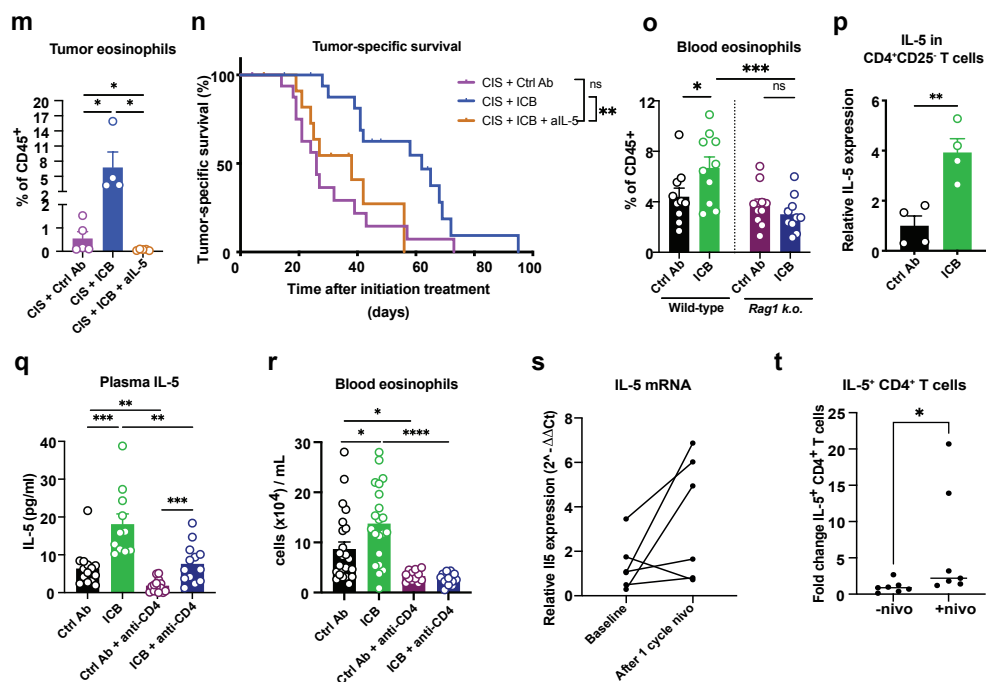


Figure 5. CD4⁺ T cell-derived IL-5 is required for ICB-induced eosinophil expansion and therapeutic benefit. (a-e) Mice with KEP-derived metastatic disease were treated as indicated (Ctrl Ab, n=10-13; ICB, n=10-13) and sacrificed 10 days after start of treatment. Frequency of total eosinophils (Live Lin⁺CD127⁺CD11b⁺CD115⁺SiglecF⁺) (a), Live Lin⁺Sca1⁺CD34⁺cKit^{int}CD125⁺Gr1⁺ eosinophil progenitors (b), representative dot plot (c) and quantification of cKit^{int}CCR3^{low} (d) and cKit⁺CCR3⁺ (e) eosinophils in bone marrow as determined by flow cytometry. (f) Relative expression of the indicated cytokines in the plasma of mice treated as described above (Ctrl Ab n=9, ICB n=10), as determined by Legend Plex, and normalized to Ctrl Ab-treated mice. (g) Fold change in IL-5 secretion by patient derived tumor fragments (PDTF) treated *ex vivo* with aPD-1 + aCTLA-4 (left) or aPD-1 (right) compared to untreated condition, measured by LEGENDplex assay, comparing PDTF-R (responders) and PDTF-NR (non-responders), defined as described previously^{45,46}. Tumor samples were collected from surgical material of patients with various tumor types (see detailed description in the Methods). (h-j) Mice with KEP-derived metastatic disease were treated with IgG2a and IgG1 control antibodies (Ctrl Abs, n=14), ICB + IgG1 (n=14), IgG2a + anti-IL-5 antibody (n=11) or ICB + anti-IL-5 (n=12) and analyzed 10 days after start of treatment. Number of eosinophils in bone marrow (h), blood (i) and lungs (j) as determined by flow cytometry. Lung eosinophils were defined as CD45⁺CD11b⁺Ly6G⁺SiglecF⁺F4/80^{int}. (k) IL-5 levels in serum of tumor-bearing KEP mice analyzed 21 days after start of indicated treatments as measured by ELISA. (l-m) Frequency of eosinophils in the blood (l) and tumor (m) of KEP mice treated as indicated and analyzed at tumor-related endpoint as determined by flow cytometry (n=4-5). Data from CIS + Ctrl Ab and CIS + ICB are the same mice as in Figure 3c & d. (n) Kaplan-Meier survival curves of KEP mice treated as indicated (CIS + Ctrl Ab, same curve as in Figure 3B); CIS + ICB, same curve as in Figure 3B; CIS + ICB + anti-IL-5, n=12, 3 censored). Log-rank (Mantel-Cox) test. (o) Number of eosinophils in blood of wild-type (wt) or Rag1 k.o. mice with KEP-derived orthotopic mammary tumors, treated as indicated (Ctrl Ab, wt n=10, Rag1 k.o. n=10; ICB, wt=10, Rag1 k.o. n=10). Treatment started when mice developed a tumor of 16 mm² and the number of eosinophils was determined by flow cytometry when tumors reached an area of 144 mm². (p) *Il5* gene expression in CD4⁺CD25⁺ T cells sorted from blood of mice with KEP-derived metastatic disease treated as described above (Ctrl Ab n=4, ICB n=4), determined by RT-qPCR. Relative expression to Ctrl Ab-treated mice is shown. (q-r) Mice with KEP-derived metastatic disease were treated with isotype control antibodies (Ctrl Ab, n=13-25), ICB (n=13-21), Ctrl Ab + anti-CD4 (n=14) or ICB + anti-CD4 (n=13) and sacrificed 10 days after start of the treatment. (q) Levels of IL-5 in plasma, measured by ELISA. (r) Number of eosinophils in the blood, as determined by flow cytometry. Pooled data of two independent experiments. (s) *Il5* gene expression determined by RT-qPCR in CD4⁺ T cells sorted from PBMCs at baseline and after one cycle of nivolumab from patients with metastatic TNBC treated in the control arm of the TONIC trial (n=6). (t) Fold change in frequency of IL-5⁺ CD4⁺ T cells among total CD4⁺ T cells from TNBC patients treated *ex vivo* with aPD1 compared to untreated condition, measured by intracellular flow cytometry. PBMCs were isolated at baseline from patients with metastatic TNBC in the control arm of the TONIC trial and stimulated with anti-CD3+anti-CD28 with or without anti-PD1 (nivolumab, as indicated) for 48 hours (n=7). All data are mean \pm S.E.M, statistical analysis by unpaired t-test or Mann-Whitney, unless differently indicated. ns, not significant, *p<0.05, **p<0.01, ***p<0.001, ****p<0.0001.

IL-33 drives eosinophil recruitment to the TME and is required for the therapeutic benefit of CIS + ICB

Although ICB alone leads to systemic eosinophil accumulation, eosinophil recruitment to the tumor and their subsequent contribution to therapeutic benefit was only observed upon cisplatin and ICB combination therapy (Figure 3). We therefore asked which eosinophil-recruiting or activating factors trigger the intratumoral accumulation of eosinophils upon cisplatin and ICB treatment. Analysis of a broad panel of eosinophil-related cytokines and chemokines revealed that IL-33 was specifically increased upon cisplatin and ICB therapy in the plasma of metastasis-bearing mice at the responsive phase of therapy (Figure 6A). Similarly, IL-33 levels were increased in tumor lysates and serum of KEP-tumor bearing mice treated with cisplatin and ICB (Figure 6B and S7A). Importantly, in patients with metastatic TNBC responding to ICB we observed a strong positive correlation between the eosinophil gene signature and IL-33 expression in metastatic lesions which was not observed in non-responders, suggesting a link between IL-33 expression and eosinophil infiltration in the TME of patients (Figure 6C). Of note, in both patients and mice, cisplatin alone was not sufficient to induce a statistically significant increase in IL33 levels (Figure 6B & S7A,B). IL-33 is an alarmin that amplifies immune responses during inflammation⁴⁸. IL-33 directly promotes eosinophil activation, adhesion and survival⁴⁹⁻⁵⁰, and IL-33 contributes to several eosinophilic disorders⁵¹. In the cancer context, IL-33 has been associated with both pro- and anti-tumor functions^{14,52,53}. To assess the functional role of IL-33 in intratumoral eosinophil accumulation, we made use of the IL-33-TRAP fusion protein, a high-affinity IL-33 antagonist⁵⁴. In line with our earlier observation that IL-5 is responsible for ICB-induced systemic eosinophilia (Figure 5), IL-33 neutralization did not affect systemic eosinophil accumulation during cisplatin and ICB therapy (Figure 6D). However, intratumoral eosinophil infiltration was abrogated upon blockade of IL-33 (Figure 6E), indicating that IL-33 is required, directly or indirectly, for eosinophil recruitment to the tumor. Importantly, IL-33 neutralization also prevented the ICB and cisplatin-induced CD8⁺ T-cell activation in tumors without affecting other immune cell populations (Figure 6F & S7C,D), phenocopying the effect achieved with eosinophil depletion (Figure 4). Importantly, IL-33-TRAP is blocking the therapeutic benefit provided by CIS + ICB (Figure 6G). In summary, these data demonstrate that IL-33 is required for eosinophil infiltration in the tumor, CD8⁺ T cell activation, and therapeutic benefit observed upon cisplatin and ICB treatment. These preclinical findings are supported by our clinical observation that increased intratumoral eosinophil infiltration is strongly correlated to IL-33 expression as well as to CD8⁺ T cells in the TME of TNBC patients responding to ICB (Figure 2C-H & 6C).

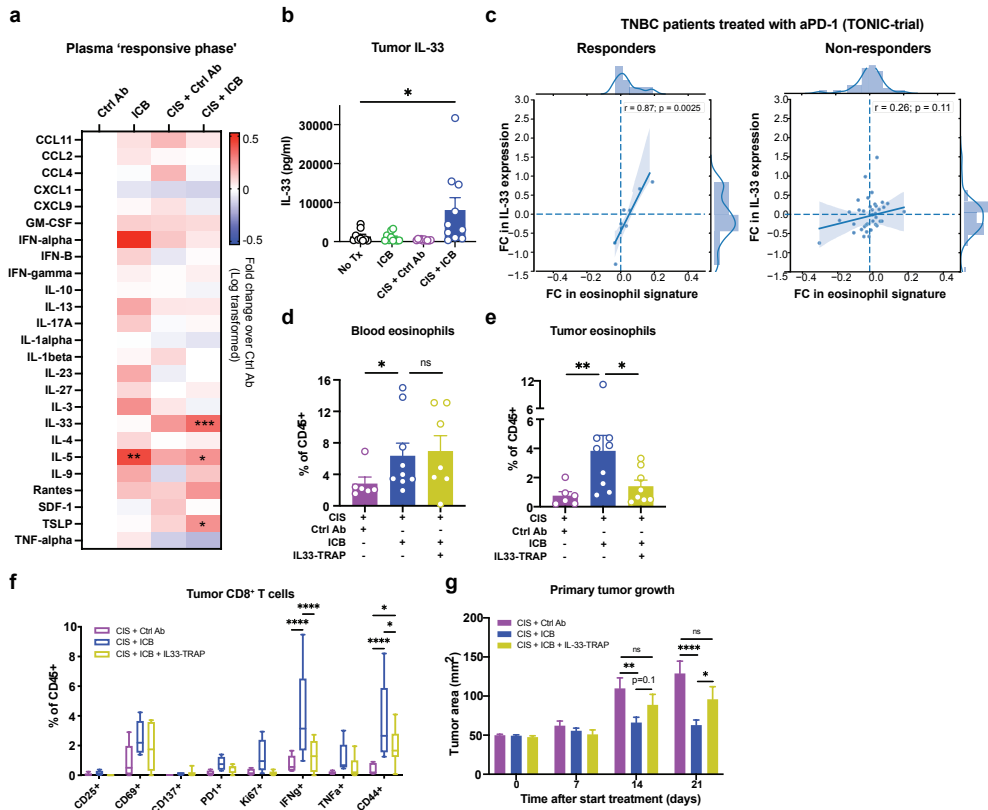


Figure 6. IL-33 drives intratumoral eosinophil infiltration and is required for the therapeutic benefit of CIS + ICB. (a) Relative expression of the indicated cytokines in plasma of metastasis-bearing mice treated as described before (Ctrl Ab n=9 (same data as in Figure 5F), ICB n=10 (same data as in Figure 5F), CIS + Ctrl Ab, n=9, CIS + ICB n=13), as determined by Legend Plex. Plasma cytokine levels were normalized to Ctrl Ab-treated mice. 1-way ANOVA or Kruskal-Wallis followed by Dunnett's or Dunn's multiple comparisons test, comparing each treatment against control-treated mice, for each cytokine. (b) IL-33 levels in tumor lysates of end-stage tumors as determined by Legend Plex (n=9-10). 1-way ANOVA followed by Dunnett's multiple comparisons test, comparing each group against untreated. (c) Paired biopsies of metastases from TNBC patients treated with nivolumab in the TONIC-trial were assessed by RNA-sequencing analysis. Correlation between the fold change (baseline to on nivo) in an eosinophil gene signature (described in Figure 2B) and the fold change (baseline to on nivo) in IL-33 in responding (left) and non-responding (right) patients with metastatic TNBC. Graph characteristics as in Figure 2. (d-e) Frequency of eosinophils in the circulation (d) and tumor (e) of KEP mice analyzed 21 days after start of treatment determined by flow cytometry (n=6-9). Mean \pm S.E.M., Mann-Whitney. (f) Frequency of CD8⁺ T cells in the tumor expressing the indicated activation markers, determined by flow cytometry (n=5-9). Data from CIS + Ctrl Ab and CIS + ICB are the same mice as in Figure 4G. Boxes represent median and interquartile range; whiskers represent full range. 2-way ANOVA followed by Tukey's multiple comparison test. (g) Average growth size \pm S.E.M. of KEP mice treated as indicated (CIS + Ctrl Ab n = 23, CIS + ICB n=32), CIS + ICB + IL33-TRAP n = 12). Unpaired t-test. ns, not significant, *p<0.05, **p<0.01, ***p<0.001, ****p<0.0001.

Recombinant IL-33 engages eosinophils and enhances response to ICB

In light of our finding that IL-33 drives eosinophil infiltration into the tumor, we hypothesized that deliberate induction of intratumoral accumulation of ICB-educated eosinophils by recombinant IL-33 (rIL-33) might represent a viable strategy to enhance the therapeutic benefit of ICB in breast cancer, in absence of

chemotherapy. Treatment of mice bearing orthotopically transplanted KEP tumors with rIL-33 alone or in combination with ICB resulted in increased eosinophils in the blood and bone marrow, as well as increased intratumoral eosinophil infiltration (Figure 7A-C). However, only the combination of ICB and rIL-33 increased CD8⁺ T-cell activation, and most notably increased the frequency of effector CD44⁺ and PD-1⁺ CD8⁺ T cells (Figure 7D), without altering other immune cell populations assessed (Figure 7E,F). Importantly, IL-33-mediated engagement of eosinophils during ICB and the resulting CD8⁺ T cell activation was accompanied by improved tumor control and extension of survival (Figure 7E,F). Collectively, these data provide proof-of-principle that rIL-33 can engage eosinophils and represents a viable strategy to enhance response to ICB in breast cancer.

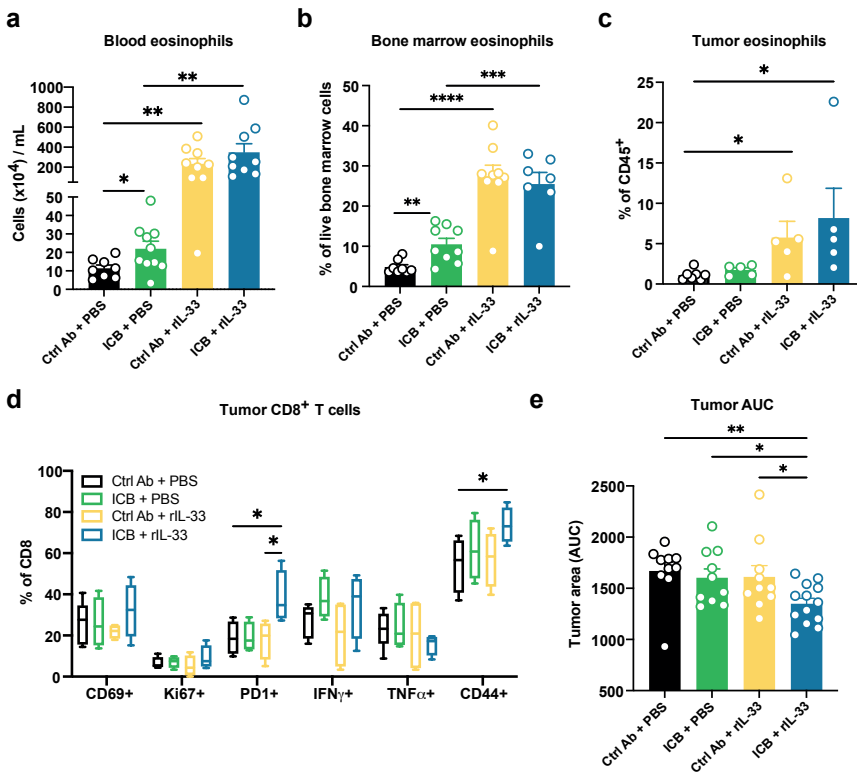


Figure 7. (continued on next page) Recombinant IL-33 therapy engages eosinophils and enhances ICB response.

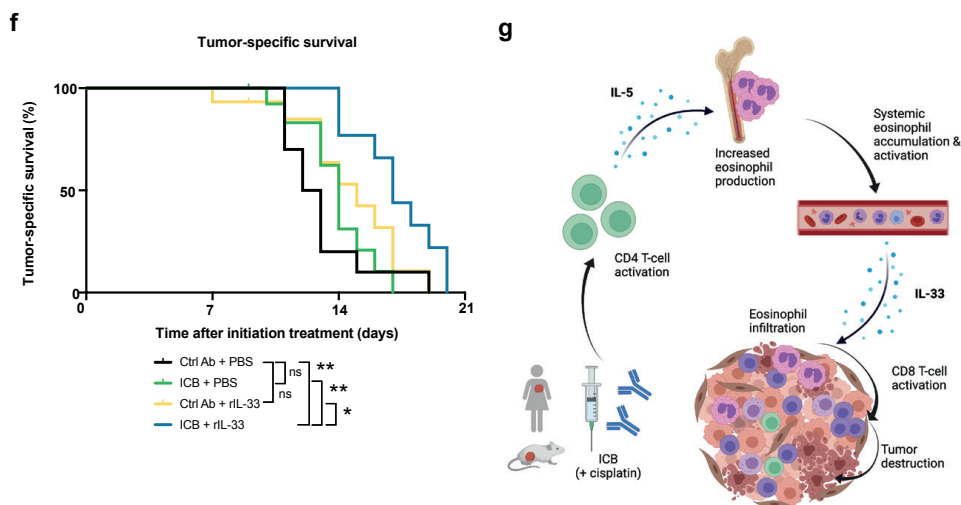


Figure 7. Recombinant IL-33 therapy engages eosinophils and enhances ICB response. (a-c) Mice bearing orthotopically transplanted KEP tumors were treated as indicated (Ctrl Ab + PBS, n=10; ICB + PBS, n=15; Ctrl Ab + rIL-33, n=15; ICB + rIL-33, n=15). Frequency of eosinophils in the circulation (a), bone marrow (b), and tumor (c) were analyzed in the responsive phase of therapy, as determined by flow cytometry. Mean \pm S.E.M., t-test. (d) Frequency of indicated activation markers expressed on CD8⁺ T cells in the tumor in responsive phase of therapy, determined by flow cytometry (n=5-7). Boxes represent median and interquartile range; whiskers represent full range. 2-way ANOVA followed by Tukey's multiple comparison test. (e) Area under curve (AUC) of growth curves was determined up to day 14 after start of treatment. Mean \pm S.E.M., 1-way ANOVA. (f) Kaplan-Meier survival curves showing tumor-related survival. Log-rank (Mantel-Cox) test. (g) Schematic summarizing figure showing how ICB and chemotherapy treatment induces IL-5 production by CD4⁺ T cells, leading to eosinophil production in the bone marrow and systemic accumulation, IL-33-driven eosinophil tumor infiltration and consequent intratumoral CD8⁺ T cell activation, which drives therapeutic benefit. Created with Biorender.com. ns, not significant, * $p < 0.05$, ** $p < 0.01$, *** $p < 0.001$, **** $p < 0.0001$.

Discussion

In this study, we take a translational approach by combining longitudinal analysis of fresh blood and tumor biopsy samples of a unique patient cohort with functional experiments in clinically relevant mouse models. We demonstrate that ICB-induced eosinophils are critical for intratumoral CD8⁺ T-cell activation and treatment response in breast cancer. Using preclinical mouse models, we mechanistically demonstrate that ICB-induced eosinophilia is mediated via CD4⁺ T cell-derived IL-5 which results in increased eosinophil production from the bone marrow and systemic eosinophil expansion. Additional induction of the alarmin IL-33, either via combination of cisplatin and ICB or rIL-33 administration, facilitates the intratumoral accumulation of ICB-induced eosinophils which, in turn, improves intratumoral CD8⁺ T-cell activation and response to ICB. In line with these preclinical findings, we demonstrate that nivolumab treatment induces IL-5 upregulation in CD4⁺ T cells of TNBC patients. Moreover, the link between IL-33 and eosinophil infiltration in the TME was validated in patients responding to ICB. In summary, we

identified the IL-5 and IL-33-eosinophil axis as a crucial mediator of ICB response in breast cancer (Figure 7G) and expose new avenues to improve the efficacy of ICB.

The effect of ICB on myeloid cells and the influence of myeloid cells on ICB response is often overlooked. We here show that an ICB-induced increase in systemic IL-5, driven by CD4⁺ T cells, pushes myelopoiesis towards increased eosinophil production resulting in systemic eosinophil accumulation. Here, parallels can be drawn with allergic conditions in which CD4⁺ T cells and eosinophils have a pathogenic function. In patients with allergic asthma, CD4⁺ T cells play a major role in the pathophysiology driving eosinophil expansion via IL-5 production^{44,55}. How ICB triggers this mechanism in the cancer context is not fully elucidated, but we demonstrated that CD4⁺ T cells of TNBC patients upregulate IL-5 *in vivo* and *in vitro* upon stimulation with nivolumab/aPD1 (Figure 5S,T), indicating that ICB can directly stimulate CD4⁺ T cells to secrete IL-5. A role for PD-1/PD-L1 signaling in controlling IL-5 secretion from CD4⁺ T cells has previously also been proposed in the context of allergy, where *in vitro* exposure of human allergen-specific CD4⁺ T cells to PD-L1 blockade stimulated their production of IL-5, among other cytokines⁵⁶. Altogether, we demonstrate that ICB-activated CD4⁺ T cells use a similar mechanism via IL-5 to drive eosinophil accumulation in cancer patients and preclinical mouse models.

Although other granulocytes, namely neutrophils and basophils, also derive from the common-myeloid progenitor (CMP) population, express IL5R and can respond to IL-5 in certain inflammatory conditions^{57,58}, IL-5 is the central cytokine specific to eosinophil development in the bone marrow⁵⁹. However, IL-33 is also implicated in eosinophil development, capable of inducing IL-5 and upregulating IL-5R α on eosinophil progenitors⁶⁰. Interestingly, we observe that ICB, in absence of chemotherapy, increases IL-5 expression but not IL-33, indicating that ICB-induced systemic IL-5 is not dependent on IL-33. This is further supported by our observation that there were no changes in systemic eosinophil abundance upon IL-33 blockade during cisplatin and ICB treatment (Figure 6D), confirming that IL-5 is the main driver of eosinophil production in the bone marrow and systemic eosinophil accumulation upon ICB.

We demonstrate that ICB can be sufficient to induce systemic eosinophil increase, but in the majority of patients and in our mouse models (which do not respond to ICB alone), this is not enough to achieve intratumoral eosinophil infiltration. We uncover that induction of IL-33 is needed to overcome this threshold and enable eosinophil infiltration into the tumor. IL-33 can either directly affect eosinophil activation and recruitment, as has been shown for eosinophils in inflammatory diseases^{49,50}, or indirectly by acting on other cells of the tumor microenvironment, for instance by promoting chemokine expression in tumor cells¹⁶. IL-33 can be passively released by epithelial cells upon cellular damage⁶¹ or actively secreted by immune cells during infection⁶² and tumor cells themselves⁶³. Importantly, in our mouse models cisplatin alone was not sufficient to increase IL-33 expression, indicating that cell damage induced by chemotherapy is not the sole driver of

increased IL-33. By combining cisplatin with ICB we were able overcome this threshold and kick start the IL-33 aspect of the cascade in our mouse models. Future research is warranted to understand which other therapeutic modalities besides cisplatin may induce intratumoral IL-33 and whether these depend on cancer cell-intrinsic features or context-dependent mechanisms remains to be elucidated. For example, in patients the net-biological effect of IL33 is influenced by levels of soluble ST2 (also known as IL1rl1), which acts as a decoy receptor for IL-33, and for which different genetic variants exist in humans⁶⁴. Thus, adding layers of complexity to the regulation of the identified immune axis.

Identifying the source of IL-33 and deciphering how its production is regulated during ICB would be important to further harness its full therapeutic potential to synergize with ICB. The synergy between rIL-33 and ICB has been studied in highly immunogenic models^{65,66}, but not, to our knowledge, in poorly immunogenic breast cancer models. Our observation that IL-33 expression correlates with an eosinophil signature in metastases of breast cancer patients that respond to ICB and our preclinical proof-of-principle study demonstrating that rIL-33 mobilizes eosinophils to improve ICB response, indicate that IL-33 represents an attractive engager of eosinophils in breast cancer patients during ICB. However, IL-33 is reported to have pleiotropic functions⁶⁷. The systemic administration of rIL-33, as performed in this study, induced an effective but modest anti-tumor response, especially in comparison with cisplatin in combination with ICB, likely because of the direct anti-tumor effect and additional immunomodulatory properties of cisplatin^{68,69}. Further studies are needed to evaluate whether IL-33 in combination with ICB could be used to specifically engage eosinophils in patients, for instance by local IL-33 administration, although, in the context of multi-organ metastatic disease, local administration of rIL-33 would be challenging.

It has previously been suggested that ICB-induced eosinophils may exert direct tumoricidal effects or enhance anti-tumor immunity by changing the tumor vasculature or reshaping the immune landscape⁶. Eosinophils can facilitate recruitment of CD8⁺ T cells by expression of T-cell chemo attractants^{11,25} or promote T-cell activation in the tumor¹³. We demonstrate that eosinophils enhance CD8⁺ T-cell activation (Figure 4G), rather than their recruitment (Figure 4F), in mammary tumors responding to ICB and chemotherapy. In line with our findings in mouse models, we observed that increased expression of an eosinophil gene signature correlated with increased CD8⁺ T-cell and IFN γ gene signatures in metastatic lesions of breast cancer patients responding to ICB (Figure 2). This suggests that in TNBC patients, eosinophils also contribute to ICB response via activation of CD8⁺ T cells, as was previously proposed for melanoma patients¹⁹. It remains to be determined whether eosinophils exert this function directly, for example by producing T-cell stimulating cytokines or chemokines, or indirectly via activation of for instance dendritic cells, as has been described during allergic inflammation⁷⁰⁻⁷².

In our study, the treatment of mice and patients differed. Where in our mouse models cisplatin and dual ICB was needed to induce responses, patients were treated with ICB alone or precluded by a brief course of different chemotherapy regimens or irradiation. Despite these differences in dosage regime and type of ICB therapy, we strikingly uncovered the same phenomena of increased eosinophils in response to ICB, indicating that the mechanism we describe in our study is a general feature of effective ICB response. This is supported by our observation that response to ICB leads to eosinophil accumulation in several cancer types (Figure S3) and further indicated by a recent small series of 14 TNBC patients in which an eosinophil increase was observed upon response to anti-PD-L1 and paclitaxel⁷³. In addition, we have validated in patients the different elements of the mechanism that we identified in our preclinical mouse models. We observed that circulating CD4⁺ T cells of TNBC patients upregulate IL-5 expression upon nivolumab treatment *in vivo* and *in vitro*. Moreover, our data demonstrating that IL-5 is secreted in tumors that show an immunological response (PDTF-R) upon *ex vivo* ICB stimulation with either aPD-1 or combined aPD-1 + aCTLA-4, further strengthens our conclusion that IL-5 induction is a common mechanism across different tumor types and ICB regimens with or without chemotherapy.

Finally, it has been suggested that increased eosinophil counts upon ICB could be used as an early predictive biomarker for response¹⁹⁻²⁴. Although we see expansion of these cells upon response to ICB in patients with metastatic TNBC, NSCLC and early-stage pMMR CC, on-treatment response biomarkers are rarely used in oncology due to widely available imaging methods for response assessment. Moreover, eosinophil expansion was not only observed in responders, but also in a proportion of non-responders as previously observed, limiting its potential for clinical decision making¹⁹⁻²⁴. Therefore, the increase in eosinophils upon ICB response, combined with our preclinical proof of their causal role in ICB response, should be considered as an important lead for the development of novel immunomodulatory strategies to engage eosinophils rather than a biomarker.

In conclusion, this study highlights that combining translational research on clinical trials with mechanistic research in preclinical mouse models is a powerful strategy to unravel novel mechanisms of ICB response. We demonstrate that eosinophils are required for ICB response by a newly identified mechanism, in which ICB induces eosinophil mobilization from the bone marrow and systemic eosinophil release via IL-5 producing CD4⁺ T cells. Additionally, we identified IL-33 as being responsible for eosinophil infiltration in the tumor site, with subsequent increased CD8⁺ T-cell activation. Our findings highlight that successful anti-tumor immune responses are not only reliant on T cells, but that crosstalk with myeloid cells is critical for an effective response to ICB, providing new avenues for future research in immunoncology.

STAR Methods

Key Resources table

The Key resources table can be found in the online version of the article.

Resource availability

Lead contact

Requests for further information and resources of this study should be directed to Karin de Visser (k.d.visser@nki.nl)

Materials availability

This study did not generate new unique reagents.

Data and code availability

- RNA-sequencing data on mouse eosinophils generated in this study has been deposited at Gene Expression Omnibus (GEO) under accession number GSE210895 and are publicly available from the date of publication. RNA-sequencing data on tumor biopsies of TNBC patients treated in the TONIC-trial stage 1 are deposited at the European Genome-phenome Archive (EGA) under accession number EGAS0001003535 and will be made available from the corresponding author on reasonable request. NanoString data from TONIC-trial stage 1 and RNAseq data of TNBC patients treated in TONIC-trial stage 2 reported in the paper are not deposited in a public repository pending ongoing work but can be made available from the corresponding authors upon reasonable request. All human data requests will be reviewed by the Institutional Review Board (IRB) of the NKI and applying researchers have to sign a data transfer agreement after IRB approval before the data can be released.
- This paper does not report original code.
- Any additional information required to re-analyze the data reported in this paper is available from the lead contact upon request.

Experimental model and subject details

Preclinical mouse models. The transgenic *Keratin14-cre;Cdh1^{F/F};Trp53^{F/F}* (KEP) model for primary mammary tumorigenesis³⁴ (FVB/N genetic background), KEP-based orthotopic mammary tumor model and the KEP-based model for spontaneous breast cancer metastasis³⁵ were used as previously described^{26,27}. Female KEP mice were monitored twice per week for spontaneous tumor formation by palpation starting at the age of 3.5 months. The perpendicular diameters of the tumors were measured using a caliper and tumor area was calculated accordingly. In the spontaneous KEP model, all treatments started when tumor area reached 50mm².

For the KEP-based orthotopic mammary tumor model, mammary tumor pieces of 1mm² size derived from KEP mice were orthotopically transplanted into the mammary glands of female FVB/N mice. In this model, treatments started when tumor area reached 25 mm². For the survival experiments and endpoint analysis

mice were sacrificed when the cumulative tumor burden reached 225mm². KEP mice were sacrificed 21 days after initiation treatment to analyze the ‘responsive phase’ or at a tumor size of 150mm² for the KEP-based orthotopic mammary tumor model. Cisplatin (Accord Healthcare Limited) was injected intravenously once every two weeks at 5mg/kg, for a maximum of 4 cycles. Anti-mouse PD-1 (RMP1-14, BioXCell), anti-mouse CTLA-4 (9D9, BioXCell) or control (2A3, BioXCell) antibodies were each given intraperitoneally at 100µg per mouse, twice per week. Anti-CD8 (2.43, BioXCell) or anti-CD4 (GK1.5, BioXCell) antibody were given intraperitoneally at 200µg per mouse, twice per week. Anti-mouse SiglecF (238047, R&D systems) and control antibody (2A3, BioXCell) were administered intraperitoneally at 20µg per mouse, three times a week. Anti-IL-5 (TRFK5, BioXCell) and control antibody (HRPN, BioXCell) were given intraperitoneally at 500µg per mouse, twice per week. Recombinant mouse IL-33 (Biolegend) was given intraperitoneally at 0,4 µg per mouse, three times a week. IL-33-TRAP (provided by Rudi Beyaert laboratory, VIB, Belgium) was given intraperitoneally at 50µg per mouse daily. For the T_{reg} depletion in *Foxp3-GFP-DTR* mice, DT (Diphtheria toxin from *Corynebacterium diphtheriae*) was given intraperitoneally at 25µg/kg, at day 0 and day 4 after start of treatment. All antibody treatments continued until the experimental endpoint was reached.

For metastasis experiments, Female FVB/N mice of 8-12 weeks of age were obtained from Janvier Labs. Mammary tumor pieces of 1mm² size derived from KEP mice were orthotopically transplanted into the mammary glands. Mammary tumors were surgically removed when they reached the size of 100mm². In the metastasis experiments, all treatments started 15 days after mastectomy, when all mice have established metastasis in the lung and/or lymph node, and treatments continued until the experimental endpoint. All treatments were performed as described above. For survival experiments, mice were sacrificed when they developed signs of distress caused by metastatic disease (respiratory distress) or when lymph node metastasis reached the size of 225mm². For analysis of ‘responsive phase’, metastasis-bearing mice were sacrificed 10 days after start of treatment for Ctrl Ab and ICB groups and 21 days for CIS+Ctrl Ab and CIS+ICB groups.

Rag1 k.o. in FVB/N genetic background were a gift from L. Coussens⁷⁴. *Cdh1*^{F/F}; *Trp53*^{F/F}; *Foxp3*^{DTR-GFP} mice⁷⁵ in FVB background were generated by the Animal Modeling Facility (AMF) of the Netherlands Cancer Institute. All mice were kept in individually ventilated cages at the animal laboratory facility of the NKI. Food and water were provided ad libitum.

Clinical trial procedures. Trial procedures were performed as described previously in the respective publications²⁸⁻³¹. All patients included in stage 1²⁸ and stage 2 of the TONIC-trial (NCT02499367) were included in the current analysis. In stage 1, 70 patients were included in the TONIC-trial, of which 67 patients received nivolumab and were available for efficacy and translational analysis, as previously described²⁸. An additional 47 patients were included in stage 2 of the trial, of which 44 patients received nivolumab and were available for efficacy and translational analysis. From these 111 patients (Supplementary Table 1), paired flow cytometry

on fresh blood (baseline, after two-week induction period and after 3 cycles of nivolumab) was performed on 55 patients and paired routine eosinophil counts were available for 90 patients (sample availability in Supplementary Table 2 and Figure S1b). Progression-free survival was measured as time between date of randomization and date of progression according to iRECIST or date of death. Overall survival was measured as time between first date of nivolumab and date of last follow-up or date of death. Data was cut-off at 1 March 2021.

Patients with metastatic NSCLC were treated in the PEMBRO-RT trial (NCT02492568)²⁹ at the NKI (paired data for n=40 from the total of 55 patients treated at the NKI and the total of 76 patients included in the trial), in which patients were randomized to pembrolizumab with or without upfront radiation²⁹. To investigate eosinophil dynamics in patients with metastatic dMMR tumors, we made use of patients treated with nivolumab in the NKI within the dMMR cohort (paired data for n=9 of the total 11 patients treated at the NKI and the total of 30 patients included in the cohort) of the DRUP-trial (NCT02925234)³¹. Finally, patients with early-stage colon cancer (either dMMR (n=21) or pMMR (n=17)) were treated in the NICHE-trial, in which patients are treated with neo-adjuvant ipilimumab (1mg/kg) and nivolumab (3mg/kg), with or without additional celecoxib in pMMR patients (NCT03026140)³⁰. In the patients with metastatic disease, response was defined as complete response (CR), partial response (PR) and stable disease (SD) of at least 24 weeks, defined according to RECIST1.1⁷⁶. Best overall response in the TONIC-trial was measured according to iRECIST⁷⁷. Response in the NICHE-trial was defined as any pathological response (>10% tumor regression), assessed on surgical material after neo-adjuvant treatment.

Study approval. All animal experiments were approved by the Animal Ethics Committee of the NKI and performed in compliance with the national and European guidelines for animal care and use. All clinical study protocols were approved by the medical-ethical committee of the NKI and conducted in accordance with the ICH Harmonized Tripartite Guideline for Good Clinical Practice and the principles of the Declaration of Helsinki. All patients provided written informed consent to participate in the clinical trial.

Method details

Flow cytometry analysis. Tumors and organs from KEP mice and FVB/N mice with metastatic breast cancer were collected in ice-cold PBS. Blood was withdrawn by tail vein or heart puncture and collected in K₂EDTA-containing tubes (BD Microtainer Blood Collection Tubes). Tumor tissues and lungs were mechanically minced using the McIlwain tissue chopper (Mickle Laboratory Engineering) and enzymatically digested at 37°C in DMEM medium containing 3mg/ml collagenase type A (Roche) plus 25µg/ml of DNase I (Sigma) for 45 min or in 100µg/mL Liberase TM (Roche) for 30 min, respectively. Half of the lymph nodes and spleen were enzymatically digested in RPMI medium containing 3mg/ml collagenase type IV (ThermoFisher Scientific), 2mM CaCl₂, 2% FCS and 25µg/mL DNase I for 30 min at 37°C and used to stain for myeloid cell populations. The other half was directly processed into

single cell suspensions and used for lymphoid cell panels. All digestion reactions were stopped by adding cold DMEM medium containing 10% FCS. For the analysis of bone marrow, tibia and femurs were flushed with PBS and processed as the other organs. Single-cell suspensions were obtained by mashing through 70 μ m filter and resuspended in PBS containing 0.5% BSA (Roche) and 2mM EDTA (Lonza). Blood, spleen, lungs and bone marrow samples were treated for 5 min at room temperature with NH₄ lysis buffer to remove erythrocytes.

For flow cytometry analysis of patient sample preparations, peripheral blood was collected in an K₂EDTA vacutainer (BD) and processed and analyzed within 24 hours. Red blood cells were lysed (lysis buffer: dH₂O, NH₄Cl, NaHCO₃, EDTA) and cells were resuspended in PBS containing 0.5% BSA and 2mM EDTA. To obtain absolute white blood cell counts per mL of human blood, the total post-lysis cell count was obtained using the NucleoCounter NC-200 (Chemometec) Automated cell counter was divided by the total volume (mL) of blood.

For intracellular cytokine staining, cells were stimulated *ex vivo* with 50ng/ml PMA, 1 μ M ionomycin and Golgi-Plug (1:1000; BD) for 3h at 37°C in IMDM medium supplemented with 8% FCS, 100 IU/ml Penicillin-Streptomycin (Roche) and 0.5% β -mercaptoethanol. For surface antigen staining, cells were first incubated with rat anti-mouse CD16/CD32 antibody (1:100; Mouse Fc Block, BD Bioscience) or human FcR Blocking Reagent (1:100 Miltenyi) for 15 min at 4°C and then incubated with fluorochrome-conjugated antibodies for 30 min at 4°C, in the dark. For intracellular antigen staining, cells were fixed with Fixation/Permeabilization solution 1X (Foxp3/Transcription Factor Staining Buffer Set, eBioscience) for 30 min at 4°C and stained with fluorochrome-conjugated antibodies in Permeabilization buffer 1X (eBioscience) for 30 min at room temperature. Viability was assessed by staining with either 7AAD staining solution (1:20; eBioscience), Zombie Red Fixable Viability Kit (1:800 BioLegend) or with Fixable Viability Dye APC-eFluor780 (1:1000; eBioscience). Data acquisition was performed on BD LSRII flow cytometer using Diva software (BD Biosciences) and data analysis was performed using FlowJo software version 10.6.2. All used flow cytometry antibodies can be found in Key Resources Table. Gating strategies are displayed in Figures S8 and S9.

Immunohistochemistry. KEP tumors were fixed for 24h in 10% neutral buffered formalin, embedded in paraffin and sectioned at 4 μ m. CD4, CD8, FOXP3 and Ly6G stainings were performed by the Experimental Animal Pathology facility of the NKI. Antibodies are listed in Key Resources Table. For MBP staining, sections were deparaffinized in xylene for 20 min, rehydrated, and incubated with 3% H₂O₂ for 10 min at room temperature. Antigen retrieval was performed using Pepsin solution (ThermoFischer Scientific) for 10 min at room temperature. As blocking solution PBS with 2.5% BSA and 10% normal goat serum was used for 30 min at room temperature. Sections were incubated with rat anti-mouse MBP antibody (1:350, clone MT-14.7.3, Lee Laboratory, Mayo Clinic) diluted in 0.5X blocking solution, overnight at 4°C. Biotinylated goat anti-rat IgG antibody (1:300, Southern Biotech) was used as secondary antibody. Streptavidin-HRP and DAB solution (DAKO) were

used following manufacturer's instructions. Sections were counterstained with hematoxylin solution. Slides were scanned using Aperio ScanScope and analyzed with Aperio ImageScope software version 12.4.3 (Aperio, Vista).

RNA-sequencing of mouse eosinophils. For the transcriptomic analysis, a minimum of 35000 eosinophils (CD11b⁺ Ly6G^{low} SSC^{high} F4/80⁺) were sorted from the blood in RLT buffer containing 1% μ -ME, using a BD FACSAria™ Fusion Cell Sorter. RNA was isolated following RNeasy Mini Kit (Qiagen) protocol, using 80% ethanol instead of RPE buffer. Smart-seq2 library preparation was performed as previously described⁷⁸, using 2100 Bioanalyzer System (Agilent) for quality control. Only samples with RIN ≥ 7 were used for RNA-sequencing analysis. The strand-specific reads (65bp single-end) were sequenced with the HiSeq 2500 System (Illumina). Demultiplexing of the reads was performed with Illumina's bcl2fastq software and demultiplexed reads were aligned against the mouse reference genome (build 38) using HISAT2. HISAT2 was supplied with known set of gene models (Ensembl version 87). Qlucore Omics Explorer (Qlucore AB, Lund, Sweden) software was used to calculate and visualize differentially expressed genes ($p < 0,05$) and sample variation, after having discarded genes with fewer than 30 mapped reads in at least 9 samples and performed data normalization by TMM method. Gene set enrichment analysis (GSEA) was performed using the GSEA program version 4.0.3 (Broad Institute). Hallmarks gene sets from Molecular Signatures Database v7.2 were used. Mouse gene symbols were remapped to human orthologues using Mouse_Gene_Symbol_Remapping_Human_Orthologs_MSigDB.v7.2.chip annotation file.

Cytokine analysis. For the analysis of cytokines and chemokines expression in mouse plasma, serum or tumor lysate, custom-made Legend Plex bead-based immunoassay (Biolegend) was used, according to manufacturer instructions. 50 μ g of total protein from lysed tissues was used for measurements. Data acquisition was performed on LSRFortessa (BD Biosciences) flow cytometer using Diva software (BD Biosciences) and analyzed using LEGENDplex™ Data Analysis Software Suite (Biolegend). In addition, mouse IL-5 ELISA detection kit (BioLegend) was used, according to manufacturer instructions.

Routine eosinophil counts in patient cohorts. Eosinophil counts were measured with a XN-2000 Hematology Analyzer of Sysmex at the diagnostic Clinical Chemistry Department. The variation coefficient was below 10%.

RNA extraction and NanoString gene expression analysis. RNA was isolated from freshly frozen sections of biopsies as previously described²⁸. For each patient, sequential biopsies were taken from the same metastatic lesion, however per patient, the site of the metastatic lesion was different (predominantly, but not only, lymph nodes, recurrent lesion in breast, liver, skin). mRNA expression was measured with the nCounter technology provided by NanoString Technologies as previously described²⁸. NanoString mRNA counts were available for patients included in stage 1 of the TONIC-trial (paired metastatic biopsies pre-nivo and on nivo $n = 26$).

RNA-sequencing on patient tumor biopsies. The RNA-sequencing data was aligned to the reference genome GRCh38 with STAR (version 2.7.1a)⁷⁹ with two-pass mode option set to “Basic”. For comparison between patients, a median of ratios normalization was performed with Deseq2 R package (version 1.24.0⁸⁰) and for within-patient comparisons TPM normalization was used. Data was analyzed using Python 3.7.6, with pandas (version 1.0.1^{81,82}) and NumPy (version 1.18.1⁸³) packages. Plots were created using Matplotlib (version 3.1.3⁸⁴) and Seaborn (version 0.10.0⁸⁵), statistical annotation was added using statannot (version 0.2.2⁸⁶). All gene-signatures are listed in Supplementary Table 3. Mean normalized expression values of individual genes were taken as a signature score. A fold change of the signature score baseline vs. on nivo was taken for each signature. RNA-sequencing on paired metastatic lesions (baseline and on nivo) was available for 48 patients, included in both stages of the trial.

RT-qPCR. Human CD3⁺ CD4⁺ T cells were sorted from TONIC patient PBMCs into RLT buffer containing 1% μ -ME, using a BD FACSAria™ Fusion Cell Sorter. RNA was isolated following RNeasy Micro Kit (Qiagen) protocol. RNA was converted to cDNA with an AMV reverse transcriptase using Oligo(dT) primers (Invitrogen). For mouse CD4⁺CD25⁻ T cells, RNA was converted to cDNA using High-capacity cDNA reverse transcription kit (ThermoFisher Scientific), following kit instructions. cDNA (20 ng per well) was analyzed by SYBR green real-time PCR with 500 nM primers using a LightCycler 480 thermocycler (Roche). *Gapdh* was used as a reference gene. Primer sequences used for each gene are listed in the Key Resources Table. Fold change in expression was calculated using $2^{-\Delta\Delta Ct}$ ($-\Delta\Delta Ct = \text{average}(\Delta Ct.\text{control})$).

Human PBMC stimulation. Patient PBMCs were seeded at a density of 500,000 cells per well in 96-well plates in DMEM (Sigma), 10% FBS (Sigma), 1 mM sodium pyruvate (Sigma), 1x MEM nonessential amino acids (Sigma), 1x Glutamax, 100 ng/ml penicillin/streptomycin, 50 nM 2-mercaptoethanol (Sigma). Cells were stimulated with a suboptimal concentration of 0.5 μ g/ml plate bound anti-CD3 (OKT3, BioLegend) and 2 μ g/ml anti-CD28 (28.2, eBioscience) for 48 hours. Anti-PD1 (Nivolumab) was added where indicated. GolgiPlug was added to each well for the final 4 hours of stimulation and cells were analyzed by flow cytometry as described above.

PDTF culture and stimulation. PDTF cultures were performed as described previously^{45,46}. Briefly, tumor samples were collected from surgical material of patients with renal cell carcinoma (anti-PD1+anti-CTLA-4 treated n=1 & anti-PD1 treated n=2), ovarian cancer (n=4 & n=1), melanoma (n=7 & n=5), non-small cell lung cancer (n=1 & n=3), and colorectal cancer (n=0 & n=1). Patient characteristics were described previously for samples stimulated with aPD-1 & aCTLA-4⁴⁶ and listed in Supplementary Table 4 for samples stimulated with aPD-1. Definition of responder and non-responder PDTFs were described previously^{45,46}. Samples were cut in fragments of 1-2 mm³ and embedded in an artificial extracellular matrix in a 96-well plate. PDTF cultures were stimulated with medium supplemented with either anti-PD1 alone (nivolumab, Bristol-Myers Squibb) at 10 μ g/ml or anti-PD-1

plus anti-CTLA4 (ipilimumab, Bristol-Myers Squibb) at 10 µg/ml where indicated. After 48 hours of culture at 37°C, supernatants were collected and IL-5 levels were measured using the LEGENDplex Human Th Cytokine (BioLegend), according to the manufacturer's protocol.

Quantifications and statistical analysis

Statistical analysis was performed in GraphPad Prism (version 8.4.3) or SPSS Statistics (version 24). All statistical tests were two-sided. All p-values are uncorrected for multiple testing unless stated otherwise. For heatmaps of human flow cytometry data (Figure S1C-F), \log_2 transformed cell count/mL or \log_2 transformed fold change were depicted, centered around the median for each population (row) separately. Hierarchical clustering was performed on populations and patients based on 1 minus Pearson correlation and Euclidian distance respectively. Complete-linkage was used for both cell populations and patients. To assess dynamics in each cell population analyzed by flow cytometry between baseline and on-nivo, the median \log_2 fold change from baseline to on-nivo ($\log_2(\text{on-nivo}) - \log_2(\text{pre-nivo})$) was plotted against Benjamini-Hochberg corrected p-values (Figure 1B). For dynamics in each cell population analyzed by flow cytometry between pre-nivo and on-nivo, linear modeling was performed (similar to a 2-way ANOVA) to predict \log_2 fold changes between pre-nivo and on-nivo counts / mL based on response and induction treatment:

$$\text{Log}_2\text{-fold_change} \sim \text{response} + \text{induction_treatment}$$

This model assumes that the response and induction treatment have an additive and independent effect on log fold changes. For each population responders were contrasted from non-responders. For Figure S2D, the regression coefficients associated with response for each population (x-axis) against the associated (Benjamini-Hochberg corrected) p-values (Wald-test) were plotted. The uncorrected (Wald-test) p-values associated with different induction treatments were estimated. For each population we performed a Shapiro-Wilk normality test on the regression residue to see if the normality assumption was violated.

Additional Resources

This paper included flow cytometry and hemocytometer data of blood samples and RNAseq data of tumor biopsies from patients with metastatic TNBC treated in the Netherlands Cancer Institute in the TONIC-trial (NCT02499367). This paper also included hemocytometer data on blood samples generated in the Netherlands Cancer Institute from patients with metastatic NSCLC treated in the PEMBRO-RT trial (NCT02492568), patients with metastatic dMMR tumors treated in the DRUP-trial (NCT02925234), and patients with early-stage colon cancer treated in the NICHE-trial (NCT03026140). Data were kindly provided by the principal investigators of the clinical trials. Further information on the clinical trial procedures and links to clinical publications can be found in the Methods section on clinical trial procedure and Key Resources Table.

Acknowledgements

We thank the patients and their families for participating in the clinical studies. We thank the Dutch Cancer Society (KWF10083, KWF13191, KWF14339) and the Swiss National Science Foundation (P2FRP3_171794 and P400PM_18318/1 to L.S.) for funding the preclinical studies. We thank the BMS-International Immunology Network (BMS/II-ON) and the Dutch Cancer Society (NKI2015-7710) for funding the TONIC study. The Dutch Cancer Society (10653ALPE) and A Sister's Hope contributed to the immunophenotyping of the TNBC patients. Research in the Kok group is funded by the Netherlands Organization for Scientific Research (NWO-VIDI 09150172010043) and the Hendrika Roet fund. Research in the De Visser laboratory is funded by the Dutch Cancer Society (KWF10623), Oncode Institute, KWF/Oncode grant 14339 and the Netherlands Organization for Scientific Research (NWO-VICI 91819616). This research was further supported by an institutional grant to the NKI of the Dutch Cancer Society and of the Dutch Ministry of Health, Welfare and Sport..S.A. holds a fundamental mandate of the Foundation against Cancer. We acknowledge the supporting staff of the clinical trials of the departments of Medical Oncology, Biometrics, Clinical Chemistry and the Triallab, in particular Daan van den Broek, Kim Kersten, Tiny Korse, Ingrid Mandjes, Els Platte, Lydia Ruiters, Karolina Sikorska and Jacqueline Zyl-de Jong. We acknowledge the Core Facility of Molecular Pathology & Biobanking and Michiel de Maaker for human RNA isolations and the Genomics Core Facility for RNA-sequencing support. We thank the Intervention Unit and the Imaging Unit of the Animal Laboratory Facility, in particular Marieke van de Ven, Renske de Korte-Grimmerink and Niels de Wit, for their support in performing the *in vivo* metastasis experiment and the MRI scans of mice with metastatic disease. We acknowledge the Experimental Animal Pathology Facility for the processing of murine tissues. Thanks to the Flow Cytometry Facility for their support throughout the entire study. Finally, we would like to thank everyone in the De Visser and Kok labs for our inspiring discussion.

Author Contributions

O.S.B., H.G., L.S., L.V., K.E.d.V and M.K. designed and performed experiments, analyzed and interpreted the data and wrote the manuscript. O.S.B., and L.S. performed the preclinical experiments with contributions from K.Ke., H.G., D.P., C.-S.H., K.V., E.A.M.R., D.K., K.Ko., I.S.A. and R.B., supervised by K.E.d.V. H.G. performed the blood phenotyping analysis of the TONIC-trial together with N.B., C.K., M.D, M.B., and K.V., supervised by K.E.d.V, and M.K.. L.V. coordinated and analyzed the data of the TONIC-trial of which M.K. is the principal investigator. O.I.I. performed bioinformatic analysis on the RNA-sequencing data of the TONIC-trial. E.v.D. performed bioinformatic and statistical analysis on blood phenotyping data of the TONIC-trial. M.C., W.T. and L.H. coordinated trial procedures and collected clinical data of the NICHE-trial, PEMBRO-RT trial and DRUP-trial, respectively. P.B. is the principal investigator of the PEMBRO-RT trial, E.E.V. is the principal investigator of the DRUP-trial. P.K. & D.S.T. developed and analyzed the data

of the PDTF platform. L.F.A.W. supervised bioinformatic and statistical analysis and contributed to interpreting the results. All authors edited and approved the manuscript.

Declaration of interests

O.S.B., H.G., L.S., L.V., O.I.I., E.v.D., N.B., C.K., M.D., K.Ke., M.B., D.P., C.S.H., K.V., E.A.M.R., D.K., L.H., K.Ko., I.S.A., P.K., R.B., and D.S.T. have no competing interests to declare. M.C. reports funding to the institute from BMS and Roche/Genentech and an advisory role for BMS, outside the submitted work. W.T. reports receiving grants from Merck Sharp & Dohme during the conduct of the PEMBRO-RT trial. P.B. reports receiving grants and medication delivery from Merck Sharp & Dohme during the conduct of the PEMBRO-RT trial as well as grants and consultancy fees from Bristol-Myers Squibb outside the submitted work. E.E.V. is legally responsible for all contracts with pharmaceutical companies at the NKI and reports research funding from BMS, outside the submitted work. L.F.A.W. reports funding to the institute from Genmab BV. K.E.d.V. reports research funding from Roche/Genentech and is consultant for Macomics, outside the scope of this work. M.K. reports funding to the institute from BMS, Roche/Genentech, AZ and an advisory role for BMS, Roche, MSD and Daiichi Sankyo, outside the submitted work.

References

1. Adams, S. et al. Pembrolizumab monotherapy for previously treated metastatic triple-negative breast cancer: cohort A of the phase II KEYNOTE-086 study. *Annals of Oncology* 30 (3), 397-404, 2019.
2. Winer, E. P. et al. Pembrolizumab versus investigator-choice chemotherapy for metastatic triple-negative breast cancer (KEYNOTE-119): a randomised, open-label, phase 3 trial. *The Lancet. Oncology* 22 (4), 499-511, 2021.
3. Schmid, P. et al. Atezolizumab plus nab-paclitaxel as first-line treatment for unresectable, locally advanced or metastatic triple-negative breast cancer (IMpassion130): updated efficacy results from a randomised, double-blind, placebo-controlled, phase 3 trial. *The Lancet. Oncology* 21 (1), 44-59, 2020.
4. Cortes, J. et al. Pembrolizumab plus chemotherapy versus placebo plus chemotherapy for previously untreated locally recurrent inoperable or metastatic triple-negative breast cancer (KEYNOTE-355): a randomised, placebo-controlled, double-blind, phase 3 clinical trial. *Lancet (London, England)* 396 (10265), 1817-1828, 2020.
5. Demaria, O. et al. Harnessing innate immunity in cancer therapy. *Nature* 574 (7776), 45-56, 2019.
6. Grisaru-Tal, S., Itan, M., Klion, A. D. & Munitz, A. A new dawn for eosinophils in the tumour microenvironment. *Nat Rev Cancer* 20 (10), 594-607, 2020.
7. Grisaru-Tal, S., Rothenberg, M. E. & Munitz, A. Eosinophil-lymphocyte interactions in the tumor microenvironment and cancer immunotherapy. *Nat Immunol* 23 (9), 1309-1316, 2022.
8. Rosenberg, H. F., Dyer, K. D. & Foster, P. S. Eosinophils: changing perspectives in health and disease. *Nature reviews. Immunology* 13 (1), 9-22, 2013.
9. Kratochvill, F. et al. TNF Counterbalances the Emergence of M2 Tumor Macrophages. *Cell reports* 12 (11), 1902-1914, 2015.
10. Zaynagetdinov, R. et al. Interleukin-5 facilitates lung metastasis by modulating the immune microenvironment. *Cancer Res* 75 (8), 1624-1634, 2015.
11. Carretero, R. et al. Eosinophils orchestrate cancer rejection by normalizing tumor vessels and enhancing infiltration of CD8(+) T cells. *Nature immunology* 16 (6), 609-617, 2015.
12. Jia, S., Li, W., Liu, P. & Xu, L. X. A role of eosinophils in mediating the anti-tumour effect of cryothermal treatment. *Sci Rep* 9 (1), 13214, 2019.
13. Arnold, I. C. et al. The GM-CSF-IRF5 signaling axis in eosinophils promotes antitumor immunity through activation of type 1 T cell responses. *J Exp Med* 217 (12), e20190706, 2020.
14. Hollande, C. et al. Inhibition of the dipeptidyl peptidase DPP4 (CD26) reveals IL-33-dependent eosinophil-mediated control of tumor growth. *Nature immunology* 20 (3), 257-264, 2019.
15. Reichman, H. et al. Activated Eosinophils Exert Antitumorogenic Activities in Colorectal Cancer. *Cancer immunology research* 7 (3), 388-400, 2019.
16. Andreone, S. et al. IL-33 Promotes CD11b/CD18-Mediated Adhesion of Eosinophils to Cancer Cells and Synapse-Polarized Degranulation Leading to Tumor Cell Killing. *Cancers (Basel)* 11 (11), 1664, 2019.
17. Varricchi, G. et al. Eosinophils: The unsung heroes in cancer? *Oncoimmunology* 7 (2), e1393134, 2018.
18. Grisaru-Tal, S. et al. Metastasis-Entrained Eosinophils Enhance Lymphocyte-Mediated Antitumor Immunity. *Cancer Res* 81 (21), 5555-5571, 2021.
19. Simon, S. C. S. et al. Eosinophil accumulation predicts response to melanoma treatment with immune checkpoint inhibitors. *Oncoimmunology* 9 (1), 1727116, 2020.
20. Delyon, J. et al. Experience in daily practice with ipilimumab for the treatment of patients with metastatic melanoma: an early increase in lymphocyte and eosinophil counts is associated with improved survival. *Ann Oncol* 24 (6), 1697-1703, 2013.
21. Gebhardt, C. et al. Myeloid Cells and Related Chronic Inflammatory Factors as Novel Predictive Markers in Melanoma Treatment with Ipilimumab. *Clinical Cancer Research* 21 (24), 5453-5459, 2015.
22. Alves, A., Dias, M., Campaignha, S. & Barroso, A. Peripheral blood eosinophilia may be a prognostic biomarker in non-small cell lung cancer patients treated with immunotherapy. *J Thorac Dis* 13 (5), 2716-2727, 2021.

23. Okauchi, S. et al. Association between peripheral eosinophils and clinical outcomes in patients with non-small cell lung cancer treated with immune checkpoint inhibitors. *Pol Arch Intern Med* 131 (2), 152-160, 2021.
24. Verhaart, S. L. et al. Real-world Data of Nivolumab for Patients With Advanced Renal Cell Carcinoma in the Netherlands: An Analysis of Toxicity, Efficacy, and Predictive Markers. *Clin Genitourin Cancer*, 2020.
25. Zheng, X. et al. CTLA4 blockade promotes vessel normalization in breast tumors via the accumulation of eosinophils. *Int J Cancer* 146 (6), 1730-1740, 2020.
26. Coffelt, S. B. et al. IL-17-producing $\gamma\delta$ T cells and neutrophils conspire to promote breast cancer metastasis. *Nature* 522 (7556), 345-348, 2015.
27. Salvagno, C. et al. Therapeutic targeting of macrophages enhances chemotherapy efficacy by unleashing type I interferon response. *Nature cell biology* 21 (4), 511-521, 2019.
28. Voorwerk, L. et al. Immune induction strategies in metastatic triple-negative breast cancer to enhance the sensitivity to PD-1 blockade: the TONIC trial. *Nat Med* 25 (6), 920-928, 2019.
29. Theelen, W. et al. Effect of Pembrolizumab After Stereotactic Body Radiotherapy vs Pembrolizumab Alone on Tumor Response in Patients With Advanced Non-Small Cell Lung Cancer: Results of the PEMBRO-RT Phase 2 Randomized Clinical Trial. *JAMA Oncol* 5 (9), 1276-1282, 2019.
30. Chalabi, M. et al. Neoadjuvant immunotherapy leads to pathological responses in MMR-proficient and MMR-deficient early-stage colon cancers. *Nature Medicine* 26 (4), 566-576, 2020.
31. van der Velden, D. L. et al. The Drug Rediscovery protocol facilitates the expanded use of existing anticancer drugs. *Nature* 574 (7776), 127-131, 2019.
32. Kikly, K. K. et al. Identification of SAF-2, a novel siglec expressed on eosinophils, mast cells, and basophils. *J Allergy Clin Immunol* 105 (6 Pt 1), 1093-1100, 2000.
33. Ayers, M. et al. IFN-gamma-related mRNA profile predicts clinical response to PD-1 blockade. *The Journal of clinical investigation* 127 (8), 2930-2940, 2017.
34. Derksen, P. W. et al. Somatic inactivation of E-cadherin and p53 in mice leads to metastatic lobular mammary carcinoma through induction of anoikis resistance and angiogenesis. *Cancer cell* 10 (5), 437-449, 2006.
35. Doornebal, C. W. et al. A preclinical mouse model of invasive lobular breast cancer metastasis. *Cancer research* 73 (1), 353-363, 2013.
36. Beyranvand Nejad, E. et al. Tumor Eradication by Cisplatin Is Sustained by CD80/86-Mediated Costimulation of CD8+ T Cells. *Cancer Res* 76 (20), 6017-6029, 2016.
37. Nolan, E. et al. Combined immune checkpoint blockade as a therapeutic strategy for BRCA1-mutated breast cancer. *Sci Transl Med* 9 (393), eaal4922, 2017.
38. Grimaldi, A. et al. Combination of chemotherapy and PD-1 blockade induces T cell responses to tumor non-mutated neoantigens. *Commun Biol* 3 (1), 85, 2020.
39. Wan, S. et al. Chemotherapeutics and radiation stimulate MHC class I expression through elevated interferon-beta signaling in breast cancer cells. *PLoS one* 7 (3), e32542, 2012.
40. Cheng, J. N. et al. Radiation-induced eosinophils improve cytotoxic T lymphocyte recruitment and response to immunotherapy. *Sci Adv* 7 (5), eabc7609, 2021.
41. Zimmermann, N. et al. Siglec-F antibody administration to mice selectively reduces blood and tissue eosinophils. *Allergy* 63 (9), 1156-1163, 2008.
42. Pfirschke, C. et al. Tumor-Promoting Ly-6G(+) SiglecF(high) Cells Are Mature and Long-Lived Neutrophils. *Cell Rep* 32 (12), 108164, 2020.
43. Iwasaki, H. et al. Identification of eosinophil lineage-committed progenitors in the murine bone marrow. *J Exp Med* 201 (12), 1891-1897, 2005.
44. Pelaia, C. et al. Interleukin-5 in the Pathophysiology of Severe Asthma. *Front Physiol* 10, 1514, 2019.
45. Voabil, P. et al. An *ex vivo* tumor fragment platform to dissect response to PD-1 blockade in cancer. *Nat Med* 27 (7), 1250-1261, 2021.
46. Kaptein, P. et al. Addition of interleukin-2 overcomes resistance to neoadjuvant CTLA4 and PD1 blockade in *ex vivo* patient tumors. *Sci Transl Med* 14 (642), eabj9779, 2022.
47. Kos, K. et al. Tumor-educated T(regs) drive organ-specific metastasis in breast cancer by impairing NK cells in the lymph node niche. *Cell Rep* 38 (9), 110447, 2022.
48. Chan, B. C. L., Lam, C. W. K., Tam, L. S. & Wong, C. K. IL33: Roles in Allergic Inflammation and Therapeutic Perspectives. *Frontiers in immunology* 10, 364, 2019.

49. Cherry, W. B., Yoon, J., Bartemes, K. R., Iijima, K. & Kita, H. A novel IL-1 family cytokine, IL-33, potently activates human eosinophils. *J Allergy Clin Immunol* 121 (6), 1484-1490, 2008.
50. Suzukawa, M. et al. Interleukin-33 enhances adhesion, CD11b expression and survival in human eosinophils. *Lab Invest* 88 (11), 1245-1253, 2008.
51. Johnston, L. K. & Bryce, P. J. Understanding Interleukin 33 and Its Roles in Eosinophil Development. *Front Med (Lausanne)* 4, 51, 2017.
52. Shani, O. et al. Fibroblast-Derived IL33 Facilitates Breast Cancer Metastasis by Modifying the Immune Microenvironment and Driving Type 2 Immunity. *Cancer Res* 80 (23), 5317-5329, 2020.
53. Lucarini, V. et al. IL-33 restricts tumor growth and inhibits pulmonary metastasis in melanoma-bearing mice through eosinophils. *Oncoimmunology* 6 (6), e1317420, 2017.
54. Holgado, A. et al. IL-33trap is a novel IL-33-neutralizing biologic that inhibits allergic airway inflammation. *J Allergy Clin Immunol* 144 (1), 204-215, 2019.
55. Ling, M. F. & Luster, A. D. Allergen-Specific CD4(+) T Cells in Human Asthma. *Ann Am Thorac Soc* 13 Suppl 1 (Suppl 1), S25-30, 2016.
56. Roskopf, S., Jahn-Schmid, B., Schmetterer, K. G., Zlabinger, G. J. & Steinberger, P. PD-1 has a unique capacity to inhibit allergen-specific human CD4(+) T cell responses. *Sci Rep* 8 (1), 13543, 2018.
57. Gorski, S. A. et al. Expression of IL-5 receptor alpha by murine and human lung neutrophils. *PLoS One* 14 (8), e0221113, 2019.
58. Kolbeck, R. et al. MEDI-563, a humanized anti-IL-5 receptor alpha mAb with enhanced antibody-dependent cell-mediated cytotoxicity function. *J Allergy Clin Immunol* 125 (6), 1344-1353.e1342, 2010.
59. Dent, L. A., Strath, M., Mellor, A. L. & Sanderson, C. J. Eosinophilia in transgenic mice expressing interleukin 5. *J Exp Med* 172 (5), 1425-1431, 1990.
60. Johnston, L. K. et al. IL-33 Precedes IL-5 in Regulating Eosinophil Commitment and Is Required for Eosinophil Homeostasis. *J Immunol* 197 (9), 3445-3453, 2016.
61. Pichery, M. et al. Endogenous IL-33 is highly expressed in mouse epithelial barrier tissues, lymphoid organs, brain, embryos, and inflamed tissues: in situ analysis using a novel IL-33-LacZ gene trap reporter strain. *J Immunol* 188 (7), 3488-3495, 2012.
62. Hung, L. Y. et al. Cellular context of IL-33 expression dictates impact on anti-helminth immunity. *Sci Immunol* 5 (53), 2020.
63. Taniguchi, S. et al. Tumor-initiating cells establish an IL-33/TGF- β 2 niche signaling loop to promote cancer progression. *Science* 369 (6501), eaay1813, 2020.
64. Saikumar Jayalatha, A. K., Hesse, L., Ketelaar, M. E., Koppelman, G. H. & Nawijn, M. C. The central role of IL-33/IL-1RL1 pathway in asthma: From pathogenesis to intervention. *Pharmacol Ther* 225, 107847, 2021.
65. Jacquelot, N. et al. Blockade of the co-inhibitory molecule PD-1 unleashes ILC2-dependent antitumor immunity in melanoma. *Nat Immunol* 22 (7), 851-864, 2021.
66. Chen, L. et al. Tumor-Derived IL33 Promotes Tissue-Resident CD8(+) T Cells and Is Required for Checkpoint Blockade Tumor Immunotherapy. *Cancer Immunol Res* 8 (11), 1381-1392, 2020.
67. Shen, J. X., Liu, J. & Zhang, G. J. Interleukin-33 in Malignancies: Friends or Foes? *Front Immunol* 9, 3051, 2018.
68. Dasari, S. & Tchounwou, P. B. Cisplatin in cancer therapy: molecular mechanisms of action. *Eur J Pharmacol* 740, 364-378, 2014.
69. de Biasi, A. R., Villena-Vargas, J. & Adusumilli, P. S. Cisplatin-induced antitumor immunomodulation: a review of preclinical and clinical evidence. *Clin Cancer Res* 20 (21), 5384-5391, 2014.
70. Jacobsen, E. A., Zellner, K. R., Colbert, D., Lee, N. A. & Lee, J. J. Eosinophils regulate dendritic cells and Th2 pulmonary immune responses following allergen provocation. *J Immunol* 187 (11), 6059-6068, 2011.
71. Kanda, A. et al. Th2-activated eosinophils release Th1 cytokines that modulate allergic inflammation. *Allergol Int* 64 Suppl, S71-73, 2015.
72. Jacobsen, E. A. et al. Allergic pulmonary inflammation in mice is dependent on eosinophil-induced recruitment of effector T cells. *J Exp Med* 205 (3), 699-710, 2008.
73. Ghebeh, H., Elshenawy, M. A., AlSayed, A. D. & Al-Tweigeri, T. Peripheral blood eosinophil count is associated with response to chemoimmunotherapy in metastatic triple-negative breast cancer. *Immunotherapy* 14 (4), 189-199, 2022.

74. de Visser, K. E., Korets, L. V. & Coussens, L. M. *De novo* carcinogenesis promoted by chronic inflammation is B lymphocyte dependent. *Cancer Cell* 7 (5), 411-423, 2005.
75. Kim, J. M., Rasmussen, J. P. & Rudensky, A. Y. Regulatory T cells prevent catastrophic autoimmunity throughout the lifespan of mice. *Nat Immunol* 8 (2), 191-197, 2007.
76. Eisenhauer, E. A. et al. New response evaluation criteria in solid tumours: revised RECIST guideline (version 1.1). *European journal of cancer (Oxford, England : 1990)* 45 (2), 228-247, 2009.
77. Seymour, L. et al. iRECIST: guidelines for response criteria for use in trials testing immunotherapeutics. *Lancet Oncol* 18 (3), e143-e152, 2017.
78. Picelli, S. et al. Full-length RNA-seq from single cells using Smart-seq2. *Nat Protoc* 9 (1), 171-181, 2014.
79. Dobin, A. et al. STAR: ultrafast universal RNA-seq aligner. *Bioinformatics* 29 (1), 15-21, 2013.
80. Love, M. I., Huber, W. & Anders, S. Moderated estimation of fold change and dispersion for RNA-seq data with DESeq2. *Genome Biology* 15 (12), 550, 2014.
81. pandas, D. t. pandas-dev/pandas: Pandas. Zenodo, 2020.
82. McKinney, W. Data Structures for Statistical Computing in Python from Proceedings of the 9th Python in Science Conference, 56 - 61, 2010.
83. Harris, C. R. et al. Array programming with NumPy. *Nature* 585 (7825), 357-362, 2020.
84. Hunter, J. D. Matplotlib: A 2D Graphics Environment. *Computing in Science & Engineering* 9 (3), 90-95, 2007.
85. Waskom, M. et al. mwaskom/seaborn: v0.8.1 (September 2017). Zenodo, 2017.
86. Weber, M. statannot 0.2.2. 2020.
87. Tateno, H., Crocker, P. R. & Paulson, J. C. Mouse Siglec-F and human Siglec-8 are functionally convergent paralogs that are selectively expressed on eosinophils and recognize 6'-sulfo-sialyl Lewis X as a preferred glycan ligand. *Glycobiology* 15 (11), 1125-1135, 2005.
88. Abu-Ghazaleh, R. I. et al. Eosinophil granule proteins in peripheral blood granulocytes. *J Leukoc Biol* 52 (6), 611-618, 1992.
89. Mori, Y. et al. Identification of the human eosinophil lineage-committed progenitor: revision of phenotypic definition of the human common myeloid progenitor. *J Exp Med* 206 (1), 183-193, 2009.
90. Hochstetter, R. et al. The CC chemokine receptor 3 CCR3 is functionally expressed on eosinophils but not on neutrophils. *Eur J Immunol* 30 (10), 2759-2764, 2000.
91. Alcover, A., Alarcón, B. & Di Bartolo, V. Cell Biology of T Cell Receptor Expression and Regulation. *Annu Rev Immunol* 36, 103-125, 2018.
92. Li, Y., Yin, Y. & Mariuzza, R. A. Structural and biophysical insights into the role of CD4 and CD8 in T cell activation. *Frontiers in immunology* 4, 206, 2013.

Supplemental Material

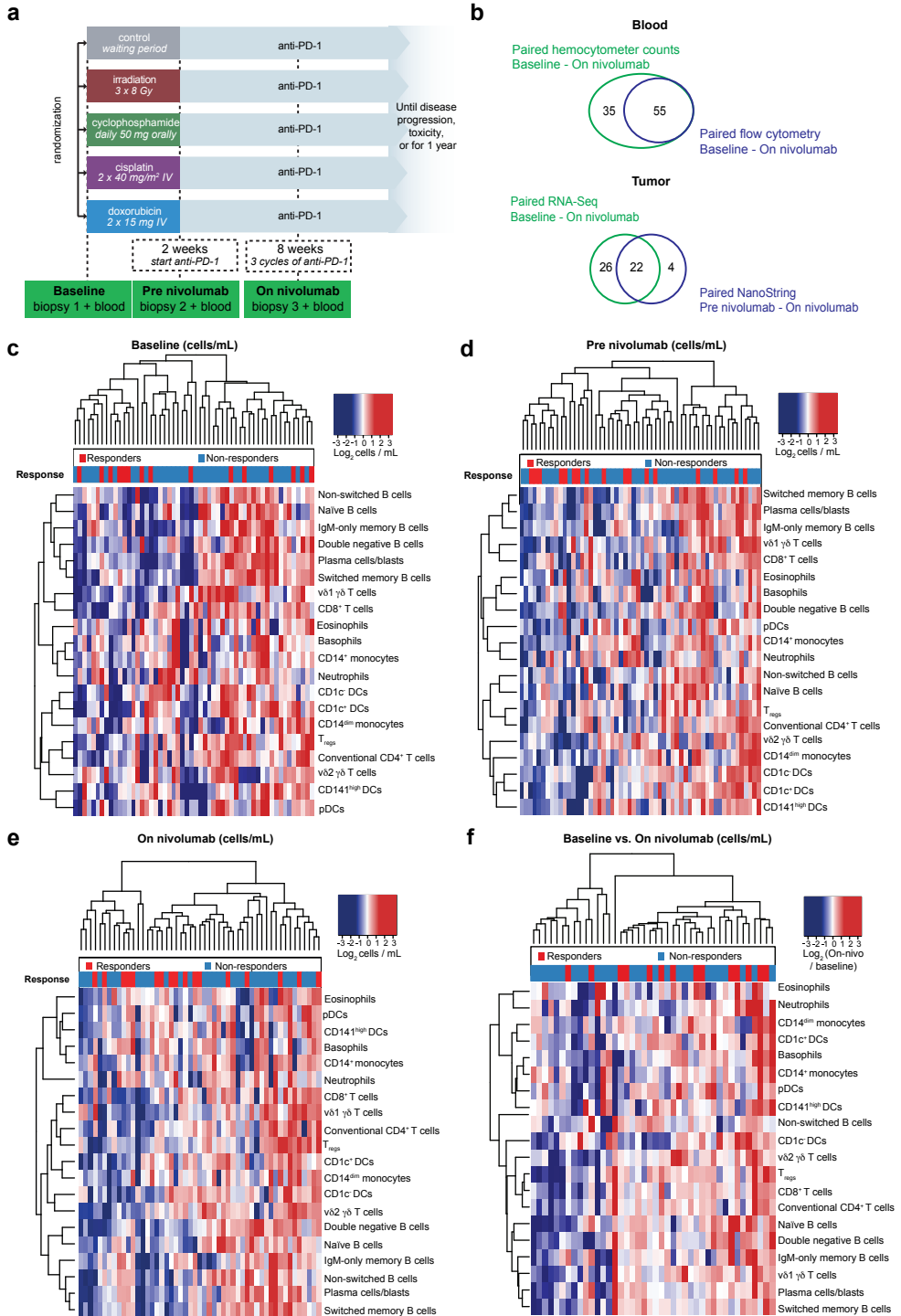


Figure S1. (See previous page) Systemic immune cell landscape of patients treated in the TONIC trial at baseline, after induction therapy and on nivolumab, related to Figure 1. (a) TONIC-trial design (NCT02499367). Patients with metastatic triple-negative breast cancer were randomized to 1 of 4 induction treatment arms (irradiation, cyclophosphamide, cisplatin or doxorubicin) or a two-week waiting period all followed by nivolumab (3mg per kg every 2 weeks) in stage 1 of the trial. In stage 2 of the trial, patients were randomized between doxorubicin induction for two weeks followed by nivolumab or immediate start of nivolumab treatment (no induction). 111 patients received at least one cycle of nivolumab (baseline characteristics in Supplementary Table 1). Blood samples and biopsies were taken at baseline, after 2 weeks of induction treatment and after 3 cycles of nivolumab. Response was determined by iRECIST. **(b)** Venn diagrams showing the relation in TONIC-trial sample availability between the different analyses. The left panel demonstrates the overlap between availability of paired flow cytometry on fresh blood and paired hemocytometer eosinophil counts from baseline to on-nivo. For 3 patients pre-nivo flow cytometry or hemocytometer data were unavailable due to logistical reasons. The right panel demonstrates overlap between tumor samples available for gene expression analysis by NanoString (pre-nivo - on-nivo) and/or RNA-sequencing (baseline - on-nivo). NanoString analysis was performed on TONIC stage 1 samples, RNA-sequencing on TONIC stage 1 and stage 2. For 4 patients there was only pre-nivo RNA and no baseline RNA available. **(c-e)** Heatmaps depicting flow cytometry analysis of immune populations at baseline **(c)**, pre-nivo (after induction) **(d)** and on-nivo **(e)**. Colors in the heatmap correspond to \log_2 transformed cells/mL and are centered to the median for each population (row) separately. **(f)** Heatmap representing the \log_2 fold change of systemic immune cell populations (cells/ml) assessed by flow cytometry from baseline to on-nivo, centered around the median for each immune cell population (row) separately. For **(c-f)**, hierarchical clustering was performed on cell populations and patients based on 1 minus Pearson correlation and Euclidian distance respectively. Complete-linkage was used for both cell populations and patients.

Figure S2. (opposite) Systemic reduction of CD1c⁺ dendritic cells and expansion of T_{regs} and eosinophils during immune checkpoint blockade response is independent of induction treatment in TONIC trial, related to Figure 1. (a-b) Paired flow cytometry analysis of systemic CD1c⁺ DCs (\log_2 transformed cells/ml) **(a)** and T_{regs} (\log_2 transformed cells/ml) **(b)** comparing baseline to on-nivo in responders and non-responders, treated in the TONIC-trial. Paired data are available for 55 patients **(a)** and **(b)**. Statistics by Wilcoxon Signed-Rank. **(c)** Fold change in systemic eosinophils (\log_2 transformed cells/ml by flow cytometry) from baseline to on-nivo in responders and non-responders, treated in the TONIC-trial. Paired data is available for 55 patients. Statistics by Mann-Whitney, median with interquartile range (IQR). **(d)** Volcano plot depicting the linear regression coefficient on the effect of response by changes in immune populations analyzed by flow cytometry (pre-nivo to on-nivo; x-axis) and Benjamini-Hochberg corrected p-values (y-axis), while respecting additive influence of induction treatment (linear modeling). The regression coefficients associated with response for each population (x-axis) against the associated (Benjamini-Hochberg corrected) p-values (Wald-test) were plotted. **(e)** Induction treatment effect on eosinophil dynamics as determined by flow cytometry shown as median count and interquartile range, statistical analysis was performed using Wilcoxon Signed-Rank test comparing baseline to on-nivo in responders and non-responders. **(f)** Paired flow cytometry analysis of eosinophils (\log_2 transformed cells/ml) comparing pre-nivo to on-nivo in responders and non-responders, treated in the TONIC-trial. Paired data was available for 52 patients. Statistics by Wilcoxon Signed-Rank. **(g)** Fold change in systemic eosinophils assessed by hemocytometer from baseline to on-nivo in responders and non-responders. Paired data is available for 90 patients. Statistics by Mann-Whitney, median with interquartile range (IQR). **(h)** Paired hemocytometer analysis of systemic eosinophils comparing pre-nivo to on-nivo in responders and non-responders. Paired data is available for 87 patients. Statistics by Wilcoxon Signed-Rank. **(i-j)** Kaplan-Meier curve of progression-free survival **(i)** or overall survival **(j)** of patients divided between a fold change in eosinophils (pre-nivo to on nivo) lower than 2 or equal to/higher than 2. Statistics with log-rank and univariate hazard ratios by Cox regression (fold change lower than 2 as reference category). Data was cut-off at 1 March 2021.

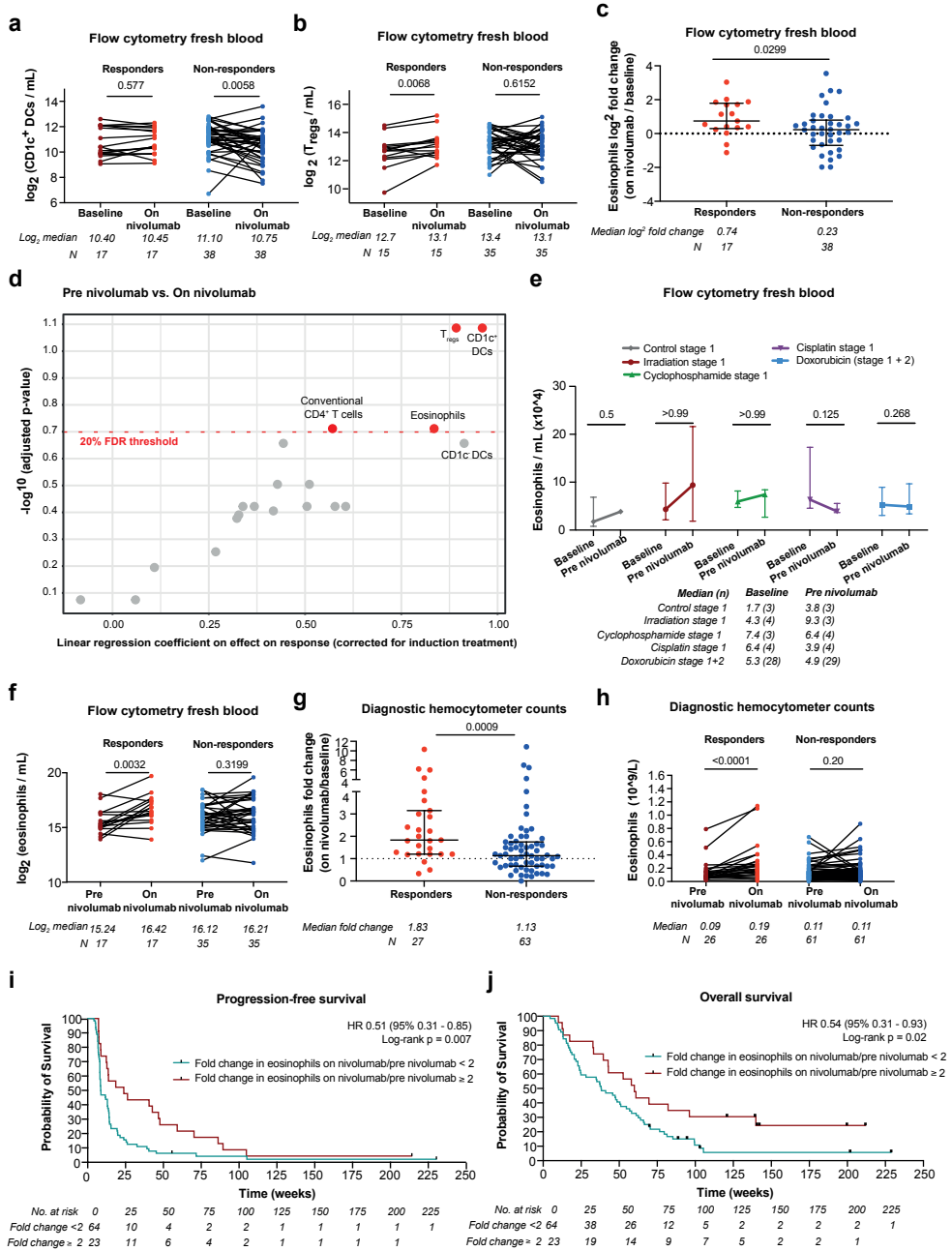


Figure S2. Systemic reduction of CD1c⁺ dendritic cells and expansion of T_{regs} and eosinophils during immune checkpoint blockade response is independent of induction treatment in TONIC trial, related to Figure 1.

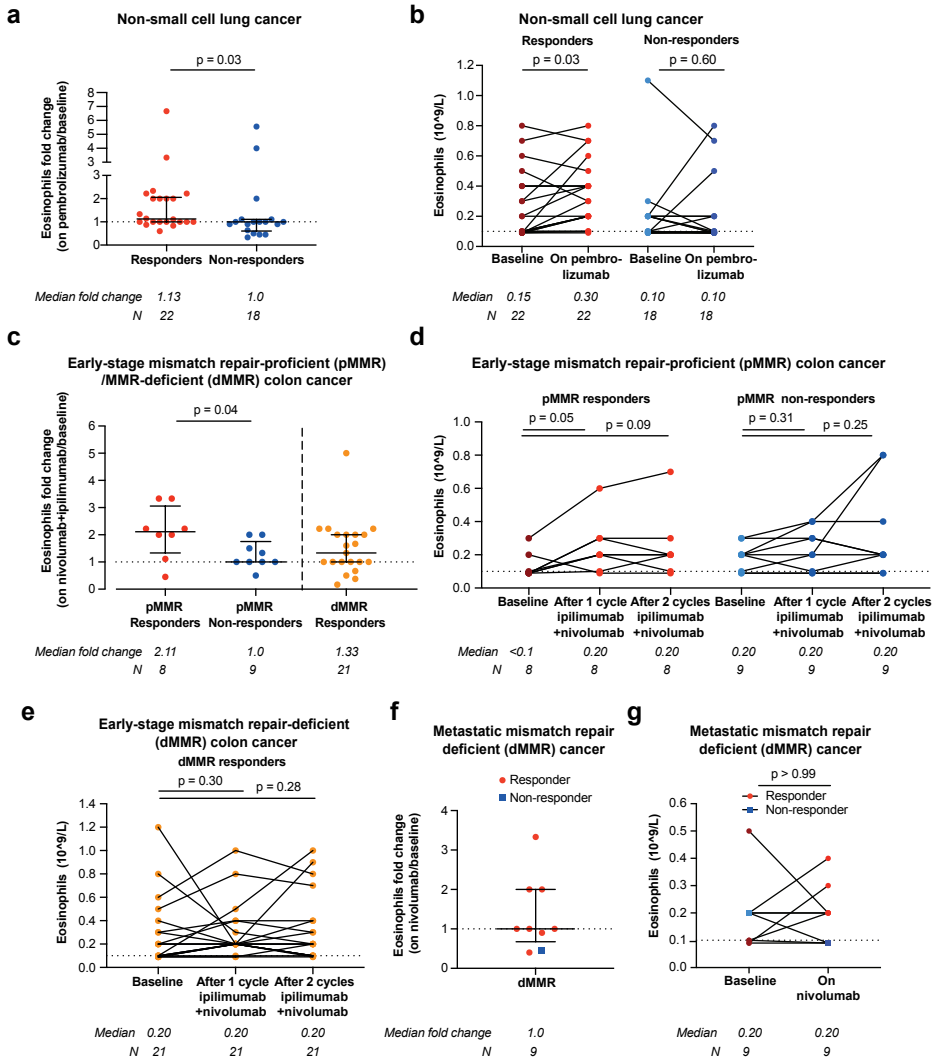


Figure S3. Systemic eosinophil accumulation after ICB and association with therapy response in different cancer types. (a) Fold change of eosinophil counts after two cycles of pembrolizumab in patients with metastatic non-small lung cancer (NSCLC) treated with pembrolizumab (200 mg, q3w) with or without upfront radiation (NCT02492568)²⁹. Paired data was available for 40 patients. (b) Paired analysis of absolute eosinophil counts in blood between baseline and two cycles of pembrolizumab in responding and non-responding patients with metastatic NSCLC. (c) Fold change of eosinophil counts after one cycle of ipilimumab/nivolumab treatment and baseline in patients with early-stage colon cancer, either mismatch repair-proficient (pMMR) or mismatch repair deficient (dMMR), treated with neoadjuvant nivolumab (day 1 and day 15, 3 mg/kg) and ipilimumab (day 1, 1 mg/kg) in the NICHE-trial (NCT03026140)³⁰. Response was defined as a pathological response (<90% tumor rest). Eosinophils were measured after 1 cycle of ipilimumab/nivolumab and after 1 additional cycle of nivo. All patients with early-stage dMMR colon cancer had a pathological response. Paired data was available for 21 patients. (d-e) Paired analysis of absolute eosinophil counts in blood between baseline and on treatment in responding and non-responding patients with mismatch repair-proficient (pMMR) (d) and mismatch repair deficient (dMMR) (e) early-stage colon cancer, treated with two cycles of neoadjuvant nivolumab and ipilimumab in the NICHE-trial. (f) Fold change of eosinophil counts after two or three cycles of nivolumab treatment in patients with metastatic dMMR tumors, treated with nivolumab (240 mg, q2w) in the dMMR cohort of the Drug Rediscovery Protocol (NCT02925234)³¹. 7 patients with colorectal cancer (6 patients with paired data), 1 patient with urothelial cell cancer (no paired data), 1 patient with cervical cancer, 1 patient with breast cancer and 1 patient with endometrial cancer were included in this cohort. (g) Paired analysis of absolute eosinophil counts between baseline and two or three cycles of nivolumab in responding and non-responding patients with metastatic

dMMR tumors, treated with nivolumab in the dMMR cohort of the Drug Rediscovery Protocol. Response was defined as complete response (CR), partial response (PR) or stable disease (SD) for 24 weeks or longer according to RECIST1.1 for (a-b and f-g). For (a,c,f), median and interquartile ranges are displayed; statistics by Mann-Whitney. For (b-e & g), statistics by Wilcoxon-signed-rank. Dashed lines indicate the threshold (0.1×10^9 cells/L) of the hemocytometer counts reported in the patient records, counts below this threshold were replaced with a value of 0.09×10^9 cells/L.

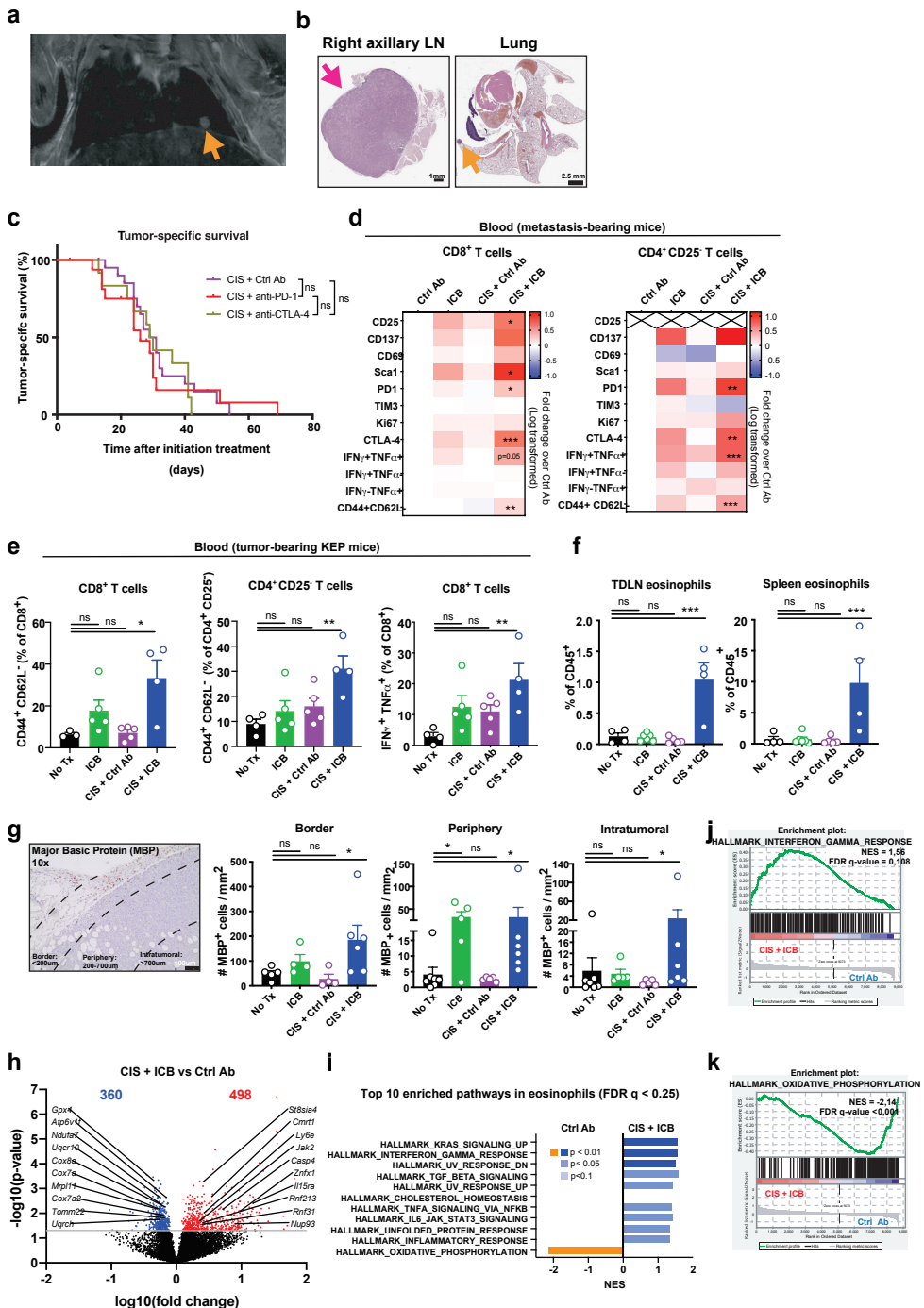


Figure S4. (see previous page) ICB and cisplatin induces systemic T-cell activation and eosinophil expansion in pre-clinical models of mammary tumorigenesis and advanced metastatic breast cancer, related to Figure 3. (a-b) MRI images displaying the lung and axillary lymph nodes (a) and H&E staining of right axillary lymph node (= primary tumor draining lymph node) and lungs (b) of mice bearing KEP-derived metastases 15 days after mastectomy. Scale bars represent 1mm (left) and 2.5mm (right). Orange arrows indicate lung metastatic nodules and pink arrows indicate a lymph node affected by metastatic disease. (c) Kaplan-Meier survival curves of KEP mice treated as indicated (CIS + Ctrl Ab, n=22, 3 censored, CIS + anti-CTLA-4, n=12, 1 censored, or CIS + anti-PD-1, n=17, 3 censored). Log-rank (Mantel-Cox) test. (d) Fold change compared to Ctrl Ab-treated mice of CD8⁺ (left) and CD4⁺ CD25⁺ (right) T cells expressing the indicated activation markers expressed in blood at metastasis-related endpoint (n=4-7), determined by flow cytometry. Log transformed data are presented. Mean \pm S.E.M., 1-way ANOVA followed by Dunnett's multiple comparisons test. (e) Frequency of effector CD8⁺ (left), effector CD4⁺ CD25⁺ (middle) T cells and IFN γ and TNF α double positive CD8⁺ T cells (right) in blood of KEP mice at tumor-related endpoint (n=4-5), determined by flow cytometry. Mean \pm S.E.M., 1-way ANOVA followed by Dunnett's multiple comparisons test. (f) Frequency of eosinophils (defined as: CD11b⁺ Ly6G^{low} F4/80^{int} SiglecF⁻) in the TDLN (left) and spleen (right) of KEP mice at tumor-related endpoint as determined by flow cytometry (n=4-6). Mean \pm S.E.M., 1-way ANOVA followed by Dunnett's multiple comparisons test. (g) Representative image and quantification of immunohistochemical staining for major basic protein (MBP) of KEP tumors at tumor-related endpoint demonstrating eosinophil distribution in intratumoral, periphery and border regions. Intratumoral areas were defined as more than 700 μ m distant from the border of the tumor tissue; tumor periphery was defined as areas between 200 μ m and 700 μ m from the border of tumor tissue; border areas were defined as areas spanning from 200 μ m inside the tumor tissue to 300 μ m into the surrounding non-tumoral tissue. Scale bar represents 100 μ m. Each dot represents the average of 4-5 different tumor areas of 0.5mm² per mouse. Mean \pm S.E.M., Kruskal-Wallis test. (h) Volcano plot demonstrating differentially expressed genes between eosinophils sorted from the blood of mice treated with Ctrl Ab or CIS + ICB in responsive phase of therapy. Genes contributing to the "Hallmark_interferon_gamma_response" and "Hallmark_oxidative_phosphorylation" gene-sets are highlighted. (i) Gene sets derived from the Molecular Signatures Database Hallmark Gene Set Collection enriched in mice treated with CIS + ICB (blue) or Ctrl Ab (orange) (FDR q < 0.25). The Normalized Enrichment Scores (NES) of the top 10 enriched gene sets are shown, ordered based on ascending q-value. (j) Enrichment plot for the gene-set "Hallmark_interferon_gamma_response" upregulated in eosinophils treated with CIS + ICB. (k) Enrichment plot for the gene-set "Hallmark_oxidative_phosphorylation" upregulated in eosinophils treated with Ctrl Ab. ns, not significant *p<0.05, **p<0.01, ***p<0.001, ****p<0.0001.

Figure S5. (opposite) Depletion of eosinophils using anti-SiglecF antibody does not promote CD4⁺ T cell or T_{reg} activation in the tumor and tumor-draining lymph node during combined ICB and cisplatin treatment, related to Figure 4. (a-c) Frequency of indicated immune cells in the tumor (a), blood (b), and lungs (c) of treated KEP mice at tumor-related endpoint as determined by flow cytometry (n=4-10). Mean \pm S.E.M., Mann-Whitney. (d) Mean Fluorescence Intensity (MFI) of SiglecF expression on eosinophils, total neutrophils or SiglecF⁻ neutrophils of KEP mice at tumor-related endpoint (n=4), measured by flow cytometry in indicated tissues. Mean \pm S.E.M., Multiple unpaired t-tests followed by Holm-Sidak for multiple comparison. (e) Quantification of IHC staining for Ly6G⁺ cells per FOV in the tumor and lung of treated KEP mice at tumor-related endpoint (n=6-10 mice, the average of 5 FOVs per mouse). (f) Quantification of IHC staining for MBP⁺ cells per mm² in the tumor and lung of treated KEP mice at tumor-related endpoint (n=4-5 mice). (g) Quantification of IHC staining for MBP of KEP tumors at tumor-related endpoint demonstrating eosinophil distribution in intratumoral (left), periphery (middle) and border regions (right), defined and analyzed as described in Figure S4G. Data of CIS + Ctrl Ab and CIS + ICB groups are the same as displayed in Figure S4G. Mean \pm S.E.M., Mann-Whitney. (h) Growth curve of mammary tumors in KEP mice treated with control antibody (n=7) or anti-SiglecF (n=3). (i-q) KEP mice were sacrificed 21 days after start of treatment (responsive phase). Untreated KEP mice were analyzed 21 days after they reached a tumor area of 50 mm², or when the tumors reached an area of 225 mm². (i-j) Number of tumor-infiltrating CD4⁺ (i) and FOXP3⁺ (j) cells in 'responsive phase' of treatment, quantified by IHC (n=5-7 mice per group. For each mouse, the average of 5-9 FOVs \pm S.E.M is displayed). Student's t-test. (k-l) Frequency of tumor-infiltrating CD4⁺CD25⁺ T cells (k) and regulatory T cells (l) expressing the indicated activation markers as determined by flow cytometry, measured 21 days after initiation of indicated treatments (n=5). (m-n) Data of (k-l) was normalized to the frequency observed in control mice. Log transformed data is presented. (o-q) Frequency of CD8⁺ T cells (o), CD4⁺CD25⁺ T cells (p) and regulatory T cells (q) expressing the indicated activation markers as determined by flow cytometry in the TDLN, measured 21 days after initiation of indicated treatments (n=5). Boxes represent median and interquartile range; whiskers represent full range. 2-way ANOVA followed by Tukey's multiple comparison test. *p<0.05, **p<0.01, ***p<0.001, ****p<0.0001.

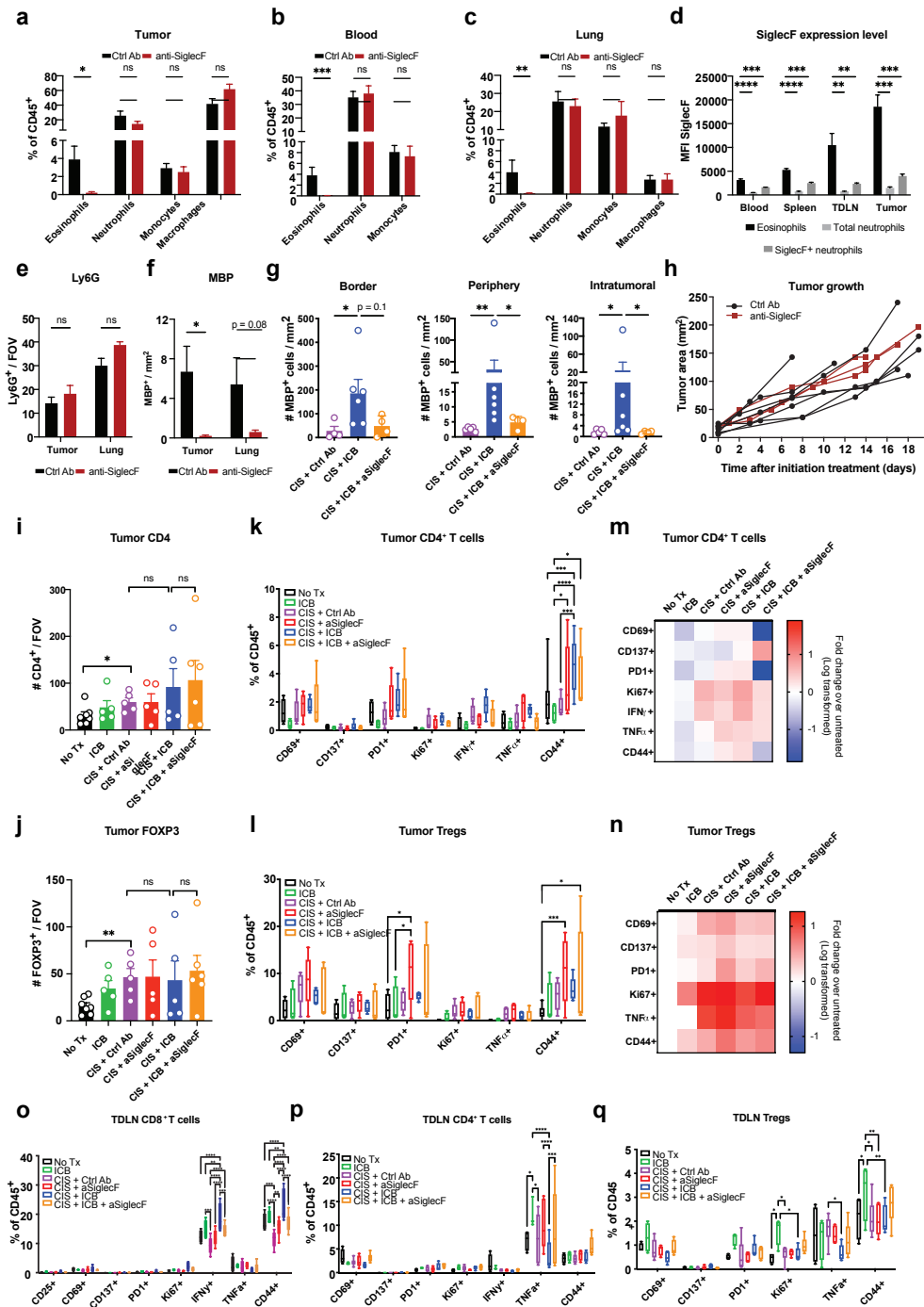


Figure S5. Depletion of eosinophils using anti-SiglecF antibody does not promote CD4⁺ T cell or T_{reg} activation in the tumor and tumor-draining lymph node during combined ICB and cisplatin treatment, related to Figure 4.

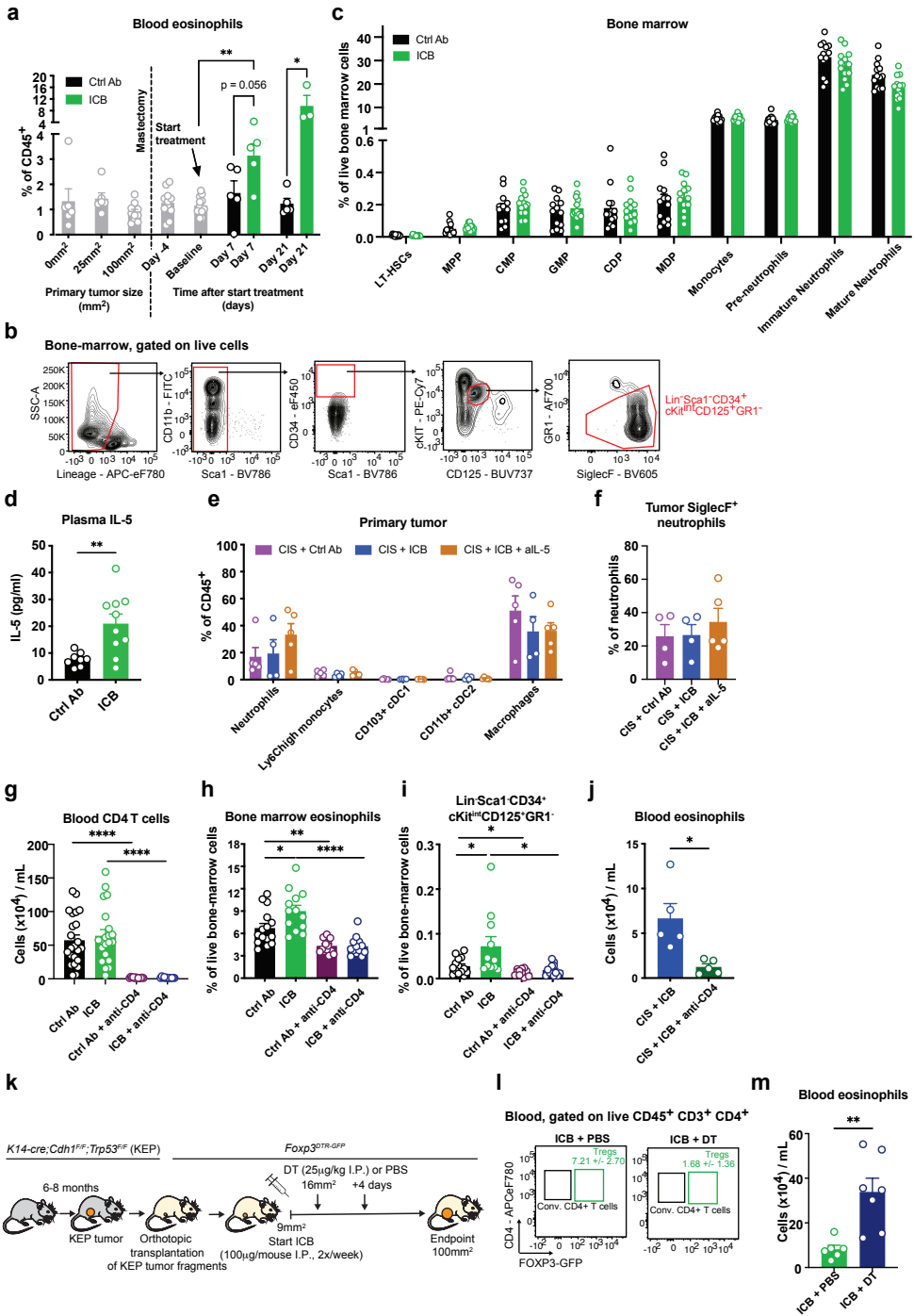


Figure S6. Dynamics and properties of ICB-induced eosinophils in mice with KEP-derived metastatic disease or mammary tumors, related to Figure 5

Figure S6. (opposite) Dynamics and properties of ICB-induced eosinophils in mice with KEP-derived metastatic disease or mammary tumors, related to Figure 5. (a) Frequency of eosinophils in blood of mice with KEP-derived metastatic disease treated as described in Figure 3E, as determined by flow cytometry at the indicated time-points (Ctrl Ab n=3-11, ICB n=3-11). (b) Gating strategy for the identification of Lin⁺Sca1⁺CD34⁺cKit^{int}CD125⁺Gr1⁻ eosinophil progenitors in the bone marrow. (c) Frequency of indicated cell types in the bone marrow of mice with KEP-derived metastatic disease treated as indicated, as determined by flow cytometry (Ctrl Ab n=13, ICB n=13). LT-HSC, long-term hematopoietic stem cell; MPP, multipotent progenitor; CMP, common myeloid progenitor; GMP, granulocyte-monocyte progenitor; CDP, common dendritic cell progenitor; MDP, macrophage-dendritic cell progenitors. Multiple unpaired t-tests followed by Holm-Sidak for multiple comparison. (d) Absolute quantification of IL-5 levels in plasma of mice with KEP-derived metastatic disease treated as indicated (Ctrl Ab n=9, ICB n=10) as measured by Legend Plex. The mice shown here are the same used for the analysis of Figure 5F. (e) Frequency of indicated immune cell populations in tumors of treated KEP mice at tumor-related endpoint, as determined by flow cytometry (n=4-5). The mice shown here are the same used for the analysis of Figure 5K-N. 1-way ANOVA. (f) Frequency of SiglecF⁺ neutrophils in primary tumor of treated KEP mice at tumor-related endpoint, as determined by flow cytometry (n=4-5). (g) Number of CD4 T cells (gated as: CD3⁺CD8⁻CD25⁻ cells) in the blood of mice with KEP-derived metastatic disease treated as described in Figure 5R, as determined by flow cytometry. Pooled data of two independent experiments. (h-i) Frequency of total eosinophils (h) and Lin⁺Sca1⁺CD34⁺cKit^{int}CD125⁺Gr1⁻ eosinophil progenitors (i) in the bone marrow of mice with KEP-derived metastatic disease treated as described in Figure 5R, as determined by flow cytometry (n=13-14). (j) Number of eosinophils in the blood of KEP-metastasis-bearing mice treated with CIS+ICB (n=5) or CIS+ICB+anti-CD4 (n=5) and analyzed on day 10 after start of treatment. (k) Experimental set-up and treatment scheme for the depletion of T_{regs} in mice with KEP-derived orthotopic mammary tumors. (l) Representative dot plots showing T_{regs} levels in the blood of mice at the experimental endpoint. Average frequency of T_{regs} as percentage of CD4⁺ cells ±S.E.M. are displayed. DT, diphtheria toxin. (m) Number of eosinophils in blood of mice treated as described in (h) (ICB + PBS, n=6, ICB + DT n=7), as determined by flow cytometry. All data are mean ±S.E.M, unpaired t-test, unless indicated otherwise. ns, not significant, *p<0.05, **p<0.01, ****p<0.001.

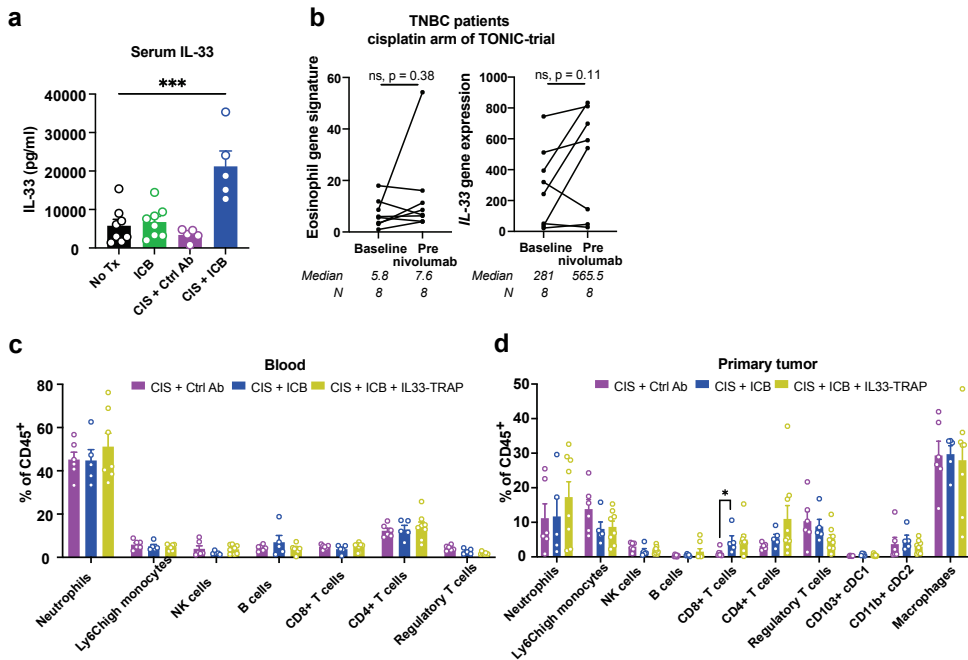


Figure S7. (continued on next page) ICB and rIL-33 specifically promote the expansion and activation of eosinophils in mice with mammary tumors, related to Figure 6 and 7.

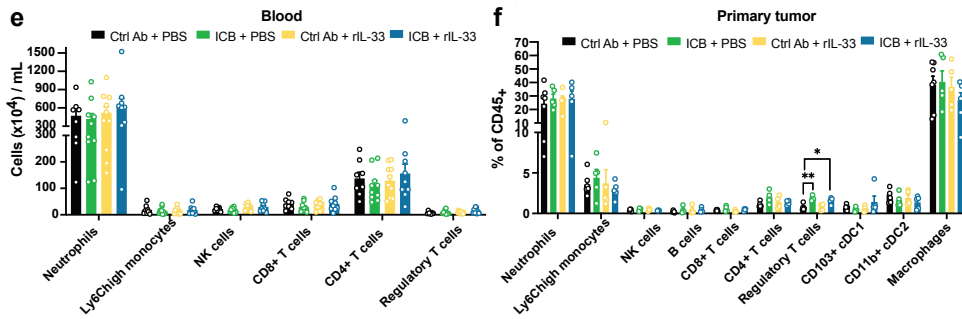


Figure S7. (continued) ICB and rIL-33 specifically promote the expansion and activation of eosinophils in mice with mammary tumors, related to Figure 6 and 7. (a) IL-33 levels in serum determined by Legend Plex of KEP mice at tumor-related endpoint treated as indicated (n=5-8). (b) Eosinophil gene signature (left) and *IL33* gene expression (right) from RNA-seq analysis of metastatic lesions of TNBC patients treated in the cisplatin arm of the TONIC trial. (c-d) Frequency of indicated immune cell populations in the blood (c) and primary tumor (d) as determined by flow cytometry of KEP mice treated as described in Figure 6D-F (n=5-8). (e-f) Frequency of indicated immune cell populations in the blood (n=8-10) (e) and primary tumor (n=5-7) (f) determined by flow cytometry of mice bearing orthotopically transplanted KEP tumors in responsive phase of therapy (i.e. tumor area of 150mm²) and treated as described in Figure 7. Statistical analysis performed by 1-way ANOVA or Kruskal-Wallis followed by Dunnett's or Dunn's multiple comparisons test, comparing each group against control mice, for each immune population. All data are mean \pm S.E.M., *p<0.05, **p<0.01, ***p<0.001.

Figure S8. (opposite) Gating strategy for flow cytometry analysis of human peripheral blood immune populations, related to STAR Methods. (a) Myeloid panel gating strategy identifying eosinophils (lineage⁻, high side scatter, CD66b⁺, CD16⁻), neutrophils (lineage⁻, high side scatter, CD66b⁺, CD16⁺), basophils (lineage⁻, low side scatter, CD66b⁻, HLA-DR⁻, FcεR1a⁺), plasmacytoid DCs (lineage⁻, low side scatter, CD66b⁻, HLA-DR⁺, CD303⁺, CD123⁺), CD141^{high} DCs (lineage⁻, low side scatter, CD66b⁻, HLA-DR⁺, CD33⁺, CD141⁺), CD14⁺ monocytes (lineage⁻, CD66b⁻, HLA-DR⁺, CD33⁺, CD14⁺), CD14^{dim} monocytes (lineage⁻, CD66b⁻, HLA-DR⁺, CD33⁺, CD14^{dim}, CD16⁺), CD1c⁺ DCs (lineage⁻, CD66b⁻, HLA-DR⁺, CD33⁺, CD14⁻, CD16⁻, CD1c⁺, FcεR1a⁺) and CD1c⁻ DCs (lineage⁻, CD66b⁻, HLA-DR⁺, CD33⁺, CD14⁻, CD16⁻, CD1c⁻, FcεR1a⁻). (b) T cell panel gating strategy to identify vd1⁺ gd T cells (CD3⁺, vd1⁺, pan gd TCR⁺), vd2⁺ gd T cells (CD3⁺, vd2⁺), CD8 T cells (CD3⁺, vd1⁻, pan gd TCR⁻, vd2⁻, CD8⁺, CD4⁻), conventional CD4 T cells (CD3⁺, vd1⁻, pan gd TCR⁻, vd2⁻, CD8⁻, CD4⁺, FoxP3⁻) and Tregs (CD3⁺, vd1⁻, pan gd TCR⁻, vd2⁻, CD8⁻, CD4⁺, FoxP3⁺, CD25^{high}). (c) Gating strategy to identify B cell subsets identifying double negative B cells (CD19⁺, CD27⁻, IgD⁻), naïve B cells (CD19⁺, CD27⁻, IgD⁺), non-switched memory B cells (CD19⁺, CD27⁺, IgD⁺), IgM-only memory B cells (CD19⁺, CD27⁺, IgD⁻, IgM⁺), switched memory B cells (CD19⁺, CD27⁺, IgD⁻, IgM⁻, CD38^{-/+}), and plasmacells/blasts (CD19⁺, CD27⁺, IgD⁻, IgM⁻, CD38^{high}).

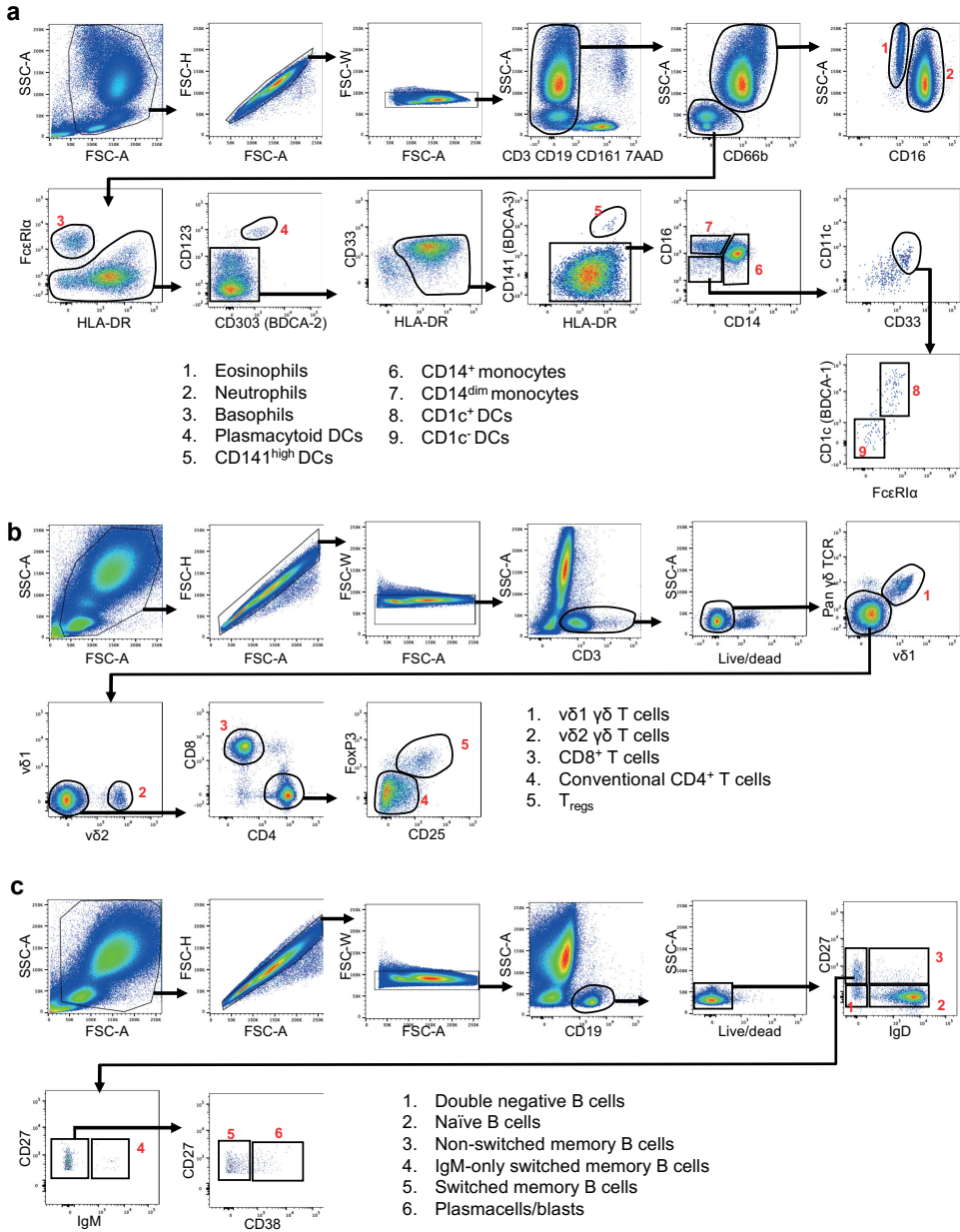


Figure S8. Gating strategy for flow cytometry analysis of human peripheral blood immune populations, related to STAR Methods.

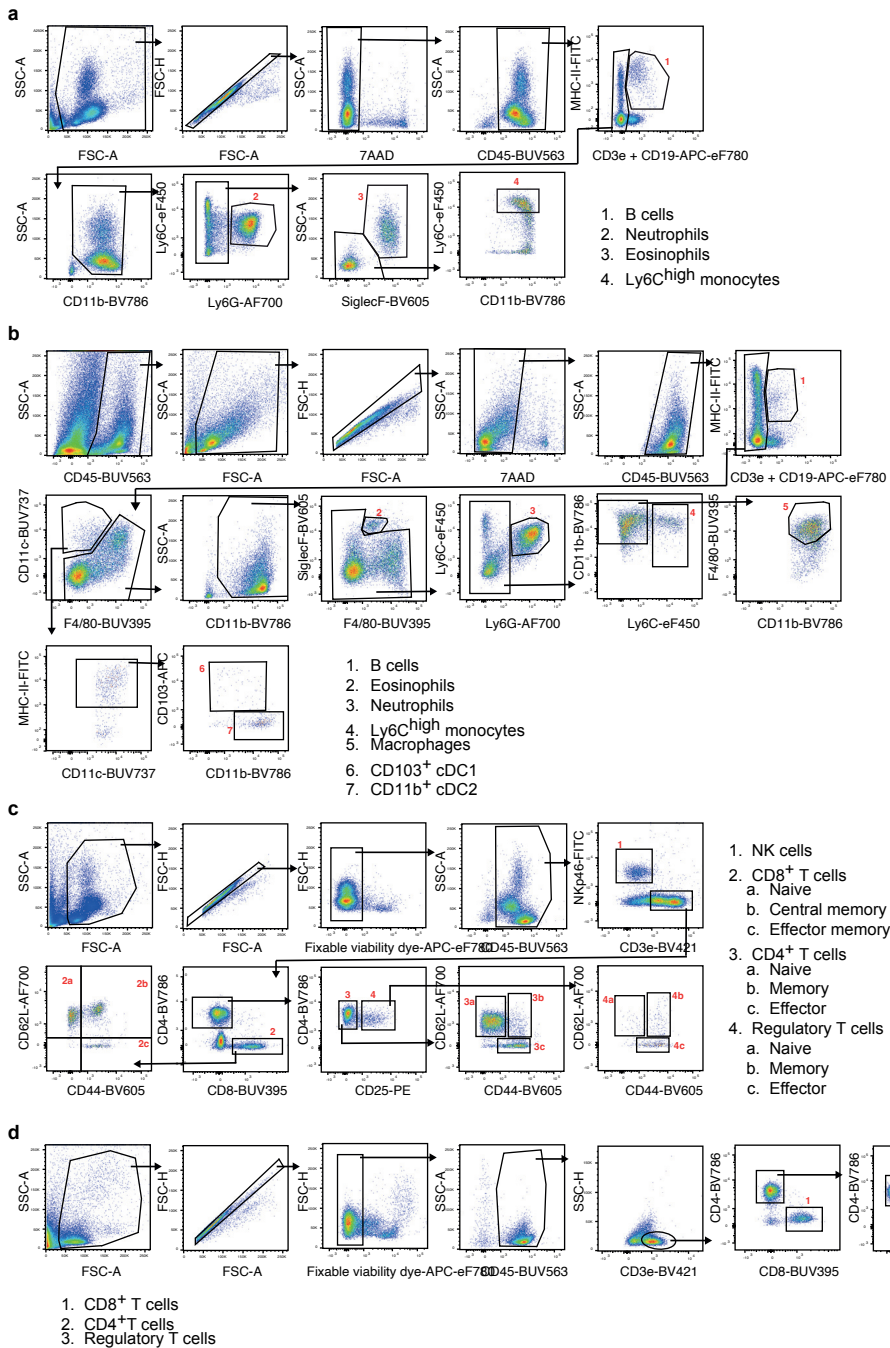


Figure S9. Gating strategy for flow cytometry to identify immune cell populations in mouse blood and tumor, related to STAR Methods. (a-b) Myeloid panel gating strategy for blood (a) and tumor (b) samples identifying B cells (CD45+, MHC-II+), neutrophils (CD45+, CD3-, CD19-, CD11b+, Ly6g+), eosinophils (in blood: CD45+, CD3-, CD19-, Ly6g-, CD11b+, SSC-Ahigh, SiglecF+; in tumor: CD45+, CD3-, CD19-, CD11b+, SiglecF+, F4/80int), Ly6chigh monocytes (CD45+, CD3-, CD19-, Ly6g-, SiglecF-, CD11b+, Ly6chigh), macrophages (in tumor: CD45+, CD3-, CD19-, SiglecF-, Ly6g-, Ly6c-, CD11b+, F4/80high), CD103+ cDC1 (in tumor: CD45+, CD3-, CD19-, F4/80-, CD11c+, MHC-II+

CD11b^{low}, CD103⁺) and CD11b⁺ cDC2 (in tumor: CD45⁺, CD3⁻, CD19⁻, F4/80⁻, CD11c⁺, MHC-II⁺, CD103⁻, CD11b⁺). (c-d) Lymphoid panel gating strategy in blood analyzed unfixed (c) and fixed (d) identifying NK cells (unfixed: CD45⁺, CD3⁻, NKp46⁺), naïve CD8⁺ T cells (unfixed: CD45⁺, NKp46⁻, CD4⁻, CD3⁺, CD8⁺; CD44⁻, CD62L⁺), central memory CD8⁺ T cells (unfixed: CD45⁺, NKp46⁻, CD4⁻, CD3⁺, CD8⁺, CD44⁺, CD62L⁺), effector memory CD8⁺ T cells (unfixed: CD45⁺, NKp46⁻, CD4⁻, CD3⁺, CD8⁺, CD44⁺, CD62L⁻), total CD8⁺ T cells (fixed: CD45⁺, CD4⁻, CD3⁺, CD8⁺), naïve CD4⁺ T cells (unfixed: CD45⁺, NKp46⁻, CD8⁻, CD25⁻, CD3⁺, CD4⁺, CD44⁻, CD62L⁺), memory CD4⁺ T cells (unfixed: CD45⁺, NKp46⁻, CD8⁻, CD25⁻, CD3⁺, CD4⁺, CD44⁺, CD62L⁺), effector CD4⁺ T cells (unfixed: CD45⁺, NKp46⁻, CD8⁻, CD25⁻, CD3⁺, CD4⁺, CD44⁺, CD62L⁻), total CD4⁺ T cells (fixed: CD45⁺, CD8⁻, FOXP3⁻, CD3⁺, CD4⁺), naïve Tregs (unfixed: CD45⁺, NKp46⁻, CD8⁻, CD25⁺, CD3⁺, CD4⁺, CD44⁻, CD62L⁺), effector Tregs (unfixed: CD45⁺, NKp46⁻, CD8⁻, CD25⁺, CD3⁺, CD4⁺, CD44⁺, CD62L⁺), memory Tregs (unfixed: CD45⁺, NKp46⁻, CD8⁻, CD25⁺, CD3⁺, CD4⁺, CD44⁺, CD62L⁻) and total Tregs (fixed: CD45⁺, CD8⁻, FOXP3⁺, CD3⁺, CD4⁺).

Supplementary Table 1: Baseline characteristics of all patients receiving at least one dose of nivolumab in the TONIC-trial (stage 1 and 2).

ULN = upper limit of normal (= 250 U/L). Related to Figure 1 and 2.

Total population (n = 111)	No. of patients	Percentage
Median age, years (range)	52 (29-74)	
WHO performance status, n (%)		
0	70	63%
1	41	37%
gBRCA1/2, n (%)		
Mutation	6	5%
Wildtype	78	70%
Unknown	27	24%
Location of metastasis, n (%)		
Lymph node only	10	9%
Visceral metastasis	79	71%
Other metastasis	22	20%
No. of prior therapies for metastatic disease, n (%)		
0	29	26%
1	56	50%
2-3	26	23%
Previous neoadjuvant or adjuvant therapy, n (%)	96	86%
Previous chemotherapy exposure, n (%)		
Taxane	101	91%
Anthracycline	95	86%
Platinum	60	54%
Capecitabine	60	54%
LDH level, n (%)		
≤ ULN	70	63%
≤ 2x ULN	41	37%

Supplementary Table 2: Sample availability in the TONIC-trial (stage 1 and 2).
Related to Figure S1B which illustrates overlap between available samples.

	No. of patients
All included patients	111
Routine eosinophil counts	
Paired baseline - on-nivo	90
Paired pre-nivo - on-nivo	87
Flow cytometry fresh blood	
Paired baseline - on-nivo	55
Paired pre-nivo - on-nivo	52
RNA-sequencing data	
Paired baseline - on-nivo	48
NanoString gene expression (TONIC stage 1 only)	
Paired pre-nivo - on-nivo	26

Supplementary Table 3: List of gene signatures used for human RNA-sequencing analysis. Related to Figure 2.

Gene signature	Genes
Eosinophil gene signature	<i>SIGLEC8</i> ⁸⁷ , <i>RNASE2</i> ⁸⁸ , <i>RNASE3</i> ⁸⁸ , <i>IL5RA</i> ⁸⁹ , <i>CCR3</i> ⁹⁰
Expanded T cell signature ³³	<i>CD3D</i> , <i>IDO1</i> , <i>CIITA</i> , <i>CD3E</i> , <i>CCL5</i> , <i>GZMK</i> , <i>CD2</i> , <i>HLA-DRA</i> , <i>CXCL13</i> , <i>IL2RG</i> , <i>NKG7</i> , <i>HLA-E</i> , <i>CXCR6</i> , <i>LAG3</i> , <i>TAGAP</i> , <i>CXCL10</i> , <i>STAT1</i> , <i>GZMB</i>
Structural CD8 ⁺ T cell signature	<i>CD3D</i> ⁹¹ , <i>CD3E</i> ⁹¹ , <i>CD3G</i> ⁹¹ , <i>CD8A</i> ⁹² , <i>CD8B</i> ⁹² , <i>TRAC</i> ⁹¹ , <i>TRBC1</i> ⁹¹ , <i>TRBC2</i> ⁹¹ , <i>CD247</i> ⁹¹
IFN γ gene signature ³³	<i>IDO1</i> , <i>CXCL9</i> , <i>CXCL10</i> , <i>HLA-DRA</i> , <i>STAT1</i> , <i>IFNG</i>

Supplementary Table 4: Patient characteristics of tumors included in PDTF analysis treated with aPD-1 alone.
Related to Figure 5G.

Patient ID	Tumor type	Tumor site	Ex vivo response to aPD-1
CRC003	Colorectal cancer	Primary	Yes
OV013-3	Ovarian cancer	Peritoneal metastasis	Yes
LU019	Non-small cell lung cancer	Primary	Yes
AKB803	Melanoma	Lymph node metastasis	Yes
MEL021	Melanoma	Lung metastasis	Yes
MEL025-1	Melanoma	Lymph node metastasis	No
LU027-2	Non-small cell lung cancer	Primary	No
MEL032	Melanoma	Metastasis muscle	No
RE015	Renal cell carcinoma	Primary	No
RE028	Renal cell carcinoma	Primary	No
MEL072	Melanoma	Lymph node metastasis	No
LU032	Non-small cell lung cancer	Primary	No
MEL077	Melanoma	Abdominal metastasis	No
LU028	Non-small cell lung cancer	Primary	No



Chapter 5

PD-L1 blockade in combination with carboplatin as immune induction in metastatic lobular breast cancer: the GELATO-trial

Leonie Voorwerk*, Olga I. Isaeva*, Hugo M. Horlings, Sara Balduzzi, Maksim Chelushkin, Noor A.M. Bakker, Elisa Champanhet, Hannah Garner, Karolina Sikorska, Claudette E. Loo, Inge Kemper, Ingrid A.M. Mandjes, Michiel de Maaker, Jasper J.L. van Geel, Jorianne Boers, Maaïke de Boer, Roberto Salgado, Marloes G.J. van Dongen, Gabe S. Sonke, Karin E. de Visser, Ton N. Schumacher, Christian U. Blank, Lodewyk F.A. Wessels, Agnes Jager, Vivianne C.G. Tjan-Heijnen, Carolien P. Schröder, Sabine C. Linn, Marleen Kok

*These authors contributed equally

In revision, Nature Cancer

Abstract

Invasive lobular breast cancer (ILC) is the second most common histological breast cancer subtype but published data on trials specific for ILC are so far lacking. Translational research revealed that a subset of ILCs may be immune-related and more sensitive to DNA-damaging agents such as platinum. In murine ILC models, synergy between immune checkpoint blockade and platinum has been observed. Here, we tested this concept in the phase II, GELATO-trial (NCT03147040), in which patients with metastatic ILC were treated with weekly carboplatin (AUC 1.5) as immune induction treatment for 12 weeks and atezolizumab (PD-L1 blockade; every three weeks) from the third week onwards until disease progression. Four out of 23 evaluable patients had a partial response (17%, 95%CI 5-39%) and two patients had stable disease for at least 24 weeks, resulting in a clinical benefit rate of 26% (95%CI 10-48%). Out of these six patients, four patients had triple-negative ILC (TN-ILC). In serial biopsies of metastatic lesions, we observed higher CD8 T-cell infiltration, expression of immune checkpoints, and exhausted T cells upon carboplatin/PD-L1 blockade. This is the first report of a clinical trial specifically for ILC and we demonstrate promising anti-tumor activity of atezolizumab with carboplatin as immune induction, in particular for TN-ILC. While activity of carboplatin/PD-L1 blockade in classical ER+ ILC was limited, our translational data yield important insights for the design of highly needed clinical trials in ILC.

Introduction

Invasive lobular breast cancer (ILC) is the second most common histological breast cancer subtype, comprising approximately 10-15% of cases¹⁻³. The non-cohesive and single file or targetoid pattern observed on routine histology is characteristic for the morphological diagnosis of ILC and loss or aberrant expression of E-cadherin supports the diagnosis of ILC⁴. Approximately 80-90% of primary ILCs express estrogen receptor (ER), have a luminal A phenotype and can be considered classic ILC^{5,6}. Approximately 5% of ILC are triple-negative (TN) and frequently exhibit a luminal phenotype implying that this subtype has a different biology compared to the majority of triple-negative breast cancer (TNBC) that is dominated by basal-like tumors^{1,7,8}.

Patients with ER+ metastatic ILC have preferred metastatic spread to the gastrointestinal tract and bone^{2,6} and a worse overall survival as compared to patients with ER+ metastatic breast cancer of no special type (NST)¹, highlighting the need for new treatment modalities. CDK4/6 inhibitors combined with endocrine treatment are an effective treatment option for patients with metastatic ER+ ILC⁹, but no other highly effective treatment options have been defined once patients become resistant to endocrine treatment. Although ILCs are a different disease entity as compared to NST, so far patients with ILC have been underrepresented in clinical trials for breast cancer¹⁰ and reports of clinical trials specifically for ILC are lacking.

Several groups have shown that based on transcriptomic profiling a subgroup of ILCs can be characterized as immune-related (IR) with high levels of immune-related genes, expression of immune checkpoints and lymphocytic infiltration^{5,11,12}. This suggests that a subset of ILCs might benefit from immune checkpoint blockade (ICB). While ICB in combination with chemotherapy has become standard of care in PD-L1 positive metastatic TNBC¹³, in patients with ER+ breast cancer only a small subgroup of patients benefits from ICB. Objective response rates (ORR) to ICB monotherapy in metastatic ER+ breast cancer (including all histological subtypes) range from 3%-12%^{14,15} to 27%-41% in combination with eribulin^{16,17}. Notably, in the KEYNOTE-028 for patients with metastatic PD-L1 positive ER+ breast cancer, two out of three responders were ILC patients¹⁵. Rational treatment combinations are needed to improve responses to ICB in ER+ breast cancer and in ILC specifically.

Previous data indicates synergy between platinum compounds and ICB in genetically engineered mouse models for ILC¹⁸. Of note, while these models strongly resemble human ILC, the field traditionally lacks models for endocrine-sensitive ILC^{19,20}. Additionally, immune-related ILCs, characterized by expression of immune-related genes, were responsive to DNA damaging agents, such as platinum, *in vitro*¹¹. Mechanistically, platinum agents have been shown to trigger the cyclic GMP-AMP synthase (cGAS) - stimulator of interferon (IFN) genes (STING) pathway by increasing the amounts of cytosolic DNA²¹ and to increase MHC class I expression²². Based on

these data, we hypothesize that the combination of platinum-based chemotherapy and ICB could be effective in patients with ILC.

Here, we report the clinical and translational results of stage I of the GELATO-trial, in which patients with metastatic ILC were treated with anti-PD-L1 until disease progression, combined with low-dose carboplatin as immune induction. To dissect the immunomodulatory effects of carboplatin alone and in combination with anti-PD-L1, we profiled immune cells in the circulation and in the tumor microenvironment of longitudinal biopsies of metastatic lesions. Besides PD-L1 expression, stromal tumor-infiltrating lymphocyte (sTIL) and CD8+ T-cell levels, deconvolution algorithms and specific immune-related gene signatures were used to dissect the effect on the various T-cell populations as well as on other elements of the cancer-immunity cycle. In addition, we studied paired primary tumors and metastatic lesions to unravel differences in the immune landscape during ILC disease progression. Finally, we studied whether carboplatin is able to modulate PD-L1 expression patterns across different metastatic lesions, using molecular imaging (^{89}Zr -atezolizumab-PET²³). The GELATO-trial is the first clinical trial specifically conducted in patients with ILC, and our results provide novel insights in the biology of metastatic ILC.

Results

Inclusion and patient demographics

In the GELATO-trial, patients with metastatic ILC (based on morphology and a negative or aberrant E-cadherin staining) were treated with weekly carboplatin (area under the curve (AUC) 1.5) for the first 12 weeks and atezolizumab (anti-PD-L1) every three weeks starting from the third cycle of carboplatin onwards (Figure 1A). The purpose of this short-term platinum-based regimen was to exploit the immunological effects of carboplatin and potentially synergize with PD-L1 blockade, and not to induce direct cytotoxic effects. The low and weekly dosing was chosen to minimize the risk of hematological toxicity in this heavily pretreated patient population^{24,25}. Following a Simon's two-stage design, 22 patients had to be accrued in the first stage of the trial. Based on a null hypothesis of 10% of patients being progression-free at 24 weeks and an alternative hypothesis of 25%, three out of 22 patients had to be progression-free at 24 weeks to allow continuation of accrual in the second stage of the trial. Between November 2017 and January 2021, 26 patients with metastatic ILC were registered in the trial, of which 23 patients started anti-PD-L1 treatment (Extended Data Figure 1) with the last two patients being registered simultaneously. Eighteen patients had ER+HER2- metastatic disease, whereas five patients had triple-negative disease (Table 1). Four out of five patients with TN-ILC had ER+ primary ILC. Six patients had non-classical ILC based on morphological assessment of a metastatic lesion biopsy. Seventy-eight percent (n=18) of patients had visceral metastases, with 52% (n=12) of patients having liver metastases and 48% (n=11) having three or more metastatic sites, all higher compared to other studies^{1,6} and inherent to our eligibility criteria for biopsy site

availability. Seventy-eight percent (n=18) of patients received prior chemotherapy, with 52% (n=12) of patients receiving prior palliative chemotherapy. Ninety-four percent (n=17) of patients with ER+ disease received prior CDK4/6 inhibitors and 40% (n=2) of patients with TN-ILC received prior platinum. Patients received a median of nine cycles of weekly carboplatin and five cycles of anti-PD-L1.

Table 1: Baseline characteristics of evaluable patients in the per protocol population.

N = 23 evaluable patients	No. of patients	Percentage
Age at inclusion, years (median, range)	60 (45-69)	
WHO performance status		
WHO 0	12	52%
WHO 1	11	48%
Histological subtype (assessed on metastatic lesion)*		
ER+HER2-	18	78%
TNBC	5	22%
HER2+	0	0%
ILC subtype (assessed on metastatic lesion)		
Classic	17	74%
Pleiomorphic [^]	4	17%
Alveolar	2	9%
Germline BRCA1/2 mutations		
gBRCA1 mutation	1	4%
No mutation	4	17%
Unknown	18	78%
Visceral metastasis	18	78%
Liver metastasis	12	52%
No. of metastatic sites		
1-2 metastatic sites	12	52%
≥ 3 metastatic sites	11	48%
LDH		
LDH ≤ ULN	15	65%
LDH ≤ 2x ULN	8	35%
Previous chemotherapy exposure		
Chemotherapy naive	5	22%
(Neo)-adjuvant	15	65%
Palliative	12	52%
Previous platinum treatment		
ER+	0	0%
TNBC	2	40% of TNBC
Previous exposure to CDK4/6 inhibitors		
ER+	17	94% of ER+
TNBC	0	0%
Disease-free interval		
De novo M1	5	22%
DFI ≤ 5 years	12	52%
DFI > 5 years	6	26%
No. of cycles carboplatin (median, range)	9 (3-12)	
No. of cycles atezolizumab (anti-PD-L1) (median, range)	5 (1-16)	

*ER+ ≥10% expression, TNBC defined as having ER and PR <10% and HER2-. 4/5 patients with a triple-negative metastasis had a primary ER+ tumor. [^]Two of the patients had TNBC. World Health Organization (WHO), lactate dehydrogenase (LDH)

Efficacy

Four patients out of the 23 evaluable patients (per protocol population) had a partial response (PR), leading to an objective response rate (ORR) of 17% (95% CI 5-39%) with two responses being short-lived. The median duration of response was 14.9 weeks. Two additional patients had stable disease (SD) or non-complete response (non-CR)/non-progressive disease (non-PD) for at least 24 weeks, resulting in a clinical benefit rate of 26% (95% CI 10-48%, Table 2, Figure 1B-D). Remarkably, four out of these six patients with clinical benefit had TN-ILC (Figure 1B). Four out of the first 22 patients were free of progression at 24 weeks, meeting the primary endpoint of the first stage of the trial for which at least three responders were needed. However, as responses were generally short-lived and observed mainly in patients with TN-ILC, the trial stopped accrual after the first stage was completed. One patient has an ongoing partial response even after PD-L1 blockade was stopped due to toxicity (Figure 1B). With a median follow-up of 23.8 months, we observed a median overall survival of 54.4 weeks and favorable survival of patients with clinical benefit (Figure 1E).

Table 2: Efficacy analysis of evaluable patients in the per protocol population.

N = 23 evaluable patients	
Best overall response (RECIST1.1), no (%)	
Complete response (CR)	0 (0)
Partial response (PR)	4 (17) [^]
Stable disease (SD) or non-CR/non-PD >24 weeks*	2 (9)
Progressive disease (PD)	17 (74)
Objective response rate (CR+PR)[^]	17% (95%CI: 5-39%)
Clinical benefit rate (CR+PR+SD>24 weeks)	26% (95%CI: 10-48%)
Median duration of response	14.9 weeks (95%CI: 6.1 weeks - not reached)
Median progression-free survival according to RECIST1.1 (22 events)	13 weeks (95%CI: 8.1 - 19.7 weeks)
Median progression-free survival according to iRECIST (22 events)	14 weeks (95%CI: 9.0 - 20.14 weeks)
Median overall survival (16 events)	54.4 weeks (95%CI: 23.6 weeks - not reached)

*1 patient had stable disease of 24 weeks according to iRECIST. Confidence interval (CI). [^]one partial response was unconfirmed.

Toxicity

Carboplatin and anti-PD-L1 were generally well tolerated, with 26% and 48% of patients, respectively, not experiencing any treatment-related adverse events (Supplementary Table 1). The most commonly observed adverse event induced by carboplatin was neutropenia, which occurred in 48% of patients (Supplementary Table 2). Anti-PD-L1 caused an increase in aspartate aminotransferase (ASAT) in 17% of patients, with only one patient having a grade 4 increase requiring corticosteroid treatment (Supplementary Table 3). Other relevant immune-related events were hypophysitis and colitis, occurring in two patients and one patient, respectively (Supplementary Table 3). No other endocrinopathies, such as thyroid

dysfunction, were reported. One patient experienced immune-related myalgia and an immune-related sarcoid-like reaction of the mediastinal lymph nodes, cytologically confirmed granulomatous inflammation, and subsequent hoarseness. This patient stopped anti-PD-L1, was treated with steroids and had an ongoing response at the time of data cut-off.

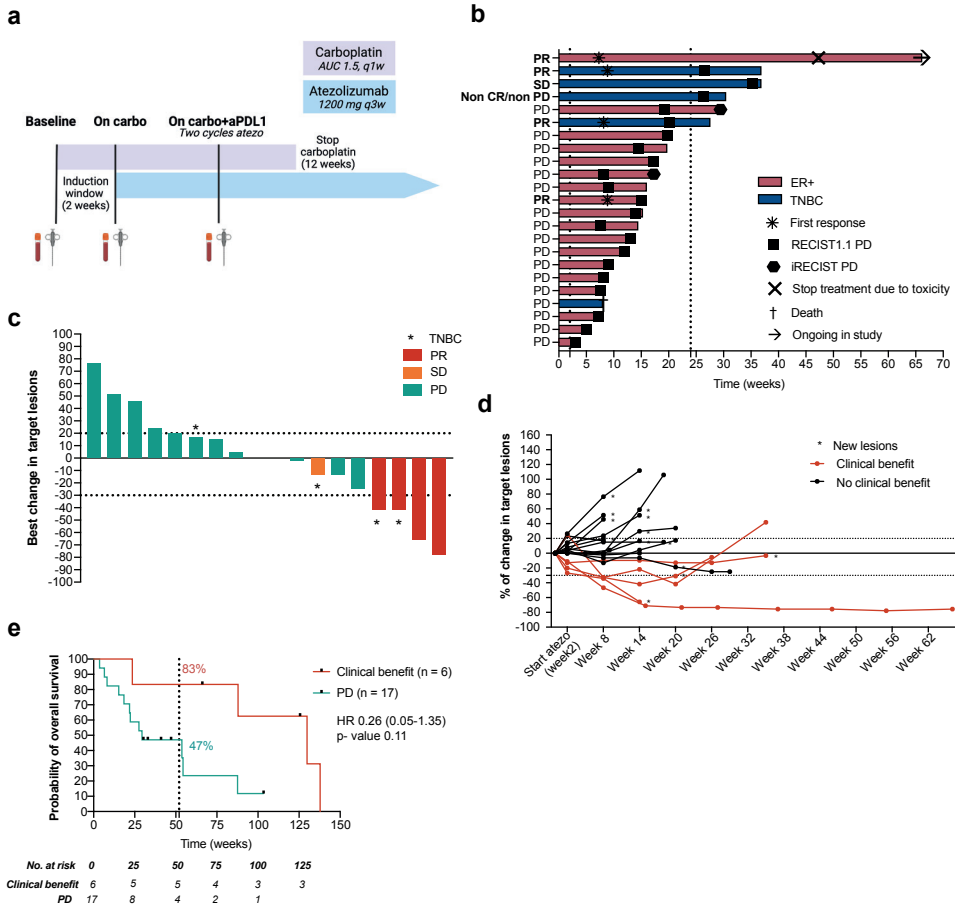


Figure 1. Design of GELATO-trial and efficacy data. (a) GELATO-trial setup. Patients were treated with 12 cycles of low-dose carboplatin. Atezolizumab (anti-PD-L1) was added from the third cycle onwards until disease progression or toxicity. Biopsies and blood were taken at baseline, before the start of anti-PD-L1 and during carboplatin+anti-PD-L1. Created with BioRender.com. (b) Swimmer's plot of all included patients. Each bar reflects one patient and is annotated with events indicated by the legend and clinical response according to RECISTv1.1. The dotted lines indicate the start of anti-PD-L1 at two weeks and the 24-week landmark of the primary endpoint. (c) Waterfall plot of patients with measurable disease (n=18). (d) Change in target lesions of patients with measurable disease. (e) Kaplan-Meier curve of overall survival in patients with clinical benefit versus no clinical benefit. The dotted line indicates one-year survival and the table lists numbers at risk at indicated timepoints. Hazard ratio was calculated using time-dependent Cox regression analysis with time to death for patients with clinical benefit calculated from the date of first partial response or from 24 weeks onwards for the patients with stable disease.

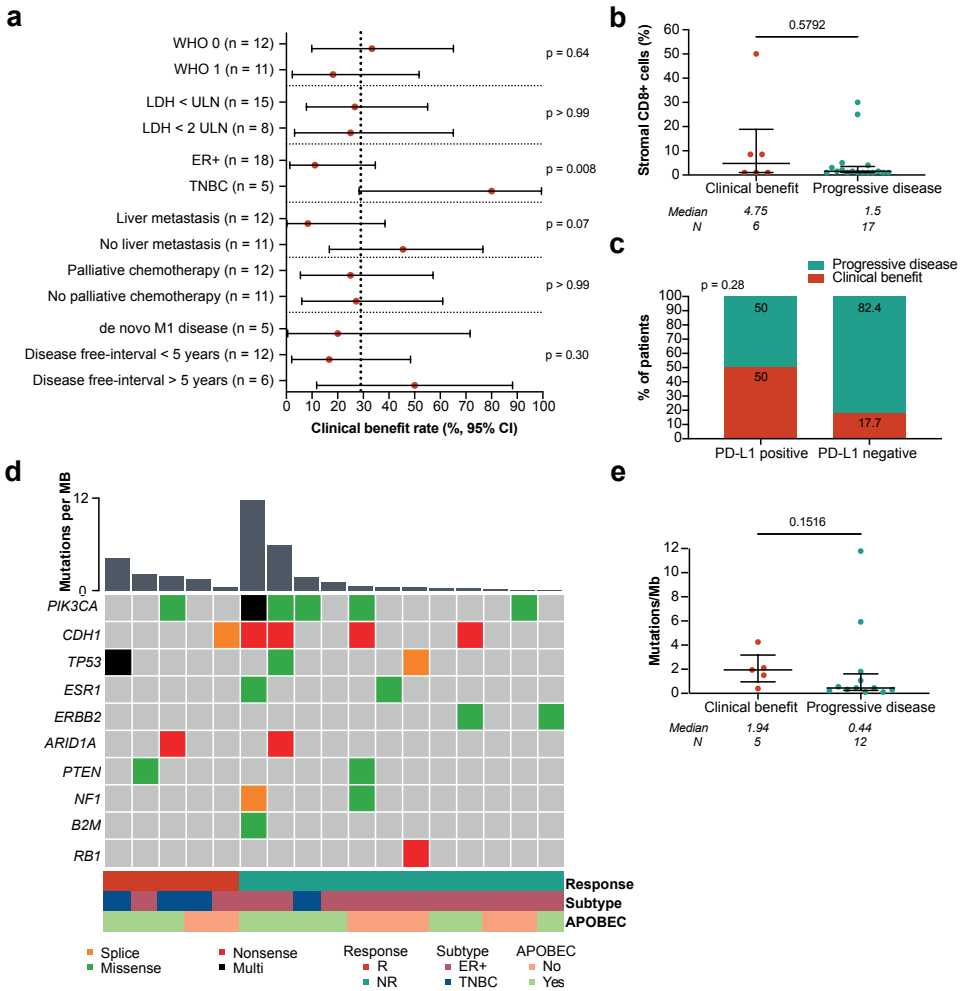


Figure 2. Association of baseline clinical features and characteristics of the tumor microenvironment with clinical benefit. (a) Clinical benefit rate and 95% confidence interval per indicated subgroup. Statistics by Fisher’s exact test (two groups) or Chi-square test (multiple groups). (b) Percentage of CD8+ cells in the stromal area of a metastatic lesion (immunohistochemistry). Median with interquartile range, statistics by Mann-Whitney-U test. (c) Percentage of patients with clinical benefit and PD-L1 expression (clone SP142). A cut-off of 1% expression on immune cells for PD-L1 positivity was used. Numbers in the graph indicate percentages, statistics by Fisher’s exact test. (d) OncoPrint of tumor mutational burden (TMB, mutations per MB) and selected genes frequently altered in metastatic ILC³¹⁻³³, assessed in biopsies of metastatic lesions. Data was available for 17 patients. Each column represents one patient and is annotated by response, subtype and enrichment of the APOBEC mutational signature. (e) TMB of metastatic lesions in relation to response. Statistics as in (a). (b)-(e) Baseline metastatic lesions correspond to metastases presented in Figure 3 and Extended Data Figure 3 and 4.

Exploratory associations with clinical benefit to carboplatin and anti-PD-L1

Patients with TN-ILC had a significantly higher clinical benefit rate as compared to patients with ER+ILC (p=0.008, Figure 2A). We observed a non-significant higher clinical benefit rate in patients without liver metastases (p=0.07), in line

with previous findings that liver metastases might have detrimental effects on immunotherapy efficacy²⁶. Looking into immune features of the metastatic lesions, we observed low baseline stromal tumor-infiltrating lymphocytes (sTILs, median 1%) and stromal CD8 T-cell levels (median 1.5%), and no association between sTILs or CD8+ T cells and clinical benefit (Figure 2B, Extended Data Figure 2A). A higher clinical benefit rate was observed in patients with PD-L1 positive tumors ($\geq 1\%$ expression on immune cells, SP142, Figure 2C), but this was not statistically significant. Using RNA sequencing, we assessed previously established gene signatures of response to ICB. An IFN γ signature²⁷, exhausted T-cell signature²⁸, tertiary lymphoid structure (TLS) signature²⁹ and a signature capturing immune checkpoint molecules³⁰, were all not significantly associated with clinical outcome (Extended Data Figure 2B-E). Of note, the patient with an ongoing durable response at data cut-off had high levels of stromal CD8+ cells (50%) and relatively high expression of immune-related genes, suggesting that, although rare in ILC, patients with high immune infiltration can benefit from ICB. We observed several genomic alterations in metastatic lesions with a well described role in metastatic ILC³¹⁻³³, with *PIK3CA* being the most frequently mutated gene (Figure 2D). There was a non-significantly higher total tumor mutational burden (TMB) in responders ($p=0.15$; Figure 2E) and in patients with TN-ILC ($p=0.10$, Extended Data Figure 2F). Additionally, 41% of the lesions demonstrated an APOBEC enrichment profile (Figure 2D)³¹, and APOBEC and cytosine deamination comprised the most prominent mutational signatures enriched in the data (Extended Data Figure 2G).

Tumor-immune evolution of primary tumors to distant metastasis

To study the evolution of the immune landscape between matched primary lesions and metastases in ILC, we collected archival primary tumors and local recurrences (characteristics of this patient subset in Supplementary Table 4). We observed slightly higher sTIL levels ($p=0.03$) in metastases compared to primary tumors, while this was not accompanied by a significant increase in PD-L1 and CD8 T cells (Extended Data Figure 3A-C). Using CIBERSORTx immune cell deconvolution³⁴ on gene expression data, we observed little immune infiltration across tumors and across timepoints, with M2 macrophages being the most abundant cell type (Extended Data Figure 4A-B) and confirmed that CD8 T-cell levels did not differ between paired primary and metastatic lesions (Figure 3A). Resting mast cells and memory B cells were the only immune cell populations that were significantly lower in metastases (Figure 3B-C). Furthermore, we applied the four previously assessed immune-related signatures and found no significant changes in expression of IFN γ -related genes, exhausted T cells, TLS or immune checkpoints (Extended Data Figure 3D-G). Looking at differences in genomic profiles, we found non-significantly higher TMB in metastases as previously described^{31,32} (Figure 3D). To assess other biological differences between paired primary tumors and metastases, we performed a gene set enrichment analysis (GSEA) of the Hallmark gene sets³⁵ (Extended Data Figure 4C-D). In metastases, we observed enrichment of glycolysis and oxidative phosphorylation gene sets (Extended Data Figure 3H-I), indicative of increased cellular respiration, and enrichment of *MYC* targets and mTOR signaling (Extended Data Figure 3J-K), suggestive of acquired signaling pathway alterations.

Altogether, we observed subtle differences between primary and metastatic lesions but the immune landscape remained largely unaffected.

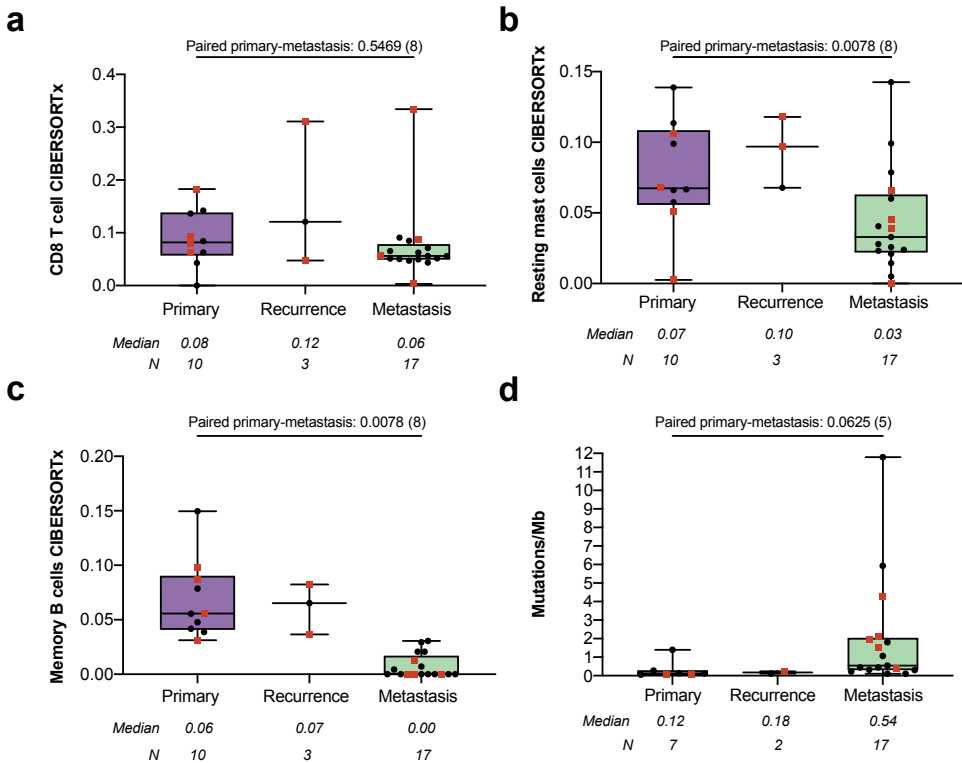


Figure 3. Tumor-immune evolution in paired primary tumors, local recurrences and metastasis. (a) Gene set expression score of CD8 T cells according to CIBERSORTx in paired primary tumors, recurrences, and metastasis. (b) Gene set expression score of resting mast cells according to CIBERSORTx in paired primary tumors, recurrences, and metastasis. (c) Gene set expression score of memory B cells according to CIBERSORTx in paired primary tumors, recurrences, and metastasis. (d) TMB in paired primary tumors, recurrences, and metastasis. (a)-(d) Boxplots display median with range. Statistics by Wilcoxon-signed-rank test on paired primary tumors and metastases, the number of patients in each analysis are listed between brackets behind the p-value. Red squares indicate patients with clinical benefit, black dots patients with no clinical benefit. Metastatic lesions correspond with baseline samples presented in Figure 2, Figure 4, Extended Data Figure 2, 4 and 6.

Carboplatin and anti-PD-L1 mediated changes in circulating immune cell populations

Several circulating immune cell populations can be affected by ICB, resulting in increased exhausted T cells, eosinophils or a decreased neutrophil-to-lymphocyte ratio (NLR)³⁶⁻³⁸. To investigate this in ILC, we characterized absolute counts of immune cell populations in fresh blood by flow cytometry at baseline, during carboplatin, and during carboplatin+anti-PD-L1 (Supplementary Table 5). After two cycles of carboplatin, no major changes were observed in circulating immune

cells (Figure 4A), but after carboplatin and anti-PD-L1 we observed a significant decrease in neutrophils, basophils, eosinophils and the NLR, probably related to the cumulative carboplatin effect (Figure 4B, Extended Data Figure 5A-B). Circulating total T cells, CD4+ and CD8+ T cell levels remained unaffected (Extended Data Figure 5C-E) but we observed a significant increase upon carboplatin and anti-PD-L1 in circulating PD-1+CTLA4+ CD8+ T cells (Extended Data Figure 5F-G). This suggests systemic reinvigoration of a dysfunctional or exhausted T cell population that is frequently used as a proxy for the presence of a tumor-reactive T-cell compartment³⁹⁻⁴¹.

Immune-mediated changes by carboplatin and anti-PD-L1 in the tumor microenvironment

Next, we assessed treatment-induced changes by carboplatin and anti-PD-L1 within the tumor microenvironment (TME) of ILC metastases. Using CIBERSORTx immune cell deconvolution³⁴, we observed increased CD8 T cells during anti-PD-L1, most notably in the patient with a durable response (Figure 4C), and the same pattern was seen when analyzing CD8 using immunohistochemistry (IHC) (Extended Data Figure 6A). sTIL levels remained largely unaffected (Extended Data Figure 6B). Interestingly, while mast cells decreased during ILC disease progression (Figure 3B), resting mast cells increased during carboplatin (Extended Data Figure 6C). Next, we assessed immune-related gene signatures and observed a significant increase after carboplatin and anti-PD-L1 in exhausted T cells²⁸, TLSs²⁹ and immune checkpoint expression³⁰, and a trend towards a higher IFN γ signature score, but only when compared to the on-carboplatin timepoint (before the start of anti-PD-L1) indicating a subtle decrease of these signatures upon carboplatin alone (Figure 4D-G). Of note, we observed no differentially expressed genes or Hallmark gene sets after carboplatin with or without anti-PD-L1 (data not shown). Next, we investigated changes in PAM50 molecular subtype during treatment in the metastatic setting. We observed that the majority of tumors (59%, 10 out of 17) were classified as HER2-enriched at baseline (Figure 4H), while patients had no HER2-overexpression or amplification. Notably, we observed that the PAM50 subtype changed in six out of 16 patients during treatment with carboplatin with or without anti-PD-L1, of which three were responders. High proportions of HER2-enriched metastases have been observed before in breast cancer, possibly due to disease progression in a more aggressive phenotype^{42,43}. Finally, we tested our preclinical hypotheses on immunogenic effects of carboplatin and, surprisingly, did not see alterations in gene signatures for cGAS-STING⁴⁴, immunogenic cell death⁴⁵, MHC class I or MHC class II (Figure 4I-J, Extended Data Figure 6D-E). In conclusion, induction with two cycles of carboplatin did not lead to major changes in the TME, but the combination of carboplatin and anti-PD-L1 was able to induce immune infiltration by CD8 T cells and increased expression of immune-related genes.

PD-L1 uptake after carboplatin induction by ⁸⁹Zr-atezolizumab-PET

To investigate the effect of carboplatin on the TME in a non-invasive fashion, which could be particularly attractive for ILC where biopsies can be challenging to obtain, we explored the use of ⁸⁹Zr-atezolizumab-PET. Repeated ⁸⁹Zr-atezolizumab-

PET could be performed in one patient, who had two measurable lesions on computed tomography (CT) scan (breast, liver), and twelve other lesions on FDG-PET at baseline (Extended Data Figure 7). Heterogeneous ^{89}Zr -atezolizumab uptake between the lesions was observed, at baseline and after two cycles of carboplatin. Contrary to the hypothesis of PD-L1 induction by carboplatin, but in line with lack of clinical treatment benefit in this patient, the median tumor-to-blood ratio (TBR) decreased after induction treatment ($p=0.01$; Figure 4K) particularly in the index breast lesion. Meanwhile the maximal standardized uptake value (SUV_{max}) of this lesion remained low (2.13 and 1.2 respectively), in line with its negative PD-L1 IHC (0% in immune cells) at baseline and after carboplatin. Concluding, repeated ^{89}Zr -atezolizumab-PET showed heterogeneity in dynamics of tracer uptake in tumor lesions and background during carboplatin treatment.

Figure 4. (opposite) Effects of carboplatin and anti-PD-L1 on circulating immune cells and the tumor microenvironment. (a) Volcano plot of the \log_2 fold change (horizontal axis) after two cycles of carboplatin to baseline in circulating immune cells, assessed by flow cytometry, and the adjusted p-value (vertical axis). The dotted horizontal line indicates the 20% false discovery rate (FDR) threshold, dotted vertical lines indicate a \log_2 fold change of 0.75. Statistics by linear modeling (Methods). For all tested populations, see Supplementary Table 5. (b) Volcano plot of \log_2 fold change after carboplatin and anti-PD-L1 to baseline in circulating immune cells assessed by flow cytometry. Statistics as in (A). (c) Gene set expression score of CD8 T cells according to CIBERSORTx in serial metastatic biopsies taken at baseline, after two cycles of carboplatin and after two cycles of anti-PD-L1 plus carboplatin. (d) Gene expression of an exhausted T-cell signature²⁸ in serial biopsies of metastatic lesions. (e) Gene expression of a tertiary lymphoid structure (TLS) signature²⁹ in serial biopsies of metastatic lesions. (f) Gene expression of an immune checkpoint signature³⁰ in serial biopsies of metastatic lesions. (g) Gene expression of an IFN γ signature²⁷ in serial biopsies of metastatic lesions. (h) PAM50 molecular subtype assessed in serial biopsies of metastatic lesions. Each row is one patient and annotated with response according to RECISTv1.1 and subtype assessed on a metastatic lesion. (i) Gene expression of a cGAS-STING signature⁴⁴ in serial biopsies of metastatic lesions. (j) Gene expression score of MHC class I related genes (*HLA-A*, *HLA-B*, *HLA-C*). (k) Tumor-to-blood ratio of ^{89}Zr -atezolizumab-PET at baseline and after two cycles of carboplatin in lesions of one patient. (c)-(g), (i)-(j) Boxplots display median with range. Statistics with Wilcoxon-signed-rank on paired samples, the number of patients in each analysis are listed between brackets behind the p-value. Red squares indicate patients with clinical benefit, black dots patients with no clinical benefit. Baseline metastatic lesions correspond to metastases presented in Figure 3 and Extended Data Figure 3 and 4.

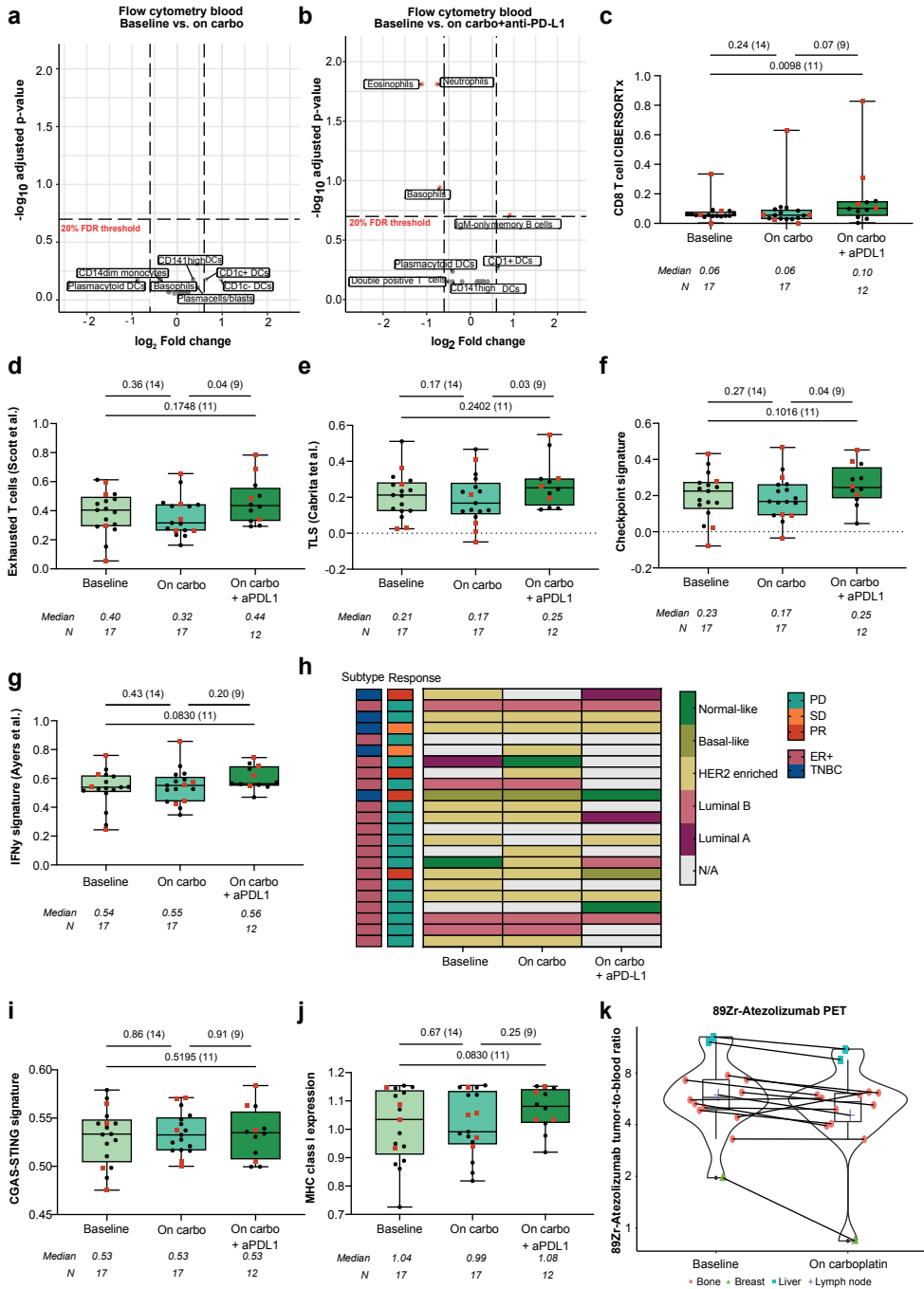


Figure 4. Effects of carboplatin and anti-PD-L1 on circulating immune cells and the tumor microenvironment.

Discussion

To our knowledge, the GELATO-trial is the first reported clinical trial conducted specifically in ILC patients based on a hypothesis founded on preclinical and translational data. While carboplatin alone neither led to significant changes in immune cell composition nor in an increase in cGAS-STING signaling or MHC class I expression, the addition of anti-PD-L1 caused an increase in CD8 T-cell infiltration and higher expression of immune-related gene signatures. Four out of the first 22 patients were progression-free at 24 weeks in the first stage of the trial, warranting expansion of the trial according to the Simon's two-stage design. However, responses were mainly observed in patients with TN-ILC and responses were not durable. This suggests that most responses could have been mainly induced by carboplatin and to a lesser extent by anti-PD-L1, since carboplatin monotherapy is effective in approximately 30% of patients with metastatic TNBC²⁴. Since ICB plus chemotherapy is now standard of care for patients with PD-L1 positive ($\geq 10\%$ combined positive score, 22C3) metastatic TNBC¹³, regardless of histological subtype, the study team decided, despite meeting the success criteria for stage I, not to proceed to the next stage of the GELATO-trial. The lack of responses to anti-PD-L1 in ER+ ILC could be partially explained by not pre-selecting patients based on a pre-existing anti-tumor immune phenotype. Important in this context is that in prior studies, the vast majority of immune-related ILCs was ER-positive. We illustrate this by one ER+ ILC patient with a clear durable response of over one year, with a TME characterized by high sTILs, CD8+ T-cell levels and positive PD-L1 expression at baseline. This indicates that, although rare, ILC patients with an immunogenic phenotype might benefit from ICB.

Recent research has suggested that TN-ILCs have different biological characteristics as compared to TN-NST and ER+-ILC, with increased androgen receptor (AR) signaling and a higher frequency of *HER2* mutations^{8,46}. Though approximately 2% of patients with primary ILC and 12-15% of patients with metastatic ILC harbor a *HER2* mutation and 90% of primary ILCs are considered AR-positive⁴⁷, among TN-ILC 20% of the tumors harbor a *HER2* mutation and 74%-94% of tumors express AR^{8,46}. In GELATO, four out of five patients with TN-ILC had ER+ primary tumors, and all patients with TN-ILC had positive AR IHC expression ($\geq 10\%$ of tumor cells). Recently, it has been shown that AR inhibition and ICB synergize *in vivo*, by reduced suppression of *Ifny* via AR signaling in CD8+ T cells⁴⁸. Also, estrogen signaling has been negatively associated with response to ICB and chemotherapy in metastatic TNBC⁴⁹ and metastatic ER+ breast cancer⁵⁰. Recently, it has been shown that estrogen might polarize tumor-associated macrophages towards an immunosuppressive state in melanoma models⁵¹. Polarized tumor-associated macrophages have been associated with residual disease post-chemotherapy in ER+ breast cancer⁵² and with poor survival in ILC patients⁵³. In our CIBERSORTx analysis, we indeed found M2 macrophages as the most abundant cell type across samples (Extended Data Figure 4A-B). Therefore, targeting AR or macrophages might help to overcome ICB resistance in ILC.

Only one patient with TN-ILC was classified as basal-like by PAM50 in the metastatic setting and four out of five patients with TN-ILCs had ER+ primary tumors. This implicates that although ER expression was lost during disease progression, TN-ILCs do not exhibit a clear basal-like phenotype. A basal-like phenotype has been associated with response to ICB and chemotherapy in early-stage high-risk ER+ breast cancer⁵⁴ and a basal-like immune-activated phenotype in metastatic TNBC⁴⁹.

Interestingly, most metastases were classified as HER2-enriched. This might be an artefact of PAM50 assessment on metastatic lesions and/or fresh-frozen material. However, also in paired lesions of the AURORA program for metastatic breast cancer and another retrospective series, a particular high proportion of HER2-enriched tumors was observed^{42,43}. The high level of HER2-enriched lesions might be due to the more aggressive features of metastatic disease, and endocrine treatment refractory disease potentially losing its luminal features upon disease progression^{42,55,56}. Furthermore, in the recent BioPER trial, after treatment with a CDK4/6-inhibitor, 37.5% of the samples showed an HER2-enriched subtype⁵⁷, suggesting that HER2-enriched tumors are prominent in patients that are heavily pretreated and/or have been exposed to CDK4/6 inhibition, as was the case for 94% of ER-positive GELATO patients. Interestingly, in GELATO 90% of primary tumors were classified as either luminal A or luminal B (data not shown), suggestive of an acquired HER2-enriched phenotype later in the disease course.

During treatment with carboplatin with or without anti-PD-L1, we also observed PAM50 subtype switching in 6/16 patients of which 5 switched towards a luminal or normal-like phenotype. Since we studied serial biopsies of the same lesions, this suggests that treatment modified the tumor-intrinsic characteristics of these lesions towards a less proliferative phenotype. Most notably, the baseline metastatic lesion of the patient with a durable response was characterized as HER2-enriched but switched to a basal-like phenotype during anti-PDL1, suggesting increased susceptibility to ICB.

On the immune cell level, we observed higher levels of CD8+ T cells in the stroma as compared to stromal TILs. As CD8+ T cells comprise the most prevalent immune cell type captured by the sTILs readout^{58,59}, this is surprising. Since both sTILs and CD8+ counts were scored by the same independent expert pathologists, it is unlikely that interrater variability played a major role here. Alternatively, we hypothesize that based on its morphology, sTILs can be easily misunderstood for tumor cells in ILC, and sTILs might therefore not be the appropriate read-out for anti-tumor immunity in ILC. Research comparing sTILs in ILC with other subtypes might have underestimated sTILs scores in ILC and incorporating a CD8 staining may improve immune assessment in patients with ILC.

Our trial is limited by a small sample size and lack of a control arm. Of note, the inclusion of a relatively small number of patients (n=23) in high-volume breast cancer centres took approximately 3.5 years. In view of the priority for translational research, patients with bone-only disease or only small lesions in, for example, the

peritoneum could not participate due to the lack of an available biopsy site, which might have slowed down inclusion. Since serial biopsies were mandatory in the trial, we included a relatively high proportion of ILC patients with visceral metastasis (18 out of 23), higher as compared to the general ILC population¹, making our cohort not fully representative of the general ILC population. Additionally, the included patients comprise a heterogeneous group characterized by different pre-treatment regimens, biopsy locations and hormone receptor status. Due to the small number of patients, our translational analyses should be considered exploratory. However, given the strong preclinical rationale behind the GELATO-trial, we would like to highlight the importance of the validation of preclinical findings in patients which was the main reason to execute the GELATO-trial.

Although ILCs comprise a separate disease entity within the breast cancer subtypes, so far reports of clinical trials specific for patients with ILC were lacking⁶⁰ and patients with metastatic ILC are often underrepresented because of a lack of measurable disease¹⁰. In our experience, several patients stopped treatment early due to rapid clinical progression (Extended Data Figure 1). These aspects of the disease complicate the inclusion of ILC patients in clinical trials. Moreover, to our knowledge only two reports of recent randomized trials for novel treatment options in ER+ metastatic breast cancer have presented prespecified subgroup analysis in ILC patients, namely benefit from CDK4/6 inhibition to endocrine treatment in ILC patients with metastatic ER+ILC⁹ and more recently a high clinical benefit rate was observed to neratinib and fulvestrant in *HER2*-mutated ILC in the phase II MutHER trial⁶¹. Targetable features of ILC are for example: high expression of ER/luminal A phenotype, synthetic lethal deficiency of ROS1/E-cadherin⁶², high tumor-mutational burden^{31,32}, high T-cell infiltration^{5,11,12} and downstream activation of the PI3K-AKT-mTOR pathway via activating *PIK3CA* mutations^{5,31}, activating *HER2* mutations^{31,33} or activation via the insulin-like growth factor 1 receptor (IGF1R)⁶³. Some of these concepts are currently under investigation in ILC-specific clinical trials, such as inducing synthetic lethality with ROS1 inhibitors in E-cadherin negative cells in both early-stage and metastatic ILC (NCT04551495, NCT03620643); exploiting sensitivity to neo-adjuvant endocrine treatment in early-stage ILC (NCT02206984, NCT01953588) or in combination with CDK4/6 inhibition (NCT02764541); and targeting activating *HER2*-mutations in metastatic ILC with neratinib and fulvestrant in a basket of the SUMMIT-trial (NCT01953926). Additionally, based on preclinical data and our work presented here, targeting the PI3K-AKT-mTOR pathway^{64,65} or macrophages⁶⁶ in combination with ICB and/or chemotherapy might be promising treatment strategies for ILC patients. Besides trials specific for ILC, subgroup analyses of ILC patients in randomized clinical trials are of vital importance to inform treatment decisions for ILC patients and thereby improve outcome for this difficult-to-treat breast cancer subtype.

In conclusion, this is the first report on a clinical trial specific for metastatic ILC representing a difficult-to-treat breast cancer subtype and we demonstrate that the combination of carboplatin and anti-PD-L1 induces clinical and immunological responses in a subset of ILC patients. Most of the responses were observed in

patients with TN-ILC, highlighting that patients with TNBC should be considered for ICB regardless of histological subtype. Our work provides novel hypotheses and paves the way for highly needed ILC-specific clinical trials.

Methods

Study design

GELATO is a phase-II, single-arm, multicenter clinical trial, conducted at four centers in the Netherlands (NCT03147040) to evaluate the efficacy of carboplatin and atezolizumab (anti-PD-L1) in patients with metastatic ILC. Lobular histology needed to be confirmed on a biopsy of a metastatic lesion with a negative or aberrant E-cadherin immunohistochemistry (IHC) staining. Eligible patients were treated with 12 cycles of weekly carboplatin (AUC of 1.5 mg/ml x min) and atezolizumab (anti-PD-L1; 1200 mg flat-dose) every three weeks starting from the third cycle of carboplatin onwards (Figure 1A). The purpose of this short-term, low-dose platinum regimen was to exploit the immunological effects of carboplatin instead of establishing a direct cytotoxic effect and avoid potential prolonged bone marrow suppression. As responses to immunotherapy in the metastatic breast cancer setting are predominantly observed within 12 weeks^{15,67,68}, the duration of carboplatin induction treatment was limited to 12 weeks. Additionally, a low carboplatin dose (AUC 1.5) was administered to minimize the risk of prolonged bone marrow suppression, as also used in prior clinical studies^{69,70}.

Anti-PD-L1 was continued until disease progression according to RECISTv1.1⁷¹, clinical progression or unacceptable toxicity. Before the start of carboplatin, after two cycles of carboplatin (two weeks from baseline) and after two cycles of anti-PD-L1 (+ 6 weekly administrations of carboplatin, 8 weeks from baseline), blood was drawn and sequential biopsies from a metastatic lesion were taken. The first six patients were included in a 3+3 phase Ib safety run-in part, with the same treatment schedule, and were included in the total number of patients. The trial was conducted in accordance with Good Clinical Practice guidelines and the Declaration of Helsinki. All patients provided written informed consent. The trial protocol, informed consent form and amendments were approved by the medical-ethical committee of the Netherlands Cancer Institute. This investigator-initiated trial was sponsored by the Netherlands Cancer Institute, atezolizumab was provided by Roche.

Eligibility criteria GELATO-trial

Eligible patients had metastatic or incurable locally advanced ILC. Patients were not preselected based on PD-L1 expression. Patients had to have a metastatic lesion or recurrence available for sequential biopsies (bone lesions were not allowed) and had to have evaluable disease according to RECISTv1.1⁷¹. In case of Estrogen Receptor (ER+) disease, patients had to have progression after endocrine treatment in the advanced setting and had to have received an anti-estrogen and an aromatase inhibitor in the early-stage or for advanced setting. A maximum of

two lines of palliative chemotherapy was allowed. Patients had to have a WHO performance status of 0 or 1, and normal bone marrow, kidney and liver functions with a Lactate Dehydrogenase (LDH) below 500 U/L (2 times upper limit of normal). Exclusion criteria were bone-only disease, symptomatic brain metastasis (stable and treated brain metastases were allowed), leptomeningeal disease localization, previous treatment with immune checkpoint inhibitors and/or a history of autoimmune disorders requiring immunosuppressive treatment. At the start of the trial, patients were eligible regardless of their receptor status. Since we aimed for a representative patient population for ILC with 10-20% ER- patients^{1,2}, inclusion of patients with triple-negative (TN)-ILC (ER and PR expression <10%, HER2-negative) was stopped after reaching 20% of total patients.

Trial procedures

Clinically stable patients with disease progression according to RECISTv1.1 were permitted to continue anti-PD-L1 until confirmation of progression on a subsequent CT scan according to iRECIST guidelines⁷². Response evaluation was performed by a CT-scan of the neck (if applicable), thorax and abdomen (including pelvis) at baseline (four weeks prior to start), before the start of anti-PD-L1, and every six weeks during treatment (every nine weeks after 24 weeks). RECISTv1.1 measurements were done by experienced breast cancer radiologists and in case of inconsistencies revised by one dedicated radiologist. Carboplatin treatment was withheld in case of hematological toxicity, such as anemia or neutropenia. Dose modification of atezolizumab was not allowed, but treatment interruptions were allowed in case of toxicity or suspicion thereof. Adverse events (AEs) were monitored every three weeks (weekly during carboplatin treatment) by laboratory assessments, vital signs and physical examinations. Grading of AEs was done per National Cancer Institute's Common Terminology Criteria for Adverse Events (NCI-CTCAE) v4.03. Supportive treatment with antiemetics, bisphosphonates, and palliative radiation (only if response could still be evaluated) was allowed. Archival formalin-fixed paraffin-embedded (FFPE) blocks of primary tumors (biopsies in case of neo-adjuvant chemotherapy or resection material) were collected via PALGA (the nationwide network and registry of histo- and cytopathology in the Netherlands)⁷³.

Trial objectives and endpoints

The primary endpoint of the trial was progression-free survival (PFS) rate at six months (24 weeks), assessed from date of registration to date of progression according to RECISTv1.1 or death from any cause. Secondary endpoints were progression-free survival (PFS) rate at six months in patients with immune-related ILC, PFS rate at 12 months, PFS according to iRECIST, overall survival (OS), objective response rate (ORR) and safety. The clinical benefit rate (CBR) comprised complete responses (CR), partial responses (PR) and stable disease (SD) for at least 24 weeks. PFS and OS were calculated from date of registration to date of progression according to RECIST1.1 and date of death or last date of follow-up, respectively. Patients were censored in case of no event at the last assessment before the data cut-off of 1 October 2021. Duration of response was calculated

from the first date of an objective response to date of progression according to RECIST1.1. Translational endpoints were the assessment of immunogenic effects of carboplatin on the TME and in the circulation using immunohistochemistry, next-generation sequencing and flow cytometry; the additive effect of anti-PD-L1 on these changes; and exploration of predictive biomarkers.

Statistical considerations

A Simon's two-stage⁷⁴ design was used to determine the sample size. The median PFS of palliative chemotherapy regimens in patients with endocrine-treatment refractory breast cancer typically lies within 2-4 months^{75,76}. If 25% of patients were free of progression at 6 months (24 weeks) in the GELATO-trial, this would warrant further investigation of the treatment regimen. The null hypothesis that the true proportion of patients progression-free at six months is 10% or lower was tested against a one-sided alternative of at least 25%. In the first stage of the trial, 22 patients had to be accrued. If two or fewer patients were progression-free at six months, the study would be stopped, otherwise 18 additional patients could be included. This design yields a type one error rate of 0.04 and power of 0.80 when the true proportion of patients progression-free at six months is 25%. The last two patients were registered in the same week and therefore both included in the trial, leading to a total inclusion of 23 patients. Primary endpoint analysis for Simon's two-stage was therefore performed separately for the first included 22 patients. Secondary and translational endpoint analyses were performed in the per protocol population (n=23, patients who received at least one dose of anti-PD-L1, Extended Data Figure 1). The data cut-off for follow-up was 1 October 2021.

Flow cytometry fresh blood

Peripheral blood was collected in an K₂EDTA vacutainer (BD) and processed within 24 hours. Three panels spanning T-cell, B-cell and myeloid cell biology were used (Supplementary Table 5 for all assessed immune cell populations, Supplementary Table 6 for antibodies, gating strategy in Extended Data Figure 8) as described before⁷⁷. Red blood cells were lysed (lysis buffer: dH₂O, NH₄Cl, NaHCO₃, EDTA) and cells were resuspended in PBS containing 0.5% BSA and 2mM EDTA. For surface antigen staining, cells were first incubated with human FcR Blocking Reagent (1:100 Miltenyi) for 15 min at 4°C and then incubated with fluorochrome-conjugated antibodies for 30 min at 4°C, in the dark. For intracellular antigen staining, cells were fixed with Fixation/Permeabilization solution 1X (Foxp3/Transcription Factor Staining Buffer Set, eBioscience) for 30 min at 4°C and stained with fluorochrome-conjugated antibodies in Permeabilization buffer 1X (eBioscience) for 30 min at room temperature. Viability was assessed by staining with either 7AAD staining solution (1:20; eBioscience) or Zombie Red Fixable Viability Kit (1:800 BioLegend). Data acquisition was performed on BD LSRII flow cytometer using Diva software (BD Biosciences) and data analysis was performed using FlowJo software version 10.6.2. To obtain absolute white blood cell counts per mL of human blood, the total post-lysis cell count was obtained using the NucleoCounter NC-200 (Chemometec) automated cell counter. To assess dynamics in each cell population with cell count/mL, linear modeling was performed using limma R package v3.46.0⁷⁸. Predicting

\log_2 transformed cell counts per mL for the same patient at different time points was done as following: $\log_2(\text{cell counts/mL}) - \text{time point} + \text{patient ID}$. The modeling was performed independently for paired samples of baseline versus post-induction (Figure 4A) and baseline versus carboplatin+anti-PD-L1 (Figure 4B). Sample pair dynamics was assessed analogously to the paired t-test. For visualization purposes, Benjamini-Hochberg corrected p-values were plotted against the corresponding \log_2 fold changes: the \log_2 fold change from baseline to pre-atezo ($\log_2(\text{pre-atezo}) - \log_2(\text{baseline})$) and the \log_2 fold change from baseline to on-atezo ($\log_2(\text{on-atezo}) - \log_2(\text{baseline})$) (Figure 4A-B). The plots were made by EnhancedVolcano R package v1.12.0⁷⁹.

TILs and immunohistochemistry

Formalin-fixed paraffin-embedded (FFPE) tumor blocks of archived primary tumor blocks and newly collected biopsies of metastatic lesions were used for sTIL assessment and CD8 and PD-L1 (SP142) immunohistochemistry staining. IHC of formalin-fixed paraffin-embedded FFPE tumor samples was performed on a BenchMark Ultra autostainer (Ventana Medical Systems). Briefly, paraffin sections were cut at 3 μm , heated at 75°C for 28 minutes and deparaffinized in the instrument with EZ prep solution (Ventana Medical Systems). Heat-induced antigen retrieval was carried out using Cell Conditioning 1 (CC1, Ventana Medical Systems) for 32 minutes at 95°C (CD8) or 48 minutes at 95°C (PD-L1). CD8 was detected using clone C8/144B (1/200 dilution, 32 minutes at 37°C, Agilent / DAKO) and PD-L1 using clone SP142 (Ready-to-Use dispenser, 16 minutes at 37°C, Roche / Ventana). Bound antibodies were detected using the OptiView DAB Detection Kit (Ventana Medical Systems). Slides were counterstained with Hematoxylin and Bluing Reagent (Ventana Medical Systems). A PANNORAMIC® 1000 scanner from 3DHISTECH was used to scan the slides at a 40x magnification. Scans of all stainings were uploaded on Slide Score (www.slidescore.com). Stromal tumor-infiltrating lymphocytes (sTILs) were assessed on an H&E slide according to international standard from the International Immuno-Oncology Biomarker Working Group (www.tilsinbreastcancer.org)⁵⁸. CD8 was assessed as percentage of positive cells in the tumor-associated stromal area, and PD-L1 as percentage of positive immune cells in the tumor and stromal area. Two expert pathologists (H.M.H. and R.S.) independently evaluated the stainings digitally and the average of scores was taken.

DNA and RNA sequencing

DNA and RNA material was isolated from FFPE sections of primary tumors or fresh-frozen (FF) tissue sections of biopsies of metastatic lesions, containing at least 30% tumor cells. DNA and RNA isolation was done simultaneously using the Qiagen AllPrep DNA/RNA FF kit for FF tissue and the Qiagen AllPrep DNA/RNA FFPE kit for FFPE blocks, according to manufacturer's instructions. Germline DNA was isolated from peripheral blood using the QIA Symphony DSP DNA midi kit. The total amount of DNA was quantified on the Nanodrop 2000 (ThermoFisher). The amount of double stranded DNA in the genomic DNA samples was quantified using the Invitrogen Qubit® dsDNA HS Assay Kit. Maximum 2000 ng of double stranded genomic DNA

was fragmented by Covaris shearing. Samples were purified using 2X Agencourt AMPure XP PCR Purification beads according to Beckman Coulter manufacturer's instructions. The sheared DNA samples were quantified and qualified on a BioAnalyzer system using the Agilent Technologies DNA7500 assay kit. With an input of maximum 1 µg sheared DNA, library preparation for Illumina sequencing was performed using the KAPA HTP Prep Kit for FF DNA (KAPA Biosystems, KK8234) or KAPA Hyper prep kit (KAPA Biosystems, KK8504) for FFPE DNA. Libraries were amplified with 4 (FF) or 6 (FFPE) PCR cycles and cleaned with 1X AMPure XP beads. Concentrations were measured with DNA7500 chips on a BioAnalyzer system. 6 pools of 6 to 7 samples were created using 500 ng of each indexed sample of FF DNA. 2 pools of 6 to 7 samples were created using 65 ng of each indexed sample of FFPE DNA. 2µl of IDT TS-mix universal blockers and 5µl Invitrogen Human Cot-1 DNA was added to each pool. Each pool was dried with a concentrator (Eppendorf). To each dried pool 8.5µl of hybridization buffer, 3.4µl Hybridization component A (SeqCap Hybridization and wash kit, Roche) and 1.1µl nuclease-free water was added to rehydrate the pool. Each pool was incubated at room temperature for 10 minutes, followed by an incubation at 96 degrees Celsius for 10 minutes. Samples were hybridized with the IDT xGen Exome Research Panel v1.0. The pool was captured and washed following the IDT protocol and amplified using 10 PCR cycles. The amplified pool was purified using AMPure® XP beads (Beckman Coulter). The purified pools were quantified on the Agilent Bioanalyzer 7500 system and one sequence pool was made by equimolar pooling. The sequence pool was diluted to a final concentration of 10nM and subjected to sequencing on an Illumina Novaseq 6000 machine with a SP 300 cycle kit for a paired end 150 bp run for FF samples and with a SP 200 cycle kit for a paired-end 100 bp run for FFPE samples, according to manufacturer's instructions.

Quality and quantity of the total RNA from was assessed by the 2100 Bioanalyzer using a Nano chip (Agilent, Santa Clara, CA). The percentage of RNA fragments > 200nt fragment distribution values (DV200) were determined using the region analysis method according to the manufacturer's instructions (Illumina, technical-note-470-2014-001). Strand-specific libraries were generated using the TruSeq RNA Exome Library Prep Kit (Illumina Inc., San Diego) according to the manufacturer's instructions (Illumina, # 1000000039582v01). Briefly, total RNA was fragmented (only for FF material), random primed and reverse transcribed using SuperScript II Reverse Transcriptase (Invitrogen, part # 18064-014) with the addition of Actinomycin D. Second strand synthesis was performed using Polymerase I and RNaseH with replacement of dTTP for dUTP. The generated cDNA fragments were 3' end adenylated and ligated to Illumina Paired-end sequencing adapters and subsequently amplified by 15 cycles of PCR. The libraries were validated on a 2100 Bioanalyzer using a 7500 chip (Agilent, Santa Clara, CA) followed by a 1-4 plex library pooling containing up to 200ng of each sample. The pooled libraries were enriched for target regions using the probe Coding Exome Oligos set (CEX, 45MB) according to the manufacturer's instructions (Illumina, # 1000000039582v01). Briefly, cDNA libraries and biotin- labeled capture probes were combined and hybridized using a denaturation step of 95°C for 10 minutes and an incubation step from 94°C to

58 °C having a ramp of 18 cycles with 1 minute incubation and 2 °C per cycle. The hybridized target regions were captured using streptavidin magnetic beads and subjected to two stringency washes, an elution step and a second round of enrichment followed by a cleanup using AMPure XP beads (Beckman, A63881) and PCR amplification of 10 cycles. The target enriched pools were analyzed on a 2100 Bioanalyzer using a 7500 chip (Agilent, Santa Clara, CA), diluted and subsequently pooled equimolar into a multi-plex sequencing pool. The libraries were sequenced with 54 paired-end reads on a NovaSeq6000 using a SP Reagent Kit v1.5 (100 cycles) (Illumina Inc., San Diego).

DNA sequencing data analysis

DNA Sequencing data was aligned to GRCh38 reference genome with bwa aligner 0.7.17⁸⁰ using the bwa-mem algorithm. Samtools fixmate 1.13⁸¹ was used to correct mate information, and duplicate reads were marked with Picard MarkDuplicates. Next, base quality scores were recalibrated with GATK BaseRecalibrator⁸², and Mutect2 2.2⁸³ was used to perform variant calling. The data that passed all Mutect2 filters was subsequently filtered with fings 1.7.1⁸⁴ and vcf2maf 1.6.21⁸⁵ was used to run VEP annotation of the variants and to produce a maf file. Variants with a variant allele frequency (VAF) >0.2 were included in final analysis. TMB was calculated with maftools 2.10.5⁸⁶ tmb function. VAF plots, mutational signature plots and oncoplot were created with maftools 2.10.5. Data was analyzed with Python 3.7.6 and R 4.1.1. Pandas 1.3.3^{87,88} was used for data handling.

RNA sequencing data analysis

RNA sequencing data has been aligned to GRCh38 with STAR 2.7.1a, with twopassMode option set to “Basic”⁸⁹. Gene counts were obtained with STAR quantMode option set to “GeneCounts”. Data quality was assessed with FastQC 0.11.5⁹⁰, FastQ Screen 0.14.0⁹¹, Picard CollectRnaSeqMetrics tool⁹² and RSeQC read_distribution.py and read_duplication.py tools 4.0.0⁹³ and found to be suitable for the downstream analysis. Data was subsequently normalised to TPM. For cell deconvolution, CIBERSORTx was run in absolute mode with LM22 Source GEP, performing the batch correction⁹⁴. Differential expression analysis was performed with DESeq2 1.34.0⁹⁵. PAM50 classification was performed with geneFu R package 2.26.0⁹⁶. Gseapy 0.9.18 ssgsea tool⁹⁷ with sample_norm_method option set to “rank” was used for gene set signature scoring. Data was analyzed with Python 3.7.6 and R 4.1.1. Pandas 1.3.3^{87,88} and NumPy 1.18.1⁹⁸ were used for data handling. Seaborn 0.10.0⁹⁹, Matplotlib 3.1.3¹⁰⁰ and statannotations 0.4.3¹⁰¹ have been used for plotting.

⁸⁹Zr-atezolizumab PET/CT imaging

Based on previous work showing superior correlation of zirconium-89 (⁸⁹Zr)-atezolizumab uptake on positron emission tomography/computerized tomography (PET/CT) with clinical response to atezolizumab, compared to immunohistochemistry- or RNA-sequencing-based predictive biomarkers²³, an imaging biomarker side study was performed in the University Medical Center Groningen (NCT04222426). At baseline and after two cycles of carboplatin, a whole body (⁸⁹Zr)-atezolizumab PET/CT was performed on a Biograph mcT 40 or 64-slice

PET/CT (Siemens/CTI, Knoxville, TN), as previously described²³. Tumor lesions were identified on standard baseline FDG-PET/CT, with a minimum width of 10mm. ⁸⁹Zr-atezolizumab-uptake was quantified in all lesions, with a maximum of 10 lesions per organ. Quantification of the ⁸⁹Zr-atezolizumab- and FDG uptake was performed using the Accurate tool¹⁰² and Syngo.via imaging software VB20/30 (Siemens), respectively. A spherical volume-of-interest (VOI) was drawn closely around all metastases. Maximum standardized uptake values (SUV_{max}) were calculated, as well as background mean SUV (SUV_{mean}). Tumor-to-blood ratio's (TBR) were calculated by dividing the SUV_{max} by the thoracic aorta SUV_{mean} ¹⁰³. Change in tumor uptake between ⁸⁹Zr-atezolizumab-PET at baseline and after two cycles of carboplatin was assessed as percentage TBR change. In addition, we calculated the median and range of the ⁸⁹Zr-atezolizumab uptake (TBR), and natural-log-transformed ⁸⁹Zr-atezolizumab uptake to obtain approximate normal distributions, yielding estimates of geometric means following back-transformation of the results.

Statistical analysis

Median time to event was calculated for PFS, OS and duration of response was calculated with the Kaplan-Meier method. Frequencies, such as response rate and clinical benefit rate, were estimated with corresponding two-sided 95% confidence intervals (Clopper-Pearson) and comparisons between frequencies were performed using Fisher's exact test. Two-sided non-parametric tests were used for translational analyses: Mann-Whitney U for two independent groups and Wilcoxon's signed-rank for paired data. Data was analyzed with GraphPad Prism v9.0, IBM SPSS statistics 24, SAS v9.4, Python 3.7.6 and R 4.1.1. Reported p-values are two-sided and unadjusted unless stated otherwise.

Data availability

DNA and RNA sequencing data will be stored in the European GenomePhenome Archive (EGA) and will be made available from the corresponding author upon reasonable request. Data requests will be reviewed by the corresponding author and Institutional Review Board of the NKI and after approval applying researchers have to sign a data transfer agreement with the NKI.

Acknowledgments

We are grateful to the patients and their families for participating in the trial. We thank all supporting clinical trial staff, in particular Myra Jansen, Greetje de Vries and the departments of Medical Oncology, Radiology, Pathology and Dermatology of participating centers. We thank the triallab of the Netherlands Cancer Institute (NKI) for handling incoming blood samples. We acknowledge the Scientific Administration departments of participating centers, particularly Abi Jayakkumar and Michiel Sondermeijer. We thank Marjo Holtkamp and Kim Kersten for patient visits and supporting the scheduling of patients. We are grateful to the

Core Facility of Molecular Pathology & Biobanking for the storage and handling of human tumor material and to the Genomics Core Facility, in particular Roel Kluin, Wim Brugman and Charline van Steenis, for DNA and RNA sequencing. We thank Marieke Bruggeman, Maxime Duijst and Chris Klaver for blood sample experiments and the Flow Cytometry Facility for support in these experiments. We acknowledge PALGA, the Dutch Pathology Registry, for enabling collection of archived material. We thank Ruud Meijer and Jeroen Paardekooper Overman from Roche for enabling the trial and arranging supply of atezolizumab.

Funding

R.S. is supported by the Breast Cancer Research Foundation (BCRF, grant nr. 17-194). Research in the Kok group is funded by the Netherlands Organization for Scientific Research (NWO-VIDI 09150172010043) and the Hendrika Roet fund. This work was supported by F. Hoffmann-La Roche Ltd, Basel, Switzerland (no grant numbers apply).

Author contributions

L.V. coordinated trial procedures, analyzed and interpreted clinical and translational data of the trial, and wrote the manuscript with O.I.I. and M.K. O.I.I. performed and interpreted computational analyses of the DNA and RNA sequencing data. H.M.H. and R.S. performed the histological scoring of the pathology slides. S.B. and K.S. performed the statistical analysis of the trial data. M.C. performed computational analyses of the flow cytometry data. N.A.M.B., E.C. and H.C.G. were responsible for blood sample processing and analysis, supervised by K.E.d.V. and M.K. and H.C.G. designed the flow cytometry panel. C.E.L. revised RECIST1.1 measurements and was together with colleagues involved in taking biopsies. I.K. was responsible for patient care. I.A.M.M. was the clinical projects manager. M.d.M. performed DNA/RNA isolations. J.J.L.v.G. and J.B. coordinated trial procedures in one participating center including the ImaGelato case. M.d.B., M.G.J.v.D., G.S.S., V.C.G.T.H., C.P.S., S.C.L. and M.K. were the main treating physicians. G.S.S., K.E.d.V., T.N.S., C.U.B., S.C.L. and M.K. wrote the trial protocol. L.F.A.W. supervised computational analyses. A.J., V.C.G.T.H, C.P.S., and M.K. were the principal investigators of the trial. All authors edited and approved the manuscript.

Conflicts of interest

L.V., O.I.I., S.B., M.C., N.A.M.B., E.C., H.G., K.S., C.E.L., I.K., I.A.M.M., M.d.M., J.J.L.v.G., J.B., M.G.J.v.D. and A.J. have no competing interests to declare. H.M.H. reports consultancy fees from Roche Diagnostics paid to the institute and is advisor for SlideScore and Ellogon from Roche Diagnostics, outside the submitted work. M.d.B. received funding from Roche, AstraZeneca, Novartis, Pfizer, Eisai and Eli

Lilly, outside the submitted work. R.S. reports non-financial support from Merck and Bristol Myers Squibb (BMS), research support from Merck, Puma Biotechnology and Roche, and personal fees from Roche, BMS and Exact Sciences for advisory boards, all outside the scope of this manuscript. G.S.S. reports research funding to the institute from Merck, Agendia, AstraZeneca, Roche and Novartis and a consulting role for Novartis, Seattle Genetics, Biovica, outside the submitted work. K.E.d.V. reports research funding from Roche and is consultant for Macomics, outside the scope of this work. T.N.S. is consultant for Third Rock Ventures and is stockholder and advisor in Allogene Therapeutics, Asher Bio, Celsius, Merus, Scenic Biotech and Neogene Therapeutics, outside this work. C.U.B. has received research grants from Novartis, BMS and NanoString, is a paid advisory board member for BMS, MSD, Roche, Novartis, GlaxoSmithKline, AstraZeneca, Pfizer, Lilly, GenMab and Pierre Fabre, and holds ownership interest in Uniti Card, Neon Therapeutics and Forty Seven, all outside this submitted work. L.F.A.W. reports funding to the institute from Genmab BV. V.C.G.T.-H. reports research funding to the institute from Roche, Eisai, Pfizer, Novartis, Lilly, Daiichi Sankyo/Astra Zeneca and Gilead Sciences, a consulting role from Pfizer, Lilly, Accord Healthcare and Novartis and honoraria from Novartis, Roche, Lilly and AstraZeneca, all outside this submitted work. C.P.S. has received research funding to the institute from Pfizer, Roche, Genentech, SNS Oncology, G1 Therapeutics, Abbvie, Synthon and CytoMx Therapeutics, outside this work. S.C.L. reports research funding to the institute from Roche/Genentech, AstraZeneca, BMS, Tesaro, Merck, Immunomedics, Eurocept Pharmaceuticals, Agendia and Novartis and a consulting role and travel grant from Daiichi Sankyo, outside this work. M.K. reports funding to the institute from BMS, Roche, AstraZeneca/MedImmune and an advisory role for BMS, Roche, MSD and Daiichi Sankyo, outside the submitted work.

References

1. Dalenc, F. *et al.* Impact of lobular versus ductal histology on overall survival in metastatic breast cancer: a French retrospective multicentre cohort study. *European journal of cancer (Oxford, England : 1990)* **164**, 70-79, 2022.
2. Pestalozzi, B. C. *et al.* Distinct clinical and prognostic features of infiltrating lobular carcinoma of the breast: combined results of 15 International Breast Cancer Study Group clinical trials. *Journal of clinical oncology : official journal of the American Society of Clinical Oncology* **26** (18), 3006-3014, 2008.
3. Sledge, G. W., Chagpar, A. & Perou, C. Collective Wisdom: Lobular Carcinoma of the Breast. *American Society of Clinical Oncology Educational Book* (36), 18-21, 2016.
4. WHO. WHO Classification of Tumours of the Breast, 5th Edition, Volume 2. 2019.
5. Ciriello, G. *et al.* Comprehensive Molecular Portraits of Invasive Lobular Breast Cancer. *Cell* **163** (2), 506-519, 2015.
6. Arpino, G., Bardou, V. J., Clark, G. M. & Elledge, R. M. Infiltrating lobular carcinoma of the breast: tumor characteristics and clinical outcome. *Breast cancer research : BCR* **6** (3), R149-R156, 2004.
7. Okines, A. *et al.* Clinical outcomes in patients with triple negative or HER2 positive lobular breast cancer: a single institution experience. *Breast Cancer Res Treat* **192** (3), 563-571, 2022.
8. Bergeron, A. *et al.* Triple-negative breast lobular carcinoma: a luminal androgen receptor carcinoma with specific ESRRA mutations. *Modern Pathology* **34** (7), 1282-1296, 2021.
9. Gao, J. J. *et al.* CDK4/6 inhibitor treatment for patients with hormone receptor-positive, HER2-negative, advanced or metastatic breast cancer: a US Food and Drug Administration pooled analysis. *The Lancet. Oncology* **21** (2), 250-260, 2020.
10. Abel, M. K. *et al.* Decreased enrollment in breast cancer trials by histologic subtype: does invasive lobular carcinoma resist RECIST? *NPJ Breast Cancer* **7** (1), 139, 2021.
11. Michaut, M. *et al.* Integration of genomic, transcriptomic and proteomic data identifies two biologically distinct subtypes of invasive lobular breast cancer. *Sci Rep* **6**, 18517-18517, 2016.
12. Du, T. *et al.* Invasive lobular and ductal breast cancer differ in immune response, protein translation efficiency and metabolism. *Sci Rep* **8** (1), 7205, 2018.
13. Cortes, J. *et al.* Pembrolizumab plus chemotherapy versus placebo plus chemotherapy for previously untreated locally recurrent inoperable or metastatic triple-negative breast cancer (KEYNOTE-355): a randomised, placebo-controlled, double-blind, phase 3 clinical trial. *Lancet (London, England)* **396** (10265), 1817-1828, 2020.
14. Dirix, L. Y. *et al.* Avelumab, an anti-PD-L1 antibody, in patients with locally advanced or metastatic breast cancer: a phase 1b JAVELIN Solid Tumor study. *Breast Cancer Res Treat* **167** (3), 671-686, 2018.
15. Rugo, H. S. *et al.* Safety and Antitumor Activity of Pembrolizumab in Patients with Estrogen Receptor-Positive/Human Epidermal Growth Factor Receptor 2-Negative Advanced Breast Cancer. *Clinical cancer research : an official journal of the American Association for Cancer Research* **24** (12), 2804-2811, 2018.
16. Tolaney, S. M. *et al.* Effect of Eribulin With or Without Pembrolizumab on Progression-Free Survival for Patients With Hormone Receptor-Positive, ERBB2-Negative Metastatic Breast Cancer: A Randomized Clinical Trial. *JAMA Oncology* **6** (10), 1598-1605, 2020.
17. Pérez-García, J. M. *et al.* Pembrolizumab plus eribulin in hormone-receptor-positive, HER2-negative, locally recurrent or metastatic breast cancer (KELLY): An open-label, multicentre, single-arm, phase-II trial. *European journal of cancer (Oxford, England : 1990)* **148**, 382-394, 2021.
18. Spagnuolo, L. *et al.* PO-365 Dissecting the synergistic effect of chemotherapy and immunotherapy on anti-tumoral T cell functions in breast cancer. *ESMO Open* **3**, A371, 2018.
19. Sflomos, G. *et al.* Atlas of Lobular Breast Cancer Models: Challenges and Strategic Directions. *Cancers* **13** (21), 5396, 2021.
20. Derksen, P. W. *et al.* Somatic inactivation of E-cadherin and p53 in mice leads to metastatic lobular mammary carcinoma through induction of anoikis resistance and angiogenesis. *Cancer cell* **10** (5), 437-449, 2006.
21. Schadt, L. *et al.* Cancer-Cell-Intrinsic cGAS Expression Mediates Tumor Immunogenicity. *Cell Rep* **29** (5), 1236-1248.e1237, 2019.

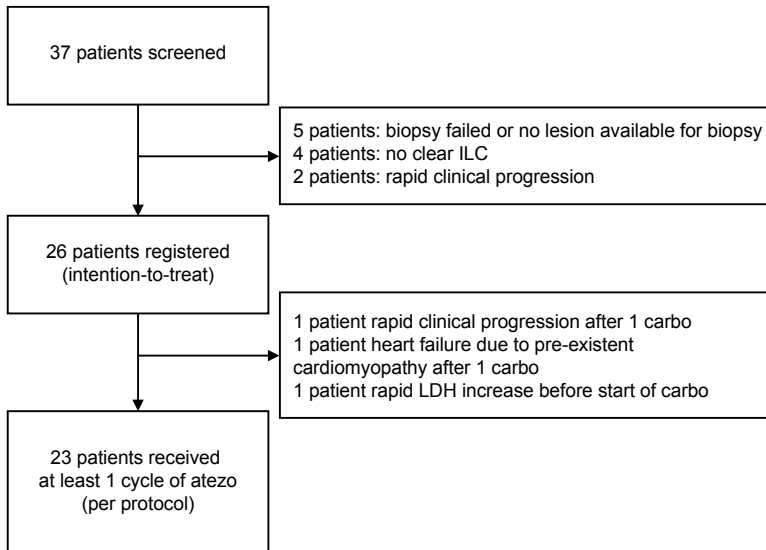
22. Wan, S. *et al.* Chemotherapeutics and radiation stimulate MHC class I expression through elevated interferon-beta signaling in breast cancer cells. *PLoS one* **7** (3), e32542, 2012.
23. Bensch, F. *et al.* (89)Zr-atezolizumab imaging as a non-invasive approach to assess clinical response to PD-L1 blockade in cancer. *Nat Med* **24** (12), 1852-1858, 2018.
24. Tutt, A. *et al.* Carboplatin in BRCA1/2-mutated and triple-negative breast cancer BRCAness subgroups: the TNT Trial. *Nat Med* **24** (5), 628-637, 2018.
25. Loibl, S. *et al.* Addition of the PARP inhibitor veliparib plus carboplatin or carboplatin alone to standard neoadjuvant chemotherapy in triple-negative breast cancer (BrighTNess): a randomised, phase 3 trial. *The Lancet. Oncology* **19** (4), 497-509, 2018.
26. Yu, J. *et al.* Liver metastasis restrains immunotherapy efficacy via macrophage-mediated T cell elimination. *Nature Medicine* **27** (1), 152-164, 2021.
27. Ayers, M. *et al.* IFN-gamma-related mRNA profile predicts clinical response to PD-1 blockade. *The Journal of clinical investigation* **127** (8), 2930-2940, 2017.
28. Scott, A. C. *et al.* TOX is a critical regulator of tumour-specific T cell differentiation. *Nature* **571** (7764), 270-274, 2019.
29. Cabrita, R. *et al.* Tertiary lymphoid structures improve immunotherapy and survival in melanoma. *Nature* **577** (7791), 561-565, 2020.
30. Bagaev, A. *et al.* Conserved pan-cancer microenvironment subtypes predict response to immunotherapy. *Cancer cell* **39** (6), 845-865.e847, 2021.
31. Pareja, F. *et al.* The genomic landscape of metastatic histologic special types of invasive breast cancer. *npj Breast Cancer* **6** (1), 53, 2020.
32. Sokol, E. S. *et al.* Loss of function of NF1 is a mechanism of acquired resistance to endocrine therapy in lobular breast cancer. *Ann Oncol* **30** (1), 115-123, 2019.
33. Richard, F. *et al.* Characterization of Stromal Tumor-infiltrating Lymphocytes and Genomic Alterations in Metastatic Lobular Breast Cancer. *Clinical cancer research : an official journal of the American Association for Cancer Research* **26** (23), 6254-6265, 2020.
34. Newman, A. M. *et al.* Determining cell type abundance and expression from bulk tissues with digital cytometry. *Nature Biotechnology* **37** (7), 773-782, 2019.
35. Liberzon, A. *et al.* The Molecular Signatures Database (MSigDB) hallmark gene set collection. *Cell Syst* **1** (6), 417-425, 2015.
36. Huang, A. C. *et al.* A single dose of neoadjuvant PD-1 blockade predicts clinical outcomes in resectable melanoma. *Nat Med* **25** (3), 454-461, 2019.
37. Simon, S. C. S. *et al.* Eosinophil accumulation predicts response to melanoma treatment with immune checkpoint inhibitors. *Oncoimmunology* **9** (1), 1727116, 2020.
38. Lalani, A.-K. A. *et al.* Change in neutrophil-to-lymphocyte ratio (NLR) in response to immune checkpoint blockade for metastatic renal cell carcinoma. *Journal for ImmunoTherapy of Cancer* **6** (1), 5, 2018.
39. Thommen, D. S. *et al.* A transcriptionally and functionally distinct PD-1+ CD8+ T cell pool with predictive potential in non-small-cell lung cancer treated with PD-1 blockade. *Nature Medicine* **24** (7), 994-1004, 2018.
40. Li, H. *et al.* Dysfunctional CD8 T Cells Form a Proliferative, Dynamically Regulated Compartment within Human Melanoma. *Cell* **176** (4), 775-789.e718, 2019.
41. Krieg, C. *et al.* High-dimensional single-cell analysis predicts response to anti-PD-1 immunotherapy. *Nat Med* **24** (2), 144-153, 2018.
42. Aftimos, P. *et al.* Genomic and Transcriptomic Analyses of Breast Cancer Primaries and Matched Metastases in AURORA, the Breast International Group (BIG) Molecular Screening Initiative. *Cancer Discov* **11** (11), 2796-2811, 2021.
43. Jørgensen, C. L. T. *et al.* PAM50 Intrinsic Subtype Profiles in Primary and Metastatic Breast Cancer Show a Significant Shift toward More Aggressive Subtypes with Prognostic Implications. *Cancers (Basel)* **13** (7), 2021.
44. An, X. *et al.* An Analysis of the Expression and Association with Immune Cell Infiltration of the cGAS/STING Pathway in Pan-Cancer. *Mol Ther Nucleic Acids* **14**, 80-89, 2019.
45. Garg, A. D., De Ruyscher, D. & Agostinis, P. Immunological metagene signatures derived from immunogenic cancer cell death associate with improved survival of patients with lung, breast or ovarian malignancies: A large-scale meta-analysis. *Oncoimmunology* **5** (2), e1069938-e1069938, 2015.

46. Conforti, F. *et al.* Biological and clinical features of triple negative Invasive Lobular Carcinomas of the breast. Clinical outcome and actionable molecular alterations. *Breast (Edinburgh, Scotland)* **59**, 94-101, 2021.
47. Mouabbi, J. A. *et al.* Invasive lobular carcinoma: an understudied emergent subtype of breast cancer. *Breast Cancer Res Treat* **193** (2), 253-264, 2022.
48. Guan, X. *et al.* Androgen receptor activity in T cells limits checkpoint blockade efficacy. *Nature*, 2022.
49. Leisha A. Emens, L. D. G., Peter Schmid, Hope S. Rugo, Sylvia Adams, Carlos H. Barrios, Andreas Schneeweiss, Veronique Dieras, Hiroji Iwata, Ching-Wei Chang, Hartmut Koeppen, Stephen Y. Chui, Sherene Loi, Luciana Molinero; . The tumor microenvironment (TME) and atezolizumab + nab-paclitaxel (A+nP) activity in metastatic triple-negative breast cancer (mTNBC): IMpassion130. *American Society of Clinical Oncology conference 2021; Journal of Clinical Oncology* **39**, 2021 (suppl 15; abstr 1006), 2021.
50. Keenan, T. E. *et al.* Molecular correlates of response to eribulin and pembrolizumab in hormone receptor-positive metastatic breast cancer. *Nat Commun* **12** (1), 5563, 2021.
51. Chakraborty, B. *et al.* Inhibition of estrogen signaling in myeloid cells increases tumor immunity in melanoma. *The Journal of clinical investigation* **131** (23), 2021.
52. Waks, A. G. *et al.* The Immune Microenvironment in Hormone Receptor-Positive Breast Cancer Before and After Preoperative Chemotherapy. *Clinical cancer research : an official journal of the American Association for Cancer Research* **25** (15), 4644-4655, 2019.
53. Tuit, S. *et al.* Transcriptional Signature Derived from Murine Tumor-Associated Macrophages Correlates with Poor Outcome in Breast Cancer Patients. *Cell Rep* **29** (5), 1221-1235.e1225, 2019.
54. Dieci, M. V. *et al.* Neoadjuvant Chemotherapy and Immunotherapy in Luminal B-like Breast Cancer: Results of the Phase II GIADA Trial. *Clinical Cancer Research* **28** (2), 308-317, 2022.
55. Cejalvo, J. M. *et al.* Intrinsic Subtypes and Gene Expression Profiles in Primary and Metastatic Breast Cancer. *Cancer research* **77** (9), 2213-2221, 2017.
56. Jørgensen, C. L. T. *et al.* PAM50 Intrinsic Subtype Profiles in Primary and Metastatic Breast Cancer Show a Significant Shift toward More Aggressive Subtypes with Prognostic Implications. *Cancers* **13** (7), 1592, 2021.
57. Albanell, J. *et al.* Palbociclib Rechallenge for Hormone Receptor-Positive/Human Epidermal Growth Factor Receptor-Negative Advanced Breast Cancer: Findings from the Phase II BioPER Trial. *Clinical cancer research : an official journal of the American Association for Cancer Research*, 2022.
58. Salgado, R. *et al.* The evaluation of tumor-infiltrating lymphocytes (TILs) in breast cancer: recommendations by an International TILs Working Group 2014. *Annals of Oncology* **26** (2), 259-271, 2015.
59. Savas, P. *et al.* Single-cell profiling of breast cancer T cells reveals a tissue-resident memory subset associated with improved prognosis. *Nat Med* **24** (7), 986-993, 2018.
60. Van Baelen, K. *et al.* Current and future diagnostic and treatment strategies for patients with invasive lobular breast cancer. *Annals of Oncology*.
61. Ma, C. X. *et al.* The Phase II MutHER Study of Neratinib Alone and in Combination with Fulvestrant in HER2-Mutated, Non-amplified Metastatic Breast Cancer. *Clinical Cancer Research* **28** (7), 1258-1267, 2022.
62. Bajrami, I. *et al.* E-Cadherin/ROS1 Inhibitor Synthetic Lethality in Breast Cancer. *Cancer Discovery* **8** (4), 498-515, 2018.
63. Nagle, A. M. *et al.* Loss of E-cadherin Enhances IGF1-IGF1R Pathway Activation and Sensitizes Breast Cancers to Anti-IGF1R/InsR Inhibitors. *Clinical cancer research : an official journal of the American Association for Cancer Research* **24** (20), 5165-5177, 2018.
64. An, Y. *et al.* Cdh1 and Pik3ca Mutations Cooperate to Induce Immune-Related Invasive Lobular Carcinoma of the Breast. *Cell Reports* **25** (3), 702-714.e706, 2018.
65. Klarenbeek, S. *et al.* Response of metastatic mouse invasive lobular carcinoma to mTOR inhibition is partly mediated by the adaptive immune system. *Oncoimmunology* **9** (1), 1724049, 2020.
66. Salvagno, C. *et al.* Therapeutic targeting of macrophages enhances chemotherapy efficacy by unleashing type I interferon response. *Nat Cell Biol* **21** (4), 511-521, 2019.
67. Nanda, R. *et al.* Pembrolizumab in Patients With Advanced Triple-Negative Breast Cancer: Phase Ib KEYNOTE-012 Study. *Journal of clinical oncology : official journal of the American Society of Clinical Oncology* **34** (21), 2460-2467, 2016.

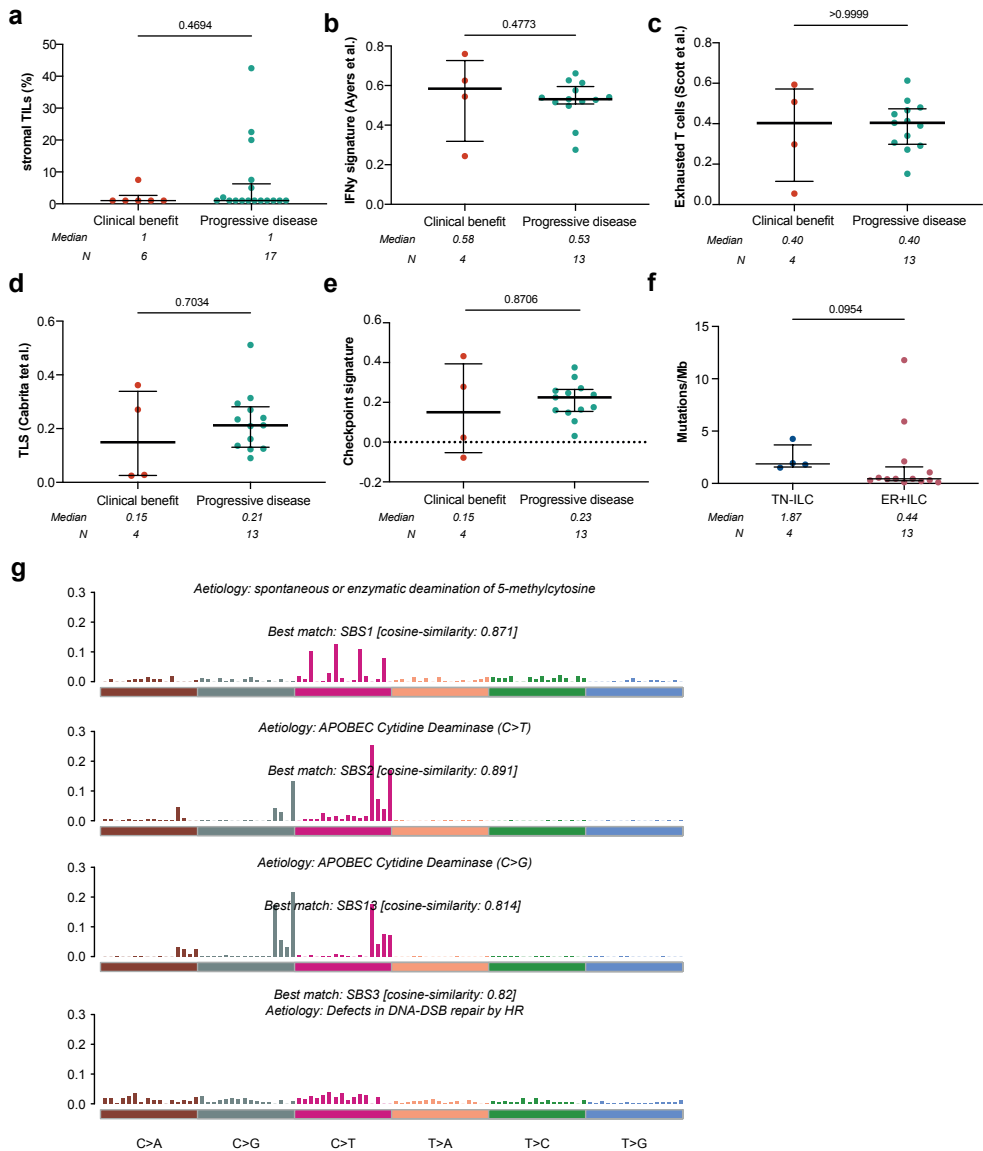
68. Weber, J. S., Kähler, K. C. & Hauschild, A. Management of immune-related adverse events and kinetics of response with ipilimumab. *Journal of clinical oncology : official journal of the American Society of Clinical Oncology* 30 (21), 2691-2697, 2012.
69. von Minckwitz, G. et al. Neoadjuvant carboplatin in patients with triple-negative and HER2-positive early breast cancer (GeparSixto; GBG 66): a randomised phase 2 trial. *The Lancet Oncology* 15 (7), 747-756, 2014.
70. Schmid, P. et al. Event-free Survival with Pembrolizumab in Early Triple-Negative Breast Cancer. *N Engl J Med* 386 (6), 556-567, 2022.
71. Eisenhauer, E. A. et al. New response evaluation criteria in solid tumours: revised RECIST guideline (version 1.1). *European journal of cancer (Oxford, England : 1990)* 45 (2), 228-247, 2009.
72. Seymour, L. et al. iRECIST: guidelines for response criteria for use in trials testing immunotherapeutics. *The Lancet. Oncology* 18 (3), e143-e152, 2017.
73. Casparie, M. et al. Pathology databanking and biobanking in The Netherlands, a central role for PALGA, the nationwide histopathology and cytopathology data network and archive. *Cell Oncol* 29 (1), 19-24, 2007.
74. Simon, R. Optimal two-stage designs for phase II clinical trials. *Control Clin Trials* 10 (1), 1-10, 1989.
75. Blum, J. L. et al. Pooled analysis of individual patient data from capecitabine monotherapy clinical trials in locally advanced or metastatic breast cancer. *Breast Cancer Res Treat* 136 (3), 777-788, 2012.
76. Cortes, J. et al. Eribulin monotherapy versus treatment of physician's choice in patients with metastatic breast cancer (EMBRACE): a phase 3 open-label randomised study. *Lancet (London, England)* 377 (9769), 914-923, 2011.
77. Voorwerk, L. et al. LBA10 Critical role of eosinophils during response to immune checkpoint blockade in breast cancer and other cancer types. *Annals of Oncology* 31, S1142, 2020.
78. Ritchie, M. E. et al. limma powers differential expression analyses for RNA-sequencing and microarray studies. *Nucleic Acids Research* 43 (7), e47-e47, 2015.
79. Blighe K., R. S., Lewis M. EnhancedVolcano: Publication-ready volcano plots with enhanced colouring and labeling. R package version 1.12.0. . <https://github.com/kevinblighe/EnhancedVolcano>, 2021.
80. Li, H. Aligning sequence reads, clone sequences and assembly contigs with BWA-MEM. arXiv, 2013.
81. Danecek, P. et al. Twelve years of SAMtools and BCFtools. *GigaScience* 10 (2), 2021.
82. McKenna, A. et al. The Genome Analysis Toolkit: a MapReduce framework for analyzing next-generation DNA sequencing data. *Genome Res* 20 (9), 1297-1303, 2010.
83. Benjamin, D. et al. Calling Somatic SNVs and Indels with Mutect2. bioRxiv, 861054, 2019.
84. Wardell, C. P., Ashby, C. & Bauer, M. A. FiNGS: high quality somatic mutations using filters for next generation sequencing. *BMC Bioinformatics* 22 (1), 77, 2021.
85. Chavan, C. K. J. G. q. M. M. A. S. Y. B. A. P. S. mskcc/vcf2maf: vcf2maf v1.6.16. Zenodo, 2018.
86. Mayakonda, A., Lin, D. C., Assenov, Y., Plass, C. & Koeffler, H. P. Maftools: efficient and comprehensive analysis of somatic variants in cancer. *Genome Res* 28 (11), 1747-1756, 2018.
87. pandas, D. t. pandas-dev/pandas: Pandas. Zenodo, 2020.
88. McKinney, W. Data Structures for Statistical Computing in Python. *Proceedings of the 9th Python in Science Conference*, 56-61, 2010.
89. Dobin, A. et al. STAR: ultrafast universal RNA-seq aligner. *Bioinformatics* 29 (1), 15-21, 2012.
90. Andrews, S. A quality control tool for high throughput sequence data., 2016.
91. Wingett, S. W. & Andrews, S. FastQ Screen: A tool for multi-genome mapping and quality control. *F1000Res* 7, 1338, 2018.
92. Institute, B. Picard (<http://broadinstitute.github.io/picard/>).
93. Wang, L., Wang, S. & Li, W. RSEQC: quality control of RNA-seq experiments. *Bioinformatics* 28 (16), 2184-2185, 2012.
94. Steen, C. B., Liu, C. L., Alizadeh, A. A. & Newman, A. M. in *Stem Cell Transcriptional Networks: Methods and Protocols* (ed Benjamin L. Kidder) 135-157 (Springer US, 2020).
95. Love, M. I., Huber, W. & Anders, S. Moderated estimation of fold change and dispersion for RNA-seq data with DESeq2. *Genome Biology* 15 (12), 550, 2014.
96. Gendoo, D. M. et al. Genefu: an R/Bioconductor package for computation of gene expression-based signatures in breast cancer. *Bioinformatics* 32 (7), 1097-1099, 2016.
97. Fang, Z. GSEAPy: Gene Set Enrichment Analysis in Python. 2020.
98. Harris, C. R. et al. Array programming with NumPy. *Nature* 585 (7825), 357-362, 2020.

99. Waskom, M. seaborn: statistical data visualization. *Journal of Open Source Software* 6, 3021, 2021.
100. Hunter, J. D. Matplotlib: A 2D Graphics Environment. *Computing in Science & Engineering* 9 (3), 90-95, 2007.
101. Github. statannotations.
102. Boellaard, R. Quantitative oncology molecular analysis suite: ACCURATE. *Journal of Nuclear Medicine* 59 (supplement 1), 1753-1753, 2018.
103. Nienhuis, P. H. et al. (18)F-BMS986192 PET Imaging of PD-L1 in Metastatic Melanoma Patients with Brain Metastases Treated with Immune Checkpoint Inhibitors: A Pilot Study. *J Nucl Med* 63 (6), 899-905, 2022.

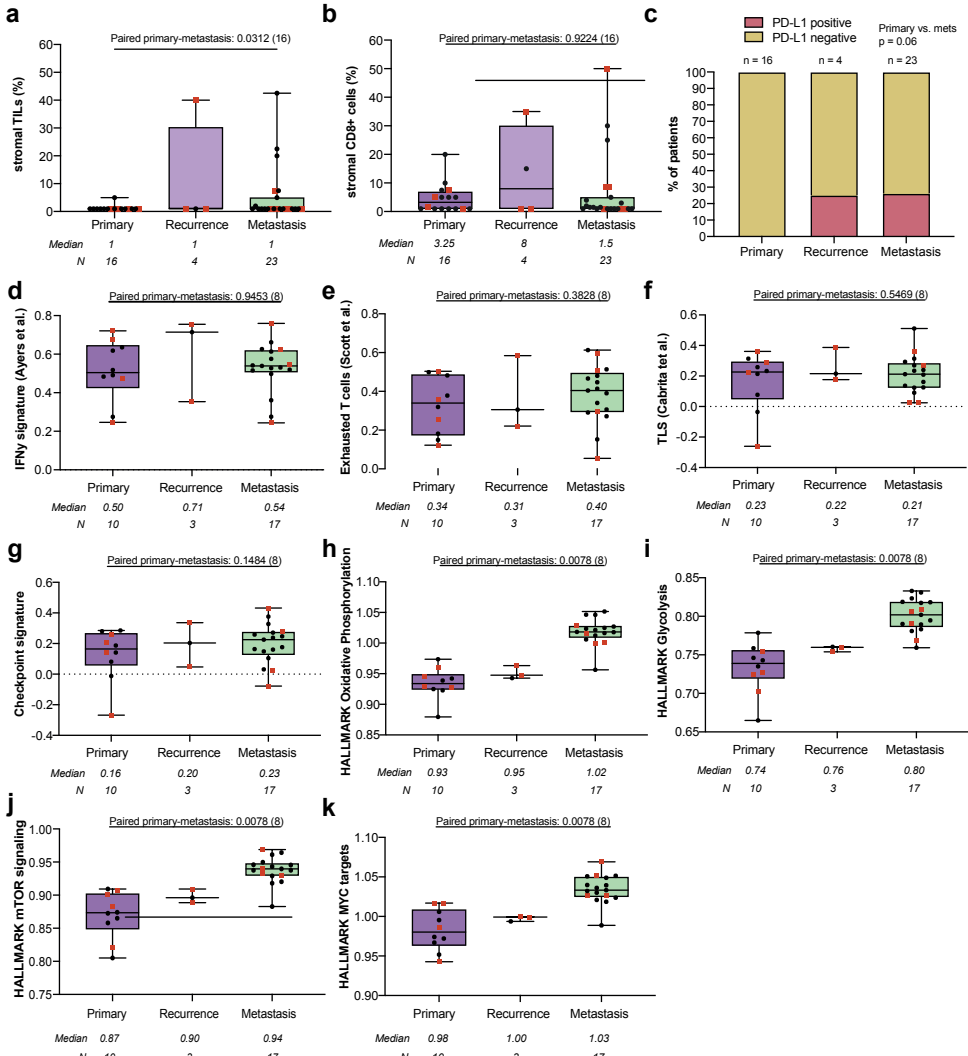
Extended Data Figures



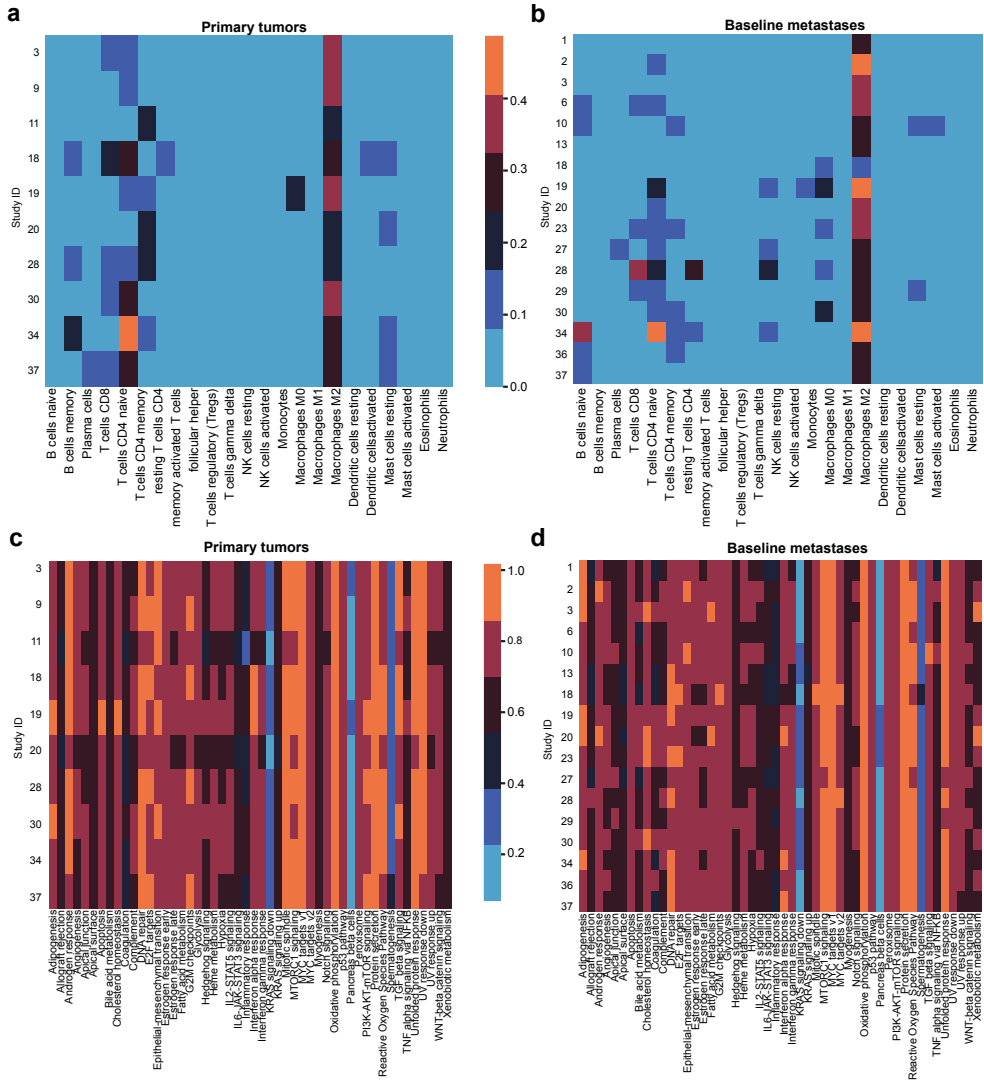
Extended Data Figure 1: Flow chart of patient inclusion in the GELATO-trial



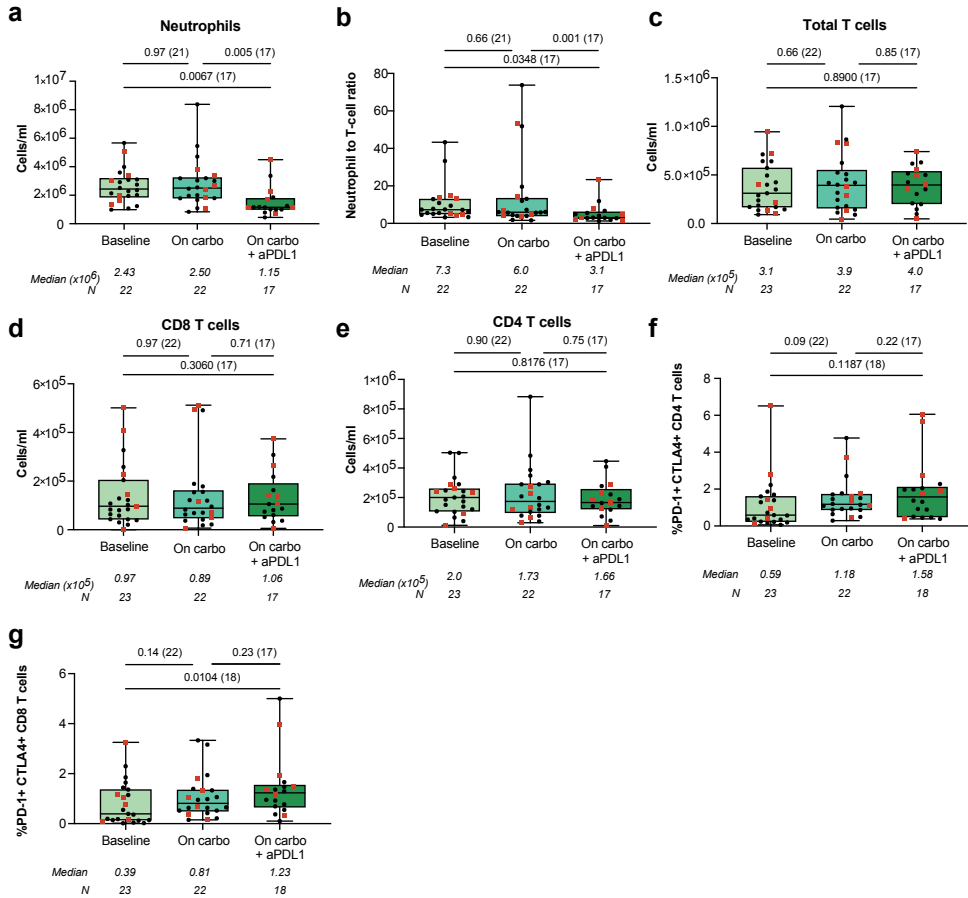
Extended Data Figure 2: Additional baseline tumor microenvironment features associated with clinical outcome. (a) Percentage of stromal tumor-infiltrating lymphocytes (sTILs). (b) Gene expression of an IFN γ signature²⁷. (c) Gene expression of an exhausted T-cell signature²⁸. (d) Gene expression of a tertiary lymphoid structure (TLS) signature²⁹. (e) Gene expression of an immune checkpoint signature³⁰. (f) Tumor mutational burden (TMB, mutations per Mb) in ER+ vs triple-negative ILC. (g) Mutational signatures enriched in metastatic lesions. (a)-(f) Median with interquartile range, statistics by Mann-Whitney-U test. Baseline metastatic lesions correspond to metastases presented in Figure 3 and Extended Data Figure 3 and 4.



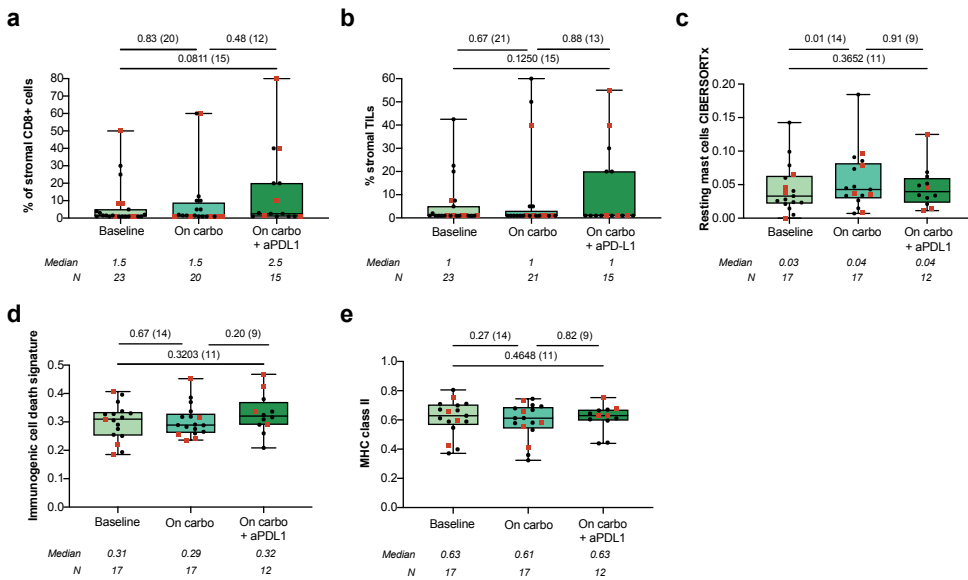
Extended Data Figure 3: Evolution of sTILs, stromal CD8+ cells, PD-L1 expression and immune-related gene sets from paired primary tumors, local recurrences and metastasis. (a) Percentage of stromal tumor-infiltrating lymphocytes (sTILs) in paired primary tumors, recurrences, and metastases. (b) Percentage of CD8+ T cells in the stromal area (immunohistochemistry). (c) Percentage of patients with clinical benefit and PD-L1 expression (clone SP142) in metastatic lesions. A cut-off of 1% expression on immune cells was used to determine PD-L1 positivity. Statistics by Fisher's exact test (primary versus metastasis) for proportions. (d) Gene expression of an IFN γ signature²⁷. (e) Gene expression of an exhausted T-cell signature²⁸. (f) Gene expression of a tertiary lymphoid structure (TLS) signature²⁹. (g) Gene expression of an immune checkpoint signature³⁰. (h) Gene set enrichment score of the HALLMARK Oxidative Phosphorylation gene set. (i) Gene set enrichment score of the HALLMARK Glycolysis gene set. (j) Gene set enrichment score of HALLMARK mTOR signaling gene set. (k) Gene set enrichment score of HALLMARK MYC targets gene set. (a)-(b), (d)-(k) Boxplots display median with range. Statistics with Wilcoxon-signed-rank on paired primary tumors and metastasis, the number of patients in each analysis are listed between brackets behind the p-value. Red squares indicate patients with clinical benefit, black dots patients with no clinical benefit. Metastatic lesions correspond with baseline samples presented in Figure 2, Figure 4, Extended Data Figure 2, 4 and 6.



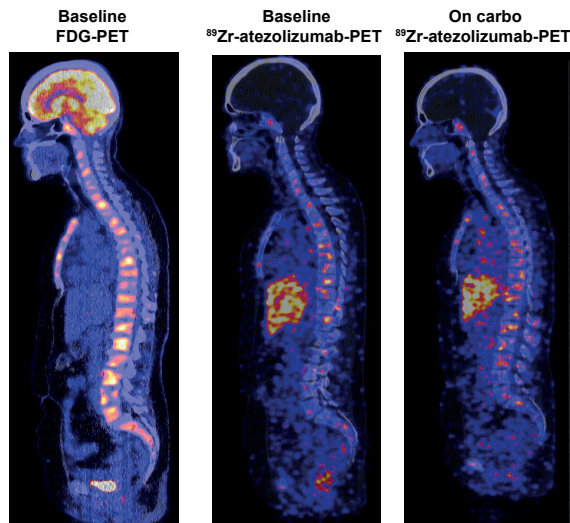
Extended Data Figure 4: Unbiased analysis of treatment-related changes in gene expression. (a) Heatmap of CIBERSORTx immune cell deconvolution³⁴ across all primary tumor samples (FFPE). Rows correspond to one sample and are annotated with patient ID. (b) Heatmap of CIBERSORTx immune cell deconvolution³⁴ across all baseline metastases (FF). Rows correspond to one sample and are annotated with patient ID. (c) Heatmap of gene-set enrichment analysis of Hallmark gene sets³⁵ across all across all primary tumor samples (FFPE). Rows correspond to one sample and are annotated with patient ID. (d) Heatmap of gene-set enrichment analysis of Hallmark gene sets³⁵ across all across all baseline metastases (FF). Rows correspond to one sample and are annotated with patient ID.



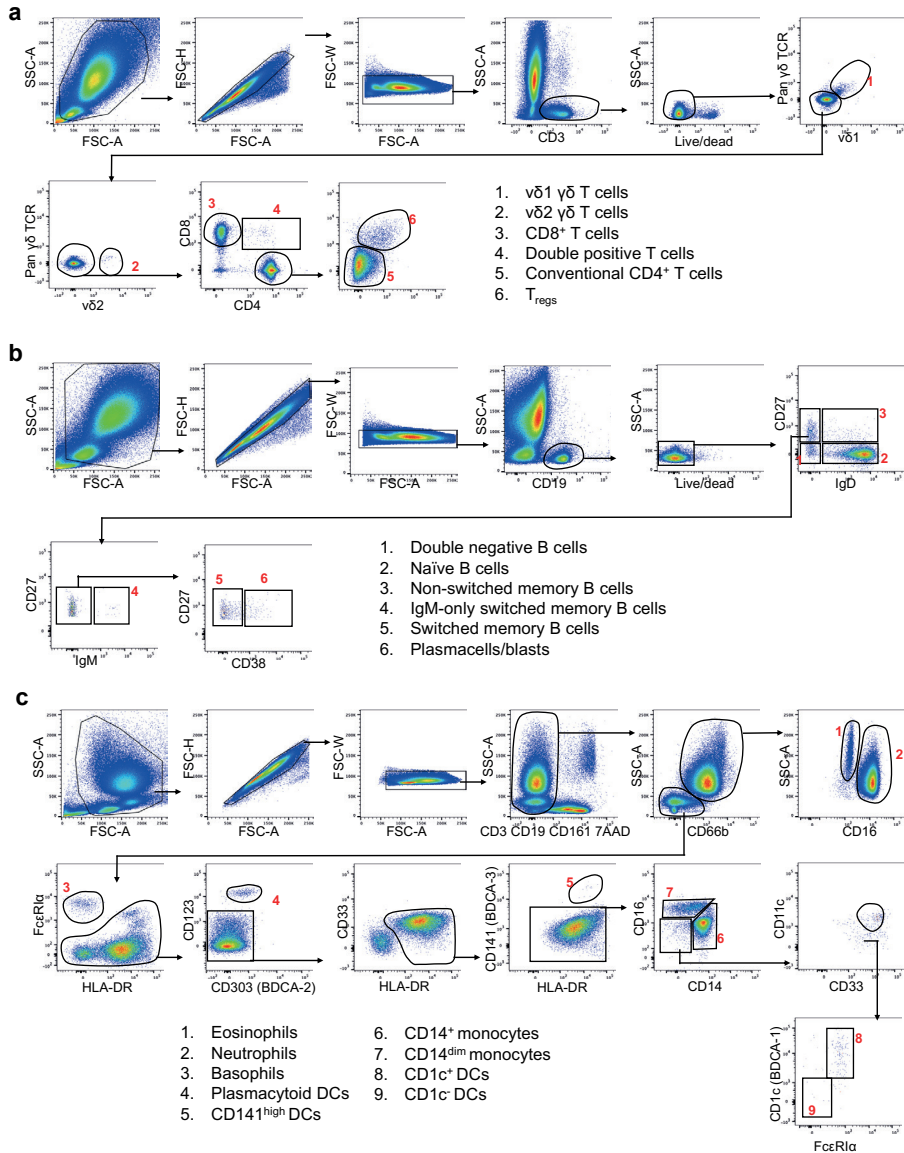
Extended Data Figure 5: Flow cytometry-based assessment of circulating immune cell populations in paired blood samples at baseline, on carboplatin and during carboplatin/anti-PD-L1. (a) Absolute circulating neutrophil counts by flow cytometry. (b) Neutrophil-to-lymphocyte ratio (total T cell count). (c) Absolute circulating total T-cell counts. (d) Absolute circulating CD8+ T-cell counts. (e) Absolute circulating CD4+ T-cell counts. (f) Percentage of circulating PD-1+CTLA-4+ CD4+ T cells. (g) Percentage of circulating PD-1+CTLA-4+ CD8+ T cells. (a)-(g). Boxplots display median with range. Statistics with Wilcoxon-signed-rank on paired samples, the number of patients in each analysis are listed between brackets behind the p-value. Red squares indicate patients with clinical benefit, black dots patients with no clinical benefit.



Extended Data Figure 6: Changes in sTILs, stromal CD8+ cells and immune-related gene sets in serial biopsies of a metastatic lesion. (a) Percentage of CD8+ T cells (immunohistochemistry) in the stromal area in serial biopsies of metastatic lesions measured at baseline, after two cycles of anti-PD-L1 plus carboplatin. (b) Percentage of stromal tumor-infiltrating lymphocytes (sTILs) in serial biopsies of metastatic lesions. (c) Gene set expression score of resting mast cells according to CIBERSORTx in serial biopsies of metastatic lesions. (d) Gene expression of an immunogenic cell death signature⁴⁵ in serial biopsies of metastatic lesions. (e) Gene expression score of MHC class II related genes (*HLA-DRA*, *HLA-DRB1*, *HLA-DOB*, *HLA-DPB2*, *HLA-DMA*, *HLA-DOA*, *HLA-DPA1*, *HLA-DPB1*, *HLA-DMB*, *HLA-DQB1*, *HLA-DQA1*, *HLA-DRB5*, *HLA-DQA2*, *HLA-DQB2*, *HLA-DRB6*). (a)-(e) Boxplots display median with range. Statistics with Wilcoxon-signed-rank on paired samples, the number of patients in each analysis are listed between brackets behind the p-value. Red squares indicate patients with clinical benefit, black dots patients with no clinical benefit. Baseline metastatic lesions correspond to metastases presented in Figure 3 and Extended Data Figure 3 and 4.



Extended Data Figure 7: Exploratory analysis of the use ⁸⁹Zr-atezolizumab-PET to evaluate PD-L1 distribution in ILC patients. Representative images of one patient imaged with FDG-PET and ⁸⁹Zr-atezolizumab-PET. Left panel depicts lateral view of baseline FDG-PET, the middle panel represents the lateral view of baseline ⁸⁹Zr-atezolizumab-PET and the right panel ⁸⁹Zr-atezolizumab-PET after two cycles of carboplatin.



Extended Data Figure 8. Gating strategies for flow cytometry analysis of peripheral blood immune populations. (a) T cell panel gating strategy identifying $v\delta 1$ $\gamma\delta$ T cells (CD3⁺, $v\delta 1$ ⁺, pan $\gamma\delta$ TCR⁺), $v\delta 2$ $\gamma\delta$ T cells (CD3⁺, $v\delta 2$ ⁺), double positive T cells (CD3⁺, $v\delta 1$ ⁺, pan $\gamma\delta$ TCR⁺, $v\delta 2$ ⁺, CD8⁺, CD4⁺), CD8 T cells (CD3⁺, $v\delta 1$ ⁺, pan $\gamma\delta$ TCR⁺, $v\delta 2$ ⁺, CD8⁺, CD4⁺), conventional CD4 T cells (CD3⁺, $v\delta 1$ ⁺, pan $\gamma\delta$ TCR⁺, $v\delta 2$ ⁺, CD8⁺, CD4⁺, FoxP3⁺) and T_{regs} (CD3⁺, $v\delta 1$ ⁺, pan $\gamma\delta$ TCR⁺, $v\delta 2$ ⁺, CD8⁺, CD4⁺, FoxP3⁺, CD25^{high}). (b) Gating strategy to identify B cell subsets identifying double negative B cells (CD19⁺, CD27⁻, IgD⁻), naïve B cells (CD19⁺, CD27⁺, IgD⁻), non-switched memory B cells (CD19⁺, CD27⁺, IgD⁻), IgM-only switched memory B cells (CD19⁺, CD27⁺, IgD⁻, IgM⁺), switched memory B cells (CD19⁺, CD27⁺, IgD⁻, IgM⁺, CD38^{high}), and plasmacells/blasts (CD19⁺, CD27⁺, IgD⁻, IgM⁺, CD38^{high}). (c) Myeloid panel gating strategy identifying eosinophils (lineage⁻, high side scatter, CD66b⁺ CD16⁺), neutrophils (lineage⁻, high side scatter, CD66b⁺ CD16⁺), basophils (lineage⁻, FcεRIα⁺, HLA-DR⁻), plasmacytoid DCs (lineage⁻, HLA-DR⁻, CD303⁺, CD123⁺), CD141^{high} DCs (lineage⁻, HLA-DR⁻, CD33⁺, CD141⁺), CD14⁺ monocytes (lineage⁻, HLA-DR⁻, CD33⁺, CD14⁺, CD16^{+/−}), CD14^{dim} monocytes (lineage⁻, HLA-DR⁻, CD33⁺, CD14^{dim}, CD16⁻), CD1c⁺ DCs (lineage⁻, HLA-DR⁻, CD33⁺, CD14⁺, CD16⁺, CD1c⁺, FcεRIα⁺) and CD1c⁻ DCs (lineage⁻, HLA-DR⁻, CD33⁺, CD14⁺, CD16⁺, CD1c⁻, FcεRIα⁻).

Supplementary Table 1: worst grade of any treatment-related adverse event.

Immune-related events are a selection of all reported atezolizumab-related events. Only grade 2 events or higher or grade 1 immune-related events were reported. 1 patient died during treatment of disease progression.

Worse grade of any adverse event, No. of patients (%)	No AE reported	Grade 1-2	Grade 3	Grade 4
Carboplatin-related	6 (26)	7 (30)	9 (39)	1 (4)
Atezolizumab-related	11 (48)	5 (22)	5 (22)	2 (9)
Immune-related event of interest	13 (57)	4 (17)	5 (22)	1 (4)

Supplementary Table 2: all reported carboplatin-related toxicity.

Only grade 2 events or higher were reported. Alanine aminotransferase (ALAT).

Carboplatin related adverse event, No. of patients (%)	Any grade	Grade 3	Grade 4
Neutrophil count decreased	11 (48)	3 (13)	1 (4)
Anemia	5 (22)	2 (9)	0 (0)
Platelet count decreased	3 (13)	2 (9)	0 (0)
Nausea	3 (13)	0 (0)	0 (0)
Fatigue	2 (9)	0 (0)	0 (0)
Abdominal pain	1 (4)	1 (4)	0 (0)
ALAT increased	1 (4)	1 (4)	0 (0)
Dehydration	1 (4)	1 (4)	0 (0)
Flu-like symptoms	1 (4)	0 (0)	0 (0)
Gastro-esophageal reflux	1 (4)	0 (0)	0 (0)
Hyperkalemia	1 (4)	0 (0)	0 (0)
Hyponatremia	1 (4)	1 (4)	0 (0)
Infusion-related reaction	1 (4)	0 (0)	0 (0)
Increased lipase	1 (4)	0 (0)	0 (0)
Obstipation	1 (4)	0 (0)	0 (0)
Peripheral neuropathy	1 (4)	0 (0)	0 (0)

Supplementary Table 3: immune-related adverse events of special interest.

Alanine aminotransferase (ALAT); aspartate aminotransferase (ASAT). *1 patient developed a grade 3 hypophysitis two months after stopping atezolizumab. ^Asymptomatic without signs of (immune-related) pancreatitis

Immune related adverse event, No. of patients (%)	Any grade	Grade 3	Grade 4
ASAT increased	4 (17)	2 (9)	1 (4)
ALAT increased	2 (9)	2 (9)	0 (0)
Flu-like symptoms	2 (9)	0 (0)	0 (0)
Hypophysitis*	2 (9)	1 (4)	0 (0)
Lipase increased^	2 (9)	1 (4)	0 (0)
Colitis	1 (4)	1 (4)	0 (0)
Dry mouth	1 (4)	0 (0)	0 (0)
Dry skin	1 (4)	0 (0)	0 (0)
Myalgia	1 (4)	0 (0)	0 (0)
Sarcoid-like reaction	1 (4)	1 (4)	0 (0)

Supplementary Table 4: characteristics of patients with collected primary tumors.

N = 17 available patients	No. of patients	Percentage
Age at diagnosis, years (median, range)	51 (33-65)	
Molecular subtype (assessed on primary tumor^{1,2})		
ER+HER2-	16	94%
ER+HER2+	1	6%
Histological grade primary tumor		
Grade 1	2	12%
Grade 2	9	53%
Grade 3	3	18%
Unknown	3	18%
Tumor stage at diagnosis		
T1	4	24%
T2	8	47%
T3	5	29%
Nodal stage at diagnosis		
N0	5	29%
N1	5	29%
N2	2	12%
N3	5	29%
Neo-adjuvant chemotherapy	6	35%
Response to neo-adjuvant chemotherapy		
pCR	0	0%
pPR (1-50% tumorrest)	1	17%
pNR (>50% tumorrest or no response)	5	83%
Disease course		
Primary-metastasis	10	59%
Primary-local recurrence-metastasis ⁴	3	18%
De novo M1 ⁵	2	12%
Primary-2 nd primary-metastasis ¹	1	6%
Primary-contralateral recurrence-metastasis ¹	1	6%
Biopsy site GELATO-trial		
Liver	7	41%
Lymph node	4	24%
Peritoneum	3	18%
Cervix	1	6%
Skin	1	6%
Thoracal wall	1	6%

¹For 1 patient with a secondary primary tumor, only the second tumor was collected (first tumor was not ILC). For 1 patient with an isolated contralateral recurrence, the first primary tumor and contralateral recurrence were collected. ²4/5 patients with a triple-negative metastasis had a primary ER+ tumor. 1 of these patients had a triple-negative contralateral recurrence. Two out of 17 patients with de novo metastatic disease had ER+ disease. ³including mixed classical and pleiomorphic. ⁴Local recurrence including recurrence in skin. 1 patient had a local ILC recurrence and contralateral breast cancer of no special type simultaneously. ⁵Breast lesions are compared with synchronous distant metastasis.

Supplementary Table 5: list of measured circulating immune cell populations as displayed in Figure 4A-B and Figure S5.

Circulating immune cell populations
Eosinophils
Basophils
Neutrophils
CD141 ^{high} dendritic cells (DCs)
CD1c ⁺ DCs
CD1c ⁻ DCs
Plasmacytoid DCs
CD14 ⁺ CD16 ⁻ monocytes
CD14 ^{dim} monocytes
Total T cells
Conventional CD4 ⁺ T cells (within total T cells)
CD8 ⁺ T cells (within total T cells)
Regulatory T cells (within total T cells)
Double positive T cells (within total T cells)
vd1 gd T cells (within total T cells)
vd2 gd T cells (within total T cells)
Total B cells
Double negative B cells (within total B cells)
Non-switched memory B cells (within total B cells)
IgM-only memory B cells (within total B cells)
Switched memory B cells (within total B cells)
Plasmacells/blasts (within total B cells)
Naïve B cells (within total B cells)

Supplementary Table 6: list of antibodies used for flow cytometry

Antigen	Fluorochrome	Clone	Dilution	Company	Catalogue number
CD3	BUV496	UCHT1	1:100	BD Bioscience	612940
CD4	BV421	RPA-T4	1:100	BD Bioscience	562424
CD8	BUV805	SK1	1:200	BD Bioscience	612754
Pan gd TCR	PE	11F2	1:100	BD Bioscience	555717
FoxP3	PE Cy5.5	FJK-16s	1:50	eBioscience/Thermofisher	35-5773-82
CCR7	APC R700	150503	1:50	BD Bioscience	565868
CD45RA	BUV737	HI100	1:400	BD Bioscience	612846
CD25	AF647	BC96	1:100	BioLegend	302618
PD-1	APC Cy7	EH12.2H7	1:100	BioLegend	329922
CTLA-4	PE CF594	BN13	1:200	BD Bioscience	562742
vd1	FITC	TS8.2	1:100	Thermofisher	TCR2730
vd2	BUV395	B6	1:100	BD Bioscience	748582
CD19	PE Cy5	HIB19	1:200	BD Bioscience	555414
CD3	PE Cy5	UCHT1	1:200	BD Bioscience	555334
CD56	PE Cy5	B159	1:100	BD Bioscience	555517
CD161	PE Cy5	DX12	1:100	BD Bioscience	551138
HLA-DR	BUV661	G46-6	1:100	BD Bioscience	612980
CD14	BUV737	M5E2	1:100	BD Bioscience	612763
CD16	BUV496	3G8	1:100	BD Bioscience	612944
CD11c	BV785	3.9	1:100	BioLegend	301644
CD1c	PE Cy7	L161	1:100	BioLegend	331516
CD141	BV711	1A4	1:100	BD Bioscience	563155
CD123	PE	6H6	1:200	BioLegend	396604
CD66b	AF647	G10F5	1:200	BD Bioscience	561645
CD33	PerCP Cy5.5	WM53	1:100	BioLegend	303414
CD303	APC vio770	REA693	1:100	Miltenyi Biotech	130-114-178
CD41a	BUV395	HIP8	1:400	BD Bioscience	740295
FceRIa	PE Dazzle 594	AER-37(CRA-1)	1:200	BioLegend	334634
CD34	FITC	581	1:100	BD Bioscience	555821
CD19	BUV395	SJ25C1	1:50	BD Bioscience	563549
IgD	APC	IA6-2	1:100	BD Bioscience	561303
CD20	BUV805	2H7	1:200	BD Bioscience	612905
CD27	PE	M-T271	1:200	BD Bioscience	555441
CD10	AF700	HI10a	1:200	BD Bioscience	563509
CD24	BB515	ML5	1:200	BD Bioscience	564521
IgM	APC Cy7	MHM-88	1:100	BioLegend	314520
CD38	BUV737	HIT2	1:400	BD Bioscience	741837
CD5	PE Dazzle 594	L17F12	1:400	BioLegend	364012
CD1d	BV786	42.1	1:200	BD Bioscience	743608
CD138	BV711	MI15	1:200	BioLegend	563184

Part II

Identification and
implementation of potential
biomarkers for immunotherapy
response in breast cancer



Chapter 6

Towards predictive biomarkers for immunotherapy response in breast cancer patients

- Review-

Leonie Voorwerk, Marije Kat, Marleen Kok

Breast cancer management, 2018; 7(1), bmt-2017-0014

Abstract

Immunotherapy using anti-PD(L)1 has revolutionized treatment for various tumor types. Early data have shown durable responses in a small subgroup of breast cancer patients. So far, the response rates appear higher for breast tumors that are triple negative, PDL1-positive and/or harbor high levels of immune cells. Both comprehensive analyses of the breast tumor microenvironment and exploiting research on biomarkers in other cancer types, such as melanoma and lung cancer, may contribute to the discovery of accurate biomarkers to select breast cancer patients for immunotherapy. Here we summarize key features of the breast tumor microenvironment as well as putative predictive biomarkers established in other tumor types. Insights from both fields can guide future studies to enable personalized breast cancer immunotherapy.

Practice points

- Although response rates to anti-PD(L)1 are moderate in breast cancer, durable responses are seen.
- No accurate biomarkers for the prediction of response to immunotherapy in breast cancer are available yet.
- Response rates to anti-PD(L)1 appear higher in triple-negative breast cancer (TNBC) and PDL1-positive breast cancer.
- Early data show that TNBC patients with a tumor harboring relatively high levels of tumor infiltrating lymphocytes have a better outcome after anti-PD(L)1.
- As seen in melanoma patients, TNBC patients with high serum lactate dehydrogenase levels are less likely to respond to anti-PD(L)1 monotherapy.
- Exploiting research on immune biomarkers in other cancer types can guide the analyses of samples of breast cancer patients treated with anti-PD(L)1 in order to find predictive biomarkers.
- It needs to be determined whether potential biomarkers predicting response to anti-PD(L)1 have solely predictive value or capture information on prognosis as well.

Immunotherapy has revolutionized cancer treatment for various tumor types. The major breakthroughs are seen with antagonistic monoclonal antibodies directed against CTLA-4, PD-1 and PD-L1. Objective response rates (ORRs) with anti-PD(L)1 treatment range from 40% in stage IV melanoma patients¹ to 19-23% in stage IV non-small-cell lung cancer (NSCLC)²⁻⁴ and 25% in renal cell carcinoma (RCC) patients⁵. Importantly, durable responses are seen in patients responding to therapy. Recently, impressive progression-free survival (PFS) benefits of anti-PDL1 were seen in stage III NSCLC patients after chemoradiotherapy as compared with placebo⁶ and longer recurrence-free survival with adjuvant anti-PD1 in stage III/IV melanoma as compared with anti-CTLA-4⁷.

Historically, breast cancer was long considered a low-immunogenic malignancy. However, accumulating data regarding the value of breast tumor-associated immune cells and early data on efficacy of immune checkpoint inhibition such as anti-PD(L)1 in metastatic breast cancer have led to reconsideration of this viewpoint. Anti-PD(L)1 is currently under investigation in breast cancer patients and promising response rates have been presented. In order to treat the right patients with the right immunomodulatory therapy, biomarkers are needed to predict response to immunotherapy. For breast cancer, no predictive biomarkers for immunotherapy are available yet. In-depth analyses of the breast cancer tumor microenvironment (TME) and the systemic immune response of breast cancer patients may help the identification of possible biomarkers. Furthermore, putative biomarkers found in other malignancies can guide the discovery of predictive biomarkers in breast cancer. In this review, we will describe the current status of biomarker research based on the small clinical trials evaluating anti-PD(L)1 in metastatic breast cancer presented so far. In addition, we summarize previous preclinical and translational research on the anti-breast cancer immune response that might be crucial for response to anti-PD(L)1. Lastly, we will discuss putative predictive biomarkers established in other tumor types that might be important for the selection of breast cancer patients for immunotherapy. Figure 1 summarizes the opportunities for the development of biomarkers to predict immunotherapy response in breast cancer.

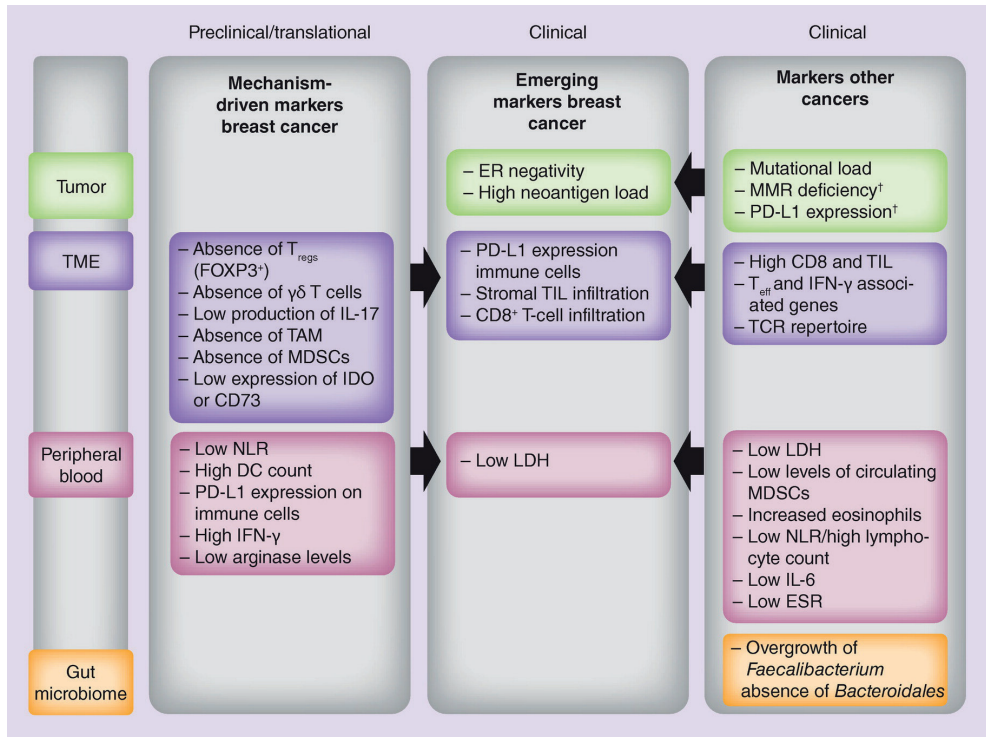


Figure 1. Opportunities for development of biomarkers to predict immunotherapy response in breast cancer. Currently, ongoing analyses of samples of breast cancer patients treated with anti-PD(L)1 have shown that ER-status, TIL, CD8 and LDH could be potential biomarkers (middle panel). New biomarker analyses can be guided by mechanism based preclinical or translational research (left panel) or from clinical trials with anti-PD(L)1 in other cancers, such as melanoma, NSCLC or bladder cancer (right panel). Information on these markers and references can be found in the text.

[†]US FDA approved biomarkers (PD-L1: $\geq 50\%$ expression on tumor cells in NSCLC).

BC: Breast cancer; DC: Dendritic cell; ER: Estrogen receptor; ESR: Erythrocyte sedimentation rate; LDH: Lactate dehydrogenase; MDSC: Myeloid-derived suppressor cell; MMR: Mismatch repair; NLR: Neutrophil-to-lymphocyte ratio; NSCLC: Non-small-cell lung cancer; TAM: Tumor-associated macrophage; TCR: T-cell receptor; T_{eff} : Effector T-cell; TIL: Tumor infiltrating lymphocyte; TME: Tumor microenvironment; T_{regs} : Regulatory T-cell.

First results of trials evaluating anti-PD(L)1 in breast cancer

In 170 patients with triple-negative breast cancer (TNBC), pretreated with chemotherapy for metastatic disease and not preselected based on PD-L1 expression (KEYNOTE-086A), an ORR of 5% was found upon treatment with anti-PD1 (pembrolizumab)⁸. In another cohort (KEYNOTE-012) of 27 patients with heavily pretreated PD-L1-positive metastatic TNBC (mTNBC), the ORR was 19%⁹. In the KEYNOTE-86B cohort of 52 patients treated with anti-PD1 as first line of therapy for metastatic disease and with PD-L1-positive tumors, the ORR was 23%¹⁰. In another Phase I study with 112 patients with mTNBC, treated with anti-PDL1 (atezolizumab), an ORR of 10% was seen¹¹. In conclusion, in mTNBC response rates

presented so far are around 5-23% and seem to be associated with PD-L1 expression and extend of previous chemotherapies.

On a smaller scale, anti-PD(L)1 has been evaluated in metastatic ER-positive disease. Dirix *et al.* found an ORR of 3% in 72 patients after treatment with anti-PDL1 (avelumab)¹². The KEYNOTE-028 study with 25 ER-positive metastatic breast cancer patients, all with PD-L1-positive tumors, revealed an ORR of 12%¹³. Currently, many trials are ongoing in metastatic breast cancer evaluating the role of anti-PD(L)1 in combination with chemotherapy. Anti-PDL1 plus nab-paclitaxel resulted in an ORR of 42% in 24 mTNBC patients¹⁴. The combination of eribulin and anti-PD1 in 39 pretreated mTNBC patients induced responses in 33% of the patients¹⁵. It still remains unclear whether this potential synergy between anti-PD(L)1 and chemotherapy is simply related to the direct effect on tumor growth or to proposed immunomodulatory aspects of chemotherapy¹⁶. Preliminary data presented at ESMO 2017 of the Phase II TONIC trial (NCT02499367) showed an ORR of 24% in 50 mTNBC patients after 2 weeks of pretreatment with either low-dose chemotherapy (cisplatin, doxorubicin and cyclophosphamide), radiotherapy or no pretreatment, followed by anti-PD1 (nivolumab)¹⁷. In-depth analyses of tumor biopsies are needed to unravel the potential immunomodulatory effect of chemotherapy/radiation on the breast TME.

Several neoadjuvant immunotherapy trials are ongoing in early breast cancer patients. In the TNBC cohort of the neoadjuvant adaptive I-SPY trial, Nanda *et al.* found three-times higher estimated complete response rates when combining anti-PD1 with paclitaxel, compared with paclitaxel monotherapy; 60 versus 20%. Furthermore, the estimated complete response rate was significantly increased in ER-positive disease with the addition of anti-PD1 (34 vs 13%)¹⁸. Schmid *et al.* described an ORR of 100% in ten early TNBC patients treated with carboplatin/nab-paclitaxel plus anti-PD1, followed by doxorubicin/cyclophosphamide (AC) and anti-PD1¹⁹. Lastly, preliminary data in a third trial showed a pathological complete response rate of 71% in seven early TNBC patients treated with anti-PDL1 (durvalumab) plus nab-paclitaxel and AC²⁰.

Potential biomarkers predicting outcome of anti-PD(L)1 in breast cancer

As described above, so far, a limited number of patients were enrolled in clinical trials evaluating anti-PD(L)1 in breast cancer. Moreover, these trials are not designed for the discovery and validation of biomarkers. In two studies PD-L1-positive TNBC had higher ORR as compared with patients with low expression of PD-L1^{11,12}. Furthermore, patients with at least 10% stromal tumor infiltrating lymphocytes (sTIL) or 1.35% CD8-positive cells (median used as cut-off) tended to have higher response rates¹¹. Recently, Loi *et al.* confirmed the predictive value of sTIL in the KEYNOTE-086 cohorts, in which significantly higher levels of sTIL were seen in mTNBC patients responding to anti-PD1. This effect was even

more pronounced in the KEYNOTE-86B cohort of PDL1-positive tumors that were not pretreated for metastatic disease. Of note, PD-L1 expression itself was not correlated with outcome after anti-PD1²¹.

Only a few studies have reported on potential biomarkers using peripheral blood. In the KEYNOTE-012 study, all five patients with a serum lactate dehydrogenase (LDH) level of above 800 U/l progressed within 8 weeks after study entry⁹. Also in the KEYNOTE-086 cohorts, LDH was associated with worse outcome after anti-PD1 treatment²¹. So far, no data are available on the predictive capacity of genetic characteristics in breast cancer, such as mutational load and gene expression. However, a slightly higher neoantigen load was seen in responders to combination therapy (anti-PDL1 plus anti-CTLA-4) in a small cohort of mTNBC and ER-positive patients²².

Breast tumor microenvironment

Besides future unbiased analyses of side studies from the trials summarized above, insights gained in the last decades from preclinical as well as translational breast cancer research may be helpful on our way to personalized breast cancer immunotherapy. Here we discuss the most important components of the breast TME that could inform future analyses of samples of patients treated with anti-PD(L)1.

Tumor intrinsic features

Genomic instability is a hallmark of cancer and an important determinant of the immunogenicity of cancer cells. Accumulation of tumor-specific nonsynonymous mutations, called mutational load, can lead to the formation of peptides that are entirely absent from the normal human genome, so-called neoantigens. This can increase the 'foreignness' of the tumor and can thereby evoke an immune response²³. In breast cancer, HER2-enriched tumors and TNBC exhibit a significantly higher mutation rate than ER-positive disease and are therefore more likely to harbor more neoantigens^{24,25}. Copy number variants are caused by stable chromosomal rearrangements and occur early in breast cancer²⁶. BRCA1/2-deficient breast cancers have impaired DNA double-strand break repair, which causes profuse copy number variant formation^{27,28}. BRCA1-mutated cancers are associated with more lymphocytic infiltration as compared with a sporadic breast cancer control group²⁹. Recently, Nolan *et al.* confirmed that TNBC tumors in the presence of a germline BRCA1 mutation have more sTIL and higher PD-L1 expression, as compared with wild-type tumors³⁰. In addition, in DNA damage response-deficient tumors, more infiltration of CD4⁺ and CD8⁺ T cells was seen³¹.

Recently, it has been shown that response rates to anti-PD1 are strikingly high in mismatch repair deficient (MMRd) tumors independent of the origin of the cancer cell³². Microsatellite instability, caused by MMRd, results in rapid accumulation of somatic mutations. MMRd is rare in breast cancer, but is present in about 1-2% of

cases³³. Profound response to anti-PD1 was seen in a breast cancer patient with a MMRd tumor³⁴. Importantly, microsatellite instability might be associated with lower survival rates as seen in a small cohort of breast cancer patients³⁵.

Tumor infiltrating lymphocytes

Considerable heterogeneity exists between mammary tumors with respect to tumor infiltrating lymphocyte (TIL) density and immune cell composition³⁶. Higher lymphocyte infiltration is correlated with ER negativity and better prognosis in general^{37,38}. Moreover, high TIL levels have been associated with improved responses to neoadjuvant chemotherapy³⁹. A distinction can be made between intratumoral and stromal lymphocytes. Stromal lymphocytes are considered a more reliable biomarker than intratumoral lymphocytes, probably due to the poor reproducibility of intratumoral TIL⁴⁰. The lymphocyte population in breast cancers is largely comprised of CD8⁺ cytotoxic T cells and CD4⁺ T-helper cells, followed by regulatory T cells and different subpopulations of B cells^{41,42}. High CD8⁺ T-cell infiltration is a positive prognostic factor generally associated with TNBC and HER2-enriched lesions⁴³. Different subpopulations of CD4⁺ T cells are present in the breast cancer TME, which include T-helper (Th) subsets, regulatory T cells (T_{regs}), $\gamma\delta$ T cells and follicular T cells^{44,45}. The presence of Th17 cells in breast cancer was associated with good prognosis, although functionally both pro- and antitumor functions have been reported⁴⁶. T_{regs} are CD4⁺ CD25⁺ FOXP3⁺ T cells with a crucial role in protecting tissues from damage due to inflammation and preventing autoimmunity⁴⁷. The presence of T_{regs} is negatively correlated with disease outcome in breast cancer⁴⁸. A small subset of T cells is represented by the $\gamma\delta$ T cells, which have an alternative T-cell receptor (TCR) that is able to recognize antigens in MHC-unrestricted fashion⁴⁹. Like T_{regs}, these $\gamma\delta$ T cells exhibit a regulatory function and were correlated to advanced stages and worse survival in breast cancer^{50,51}. Conversely, follicular T cells have an antitumor role since they were associated with better prognosis in HER2- positive breast cancer⁴⁵. Tumor-reactive B cells can produce antibodies that recognize neoantigen epitopes, which potentiates tumor elimination by T cells and innate immune cells⁵². Tumor-evoked regulatory B cells (B_{regs}) were shown to secrete immunosuppressive cytokines, which inhibited proliferation of CD4⁺ T cells. In addition, PD-L1 expression on B cells was shown to inhibit antitumor T-cell responses⁵³.

Tumor infiltrating myeloid cells

Tumor-associated macrophages (TAMs) are known to facilitate metastasis^{54,55}. In breast cancer, TAMs have been associated with ER negativity, higher histological grade and poor prognosis⁵⁶. Neutrophils reduce T-cell proliferation and therefore suppress effector function. Alongside $\gamma\delta$ T cells, neutrophils have a role in promoting breast cancer metastasis⁵⁷. In a mechanistic mouse study, it was shown that inflamed mammary tumors secrete chemokine IL-1 β , which attracts $\gamma\delta$ T cells and induces them to produce anti-inflammatory cytokine IL-17 and G-CSF. Neutrophils are recruited by these factors and secrete inducible NOS, which in turn suppresses antitumor CD8⁺ T-cell effector function and therefore facilitates metastasis⁵⁷. Lastly, myeloid-derived suppressive cells (MDSCs) are immature myeloid cells that exhibit

immunosuppressive capacity. MDSCs inhibit effector functions of T cells, natural killer (NK) cells and dendritic cells (DCs), while stimulating protumor functions of T_{regs} , TAMs and Th2 cells through various mechanisms. Infiltrating MDSCs have been associated with unfavorable outcome in breast cancer⁵⁸. Of note, new insights concerning tumor infiltrating myeloid cells have also generated confusion due to, for example, the lack of consensus on phenotypic markers to detect polarized macrophages or MDSCs⁵⁹.

Other features of immunosuppression in breast cancer

A balance between stimulatory and inhibitory signals regulates T-cell activity. One of the most important immune checkpoints in peripheral immunological tolerance is governed by PD-1. This co-inhibitory immune receptor represses the effector function of cytotoxic T cells to prevent autoimmunity⁶⁰. PD1 expression is induced on T cells upon TCR activation^{61,62}. Besides activated T cells, also activated B cells, NK cells and several other immune lineages were shown to express PD1⁶³. PD-L1, also known as B7-H1, is broadly expressed among different populations of immune cells and certain tissues, whereas PD-L2 is mainly limited to DCs. Cytokine IFN- γ , secreted by activated T cells, is shown to induce expression of both PD-L1 and PD-L2^{64,65}. Remarkably, in breast cancer PD-L1 expression was mainly observed on immune cells as opposed to tumor cells in other cancers⁶⁶.

IFN- γ secreted in the TME induces expression of IDO⁶⁷. *IDO* was linked to high TIL density in breast cancer⁶⁸. Conversely, in a breast cancer murine model, high *IDO* expression was reported to have an immunosuppressive function on T cells, and might interfere with immunotherapy efficacy⁶⁹. IDO inhibition is currently being evaluated in Phase I clinical trials in combination with immune checkpoint blockade⁷⁰. Lastly, CD73 is upregulated by T_{regs} as another immune escape mechanism⁷¹. As a result of enzymatic activity of CD73, the A2a receptor (A2aR) on T cells is activated, which in turn enhances PD1 expression^{72,73}. CD73 expression has been associated with poor outcome in TNBC⁷⁴. Both CD73 and A2aR antagonist therapies synergize with PD1 blockade in mouse models^{73,75}.

Systemic immune response in breast cancer

In contrast to chemotherapy or targeted therapy, immunotherapy is not directed against the cancer cells but can modulate the patient's immune system. Emerging data in the field of clinical melanoma research show that circulating immunosuppressive cells or factors are associated with poor outcome after immunotherapy. Here we summarize the current knowledge on features of this systemic immune response in breast cancer.

Circulating immune cells

It was shown that breast cancer patients have decreased peripheral lymphocyte levels, but differences were only statistically significant for CD8⁺ and CD4⁺ T cells⁷⁶. Compared with healthy controls, higher peripheral blood T_{reg} counts were found in

breast cancer patients^{77,78}. Elevated neutrophil-to-lymphocyte ratio as a measure for systemic inflammation has recently been associated with lower survival rates⁷⁹. Peripheral blood DC counts, myeloid-derived DCs in particular, were shown to be consistently reduced in breast cancer patients⁸⁰. In advanced breast cancer patients, DC count was dramatically lower as compared with early breast cancer, where more immature DCs were observed^{80,81}. Finally, PD-L1 mRNA expression in immune cells detected in peripheral blood might be associated with disease progression⁸². Interestingly, circulating metastatic breast cancer cells expressing PD-L1 were also detectable⁸³.

Secreted immunological mediators

In cancer patients, predominance of Th2-related cytokines was observed in peripheral blood, whereas Th1 cytokines were decreased⁸⁴. Significantly reduced levels of IFN- γ (Th1 associated) were measured in breast cancer patients, suggesting that IFN- γ production by lymphocytes is partially or completely impaired⁷⁶. Arginase serum levels were found to be elevated and increased during disease progression in breast cancer patients⁸⁵. Treatment with VEGF antagonist bevacizumab inhibited the infiltration of suppressive immune cells (i.e., T_{regs}, TAMs and MDSCs) in a breast cancer xenograft model⁸⁶. As discussed above, serum LDH levels are associated with outcome after anti-PD1 in TNBC, but LDH does also correlate with disease outcome in cancer. This suggests that LDH might not be a pure predictive factor for breast cancer immunotherapy response, but also captures prognostic information⁸⁷. Acidification of the TME, as a result of conversion of pyruvate into lactate by LDH, has detrimental consequences for infiltrating T cells, such as impaired cytokine production and lytic activity⁸⁸.

Putative biomarkers for immunotherapy in other malignancies

Research in melanoma, bladder cancer and NSCLC has already given important insights into features of the TME that predict response to anti-PD(L)1. This information can be exploited with the aim to identify putative predictive biomarkers in breast cancer. According to the ‘cancer immunogram’ presented by Blank *et al.*, seven parameter classes can be used to describe the interaction between cancer and the immune system⁸⁹. In this section, possible biomarkers found in other malignancies than breast cancer, will be described according to these classes.

Tumor foreignness

In patients with MMRd tumors treated with anti-PD1, high response rates are seen, independent of cancer type³². This led to the US FDA approval of MMRd as a biomarker for immunotherapy. A relationship was shown between high nonsynonymous mutation burden and improved response to anti-PD1 in NSCLC patients⁹⁰. The significance of mutational load as a predictive marker was also confirmed in bladder cancer⁹¹. Frameshift indel mutations, small insertions or deletions, were associated with better response to checkpoint inhibition in

melanoma⁹². Furthermore, poor outcome after anti-CTLA-4 treatment was seen in patients with melanoma with tumor aneuploidy and higher burden of copy number loss^{93,94}. Clonal neoantigens but not the subclonal mutations were predictive of response to anti-PD1 in NSCLC⁹⁵.

General immune status

Increases in peripheral blood lymphocyte count during treatment has been correlated to improved anti-CTLA-4 response, whereas a high neutrophil-to-lymphocyte ratio was associated with inferior outcome in anti-PD1-treated NSCLC patients^{96,97}. Higher rates of MDSCs were associated with lower response rates in anti-CTLA-4 refractory melanoma patients treated with anti-PD1⁹⁸ and lower overall survival (OS) in melanoma patients treated with anti-CTLA-4⁹⁹. In addition, it was seen that responders to anti-CTLA-4 had a higher increase of eosinophils after one infusion as compared with non-responders. Also, monocyte and neutrophil count at baseline were significantly lower in responders. A decrease in monocytic MDSCs, a reduction in PD-L1 expression on MDSCs seemed predictive of response to anti-CTLA-4 in the same cohort¹⁰⁰.

Immune cell infiltration

Increased TILs and CD8⁺ T cells in particular have been linked with therapeutic efficacy of PD(L)1 checkpoint blockade in different cancer types, especially in melanoma^{101,102}. An increase in TIL after treatment and higher baseline levels of FOXP3 and IDO were associated with better clinical outcome in melanoma patients treated with anti-CTLA-4¹⁰³. Higher frequencies of FOXP3⁺ CD4⁺ T cells were also associated with better survival in melanoma patients treated with anti-CTLA-4¹⁰⁴. CTLA4 is known to be expressed on FOXP3⁺ T_{regs} and therefore might be important for anti-CTLA-4 efficacy¹⁰⁵. FOXP3 in relation to response to anti-PD(L)1 has not been well described. In RCC patients treated with anti-PDL1 a subtle higher ratio of effector T cells to regulatory T cells was seen in responders, as measured by gene expression¹⁰⁶.

T-cell checkpoints

PD-L1 expression on tumors has been linked with better responses to immunotherapy across different cancers. However, PD-L1 expression does not appear to be a requisite for immunotherapeutic responses and PDL1-positive tumors are not always responsive^{107,108}. Interestingly in some tumor types, such as bladder cancer, PD-L1 expression on immune cells appears to be more predictive of anti-PD(L)1 response than its expression on tumor cells^{108,109}, as might be the case for breast cancer.

Soluble inhibitors

Low baseline levels of the erythrocyte sedimentation rate were associated with better OS in melanoma patients treated with anti-CTLA-4¹¹⁰. In a small cohort of 40 melanoma patients, high IL-6 levels were associated with worse outcome after anti-CTLA-4 treatment⁹⁶.

Inhibitory tumor mechanisms

LDH has been shown to inhibit function and survival of T cells and NK cells¹¹¹. High levels of serum LDH are correlated with worse response to anti-CTLA-4 in melanoma patients¹¹⁰. Furthermore, higher response rates were seen in melanoma patients with normal LDH treated with anti-PD1¹¹². Whether LDH is mainly a prognostic factor or also predictive for immunotherapy response needs to be further established.

Immune infiltrate activation

T-effector- and IFN- γ -associated genes were associated with better OS in NSCLC patients treated with anti-PDL1¹¹³. This was also shown in melanoma patients that responded to anti-CTLA-4 or anti-PD1, in which higher expression levels of genes were found related to CD8⁺ T cells, $\gamma\delta$ T and NK cells, and lower levels of genes associated with MDSCs and T_{regs}¹¹⁴. Higher IFN- γ associated gene expression levels were associated with better response to anti-PDL1 in urothelial cell carcinoma and anti-CTLA-4 in melanoma^{108,115}. Deep sequencing of the T-cell receptor in peripheral blood samples of melanoma patients showed a correlation between TCR repertoire and better OS after immune checkpoint blockade¹¹⁶. An increased clinical benefit to anti-CTLA-4 was observed in patients with higher baseline TCR diversity measured from peripheral blood of melanoma patients¹¹⁷. In addition, it was found that melanoma patients who responded to neoadjuvant anti-PD1 and anti-CTLA-4, had more newly detectable TCR clones after 6 weeks of treatment¹¹⁸.

Gut microbiome

Accumulating evidence indicates that an overgrowth or absence of specific gut bacteria might predict response to immunotherapy. In mice with melanoma, *Bifidobacterium* was needed for anti-PDL1 response. After oral administration of this gut microbiome bacterium, tumors were reduced in size to the same extent as with anti-PDL1 alone¹¹⁹. In patients with metastatic melanoma treated with anti-PD1, response was associated with a 'favorable' gut microbiome. More diversity, high abundance of *Faecalibacterium* and low abundance of *Bacteroidales* was associated with response to anti-PD1 and longer PFS. Fecal microbiome transplant of germ-free mice with feces obtained from melanoma patients responding to anti-PD1, resulted in reduced tumor growth¹²⁰. Another study showed that NSCLC and RCC patients treated with antibiotics during the course of anti-PD1 had shorter PFS and/or OS, as compared with patients not treated with antibiotics. This effect remained statistically significant in a multivariate analysis including other prognostic markers. An association between the abundance of *Akkermansia muciniphila* and a favorable clinical outcome was seen. Fecal microbiome transplant with *A. muciniphila* in sarcoma bearing mice restored response to anti-PD1 after treatment with antibiotics¹²¹.

Future perspective

Knowledge on the breast TME, the systemic immune response in breast cancer patients and biomarkers found in other malignancies can guide the search for new biomarkers in breast cancer. In addition, understanding the mechanisms of response to immunotherapy in breast cancer will be crucial to increase benefit, including cure and quality of life of our breast cancer patients. To obtain this knowledge, comprehensive analysis of different types of data is essential. Therefore, large scale acquisition of cancer tissue, peripheral blood and other biospecimens is critical for the development of a robust classifier that can be used in the clinic to predict response and toxicity of immunotherapy in early and metastatic breast cancer patients.

Financial & competing interests disclosure

M Kok has received an unrestricted research grant from Bristol-Meyers-Squibb paid to the institute and a translational fellowship of the Dutch Cancer Society (KWF) paid to the institute. The authors have no other relevant affiliations or financial involvement with any organization or entity with a financial interest in or financial conflict with the subject matter or materials discussed in the manuscript apart from those disclosed. No writing assistance was utilized in the production of this manuscript.

Acknowledgements

We apologize to colleagues whose work was not cited in this review due to space constraints.

References

1. Robert C, Long GV, Brady B et al. Nivolumab in previously untreated melanoma without BRAF mutation. *The New England journal of medicine* 372(4), 320-330, 2015
2. Garon EB, Rizvi NA, Hui R et al. Pembrolizumab for the treatment of non-small-cell lung cancer. *The New England journal of medicine* 372(21), 2018-2028, 2015
3. Borghaei H, Paz-Ares L, Horn L et al. Nivolumab versus Docetaxel in Advanced Nonsquamous Non-Small-Cell Lung Cancer. *The New England journal of medicine* 373(17), 1627-1639, 2015
4. Gettinger S, Rizvi NA, Chow LQ et al. Nivolumab Monotherapy for First-Line Treatment of Advanced Non-Small-Cell Lung Cancer. *Journal of clinical oncology* 34(25), 2980-2987, 2016
5. Motzer RJ, Escudier B, McDermott DF et al. Nivolumab versus Everolimus in Advanced Renal-Cell Carcinoma. *The New England journal of medicine* 373(19), 1803-1813, 2015
6. Antonia SJ, Villegas A, Daniel D et al. Durvalumab after Chemoradiotherapy in Stage III Non-Small-Cell Lung Cancer. *The New England journal of medicine* doi:10.1056/NEJMoa1709937, 2017
7. Weber J, Mandala M, Del Vecchio M et al. Adjuvant Nivolumab versus Ipilimumab in Resected Stage III or IV Melanoma. *The New England journal of medicine* doi:10.1056/NEJMoa1709030, 2017
8. Adams S, Schmid P, Rugo HS et al. Phase 2 study of pembrolizumab (pembro) monotherapy for previously treated metastatic triple-negative breast cancer (mTNBC): KEYNOTE-086 cohort A. *Journal of Clinical Oncology* 35(15_suppl), 1008, 2017
9. Nanda R, Chow LQ, Dees EC et al. Pembrolizumab in Patients With Advanced Triple-Negative Breast Cancer: Phase Ib KEYNOTE-012 Study. *Journal of clinical oncology* 34(21), 2460-2467, 2016.
***The KEYNOTE-012 is the first published clinical trial investigating anti-PD1 in breast cancer, showing durable responses in a subset of patients.**
10. Adams S, Loi S, Toppmeyer D et al. Phase 2 study of pembrolizumab as first-line therapy for PD-L1-positive metastatic triple-negative breast cancer (mTNBC): Preliminary data from KEYNOTE-086 cohort B. *Journal of Clinical Oncology* 35(15_suppl), 1088, 2017
11. Schmid P, Cruz C, Braithes FS et al. Abstract 2986: Atezolizumab in metastatic TNBC (mTNBC): Long-term clinical outcomes and biomarker analyses. *Cancer Research* 77(13 Supplement), 2986-2986, 2017
12. Dirix LY, Takacs I, Jerusalem G et al. Avelumab, an anti-PD-L1 antibody, in patients with locally advanced or metastatic breast cancer: a phase 1b JAVELIN Solid Tumor study. *Breast cancer research and treatment* doi:10.1007/s10549-017-4537-5, 2017
13. Rugo H, Delord J-P, Im S-A et al. Abstract S5-07: Preliminary efficacy and safety of pembrolizumab (MK-3475) in patients with PD-L1-positive, estrogen receptor-positive (ER+)/HER2-negative advanced breast cancer enrolled in KEYNOTE-028. *Cancer Research* 76(4 Supplement), S5-07-S05-07, 2016
14. Adams S, Diamond JR, Hamilton EP et al. Phase Ib trial of atezolizumab in combination with nab-paclitaxel in patients with metastatic triple-negative breast cancer (mTNBC). *Journal of Clinical Oncology* 34(15_suppl), 1009, 2016
15. Tolaney S, Savulsky C, Aktan G et al. Abstract P5-15-02: Phase 1b/2 study to evaluate eribulin mesylate in combination with pembrolizumab in patients with metastatic triple-negative breast cancer. *Cancer Research* 77(4 Supplement), P5-15-02, 2017
16. Kersten K, Salvagno C, De Visser KE. Exploiting the Immunomodulatory Properties of Chemotherapeutic Drugs to Improve the Success of Cancer Immunotherapy. *Frontiers in immunology* 6 516, 2015
17. Kok M, Horlings HM, Van De Vijver K et al. LBA 14 - Adaptive phase II randomized non-comparative trial of nivolumab after induction treatment in triple negative breast cancer: TONIC-trial. *Ann Oncol; ESMO abstracts* (2017).
18. Nanda R, Liu MC, Yau C et al. Pembrolizumab plus standard neoadjuvant therapy for high-risk breast cancer (BC): Results from I-SPY 2. *Journal of Clinical Oncology* 35(15_suppl), 506, 2017
19. Schmid P, Park YH, Muñoz-Couselo E et al. Pembrolizumab (pembro) + chemotherapy (chemo) as neoadjuvant treatment for triple negative breast cancer (TNBC): Preliminary results from KEYNOTE-173. *Journal of Clinical Oncology* 35(15_suppl), 556, 2017

20. Pusztai L, Silber A, Hofstatter EW et al. Safety of MEDI4736 (anti-PD-L1 antibody) administered concomitant with weekly nab-paclitaxel and dose dense doxorubicin/cyclophosphamide (ddAC) as neoadjuvant chemotherapy for stage I-III triple negative breast cancer (TNBC): A Phase I/II trial. *Journal of Clinical Oncology* 35(15_suppl), 572, 2017
21. Loi S, Adams S, Schmid P et al. LBA13 - Relationship between tumor infiltrating lymphocyte (TIL) levels and response to pembrolizumab (pembro) in metastatic triple-negative breast cancer (mTNBC): Results from KEYNOTE-086. *Ann Oncol; ESMO abstracts* (2017).
22. Santa-Maria CA, Kato T, Park J-H et al. Durvalumab and tremelimumab in metastatic breast cancer (MBC): Immunotherapy and immunopharmacogenomic dynamics. *Journal of Clinical Oncology* 35(15_suppl), 3052, 2017
23. Schumacher TN, Schreiber RD. Neoantigens in cancer immunotherapy. *Science* 348(6230), 69-74, 2015
***Schumacher et al. clearly describe the mechanisms and consequences of neoantigen formation in tumors and the cytotoxic T-cell response directed to these neoantigens.**
24. Shah SP, Roth A, Goya R et al. The clonal and mutational evolution spectrum of primary triple-negative breast cancers. *Nature* 486(7403), 395-399, 2012
25. Network TCGA. Comprehensive molecular portraits of human breast tumours. *Nature* 490(7418), 61-70, 2012
26. Wang Y, Waters J, Leung ML et al. Clonal evolution in breast cancer revealed by single nucleus genome sequencing. *Nature* 512(7513), 155-160, 2014
27. Van Beers EH, Van Welsem T, Wessels LF et al. Comparative genomic hybridization profiles in human BRCA1 and BRCA2 breast tumors highlight differential sets of genomic aberrations. *Cancer Res* 65(3), 822-827, 2005
28. Natrajan R, Weigelt B, Mackay A et al. An integrative genomic and transcriptomic analysis reveals molecular pathways and networks regulated by copy number aberrations in basal-like, HER2 and luminal cancers. *Breast cancer research and treatment* 121(3), 575-589, 2010
29. Lakhani SR, Jacquemier J, Sloane JP et al. Multifactorial analysis of differences between sporadic breast cancers and cancers involving BRCA1 and BRCA2 mutations. *Journal of the National Cancer Institute* 90(15), 1138-1145, 1998
30. Nolan E, Savas P, Policheni AN et al. Combined immune checkpoint blockade as a therapeutic strategy for BRCA1-mutated breast cancer. *Science translational medicine* 9(393), 2017
31. Parkes EE, Walker SM, Taggart LE et al. Activation of STING-Dependent Innate Immune Signaling By S-Phase-Specific DNA Damage in Breast Cancer. *Journal of the National Cancer Institute* 109(1), 2017
32. Le DT, Durham JN, Smith KN et al. Mismatch repair deficiency predicts response of solid tumors to PD-1 blockade. *Science* 357(6349), 409-413, 2017
**** Based on this clinical trial, the US FDA approved MMRd as a biomarker for anti-PD1 (pembrolizumab), which is the first biomarker not linked to a certain tumor type.**
33. Davies H, Morganella S, Purdie CA et al. Whole-Genome Sequencing Reveals Breast Cancers with Mismatch Repair Deficiency. *Cancer Research* doi:10.1158/0008-5472.can-17-1083, 2017
34. Kok M, Horlings HM, Snaebjornsson P et al. Profound Immunotherapy Response in Mismatch Repair-Deficient Breast Cancer. *JCO Precision Oncology* doi:10.1200/po.17.00052(1), 1-3, 2017
35. Paulson TG, Wright FA, Parker BA, Russack V, Wahl GM. Microsatellite instability correlates with reduced survival and poor disease prognosis in breast cancer. *Cancer Res* 56(17), 4021-4026, 1996
36. Stanton SE, Adams S, Disis ML. Variation in the Incidence and Magnitude of Tumor-Infiltrating Lymphocytes in Breast Cancer Subtypes: A Systematic Review. *JAMA Oncol* 2(10), 1354-1360, 2016
37. Adams S, Gray RJ, Demaria S et al. Prognostic value of tumor-infiltrating lymphocytes in triple-negative breast cancers from two phase III randomized adjuvant breast cancer trials: ECOG 2197 and ECOG 1199. *J Clin Oncol* 32(27), 2959-2966, 2014
38. Salgado R, Denkert C, Campbell C et al. Tumor-Infiltrating Lymphocytes and Associations With Pathological Complete Response and Event-Free Survival in HER2-Positive Early-Stage Breast Cancer Treated With Lapatinib and Trastuzumab: A Secondary Analysis of the NeoALTTO Trial. *JAMA Oncol* 1(4), 448-454, 2015
39. Mao Y, Qu Q, Zhang Y, Liu J, Chen X, Shen K. The Value of Tumor Infiltrating Lymphocytes (TILs) for Predicting Response to Neoadjuvant Chemotherapy in Breast Cancer: A Systematic Review and Meta-Analysis. *PLOS ONE* 9(12), e115103, 2014

40. Salgado R, Denkert C, Demaria S et al. The evaluation of tumor-infiltrating lymphocytes (TILs) in breast cancer: recommendations by an International TILs Working Group 2014. *Annals of Oncology* 26(2), 259-271, 2015
***The tumor-infiltrating lymphocyte working group provides clear guidelines on the scoring of stromal tumor-infiltrating lymphocytes in several stages of breast cancer.**
41. Ruffell B, Au A, Rugo HS, Esserman LJ, Hwang ES, Coussens LM. Leukocyte composition of human breast cancer. *Proc Natl Acad Sci U S A* 109(8), 2796-2801, 2012
42. Burugu S, Asleh-Aburaya K, Nielsen TO. Immune infiltrates in the breast cancer microenvironment: detection, characterization and clinical implication. *Breast Cancer* 24(1), 3-15, 2017
43. Ali HR, Provenzano E, Dawson SJ et al. Association between CD8+ T-cell infiltration and breast cancer survival in 12,439 patients. *Ann Oncol* 25(8), 1536-1543, 2014
44. Coventry BJ, Weightman MJ, Bradley J, Skinner JM. Immune profiling in human breast cancer using high-sensitivity detection and analysis techniques. *JRSM Open* 6(9), 2054270415603909, 2015
45. Gu-Trantien C, Loi S, Garaud S et al. CD4⁺ follicular helper T cell infiltration predicts breast cancer survival. *J Clin Invest* 123(7), 2873-2892, 2013
46. Yang L, Qi Y, Hu J, Tang L, Zhao S, Shan B. Expression of Th17 cells in breast cancer tissue and its association with clinical parameters. *Cell biochemistry and biophysics* 62(1), 153-159, 2012
47. Fontenot JD, Gavin MA, Rudensky AY. Foxp3 programs the development and function of CD4⁺CD25⁺ regulatory T cells. *Nature immunology* 4(4), 330-336, 2003
48. Demir L, Yigit S, Ellidokuz H et al. Predictive and prognostic factors in locally advanced breast cancer: effect of intratumoral FOXP3⁺ Tregs. *Clinical & experimental metastasis* 30(8), 1047-1062, 2013
49. Shin S, El-Diwany R, Schaffert S et al. Antigen recognition determinants of gammadelta T cell receptors. *Science* 308(5719), 252-255, 2005
50. Ma C, Zhang Q, Ye J et al. Tumor-infiltrating gammadelta T lymphocytes predict clinical outcome in human breast cancer. *Journal of immunology* 189(10), 5029-5036, 2012
51. Peng G, Wang HY, Peng W, Kiniwa Y, Seo KH, Wang R-F. Tumor-Infiltrating $\gamma\delta$ T Cells Suppress T and Dendritic Cell Function via Mechanisms Controlled by a Unique Toll-like Receptor Signaling Pathway. *Immunity* 27(2), 334-348, 2007
52. Kotlan B, Simsa P, Teillaud JL et al. Novel ganglioside antigen identified by B cells in human medullary breast carcinomas: the proof of principle concerning the tumor-infiltrating B lymphocytes. *J Immunol* 175(4), 2278-2285, 2005
53. Zhang Y, Morgan R, Chen C et al. Mammary-tumor-educated B cells acquire LAP/TGF- β and PD-L1 expression and suppress anti-tumor immune responses. *Int Immunol* 28(9), 423-433, 2016
54. Wyckoff JB, Wang Y, Lin EY et al. Direct visualization of macrophage-assisted tumor cell intravasation in mammary tumors. *Cancer Res* 67(6), 2649-2656, 2007
55. Valković T, Dobrila F, Melato M, Sasso F, Rizzardi C, Jonjić N. Correlation between vascular endothelial growth factor, angiogenesis, and tumor-associated macrophages in invasive ductal breast carcinoma. *Virchows Arch* 440(6), 583-588, 2002
56. Mahmoud SM, Lee AH, Paish EC, Macmillan RD, Ellis IO, Green AR. Tumour-infiltrating macrophages and clinical outcome in breast cancer. *Journal of clinical pathology* 65(2), 159-163, 2012
57. Coffelt SB, Kersten K, Doornebal CW et al. IL-17-producing $\gamma\delta$ T cells and neutrophils conspire to promote breast cancer metastasis. *Nature* 522(7556), 345-348, 2015
***Coffelt et al. describe the underlying mechanism of mammary tumor metastasis formation in vivo by studying the role of $\gamma\delta$ T cells and neutrophils in systemic inflammation.**
58. Markowitz J, Wesolowski R, Papenfuss T, Brooks TR, Carson WE. Myeloid-derived suppressor cells in breast cancer. *Breast Cancer Res Treat* 140(1), 13-21, 2013
59. Elliott LA, Doherty GA, Sheahan K, Ryan EJ. Human Tumor-Infiltrating Myeloid Cells: Phenotypic and Functional Diversity. *Frontiers in immunology* 8(86), 2017
60. Crawford A, Wherry EJ. The diversity of costimulatory and inhibitory receptor pathways and the regulation of antiviral T cell responses. *Current opinion in immunology* 21(2), 179-186, 2009
61. Nishimura H, Agata Y, Kawasaki A et al. Developmentally regulated expression of the PD-1 protein on the surface of double-negative (CD4⁻CD8⁻) thymocytes. *International immunology* 8(5), 773-780, 1996
62. Vibhakar R, Juan G, Traganos F, Darzynkiewicz Z, Finger LR. Activation-induced expression of human programmed death-1 gene in T-lymphocytes. *Experimental cell research* 232(1), 25-28, 1997

63. Keir ME, Butte MJ, Freeman GJ, Sharpe AH. PD-1 and its ligands in tolerance and immunity. *Annual review of immunology* 26 677-704, 2008
64. Freeman GJ, Long AJ, Iwai Y et al. Engagement of the PD-1 immunoinhibitory receptor by a novel B7 family member leads to negative regulation of lymphocyte activation. *The Journal of experimental medicine* 192(7), 1027-1034, 2000
65. Latchman Y, Wood CR, Chernova T et al. PD-L2 is a second ligand for PD-1 and inhibits T cell activation. *Nature immunology* 2(3), 261-268, 2001
66. Cimino-Mathews A, Thompson E, Taube JM et al. PD-L1 (B7-H1) expression and the immune tumor microenvironment in primary and metastatic breast carcinomas. *Hum Pathol* 47(1), 52-63, 2016
67. Spranger S, Spaapen RM, Zha Y et al. Up-regulation of PD-L1, IDO, and T(regs) in the melanoma tumor microenvironment is driven by CD8(+) T cells. *Sci Transl Med* 5(200), 200ra116, 2013
68. Denkert C, Von Minckwitz G, Brase JC et al. Tumor-infiltrating lymphocytes and response to neoadjuvant chemotherapy with or without carboplatin in human epidermal growth factor receptor 2-positive and triple-negative primary breast cancers. *J Clin Oncol* 33(9), 983-991, 2015
69. Yu J, Wang Y, Yan F et al. Noncanonical NF-kappaB activation mediates STAT3-stimulated IDO upregulation in myeloid-derived suppressor cells in breast cancer. *Journal of immunology* 193(5), 2574-2586, 2014
70. Spira AI, Hamid O, Bauer TM et al. Efficacy/safety of epacadostat plus pembrolizumab in triple-negative breast cancer and ovarian cancer: Phase I/II ECHO-202 study. *Journal of Clinical Oncology* 35(15_suppl), 1103-1103, 2017
71. Deaglio S, Dwyer KM, Gao W et al. Adenosine generation catalyzed by CD39 and CD73 expressed on regulatory T cells mediates immune suppression. *J Exp Med* 204(6), 1257-1265, 2007
72. Antonioli L, Yegutkin GG, Pacher P, Blandizzi C, Haskó G. Anti-CD73 in cancer immunotherapy: awakening new opportunities. *Trends Cancer* 2(2), 95-109, 2016
73. Allard B, Pommey S, Smyth MJ, Stagg J. Targeting CD73 enhances the antitumor activity of anti-PD-1 and anti-CTLA-4 mAbs. *Clinical cancer research* 19(20), 5626-5635, 2013
74. Loi S, Pommey S, Haibe-Kains B et al. CD73 promotes anthracycline resistance and poor prognosis in triple negative breast cancer. *Proc Natl Acad Sci U S A* 110(27), 11091-11096, 2013
75. Mittal D, Young A, Stannard K et al. Antimetastatic effects of blocking PD-1 and the adenosine A2A receptor. *Cancer Res* 74(14), 3652-3658, 2014
76. Caras I, Grigorescu A, Stavaru C et al. Evidence for immune defects in breast and lung cancer patients. *Cancer Immunol Immunother* 53(12), 1146-1152, 2004
77. Liyanage UK, Moore TT, Joo HG et al. Prevalence of regulatory T cells is increased in peripheral blood and tumor microenvironment of patients with pancreas or breast adenocarcinoma. *J Immunol* 169(5), 2756-2761, 2002
78. Wolf AM, Wolf D, Steurer M, Gastl G, Gunsilius E, Grubeck-Loebenstien B. Increase of regulatory T cells in the peripheral blood of cancer patients. *Clin Cancer Res* 9(2), 606-612, 2003
79. Ethier JL, Desautels D, Templeton A, Shah PS, Amir E. Prognostic role of neutrophil-to-lymphocyte ratio in breast cancer: a systematic review and meta-analysis. *Breast Cancer Res* 19(1), 2, 2017
80. Della Bella S, Gennaro M, Vaccari M et al. Altered maturation of peripheral blood dendritic cells in patients with breast cancer. *Br J Cancer* 89(8), 1463-1472, 2003
81. Pinzon-Charry A, Ho CS, Maxwell T et al. Numerical and functional defects of blood dendritic cells in early- and late-stage breast cancer. *Br J Cancer* 97(9), 1251-1259, 2007
82. Kawaguchi K, Suzuki E, Yamaguchi A, Yamamoto M, Morita S, Toi M. Altered expression of major immune regulatory molecules in peripheral blood immune cells associated with breast cancer. *Breast Cancer* 24(1), 111-120, 2017
83. Mazel M, Jacot W, Pantel K et al. Frequent expression of PD-L1 on circulating breast cancer cells. *Mol Oncol* 9(9), 1773-1782, 2015
84. Goto S, Sato M, Kaneko R, Itoh M, Sato S, Takeuchi S. Analysis of Th1 and Th2 cytokine production by peripheral blood mononuclear cells as a parameter of immunological dysfunction in advanced cancer patients. *Cancer immunology, immunotherapy* 48(8), 435-442, 1999
85. Polat MF, Taysi S, Polat S, Böyük A, Bakan E. Elevated serum arginase activity levels in patients with breast cancer. *Surg Today* 33(9), 655-661, 2003
86. Roland CL, Lynn KD, Toombs JE, Dineen SP, Udugamasooriya DG, Brekken RA. Cytokine levels correlate with immune cell infiltration after anti-VEGF therapy in preclinical mouse models of breast cancer. *PLoS One* 4(11), e7669, 2009

87. Zhang J, Yao YH, Li BG, Yang Q, Zhang PY, Wang HT. Prognostic value of pretreatment serum lactate dehydrogenase level in patients with solid tumors: a systematic review and meta-analysis. *Sci Rep* 5 9800, 2015
88. Fischer K, Hoffmann P, Voelkl S et al. Inhibitory effect of tumor cell-derived lactic acid on human T cells. *Blood* 109(9), 3812-3819, 2007
89. Blank CU, Haanen JB, Ribas A, Schumacher TN. *CANCER IMMUNOLOGY*. The “cancer immunogram”. *Science* 352(6286), 658-660, 2016
****This paper provides an informative framework for possible biomarkers and resistance mechanisms of immunotherapy.**
90. Rizvi NA, Hellmann MD, Snyder A et al. Cancer immunology. Mutational landscape determines sensitivity to PD-1 blockade in non-small cell lung cancer. *Science* 348(6230), 124-128, 2015
91. Rosenberg JE, Hoffman-Censits J, Powles T et al. Atezolizumab in patients with locally advanced and metastatic urothelial carcinoma who have progressed following treatment with platinum-based chemotherapy: a single-arm, multicentre, phase 2 trial. *Lancet* 387(10031), 1909-1920, 2016
92. Turajlic S, Litchfield K, Xu H et al. Insertion-and-deletion-derived tumour-specific neoantigens and the immunogenic phenotype: a pan-cancer analysis. *The Lancet. Oncology* 18(8), 1009-1021, 2017
93. Davoli T, Uno H, Wooten EC, Elledge SJ. Tumor aneuploidy correlates with markers of immune evasion and with reduced response to immunotherapy. *Science* 355(6322), 2017
94. Roh W, Chen PL, Reuben A et al. Integrated molecular analysis of tumor biopsies on sequential CTLA-4 and PD-1 blockade reveals markers of response and resistance. *Science translational medicine* 9(379), 2017
95. Mcgranahan N, Furness AJS, Rosenthal R et al. Clonal neoantigens elicit T cell immunoreactivity and sensitivity to immune checkpoint blockade. *Science* 351(6280), 1463-1469, 2016
96. Bjoern J, Juul Nitschke N, Zeeberg Iversen T, Schmidt H, Fode K, Svane IM. Immunological correlates of treatment and response in stage IV malignant melanoma patients treated with Ipilimumab. *Oncoimmunology* 5(4), e1100788, 2016
97. Bagley SJ, Kothari S, Aggarwal C et al. Pretreatment neutrophil-to-lymphocyte ratio as a marker of outcomes in nivolumab-treated patients with advanced non-small-cell lung cancer. *Lung Cancer* 106 1-7, 2017
98. Weber J, Gibney G, Kudchadkar R et al. Phase I/II Study of Metastatic Melanoma Patients Treated with Nivolumab Who Had Progressed after Ipilimumab. *Cancer immunology research* 4(4), 345-353, 2016
99. Kitano S, Postow MA, Ziegler CG et al. Computational algorithm-driven evaluation of monocytic myeloid-derived suppressor cell frequency for prediction of clinical outcomes. *Cancer Immunol Res* 2(8), 812-821, 2014
100. Gebhardt C, Sevko A, Jiang H et al. Myeloid Cells and Related Chronic Inflammatory Factors as Novel Predictive Markers in Melanoma Treatment with Ipilimumab. *Clinical cancer research* 21(24), 5453-5459, 2015
101. Hamid O, Robert C, Daud A et al. Safety and tumor responses with lambrolizumab (anti-PD-1) in melanoma. *N Engl J Med* 369(2), 134-144, 2013
102. Tumei PC, Harview CL, Yearley JH et al. PD-1 blockade induces responses by inhibiting adaptive immune resistance. *Nature* 515(7528), 568-571, 2014
103. Hamid O, Schmidt H, Nissan A et al. A prospective phase II trial exploring the association between tumor microenvironment biomarkers and clinical activity of ipilimumab in advanced melanoma. *Journal of translational medicine* 9 204, 2011
104. Martens A, Wistuba-Hamprecht K, Geukes Foppen M et al. Baseline Peripheral Blood Biomarkers Associated with Clinical Outcome of Advanced Melanoma Patients Treated with Ipilimumab. *Clinical cancer research* 22(12), 2908-2918, 2016
105. Tang AL, Teijaro JR, Njau MN et al. CTLA4 expression is an indicator and regulator of steady-state CD4+ FoxP3+ T cell homeostasis. *Journal of immunology* 181(3), 1806-1813, 2008
106. McDermott DF, Sosman JA, Szoln M et al. Atezolizumab, an Anti-Programmed Death-Ligand 1 Antibody, in Metastatic Renal Cell Carcinoma: Long-Term Safety, Clinical Activity, and Immune Correlates From a Phase Ia Study. *Journal of clinical oncology* 34(8), 833-842, 2016
107. Patel SP, Kurzrock R. PD-L1 Expression as a Predictive Biomarker in Cancer Immunotherapy. *Mol Cancer Ther* 14(4), 847-856, 2015
108. Herbst RS, Soria JC, Kowanetz M et al. Predictive correlates of response to the anti-PD-L1 antibody MPDL3280A in cancer patients. *Nature* 515(7528), 563-567, 2014

109. Powles T, Eder JP, Fine GD et al. MPDL3280A (anti-PD-L1) treatment leads to clinical activity in metastatic bladder cancer. *Nature* 515(7528), 558-562, 2014
110. Kelderman S, Heemskerk B, Van Tinteren H et al. Lactate dehydrogenase as a selection criterion for ipilimumab treatment in metastatic melanoma. *Cancer immunology, immunotherapy* 63(5), 449-458, 2014
111. Brand A, Singer K, Koehl GE et al. LDHA-Associated Lactic Acid Production Blunts Tumor Immunosurveillance by T and NK Cells. *Cell metabolism* 24(5), 657-671, 2016
112. Ribas A, Hamid O, Daud A et al. Association of Pembrolizumab With Tumor Response and Survival Among Patients With Advanced Melanoma. *Jama* 315(15), 1600-1609, 2016
113. Fehrenbacher L, Spira A, Ballinger M et al. Atezolizumab versus docetaxel for patients with previously treated non-small-cell lung cancer (POPLAR): a multicentre, open-label, phase 2 randomised controlled trial. *Lancet* 387(10030), 1837-1846, 2016
114. Charoentong P, Finotello F, Angelova M et al. Pan-cancer Immunogenomic Analyses Reveal Genotype-Immunophenotype Relationships and Predictors of Response to Checkpoint Blockade. *Cell reports* 18(1), 248-262, 2017
115. Ji RR, Chasalow SD, Wang L et al. An immune-active tumor microenvironment favors clinical response to ipilimumab. *Cancer immunology, immunotherapy* 61(7), 1019-1031, 2012
116. Cha E, Klinger M, Hou Y et al. Improved survival with T cell clonotype stability after anti-CTLA-4 treatment in cancer patients. *Sci Transl Med* 6(238), 238ra270, 2014
117. Postow MA, Manuel M, Wong P et al. Peripheral T cell receptor diversity is associated with clinical outcomes following ipilimumab treatment in metastatic melanoma. *J Immunother Cancer* 3 23, 2015
118. Rozeman EA, Blank CU, Akkooi ACJV et al. Neoadjuvant ipilimumab + nivolumab (IPI+NIVO) in palpable stage III melanoma: Updated data from the OpACIN trial and first immunological analyses. *Journal of Clinical Oncology* 35(15_suppl), 9586-9586, 2017
119. Sivan A, Corrales L, Hubert N et al. Commensal Bifidobacterium promotes antitumor immunity and facilitates anti-PD-L1 efficacy. *Science* 350(6264), 1084-1089, 2015
120. Gopalakrishnan V, Spencer CN, Nezi L et al. Gut microbiome modulates response to anti-PD-1 immunotherapy in melanoma patients. *Science* doi:10.1126/science.aan4236 (2017).
121. Routy B, Le Chatelier E, Derosa L et al. Gut microbiome influences efficacy of PD-1-based immunotherapy against epithelial tumors. *Science* doi:10.1126/science.aan3706 (2017).



Chapter 7

Application of a risk-management framework for integration of stromal tumor-infiltrating lymphocytes in clinical trials

Jan Hudeček*, **Leonie Voorwerk***, Maartje van Seijen, Iris Nederlof, Michiel de Maaker, Jose van den Berg, Koen K. van de Vijver, Karolina Sikorska, Sylvia Adams, Sandra Demaria, Giuseppe Viale, Torsten O. Nielsen, Sunil S. Badve, Stefan Michiels, William Fraser Symmans, Christos Sotiriou, David L. Rimm, Stephen M. Hewitt, Carsten Denkert, Sibylle Loibl, Sherene Loi, John M.S. Bartlett, Giancarlo Pruneri, Deborah A. Dillon, Maggie C.U. Cheang, Andrew Tutt, Jacqueline A. Hall, Zuzana Kos, Roberto Salgado, Marleen Kok, Hugo M. Horlings and International Immuno-Oncology Biomarker Working Group[#]

*These authors contributed equally

[#]A full list of authors and affiliations of the Working Group appears in the online version of the manuscript.

Abstract

Stromal tumor-infiltrating lymphocytes (sTILs) are a potential predictive biomarker for immunotherapy response in metastatic triple-negative breast cancer (TNBC). To incorporate sTILs into clinical trials and diagnostics, reliable assessment is essential. In this review, we propose a new concept, namely the implementation of a risk-management framework that enables the use of sTILs as a stratification factor in clinical trials. We present the design of a biomarker risk-mitigation workflow that can be applied to any biomarker incorporation in clinical trials. We demonstrate the implementation of this concept using sTILs as an integral biomarker in a single-center phase II immunotherapy trial for metastatic TNBC (TONIC trial, NCT02499367), using this workflow to mitigate risks of suboptimal inclusion of sTILs in this specific trial. In this review, we demonstrate that a web-based scoring platform can mitigate potential risk factors when including sTILs in clinical trials, and we argue that this framework can be applied for any future biomarker-driven clinical trial setting.

Introduction

Clinical trials in cancer research are increasingly incorporating biomarkers, for example, as an inclusion criterion or for stratification of patients to control for confounding factors. Practical challenges, such as interobserver variation in the assessment of biomarkers during the execution of the trial, are often overlooked. If not handled appropriately, these challenges can limit the effectiveness and ability to complete the biomarker and drug development process. According to Hall et al.¹, the risks inherent to biomarker integration can be divided into risks to patients, operational risks, and direct risks to biomarker development. A practical risk-management framework developed by a National Cancer Institute (NCI), National Cancer Research Institute (NCRI), and European Organization for Research and Treatment of Cancer (EORTC) Working Group¹ was proposed to manage the risks inherent to biomarker integration into clinical trials.

Stromal tumor-infiltrating lymphocytes (sTILs) have been strongly associated with prognosis in early-stage triple-negative breast cancer (TNBC) and HER2-positive breast cancer. In addition, sTILs are predictive for neo-adjuvant chemotherapy response in early breast cancer^{2,3}. Furthermore, sTILs correlate with outcome after immune checkpoint blockade in metastatic TNBC⁴⁻⁶. The readout of sTILs, however, can be challenging impeding its effective use as a biomarker and its usage in the clinic⁷. The International Immuno-Oncology Biomarker Working Group (hereafter called the TIL Working Group) has provided guidelines for the scoring of sTILs in breast cancer⁸, and the St. Gallen Breast Cancer Conference of 2019 endorsed sTILs being routinely characterized in TNBC and reported according to these guidelines⁸.

Risks associated with integration of biomarkers in clinical trials

In contemporary clinical research there is an increasing trend toward the use of biomarker results obtained in daily practice to select patients for inclusion in clinical trials. Although biomarker research is more and more prominent in clinical trials, most biomarkers will not make into the clinic⁹. Therefore, continuous monitoring of the predefined risks and the solutions can improve the quality of the biomarker, which can be applied in a clinical trial setting, as well as in daily practice. The recommendations of the TIL Working Group^{8,10} for appropriate scoring, and the risk-management framework of the NCI, NCRI, and EORTC Working Groups¹ will help to effectively and efficiently improve the incorporation of biomarkers in clinical trials in first instance.

Several risks are associated with biomarker development and integration of biomarkers in clinical trials. Roughly, risks can be divided into three categories: risks to patient safety, operational risks, and risks to biomarker development. Not all risks are applicable to all clinical trials and upon designing a biomarker-incorporating clinical trial, risks should be defined and mitigation approaches formulated. It is highly recommended that during a clinical trial, risks are not

only pre-identified but are also continuously monitored to prevent stagnation in biomarker development¹. For example, incorporating biomarkers in a large multi-center international clinical trial involves different risks than a small single-center trial. In the first case, there might be different legislation regarding data confidentiality, and inter-laboratory variability can be an issue. When incorporating a biomarker as inclusion criterion or stratification factor in clinical trials, rapid turnaround times are needed and the highest level of quality is necessary for correct interpretation of the results. In the next steps of biomarker development, high-quality results are needed to ensure implementation in daily clinical practice.

Use of digital pathology in clinical trials and development of a novel web application

In larger trials, usually phase II-III, central pathology review (CPR) plays an important role in the reliable assessment of biomarker scoring. However, logistical issues, such as the sending of tumor blocks or slides, can be time consuming, costly for the pathology laboratory, and error prone with significant consequences for patient inclusion if the wrong material is sent to the central lab. Digital sharing of histology slides and patient data simplifies logistics for CPR¹¹. Besides digital sharing and scoring of slides, digital image analysis and machine learning approaches are emerging in clinical research^{12,13}. The use of digital pathology or digital evaluation of histology slides most prominently mitigates risks associated with operational processes. It can reduce the number of missing samples, since the sharing of material is simplified; it enables rapid turnaround times; reduces manual errors; and can streamline local versus central assessment of biomarker.

For clinicians and researchers to use digital pathology, applications and websites should be user-friendly and intuitive. As an example, a web-based tool called Slide Score (www.slidescore.com) was developed as a cross-platform web application to facilitate the scoring of whole slide images and tissue microarray (TMA) cores. Application programming interface (API) was implemented that allowed programmatic administration of studies, uploading slides, fetching results, and retrieving pixel data for regions of images. This API enabled automating creation of new studies from internal database system for managing biobanking workflows. Additionally, a plugin was developed for QuPath¹⁴ - open-source image analysis software - which uses this API to run image analysis algorithms on slides stored on the Slide Score platform avoiding the need to download the slides. This web-based platform was used in high-impact projects^{6,15}, for example, for the digital scoring of biomarkers in the first stage of the TONIC trial⁶, and the estimation of the immune infiltrate of tumors of melanoma patients used for single-cell sequencing¹⁵. Furthermore, the web-based platform is currently used for several other types of research, such as interrater variability studies, retrospective TMA, and whole slide scoring and prospective biomarker scoring.

Design of a workflow to mitigate risks associated with biomarker development: an example

We identified seven distinct risks with the risk-management framework published by Hall et al.¹ as possibly interfering with the quality and integration of prospective sTILs scores in a clinical trial, and designed our workflow accordingly (Table 1). These risks are specific for this trial, but some of them are applicable also to other trials. They span all three categories mentioned above¹ and included (1) poor-quality biopsies, (2) possible loss of data confidentiality, (3) interrater variability, (4) poor sample quality, (5) poor scoring quality, (6) delay in patient registration, and (7) manual errors (Table 1). We then defined solutions to mitigate these risks and integrated these solutions in a workflow that can be applied across clinical trials and across biomarkers (Figure 1). The workflow can be modified according to local guidelines, research questions, and clinical trial designs. We used the following workflow to obtain timely and reliable sTILs scores (summary in Supplementary Figure 1).

After obtaining informed consent of a patient, three biopsies of one metastatic lesion (lymph node, skin, liver, or other) were obtained in this trial. Previous research has shown that three 14 G core needle biopsies should be sufficient for accurate breast cancer diagnosis¹⁶. A hematoxylin and eosin (H&E)-stained slide of one biopsy was then evaluated, to ensure that the biopsy contained enough tumor cells (more than 100 cells) for further analysis (risk 1). Next, a high-resolution digital scan was obtained and automatically pseudonymized with study-specific identifiers (risk 2) before uploading to Slide Score. Display of the original labels was masked to ensure confidentiality of all data within Slide Score (Supplementary Figure 2b). Pathologists and administrators had to login with their username and password to access the slides and were able to add a two-factor authentication application. Four well-trained breast pathologists, based in three different institutes and in two different countries, were notified via email to score each slide using existing sTIL scoring guidelines of the TIL Working Group^{8,10} to reduce interrater variability (risk 3). sTILs are scored as the percentage of lymphocytes in the total stromal area (in close proximity of the tumor cells). Interrater variability can lead to bias in the results, when assessment of a biomarker is skewed towards either the lower or higher ranges. When there was a disagreement (using a 5% cut-off) a concordance-score was agreed upon (Supplementary Figure 1). Low-quality, inaccurate collection or processing of samples can result in low sample availability and introduce batch effects or bias in the results (risk 4) and lead to non-consistent scores (risk 5). High quality of samples was ensured by standardization of our workflow in which all steps were performed in the same manner for every biopsy (Supplementary Figure 1). Oversight of the entire workflow by one person, referred to as the central manager, is essential for timely identification of technical errors. The central manager tracked the timing of the biopsies, notified the pathologists immediately after the scan was uploaded and sent reminders if necessary, kept track of the scores and timing, and noted the score in the patient record for trial office notification. We predefined acceptable timeframes for obtaining the scores

of the reviewers and tracked these during the study progress (risk 6; Supplementary Figure 1). Pathologists were notified via email the next working day when the slide was not scored yet to minimize the waiting period to start treatment (risk 6). Finally, using Slide Score, we reduced the risks of typos and other manual errors by collecting all slides within one online study group (collection of slides) and a customized scoring form was built to standardize scores and obtain structured data (risk 7).

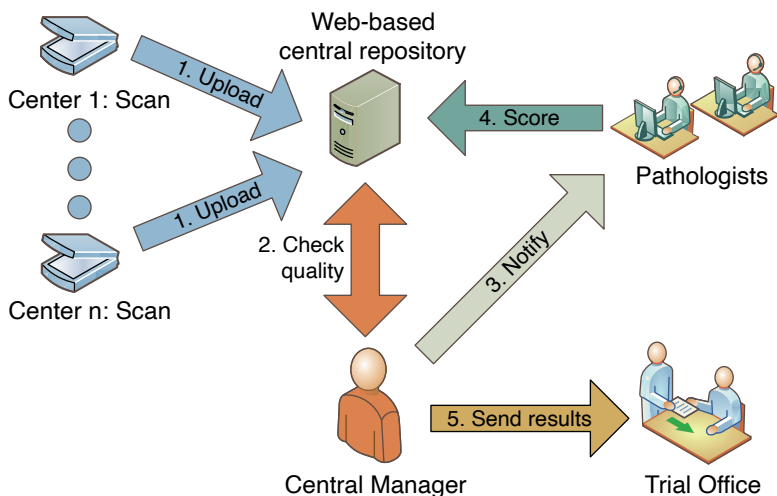


Figure 1: Organization of a workflow for reliable and timely biomarker scoring in a general single-center or multi-center trial. Personnel at individual centers scan the slides after processing by the local pathology department. Digital slides are uploaded to a central web-based repository, such as Slide Score. A study-specific identifier is assigned to each sample. The central manager is notified by the system when new slides are available and requests pathologists to review it. When a consensus score is obtained, the trial office is notified for randomization of the patient.

Implementation of workflow in the TONIC-trial

The TONIC trial (NCT02499367)⁶ is a phase II, non-comparative randomized multi-cohort single-center trial (full title: Adaptive phase II randomized non-comparative Trial Of Nivolumab after Induction treatment in TNBC patients), designed to assess the efficacy of induction of an anti-cancer immune response by low-dose chemotherapy or irradiation to increase response to anti-PD-1 in patients with metastatic TNBC. In the first part of the trial⁶, patients with metastatic TNBC were randomized to nivolumab (1) without induction or two-week low-dose induction, with (2) irradiation (3×8 Gy), (3) cyclophosphamide, (4) cisplatin, or (5) doxorubicin, all followed by nivolumab (anti-PD-1; 3 mg/kg). Based on a Simon's two-stage design¹⁷ and prespecified pick-the-winner criteria, only the doxorubicin cohort was allowed to continue in the second part of the trial⁶. In the second part of the TONIC trial, patients were randomized between anti-PD-1 monotherapy (control group) and two cycles of low-dose doxorubicin (15 mg flat

dose, weekly), followed by anti-PD-1 (Supplementary Figure 2a). Randomization was stratified for sTILs. Stratification is done by dividing patients in two categories, namely sTIL_{high} (equal or exceeding 5%) and sTIL_{low} (lower than 5%). The cut-off was determined based on data obtained in the first part of the TONIC trial, in which we observed that sTILs were predictive of response to anti-PD-1, both continuous and when a cut-off of 5% was used⁶. These data confirmed the predictive value of sTILs of at least 5% in another trial, which tested the efficacy of anti-PD-1 in patients with metastatic TNBC⁴. The full protocol, including four amendments, and the informed consent form were approved by the medical-ethical committee of The Netherlands Cancer Institute. All patients provided written informed consent before enrollment. The trial was registered on 17 August 2015. The 47 patients of the second part of the trial were randomized between March 2018 and July 2019. Full eligibility criteria and trial procedures have been described previously⁶.

In the second part of the TONIC trial, we could implement our workflow with a focus on accurate and reproducible sTIL scores within a reasonable timeframe after a biopsy was taken (72 h). For all 47 patients included in the trial, reliable sTIL scores were obtained with 45 biopsies scored within the 72-h timeframe (Supplementary Figure 3). During the course of the study, the server of Slide Score was available 99.9% of the time. Five biopsies had to be re-evaluated due to a discrepancy in the categorical scores, when not all pathologists agreed on the appropriate category of the sTIL score (lower than 5% versus higher or equal to 5%). In three of these cases the score of one pathologist was higher (5 or 10%) than the score of the other two or three pathologists (0-3%). The average sTIL score was obtained and the pathologist causing the disagreement was notified. In the fourth and fifth case, two pathologists scored 5 and 10%, whereas the other pathologists scored 1%. All four pathologists were notified of the disagreement and a consensus score of 5% was obtained. We observed an intraclass correlation coefficient of 0.94 (95% confidence interval (CI): 0.91-0.97) for sTILs as a continuous variable. Interrater agreement for the categorical variable used in the stratification (sTILs <5% or ≥5%) was 0.86 (multirater Fleiss' κ^{18} ; 95% CI: 0.73-1; Supplementary Figure 2c). In the anti-PD-1 monotherapy cohort, we observed that 13 out of 23 patients (56.5 %) had sTILs below 5%, as compared to 15 out of 24 patients in the doxorubicin cohort (62.5 %; Fisher's exact test p value 0.77). The distribution of the sTIL scores is depicted in Supplementary Figure 2d. These data indicate effective stratification based on the cut-off of 5%, but a slightly uneven distribution in the higher ranges of sTIL scores (10% or higher) inherent to the use of our cut-off. We observed a median time from biopsy until the scanning of the H&E slide of 30 h (range 24-98 h) and a median time from the biopsy until at least three scores were obtained of 43 h (range 27-106 h). In total, the median time from biopsy until registration in the patient records was 49 h (range 41-106 h; Supplementary Figure 2e), with 96% of biopsies scored within 72 h. Two biopsies were not scored within the 72-h time limit, due to additional processing of one sample and one delay in registration time due to the absence of the central manager (Supplementary Figures 1 and 3).

Table 1: Risks with possible high impact identified in a phase II immunotherapy trial⁶ based on the perspectives of Hall et al.¹ with our approach to mitigation of that risk.

Type of risk	Risk	Description of risk	Mitigation approach
1. Risks to patients	No stroma or tumor cells in biopsy	Discomfort and risks associated with a sampling intervention	Take multiple biopsies from one lesion at the same time (a minimum of three biopsies per lesion ⁹) and check amount of tumor cells before analysis of sTILs and inclusion in the trial
2. Risks to patients	Loss of data confidentiality	Patient samples sent to multiple institutions and reviewers	Pseudonymization should be applied, hide slide labels, implement strict access control, ensure no metadata is linked to a slide
3. Risks to biomarker development	Inter-laboratory variability and interobserver variability	Different methodologies used to score slides, interrater variability	Use of international guidelines for scoring and training, use consensus score of four expert pathologists from three institutes
4. Operational risks	Failure of sample collection, processing and quality	Missing or poor-quality samples resulting in poor consensus scoring	Standardized tissue processing, workflow management
5. Operational risks	Inadequate image quality or no ability to access image	Missing, poor or inaccurate scoring	Track the scores of all pathologists and notify when scores are inconsistent
6. Operational risks/risks to patients	Long turnaround time	Delay in patient randomization and treatment	Timeline tracking incorporated in workflow
7. Operational risks	Data management failure	Errors in collecting manual scores, typos, data conversion issues	Structured digital scores from pathologist to the analyst

Advantages and limitations of a web-based risk-mitigation workflow

Our proposed solutions involved standardization of our workflow, obtaining digital images and the use of a web-based tool such as Slide Score for the managing and scoring of digital images. Anticipating the incorporation of digital images in routine diagnostics, our workflow shows that it is feasible for a pathologist to score digital images with high reliability. Moreover, a web-based tool can facilitate the process of coordinated uploading of digital images, pseudonymizing slides, and regulate access to studies and proper data management. Web-based platforms are therefore of high interest in biomarker research and can help with automation that can be transferred to clinical practice in the future.

In this study, we obtained sTIL scores within 72 h after a biopsy was taken, which is a reasonable timeframe for clinicians to start randomization of patients to treatment arms in a clinical trial. We observed an excellent interrater agreement score between our panel of four expert pathologists. In an accompanying paper⁷ we demonstrate using data from three RING studies of the TIL Working Group that the concordance achieved using a risk-management approach as detailed in this study is substantially higher than observed outside this risk-management perspective as observed in the three RING studies and in other published studies^{19,20}. However, our sample size is small and the four pathologists in the current study were trained and experienced in the scoring of sTILs in breast cancer. Also, the biopsies used in this study were checked for containing sufficient tumor cells (≥ 100 cells) before the slide was scored for sTILs, which could have further improved our results. In the future, it is to be expected that computational workflows will further improve the scoring of sTILs¹³. Although we obtained reliable and timely results in 96% of cases, the presence of a central manager is crucial. In one case there was a delay in registration time due to the absence of the central manager. The manual intervention of quality checks, processing of the slides, and data cannot be circumvented in our workflow.

Stratification in this study was performed using sTILs as a binary variable (lower than 5% versus higher or equal to 5%). Consequently, we observed an uneven distribution in continuous sTILs scores between the cohorts (Supplementary Figure 2d). This was mainly due to more patients with sTILs scores above 10% in the anti-PD-1 monotherapy cohort. Inherent to the use of a binary cut-off for stratification, the median of the continuous measurement might still differ between cohorts. Alternatively, multiple categories for the same variable can be used in stratification. However, this approach generates more strata, with lower number of patients in each stratum, possibly leading to an imbalance in distribution^{21,22}. Moreover, at the time of writing of this paper no cut-offs for sTILs are established and/or properly validated for predictive purposes.

During the trial, we continuously monitored whether our strategy was still feasible within the set timeframe by means of regular evaluation by the pathologists and the study coordinators. This led to rapid adjustment of the workflow if needed,

ensuring the quality of the sTIL scores. For example, pathologists could easily login remotely and score a digital H&E outside the hospital ensuring that sTILs were still scored within 72 h after biopsy. Ongoing evaluation during the clinical trial is of critical importance for risk mitigation in biomarker research¹.

Future applications of the workflow

Our strategy can serve as a template for risk management and mitigation of all identified risks in future clinical trials incorporating biomarkers for inclusion, enrichment, or stratification. By no means will risks identified in this study be similar for all clinical trials. Each trial will have its own risks that need to be mitigated, although there will be similarities between the risks across clinical trials. Defining the risks that come with biomarker development will help tested biomarkers eventually make their way to the clinic. However, one may even argue that a similar risk-management strategy can be applied in daily practice. In the BELLINI trial (NCT03815890), two cycles of neo-adjuvant anti-PD-1 are administered in patients with early-stage TNBC or luminal B breast cancer. All patients are required to have at least 5% sTILs in the pretreatment biopsy and patients are thereafter stratified in three sTIL categories. Our workflow will be used to ensure timely and reliable sTIL scores for the right patient selection. By using our workflow, scoring of sTILs is highly standardized, allowing also smaller centers with less extensive experience in sTILs scoring to participate in a clinical trial.

Conclusions

In contemporary clinical research there is an increasing trend toward the use of biomarker results obtained in daily practice to select patients for inclusion in clinical trials. Therefore, continuous monitoring of the predefined risks and the solutions can improve the quality of the biomarker, as can be applied in a clinical trial setting, as well as in daily practice. The recommendations of the TIL Working Group^{8,10} for appropriate scoring, the risk-management framework of the NCI, NCRI, and EORTC Working Groups¹, as well as our proposed strategies to reduce risks will help to effectively and efficiently improve the incorporation of biomarkers in clinical trials in first instance, herewith illustrated using sTILs as a paradigm of this development.

Data availability

The data that support the findings of this study are available from the corresponding author upon reasonable request.

Acknowledgements

The department of Pathology of the Netherlands Cancer Institute is thanked for the support of this study and ensuring the rapid turnaround times. The Breast Cancer Research Foundation and Bristol-Myers-Squibb (BMS) are thanked for financial support. We thank the BMS-International Immuno-Oncology Network (BMS/II-ON) and the Dutch Cancer Society (NKI2015-7710) for funding the clinical trial costs and this feasibility study (NKI2016-10510). S.L., R.S. and M.K. are supported by a grant from the Breast Cancer Research Foundation (BCRF, NY, US).

Author contributions

J.H. developed Slide Score and wrote the manuscript with L.V., R.S., M.K. and H.M.H. L.V. coordinated study procedures and performed data-analyses. M.v.S., I.N., S.A., S.D., G.V., T.O.N., S.S.B., S.M., W.F.S., C.S., D.L.R., S.H., C.D., S.L., Sh.L., J.M.S.B., G.P., D.A.D., M.C., U.C., A.T., J.A.H. and Z.K. gave critical input. M.d.M. provided logistical support with the sample processing. J.v.d.B., K.K.v.d.V., R.S. and H.M.H. scored the slides. K.S. performed the statistical analysis. M.K. is the principal investigator of the TONIC trial. J.H., L.V., R.S., M.K. and H.M.H. designed this feasibility study. All authors edited and approved the manuscript.

Competing interests

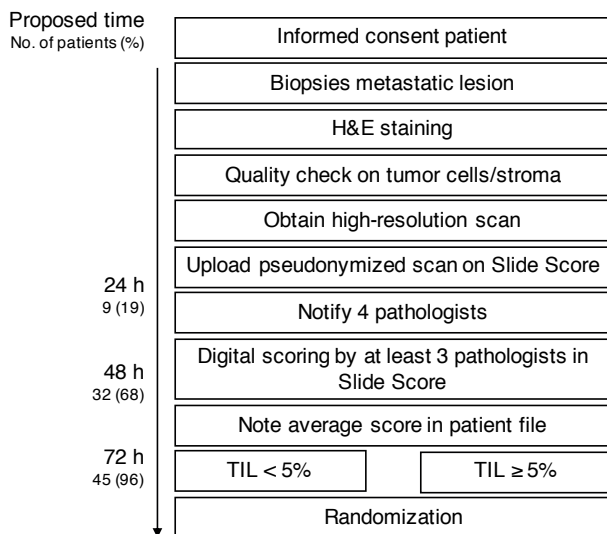
J.H. is the owner of Slide Score. B.V. L.V., M.v.S., I.N., M.d.M., J.v.d.B., K.K.v.d.V., K.S., S.A., S.D., G.V., S.S.B., S.M., W.F.S., C.S., S.M.H., C.D., S.L., G.P., M.C.U.C., Z.K., and H.M.H. have nothing to disclose. T.O.N. has consulted for Nanostring and received compensation and has intellectual property rights/ownership interests from Bioclassifier LLC, not related to the subject material under consideration and received funding support from the Canadian Cancer Society. D.L.R. reports research funding from AstraZeneca, Cepheid, Navigate BioPharma, NextCure, Lilly, and Ultivue; instrument support from Ventana, Akoya/PerkinElmer, and NanoString; advisory board of Amgen, AstraZeneca, Cell Signaling Technology, Cepheid, Daiichi Sankyo, GSK, Konica/Minolta, Merck, NanoString, PerkinElmer, Ventana, and Ultivue; consultancy for Biocept; honorarium and travel support from BMS; royalties from Rarecyte and is a founder and equity holder of PixelGear. Sh.L. receives research funding to her institution from Novartis, Bristol Meyers Squibb, Merck, Roche-Genentech, Puma Biotechnology, Pfizer, and Eli Lilly, acted as consultant (not compensated) to Seattle Genetics, Pfizer, Novartis, BMS, Merck, AstraZeneca, and Roche-Genentech and acted as consultant (paid to her institution) to Aduro Biotech. J.M.S.B. reports research funding from ThermoFisher, Genoptix, Agendia, NanoString Technologies, Stratifyer GmbH, and Biotheranostics and advisory roles for Insight Genetics, BioNTech AG, Biotheranostics, Pfizer, RNA Diagnostics, and OncoXchange. J.M.S.B. reports the following patents: Methods and Devices for Predicting Anthracycline Treatment Efficacy, US utility (January

2017; 15/ 325,472; EPO - 15822898.1; Canada - not yet assigned), Systems, Devices and Methods for Constructing and Using a Biomarker, US utility (January 2017; 15/ 328,108; EPO - 15824751.0; Canada - not yet assigned), Histone gene module predicts anthracycline benefit (October 2016; PCT/CA2016/000247), 95-Gene Signature of Residual Risk Following Endocrine Treatment (December 2016; PCT/ CA2016/000304), Immune Gene Signature Predicts Anthracycline Benefit (December 2016; PCT/CA2016/000305). D.A.D. is on the advisory board and consults for Oncology Analytics Inc., and has consulted for and received travel funds from Novartis for work unrelated to the current manuscript. A.T. reports benefits from ICR's Inventors Scheme associated with patents for one of PARP inhibitors in BRCA1/2- associated cancers. A.T. also reports Honoraria from Pfizer, Vertex, Prime Oncology, and Artios, honoraria and stock in InBioMotion, honoraria and financial support for research from AstraZeneca, Medivation, Myriad Genetics, and Merck Serono. J.A.H. is the director and owner of Vivactiv Ltd. R.S. reports research funding from Roche, Puma, and Merck; advisory board and consultancy for BMS; travel funding from Roche, Merck, and AstraZeneca, outside the scope of this work. M.K. reports funding to the institute from BMS, Roche and an advisory role for BMS, outside the submitted work.

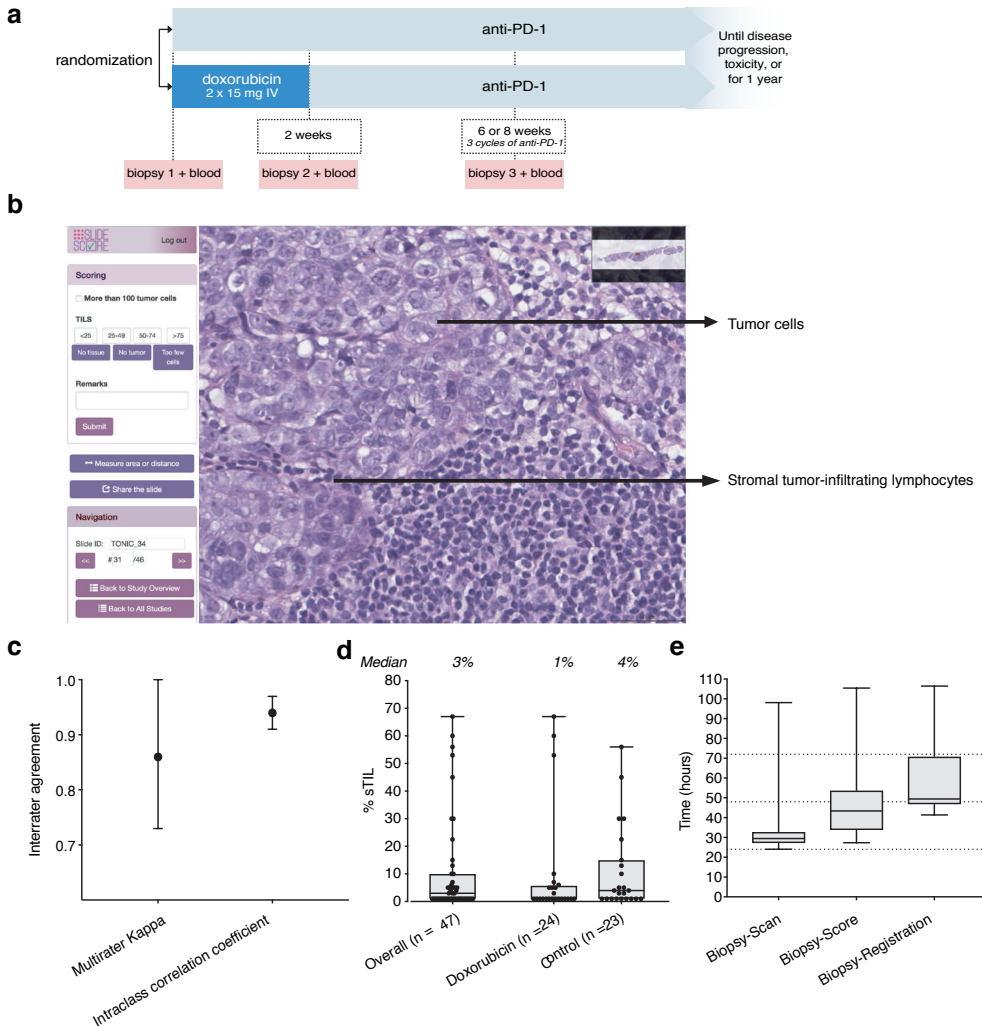
References

1. Hall, J. A., Salgado, R., Lively, T., Sweep, F. & Schuh, A. A risk-management approach for effective integration of biomarkers in clinical trials: perspectives of an NCI, NCRI, and EORTC working group. *The Lancet Oncology* 15, e184-193, 2014
2. Loi, S. et al. Tumor-Infiltrating Lymphocytes and Prognosis: A Pooled Individual Patient Analysis of Early-Stage Triple-Negative Breast Cancers. *Journal of Clinical Oncology* 37, 559-569, 2019
3. Denkert, C. et al. Tumour-infiltrating lymphocytes and prognosis in different subtypes of breast cancer: a pooled analysis of 3771 patients treated with neoadjuvant therapy. *The Lancet Oncology* 19, 40-50, 2018
4. Loi, S. et al. LBA13 - Relationship between tumor infiltrating lymphocyte (TIL) levels and response to pembrolizumab (pembro) in metastatic triple-negative breast cancer (mTNBC): Results from KEYNOTE-086. *Annals of Oncology* 28(Suppl_5), v605-49, 2017
5. Emens, L. A. et al. Long-term Clinical Outcomes and Biomarker Analyses of Atezolizumab Therapy for Patients With Metastatic Triple-Negative Breast Cancer: A Phase 1 Study. *JAMA Oncology*, 2018.4224, 2018
6. Voorwerk, L. et al. Immune induction strategies in metastatic triple-negative breast cancer to enhance the sensitivity to PD-1 blockade: the TONIC trial. *Nat Med* 25 (6), 920-928, 2019.
7. Kos, Z. et al. Pitfalls in Assessing Stromal Tumour Infiltrating Lymphocytes (sTILs) in Breast Cancer: How to Avoid Them and Clinical Implications if You Don't. A report from the International Immunology Biomarker Group. *npj Breast Cancer*, 2020
8. Salgado, R. et al. The evaluation of tumor-infiltrating lymphocytes (TILs) in breast cancer: recommendations by an International TILs Working Group 2014. *Annals of Oncology* 26, 259-271, 2015
9. Hayes, D. F. et al. Breaking a vicious cycle. *Science Translational Medicine* 5, 196cm196, 2013
10. Hendry, S. et al. Assessing Tumor-infiltrating Lymphocytes in Solid Tumors: A Practical Review for Pathologists and Proposal for a Standardized Method From the International Immunooncology Biomarkers Working Group: Part 1: Assessing the Host Immune Response, TILs in Invasive Breast Carcinoma and Ductal Carcinoma In Situ, Metastatic Tumor Deposits and Areas for Further Research. *Advances in anatomic pathology* 24, 235-251, 2017
11. Mroz, P., Parwani, A. V. & Kulesza, P. Central pathology review for phase III clinical trials: the enabling effect of virtual microscopy. *Archives of Pathology & Laboratory Medicine* 137, 492-495, 2013
12. Pell, R. et al. The use of digital pathology and image analysis in clinical trials. *Journal of Pathology: Clinical Research* 5, 81-90, 2019
13. Amgad, M. et al. Key issues in computational assessment of Tumor Infiltrating Lymphocytes in solid tumors. A report from the International Immunology Biomarker Working group. *npj Breast Cancer*, 2020
14. Bankhead, P. et al. QuPath: Open source software for digital pathology image analysis. *Scientific Reports* 7, 16878, 2017
15. Li, H. et al. Dysfunctional CD8 T Cells Form a Proliferative, Dynamically Regulated Compartment within Human Melanoma. *Cell* 176, 775-789.e718, 2019
16. Sauer, G. et al. Ultrasound-guided large-core needle biopsies of breast lesions: analysis of 962 cases to determine the number of samples for reliable tumour classification. *British Journal of Cancer* 92, 231-235, 2005
17. Simon, R. Optimal two-stage designs for phase II clinical trials. *Controlled Clinical Trials* 10, 1-10, 1989
18. Fleiss, J. L. *Statistical methods for rates and proportions*. Second edition, 1981
19. Tramm, T. et al. Standardized assessment of tumor-infiltrating lymphocytes in breast cancer: an evaluation of inter-observer agreement between pathologists. *Acta Oncologica* 57, 90-94, 2018
20. Dieci, V. et al. Association of tumor-infiltrating lymphocytes with distant disease-free survival in the ShorthER randomized adjuvant trial for patients with early HER2+ breast cancer. *Annals of Oncology* 30, 418-423, 2019
21. Therneau, T. M. How many stratification factors are "too many" to use in a randomization plan? *Controlled Clinical Trials* 14, 98-108, 1993
22. Silcocks, P. How many strata in an RCT? A flexible approach. *British Journal of Cancer* 106, 1259-1261, 2012

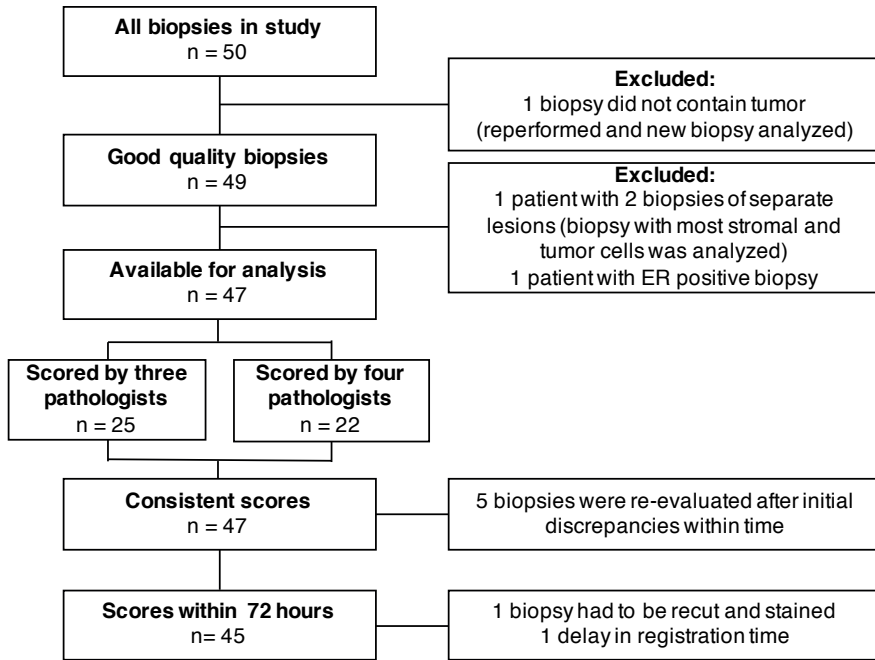
Supplemental material



Supplementary Figure 1: Workflow for risk mitigation for the use of sTILs as a stratification factor in the TONIC-trial. Every block represents one step in the workflow. On the left side of the workflow, the proposed timeline is depicted. Numbers below the timestamps reflect the number of patients and percentage of total patients that finalized the step within the proposed time.



Supplementary Figure 2: Implementation of the workflow in the second part of the TONIC-trial⁶. (a) Setup of part 2 of the adaptive phase II TONIC-trial⁶. Patients are randomized between anti-PD-1 monotherapy (control cohort) or start with two cycles of low-dose doxorubicin followed by anti-PD-1. Before the start of treatment biopsies are taken. (b) User interface of Slide Score. A customized sTILs scoring form is depicted in the image. Users can zoom in on the whole image with high resolution. A representative lymph node biopsy is displayed. (c) Interrater agreement sTILs. The intraclass correlation coefficient (ICC) is calculated over continuous sTILs of all raters. Fleiss' Kappa is calculated over categorical sTILs (5% or higher versus lower than 5%) of all raters. Error bars represent the 95% confidence intervals. (d) Distribution of sTILs over all patients and per cohort. The final sTILs scores that are used for stratification are depicted (average of three or four pathologists). Every dot represents one score, boxplots represent the median with 25-75% percentile, error bars represent the range. (e) Turnaround time sTILs. Depicted is the time in hours that it takes from the biopsy to the scan, the biopsy to the final score of the panel of pathologists and the biopsy to the registration of sTILs in the patient records (availability of scores). Boxplots represent the median with 25-75% percentile, error bars represent the range.



Supplementary Figure 3: Diagram of biopsies and sTILs scores available for stratification in the TONIC-trial.



Chapter 8

Immune landscape of breast tumors
with low and intermediate estrogen
receptor expression

Leonie Voorwerk, Joyce Sanders, Milou S. Keusters, Sara Balduzzi, Sten Cornelissen, Maxime Duijst, Esther H. Lips, Gabe S. Sonke, Sabine C. Linn, Hugo M. Horlings, Marleen Kok

In revision, npj Breast Cancer

Abstract

Immune checkpoint blockade (ICB) is currently approved for patients with triple-negative breast cancer (TNBC), whereas responses to ICB are also observed in a small subgroup of Estrogen Receptor (ER)-positive breast cancer. The cut-off for ER-positivity ($\geq 1\%$) is based on likelihood of endocrine treatment response, but ER-positive breast cancer represents a very heterogeneous group. This raises the question whether selection based on ER-negativity should be revisited to select patients for ICB treatment in the context of clinical trials. Stromal tumor-infiltrating lymphocytes (sTILs) and other immune parameters are higher in TNBC compared to ER-positive breast cancer, but it is unknown whether lower ER levels are associated with more inflamed tumor microenvironments (TME). We collected a consecutive series of primary tumors from 173 HER2-negative breast cancer patients, enriched for tumors with ER expression between 1 and 99% and found levels of stromal TILs, CD8+ T cells, and PD-L1 positivity in breast tumors with ER 1-9% and ER 10-50% to be comparable to tumors with ER 0%. Expression of immune-related gene signatures in tumors with ER 1-9% and ER 10-50% was comparable to ER 0%, and higher than in tumors with ER 51-99% and ER 100%. Our results suggest that the immune landscape of ER low tumors (1-9%) and ER intermediate tumors (10-50%) mimic that of primary TNBC.

Introduction

Estrogen receptor (ER) expression assessment is one of the cornerstones in the diagnostic work-up for breast cancer and is an essential biomarker for prediction of endocrine treatment efficacy^{1,2}. Current ASCO/CAP recommendations define ER-positive tumors as having $\geq 1\%$ ER expression and tumors with ER expression between 1 and 10% as ER low-positive tumors². This cut-off is based on studies that reported lack of responses to endocrine treatment in tumors with no ER expression^{3,4}, but a pragmatic cut-off of 10% is sometimes used in clinical trials⁵⁻⁸ and in daily practice⁹. Although the cut-off was originally meant for endocrine treatment response, it is also being used for selecting breast cancer for novel treatments such as immune checkpoint blockade (ICB). Approximately 2-5% of HER2-negative patients have breast cancer with low-positive ER (1-9%) expression¹⁰⁻¹². Recently, several studies demonstrated that patients with ER low-positive HER2-negative breast cancer have similar outcomes as compared to triple-negative breast cancer (TNBC) patients¹⁰⁻¹⁴. ER low-positive breast tumors have comparable progesterone receptor (PR) levels^{12,15}, tumor grade^{10-13,16} and Ki-67 expression^{11,13,16} to TNBC and are usually classified as basal-like or HER2-enriched^{11,15,17}. Intermediate ER expression of 10-50% is common in approximately 5-10% of breast tumors^{18,19} and we hypothesize that this group might share basal-like features with TNBC similar to the ER low-positive group.

In general, as compared to ER-positive tumors, ER-negative tumors have a more inflamed tumor microenvironment (TME), characterized by prominent stromal tumor-infiltrating lymphocyte (sTIL) infiltration²⁰, CD8+ T-cells²¹ and higher expression of immune-related gene sets²². sTILs and CD8+ T cells are positively associated with prognosis and chemotherapy efficacy in early-stage TNBC^{20,21,23-26}, while in ER-positive breast cancer the role of immune cell infiltration is less clear^{20,27,28}. Responses to ICB are also more prominent in patients with TNBC²⁹. Neo-adjuvant ICB plus chemotherapy is currently approved for early-stage TNBC³⁰ and promising results have been observed in high-risk ER-positive breast cancer^{8,31,32}. Exploratory biomarker studies from these and other trials demonstrated that expression of immune-related genes are associated with response³³ or survival³⁴ to neo-adjuvant ICB in early-stage TNBC, while sTILs and PD-L1 expression mainly have predictive value in the metastatic setting^{35,36}. It is currently not known whether breast tumors with low-positive (1-9%) or intermediate-positive (10-50%) ER expression are comparable to TNBC in terms of immune characteristics that are relevant for ICB response and whether these patients are therefore more likely to respond to ICB.

In this study, we aim to explore immunological characteristics of HER2-negative breast tumors with low-positive (1-9%) or intermediate-positive (10-50%) ER expression, as compared to TNBC and tumors with high ER expression (>50%). Using a consecutive series of tumor blocks, enriched for tumors with ER expression between 1 and 99%, we investigated clinicopathological characteristics and features of the TME that have previously been associated with response to ICB in breast cancer.

Results

Clinicopathological characteristics in relation to ER expression levels

A series of tumor blocks from 173 HER2-negative patients was collected, enriched for ER expression between 1-9%, 10-50% and 51-99%. All patients diagnosed in the Netherlands Cancer Institute between 2011 and 2019 with HER2-negative primary breast cancer with ER expression between 1 and 50% and for whom tumor material was available were identified, of which 17 patients had tumors with ER1-9% (low-positive) and 22 patients with ER10-50% (intermediate-positive; Supplementary Figure 1). Subsequently, a consecutive series of tumors with ER0% (negative; n=46), ER51-99% (high; n=37) and ER100% (ultrahigh; n=51) within these diagnosis years were collected, aiming for balanced group sizes. For each patient, an in-house tumor block of a pre-treatment biopsy (in case of neo-adjuvant treatment) or resection was collected. We observed slight differences in tumor size and nodal stage between the groups, with the highest proportion of small tumors within the ER100% group and the highest proportion of lymph node-negative tumors in the group with ER1-9% (Table 1). Four patients had a germline *BRCA1* mutation within the ER0% group and three patients had a germline *BRCA2* mutation within the ER100% group. As expected, ER expression highly correlated with PR expression and negatively correlated with tumor grade and Ki67 levels (Table 1, Supplementary Figure 2A-C). In the groups with low-positive and intermediate-positive ER expression we observed a lower proportion of grade 3 tumors and lower Ki-67 expression levels as compared to ER-negative tumors, but a higher proportion of grade 3 tumors as compared to the groups with high ER expression (>50%; Supplementary Figure 2B-C).

sTILs, CD8+ T cells and PD-L1 expression of tumors with low-positive and intermediate-positive ER expression

First, we assessed immune cell composition by investigating sTILs, stromal CD8+ T-cells and PD-L1 expression (assay 22C3, combined positive score). We observed highest levels of sTILs and continuous PD-L1 expression in the ER0% and ER10-50% groups, followed by the ER1-9% group (Figure 1A-B). Median CD8+ T-cell levels were equal in the groups with ER0%, ER1-9% and ER10-50%, and higher as compared to the groups with ER51-99% and ER100% (Figure 1C). Next, we assessed the proportion of PD-L1 positive tumors in the different groups using a cut-off of $\geq 1\%$ and $\geq 10\%$. We observed that 86%, 82% and 77% of patients with ER0%, ER1-9% and ER10-50%, respectively, had PD-L1 positive tumors using a 1% cut-off, whereas this was only 68% and 52% for the groups with ER51-99% and ER100% (Figure 1D). The same patterns were observed using the higher PD-L1 cut-off of 10%, with approximately 40-50% of tumors within the ER0%, ER1-9% and ER10-50% groups and only 11% and 10% with ER51-99% and ER100%, respectively, being PD-L1 positive (Figure 1D). Investigating sTILs, CD8+ T-cell levels and PD-L1 expression in relation to age and menopausal status, we observed slightly higher sTIL levels in younger patients (Supplementary Figure 3A-F). Higher PD-L1 expression and only slightly higher sTILs and CD8+ T-cell levels were seen in grade 3 tumors or tumors with high Ki-67 expression (Supplementary Figure 3G-L), suggesting that these features are

mainly associated with ER expression and may play a less dominant role in immune cell composition. Altogether, these data demonstrate that breast tumors with low-positive (1-9%) and intermediate-positive (10-50%) ER expression are comparable to ER-negative tumors in terms of sTILs, CD8+ T cells and PD-L1 expression.

Table 1. Patient characteristics. Difference between groups was tested by Fisher's exact test with excluded missing values. The median difference between age was tested by Kruskal-Wallis. Not applicable (NA), germline *BRCA* (g*BRCA*)

N = 173 No. of patients (%)		ER 0% (n=46)	ER 1-9% (n=17)	ER 10-50% (n=22)	ER 51-99% (n=37)	ER 100% (n=51)	P-value
Age	Median (range)	55 (26-79)	64 (35-89)	56 (38-84)	54 (28-82)	59 (31-80)	0.26
	≤50	21 (46)	7 (41)	8 (36)	18 (49)	19 (37)	0.80
	>50	25 (54)	10 (59)	14 (64)	19 (51)	32 (63)	
	≤60	29 (63)	7 (41)	12 (55)	27 (73)	29 (57)	0.22
	>60	17 (37)	10 (59)	10 (45)	10 (27)	22 (43)	
Menopausal status	Pre/peri	18 (39)	5 (29)	6 (27)	17 (46)	17 (33)	0.60
	Post	27 (59)	10 (59)	11 (50)	15 (41)	29 (57)	
	Unknown/NA	1 (2)	2 (12)	5 (23)	5 (14)	5 (10)	
Tumor stage	T1	17 (37)	11 (65)	15 (68)	20 (54)	38 (75)	0.01
	T2	24 (52)	6 (35)	5 (23)	15 (41)	12 (24)	
	T3	5 (11)	0 (0)	2 (9)	2 (5)	1 (2)	
Nodal stage	N0	36 (78)	15 (88)	15 (68)	22 (59)	39 (76)	0.09
	N1	7 (15)	2 (12)	3 (14)	13 (35)	11 (22)	
	N2-N3	3 (6)	0 (0)	4 (18)	2 (5)	1 (2)	
gBRCA mutation	<i>BRCA1</i>	4 (9)	0 (0)	1 (5)	0 (0)	0 (0)	0.07
	<i>BRCA2</i>	0 (0)	0 (0)	0 (0)	0 (0)	3 (6)	
	No mutation	29 (63)	10 (59)	10 (45)	14 (38)	13 (25)	
	Unknown	13 (28)	7 (41)	11 (50)	23 (62)	35 (69)	
PR expression	PR 0%	39 (85)	10 (59)	7 (32)	6 (16)	9 (18)	<0.0001
	PR1-9%	7 (15)	7 (41)	4 (18)	3 (8)	5 (10)	
	PR ≥ 10%	0 (0)	0 (0)	11 (50)	28 (76)	37 (73)	
Tumor grade	Grade 1	0 (0)	2 (12)	2 (9)	9 (24)	13 (25)	<0.0001
	Grade 2	2 (4)	4 (24)	11 (50)	22 (59)	31 (61)	
	Grade 3	44 (96)	9 (53)	7 (32)	6 (16)	7 (14)	
	Unknown	0 (0)	2 (9)	2 (9)	0 (0)	0 (0)	
Ki-67 expression	Ki-67 <20%	4 (9)	7 (41)	11 (50)	27 (73)	37 (73)	<0.0001
	Ki-67 ≥ 20%	42 (91)	10 (59)	11 (50)	10 (27)	14 (27)	

Intrinsic molecular subtypes of tumors with low-positive or intermediate-positive ER expression

As a basal-like molecular subtype has been described as possibly predictive of ICB response^{8,37}, we assessed PAM50 subtypes (NanoString)^{38,39}. We observed basal-like tumors in the groups with ER expression of 0% (91% of total), 1-9% (54% of total) and 10-50% (12% of total), but not in the groups with higher ER expression (Figure 1E). In the low-positive and intermediate-positive ER groups, 31% and 59% of tumors, respectively, were classified as luminal A or B, as compared to 97% in the ER-high and 100% in the ER-ultrahigh groups, underlining the heterogeneous nature of the groups with ER expression between 1-50% (Figure 1E). Next, we assessed the TNBC subtypes by Burstein *et al.*⁴⁰ in the ER0%, ER1-9% and ER10-50% groups, as a basal-like immune-activated (BLIA) phenotype has been associated with response

to ICB as well³⁷. In our dataset, tumors with a BLIA phenotype were restricted to ER expression of 50% or lower. Interestingly, 15% and 12% of tumors with ER1-9% and ER10-50% expression, respectively, were classified as BLIA, as compared to 42% of tumors with ER0% (Figure 1F). PD-L1 expression was highest in the BLIA tumors (Supplementary Figure 3M). These findings demonstrate that within the breast cancer groups with low-positive or intermediate-positive ER expression, a subset of tumors is inflamed and exhibits molecular features of TNBC.

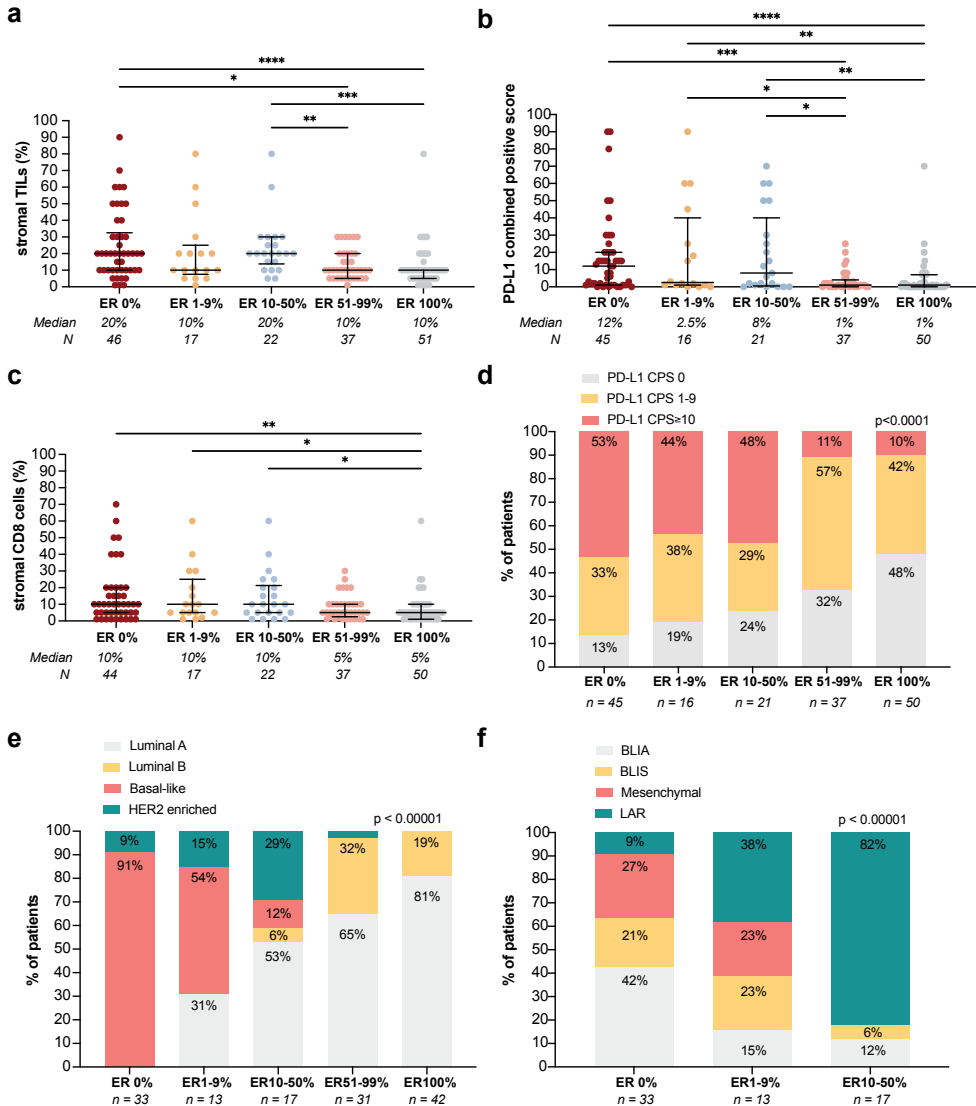


Figure 1: Immune cell composition in relation to estrogen receptor (ER) expression levels.

Figure 1: (opposite) Immune cell composition in relation to estrogen receptor (ER) expression levels. (a) Levels of stromal tumor infiltrating lymphocytes (sTILs) in relation to ER expression. Median with interquartile range, statistics by Kruskal-Wallis with post-hoc Dunn's test. Only statistically significant comparisons are shown. * $p < 0.05$, ** $p < 0.01$, *** $p < 0.001$, **** $p < 0.0001$. (b) PD-L1 expression (clone 22C3), assessed as combined positive score (CPS) in relation to ER expression. Statistics as in (a). PD-L1 staining was unavailable for 5 patients. (c) Levels of stromal CD8+ T cells (percentage of CD8+ T cells of the stromal area) in relation to ER expression. Statistics as in (a). CD8 staining was unavailable for 3 patients. (d) Proportion of patients with PD-L1 positive tumors (CPS) using different cut-offs (0%, 1-9%, $\geq 10\%$) in relation to ER expression. Numbers display percentage per group, statistics by Fisher's exact test. (e) Proportion of patients with luminal A, luminal B, basal-like and HER2 enriched tumors in relation to ER expression. Molecular subtypes were assessed according to PAM50 with the NanoString nCounter® Breast Cancer 360™ panel. Statistics as in (d). (f) Proportion of patients with basal-like immune activated (BLIA), basal-like immune-suppressed (BLIS), mesenchymal or luminal androgen receptor (LAR) tumors in relation to ER expression. TNBC subtypes were assessed with the NanoString nCounter® Breast Cancer 360™ panel. Statistics as in (d).

Higher expression of immune-related genes in ER-negative, low-positive, and intermediate-positive tumors, as compared to ER high-positive tumors

To gain more insight in the immune biology of tumors with low-positive or intermediate-positive ER expression, we next analyzed expression of immune signatures using the NanoString nCounter® Breast Cancer 360™ panel. Within each ER subgroup there was a wide range of expression of all immune signatures, but in general immune signatures were most highly expressed in ER0%, ER1-9% and ER10-50% (Figure 2A). Zooming in on the signatures that were significantly different between groups, we observed highest median levels of the CD8+ T cell signature, *PD1* mRNA expression and regulatory T-cell (T_{reg}) signature in the group with ER10-50%. These levels were not significantly different from the groups with ER1-9% and ER0%, but significantly higher as compared to the ER51-99% and/or ER100% groups (Figure 2B-D). Median expression levels of signatures reflecting antigen presenting machinery (APM), $IFN-\gamma$ signature, inflammatory chemokines and tumor-inflammation score (TIS) were all highest in breast tumors with no ER expression, not significantly different from the groups with low- or intermediate-positive ER expression and statistically significantly higher when comparing to the ER51-99% or ER100% groups (Figure 2E-H). Mast cells were the only immune cells that were more abundantly present in the TME of ER-positive tumors, increasing with ER expression (Figure 2A,I). Using pre-treatment gene expression data from an independent validation cohort of stage I-III breast cancer patients treated with neo-adjuvant chemotherapy⁴¹, we also observed higher levels of the CD8+ T-cell signature and $IFN-\gamma$ signature in breast tumors with 0%, 1-9% and 10-50% ER expression, as compared to tumors with ER expression $> 50\%$ (Supplementary Figure 4A-D). Additionally, also in this cohort we observed higher expression of mast-cell related genes in ER-positive tumors, as compared to ER-negative or ER low-positive tumors (Supplementary Figure 4E-F).

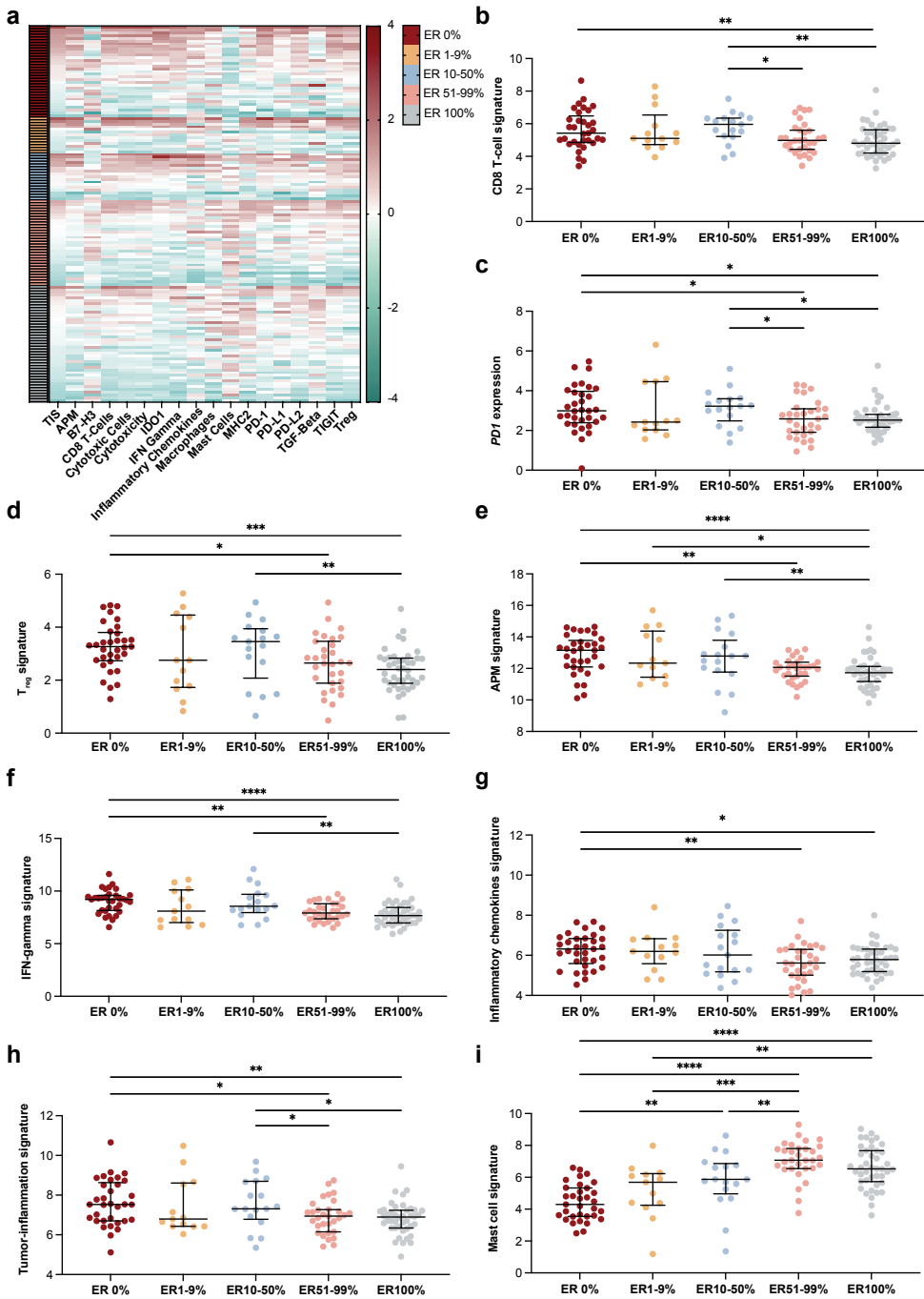


Figure 2: Expression of immune signatures in relation to estrogen receptor (ER) expression levels. (a) Heatmap of expression of immune signatures (z-scores), grouped by ER expression and sorted by tumor-inflammation signature (TIS)⁶⁴ per group. **(b)** CD8+ T-cell signature expression in relation to ER expression. Genes included: *CD8A*, *CD8B*. **(c)** *PD1* expression in relation to ER. **(d)** Regulatory T-cell (T_{reg}) signature in relation to ER expression. Genes included:

FOXP3. (e) Antigen presenting machinery (APM) signature expression in relation to ER. Genes included: *TAP1*, *TAP2*, *TAPBP*, *HLA-A*, *HLA-B*, *HLA-C*. (f) Interferon (IFN)- γ signature expression in relation to ER expression. Genes included: *CXCL9*, *CXCL10*, *STAT1*. (g) Inflammatory chemokine signature expression in relation to ER expression. Genes included: *CCL2*, *CCL3L1*, *CCL4*, *CCL7*, *CCL8*. (h) TIS in relation to ER expression. Genes included: *CCL5*, *CD27*, *CD274*, *CD276*, *CD8A*, *CMKRL1*, *CXCL9*, *CXCR6*, *HLA-DQA1*, *HLA-DRB1*, *HLA-E*, *IDO1*, *LAG3*, *NKG7*, *PDCD1LG2*, *PSMB10*, *STAT1*, *TIGIT*. (i) Mast cell signature expression in relation to ER expression. Genes included: *MS4A2*, *CPA3*, *HDC*, *TPSAB1*. (b)-(i) Median with interquartile range, statistics by Kruskal-Wallis with post-hoc Dunn's test. Only statistically significant comparisons are shown. * $p < 0.05$, ** $p < 0.01$, *** $p < 0.001$, **** $p < 0.0001$.

To assess transcriptomic differences including non-immune-related processes in relation to ER expression, we analyzed all 42 signatures of the NanoString panel and started with unbiased clustering of the tumors. Using a principal component analysis, we observed that tumors with 0% ER expression tended to cluster away from breast tumors with >50% ER expression, but tumors with ER1-9% and ER10-50% seemed to mix between the tumors with 0% and >50% ER expression (Supplementary Figure 5A). With unsupervised clustering, two clusters were dominated by ER0% tumors and also included ER1-9% and ER10-50% tumors, which were characterized by either high expression of immune signatures or by genomic instability (Supplementary Figure 5B). Comparing expression of each signature between the groups with ER0% and ER1-9%, we saw significantly lower expression of signatures characterizing genomic instability and p53 biology and, as expected, higher expression of ER-related signaling in the group with ER1-9% expression, but no significant differences in immune signatures (Figure 3A). Investigating differential expression between tumors with ER10-50% and ER1-9%, we observed higher expression of ER signaling in the ER10-50% group, but again no significant differences in immune signatures (Figure 3B). Comparing ER51-99% tumors with the group of ER10-50%, we observed higher expression of immune pathways in the tumors with ER expression between 10-50% and lower expression of ER signaling and mast cells (Figure 3C). Between the groups with ER51-99% and ER100%, mainly a difference in *ESR1* expression was seen (Figure 3D). To increase statistical power, we pooled the ER low-positive and intermediate-positive groups (ER1-50%) and confirmed our findings (Supplementary Figure 6A-B). In summary, we observed that the expression of immune signatures was significantly higher in tumors with negative and low-positive or intermediate-positive ER expression as compared to tumors with high-positive ER expression, in line with our data on sTILs, CD8+ T cells and PD-L1 expression. Comparing to ER-negative tumors, we observed that ER low-positive and intermediate-positive breast tumors differ in ER signaling and genomic instability, but not in expression in immune pathways.

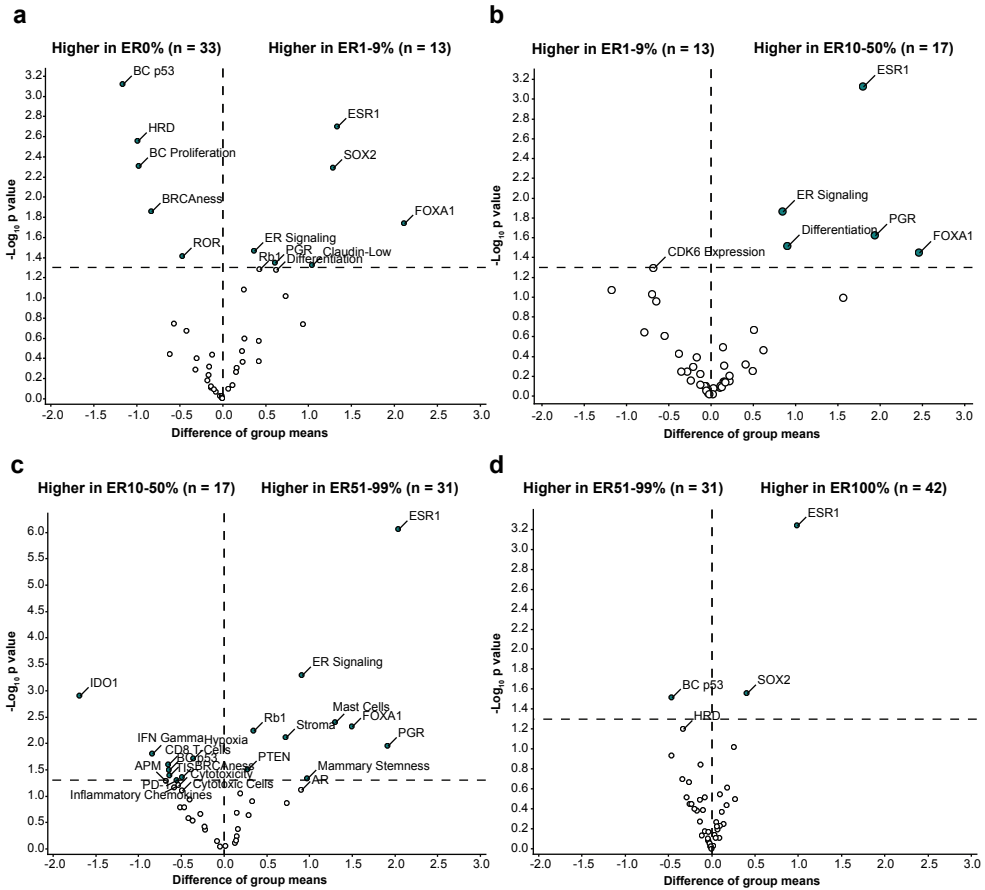


Figure 3: Differential gene expression of NanoString Breast Cancer 360™ signatures. (a) Difference in gene expression of signatures between the group with 0% ER expression and 1-9% ER expression. (b) Difference in gene expression of signatures between the group with 1-9% ER expression and 10-50% ER expression. (c) Difference in gene expression of signatures between the group with 10-50% ER expression and 51-99% ER expression. (d) Difference in gene expression of signatures between the group with 51-99% ER expression and 100% ER expression. (a)-(d). On the x-axis the difference in group means is displayed, on the y-axis the unadjusted p-value per variable by student t-tests. The vertical line indicates no change, the horizontal line indicates a p-value of 0.05.

Discussion

Breast cancer is a heterogeneous disease with ER expression being one of the most widely used biomarkers. The current cut-off of $\geq 1\%$ for positive ER expression is based on early studies in which no benefit was seen with endocrine treatment in patients with no ER expression. Consequently, most translational studies and clinical trials focus on differences between TNBC and ER-positive breast cancer, with no further distinction in ER-positive breast cancer. In this study, we explore the immune landscape of early-stage breast tumors with different levels of ER

expression. We are, to our knowledge, the first to demonstrate that early-stage breast tumors with low-positive (1-9%) and intermediate-positive (10-50%) ER expression have more similarities in immune biology to TNBC than to their highly ER-positive counterparts, based on sTILs, CD8+ T-cell presence, PD-L1 expression and expression of immune pathways. Our data highlight that clinical trials investigating ICB in ER-positive breast cancer should consider efficacy analysis in subgroups of patients with low-positive or intermediate-positive breast cancer.

Two phase II trials have reported results of neo-adjuvant ICB plus chemotherapy in high-risk ER-positive breast cancer. In the I-SPY2 trial, two arms with ICB-combinations graduated: pembrolizumab plus chemotherapy (taxane, followed by AC)³¹ and durvalumab/olaparib plus chemotherapy³². In both arms, it was shown that pCR rates were higher in the experimental arms as compared to the control arms in the high-risk (based on MammaPrint) ER-positive subgroup. Importantly, in an exploratory analysis, patients with an ultrahigh MammaPrint signature derived most benefit from the addition of durvalumab/olaparib to chemotherapy, which correlated with low *ESR1* and *PGR* expression and high proliferation³². Additionally, low *ESR1* and *PGR* expression was associated with higher pCR rates in the pembrolizumab arm⁴². In the single-arm GIADA-trial, a pCR rate of 15% was observed after neo-adjuvant chemotherapy (AC) plus nivolumab and exemestane in high-risk ER+ ($\geq 10\%$) breast cancer, defined by high Ki-67 expression and/or tumor grade 3⁸. In this trial, a basal-like subtype highly correlated with response⁸. Additionally, in metastatic ER-positive breast cancer, estrogen signaling was negatively associated with response to pembrolizumab and eribulin⁴³. Results of these trials indicate that ICB responses are not limited to TNBC and that exploratory subgroup analysis of response in clinical trials investigating ICB in ER-positive breast cancer are of great importance to confirm the association between low and intermediate ER expression levels and ICB response.

While sTILs and CD8+ T cells are positively associated with outcome in early-stage TNBC^{20,21,23-26}, this association is not clear in ER-positive breast cancer^{20,27,28}, suggesting that T-cell functioning is hampered in ER-positive tumors. Several immune cells, particularly myeloid cells, express ER⁴⁴. Estrogen signaling has been shown to increase mobilization and immune-suppressive functions of myeloid-derived suppressor cells (MDSCs) *in vivo* which drives disease progression⁴⁵. Moreover, a recent study demonstrated that estrogen signaling in a murine melanoma model promoted the accumulation of immune-suppressive macrophages in the TME, reduced cytotoxicity of CD8+ T cells and promoted tumor growth⁴⁶. In breast cancer, high levels of tumor-associated macrophages (TAMs) and mast cells with pleiotropic functions have been described^{47,48}. Interestingly in this model, this detrimental effect could be reverted by treatment with fulvestrant and ICB⁴⁶. In turn, immune signaling, via interferons and STAT1, has been implicated in increased transcription of ER in tumor cells⁴⁹, indicating a positive feedback loop between estrogen and interferon signaling and highlighting the complex crosstalk between immune cells in the TME and ER signaling. In breast cancer, high levels of tumor-associated macrophages (TAMs) and mast cells with pleiotropic functions

have been described^{47,48}. Mast cells are more abundant in the TME of luminal breast cancers, as compared to basal-like tumors⁵⁰ and have been correlated to residual disease after neo-adjuvant chemotherapy⁵¹ and a non-pCR in the pembrolizumab and durvalumab/olaparib arm in the ER-positive subgroup of the I-SPY2 trial^{32,42}. In our study we observed high levels of mast cell-related gene expression in ER-high tumors as compared to TNBC or ER low/intermediate tumors. Altogether, we hypothesize that the level of ER signaling shapes the TME of ER-positive breast cancer potentially promoting an immune-suppressive state.

Subgroup analysis in ongoing phase III trials testing neo-adjuvant ICB-chemotherapy in high-risk ER-positive breast cancer (NCT03725059, NCT04109066) and future trials are needed to validate whether patients with low-positive or intermediate-positive ER expression derive more benefit from ICB than patients with high expression of ER. Since responses to endocrine treatment have been observed in some patients with low-positive ER tumors⁵² and CDK4/6 inhibitors have clinical activity in patients with intermediate-positive ER tumors (<50%) albeit to a lesser extent than patients with ER-high tumors⁵³, it remains to be determined what the optimal (combination) treatment regimen is. Ideally, a basket trial specifically for patients with low- and/or intermediate-positive breast cancer could provide answers on this question, testing neo-adjuvant ICB-combinations such as anti-PD1 plus endocrine treatment, ICB with other immuno-oncology agents such as anti-CTLA4 plus anti-PD1⁵⁴. In our cohort, we did not observe higher levels of sTILs, CD8+ T cells or PD-L1 expression in grade 3 or highly proliferative (Ki-67 expression $\geq 20\%$) tumors with ER expression >50% (data not shown), suggesting that patients most likely to respond to CDK4/6 inhibitors^{53,55} don't have particularly immunogenic tumors. This is important in light of the substantial toxicity that has been observed with anti-PD1 plus CDK4/6 inhibitors⁵⁶. Recently, Wolf and colleagues proposed a novel model on the redefinition of early-stage breast cancer subtypes based on the pathological response to targeted agents or ICB. Within the ER-positive HER2-negative immune-enriched subtype, an estimated pCR rate to neo-adjuvant pembrolizumab plus chemotherapy of 69% was seen⁵⁷. Based on our data, we hypothesize that this immune-enriched subtype might mostly be comprised of breast tumors with low-positive or intermediate-positive ER expression.

Our study is limited by its small sample size of the ER low-positive and intermediate-positive groups, although this is inherent to the relatively low incidence of these breast cancers in a single centre and the lack of reporting of continuous ER expression in most cancer registries and pathology laboratories. Furthermore, it has been proposed that low-positive ER tumors are an artefact of a low intensity staining⁵⁸. However, in our study all ER stainings were done in concordance with Dutch guidelines for breast cancer diagnostics⁹ in one expert centre laboratory, including both internal controls and control tissues to ensure accurate receptor staining and were scored by dedicated breast pathologists. Third, we collected tumor blocks of the ER-negative and the two high-positive groups in a short consecutive series to roughly match the group size of the pooled ER low-positive and intermediate-positive group. This series was not matched in terms of TNM stage,

resulting in slightly unbalanced T-stage and N-stage between groups. Since sTILs, CD8+ T cells and PD-L1 levels did not differ between T-stages and N-stages (data not shown), we believe that the effect of this disbalance is probably limited. Our study focused on early-stage breast tumors, and therefore our conclusions cannot directly be applied to the metastatic setting. Since our series is not representative of the breast cancer population due to our enrichment of breast tumors with ER expression between 1-99%, it should be noted that our series is not suitable for epidemiological studies or real-world interpretation but instead our results should be considered as hypothesis-generating.

In this study, we demonstrate that early-stage breast tumors with low-positive (1-9%) and intermediate-positive (10-50%) ER expression have immunological properties with more similarities to ER-negative tumors than to ER-high tumors. Since ICB is currently only approved for TNBC, these findings highlight that the identification based on ER-negativity of breast tumors that might benefit from ICB needs revisiting. Our study encourages adequately powered subgroup analysis of patients with low-positive and intermediate ER expression in clinical trials for ICB in ER-positive breast cancer and highlights that the traditional selection based on ER expression might not be optimal for ICB treatment.

Methods

Study population and tissue collection

All patients presenting with primary breast cancer with ER expression on tumor cells between 1-50% in the Netherlands Cancer Institute between January 2011 and September 2019 were identified via the local Tumor Registry. All patients were considered to be included if they had early-stage disease, HER2-negative breast cancer and availability of tumor blocks within our institute. To ensure accurate continuous ER scoring and HER2 assessment, we only collected tumor blocks after 2011. Available archival formalin-fixed paraffin-embedded (FFPE) tumor blocks within the Netherlands Cancer Institute with known ER expression were collected in the study. Using the same inclusion criteria, we collected a longitudinal series of tumor blocks with ER expression of 0%, 51-99% and 100%. Given that these groups are more prevalent and to roughly match the sample size of the group with ER expression between 1-50%, a random shorter period within the diagnosis years of 2011-2019 was used to collect the tumor blocks for the groups with ER expression of 0%, 51-99% and 100% (Supplementary Figure 1). When available, resection material was collected and, in case of neo-adjuvant endocrine treatment or chemotherapy, biopsies were collected. All patients with metastatic disease, or tumor blocks of local recurrences and non-invasive breast tumors were excluded. Clinical data was extracted from the local Tumor Registry from the selected patients and additional clinical data was collected directly from the patient records. Pathological characteristics, such as ER expression, PR expression, HER2 status, Ki-67 expression, and tumor grade, were obtained from the pathology reports. All histological assessments were performed in a single

pathology laboratory of the Netherlands Cancer Institute in concordance with Dutch guidelines for breast cancer diagnostics⁹ including the required controls to ensure accurate receptor staining. Scoring was performed by dedicated breast cancer pathologists. The study was approved by the Institutional Review Board of the Netherlands Cancer Institute (IRBdm20-044).

H&E and immunohistochemistry stainings

New hematoxylin and eosin (H&E) stainings were obtained from FFPE tumor blocks and tumor blocks with a tumor-cell percentage below 20% were disregarded. Immunohistochemistry of the FFPE tumor samples was performed on a BenchMark Ultra autostainer (Ventana Medical Systems). Briefly, paraffin sections were cut at 3 μm , heated at 75 °C for 28 minutes and deparaffinized in the instrument with EZ prep solution (Ventana Medical Systems). Heat-induced antigen retrieval was carried out using Cell Conditioning 1 (CC1, Ventana Medical Systems) for 32 minutes at 95 °C (CD8) or 64 minutes at 95 °C (PD-L1). CD8 was detected using clone C8/144B (1/200 dilution, 32 minutes at 37 °C, Agilent/DAKO) and PD-L1 using clone 22C3 (1/40 dilution, 1 hour at room temperature, Agilent/DAKO). Bound antibody was detected using the OptiView DAB Detection Kit and slides were counterstained with Hematoxylin and Bluing Reagent (Ventana Medical Systems). Slides were scanned with a PANNORAMIC® 1000 scanner (3DHISTECH; 40x magnification) and uploaded on SlideScore for digital assessment (www.slidescore.com). On the H&E, sTILs were assessed by an experienced pathologist (J.S.) according to established guidelines for sTIL scoring in breast cancer⁵⁹. CD8+ T cells were scored as percentage of positive cells within the tumor-associated stromal area by the same pathologist. sTILs and CD8 scores were revised by an independent second pathologist (H.M.H.). PD-L1 expression was assessed by a dedicated breast pathologist (H.M.H.) as the combined positive score (CPS), which was defined as the number of PD-L1 positive cells (tumor cells and immune cells) divided by the total number of tumor cells multiplied by 100, as described before⁶⁰.

NanoString gene expression analysis

The tumor and tumor-associated stromal area was annotated on a H&E slide for subsequent RNA isolation. In case of an area of at least 8 mm² and a TCP of 20%, RNA was isolated in 5-15 10 μm sections of FFPE tumor blocks (depending on area size). DNA and RNA was isolated simultaneously with the AllPrep DNA/RNA FFPE kit (Qiagen, #80234) using the QIAcube, according to the manufacturer's instructions. The RNA concentration was measured by NanoDrop. 200 ng of RNA (or max. 12 μl in case of low concentrations) was used as input on a NanoString nCounter® platform and gene expression was assessed by the NanoString nCounter® Breast Cancer 360™ panel⁶¹. Kits and probes were obtained from NanoString and samples were processed by the manufacturer's instructions. The Breast Cancer 360™ panel contains 758 genes of interest with 18 additional genes for internal reference. Only samples passing the quality control of housekeeping gene expression were included in the subsequent analysis. Genes not included in the tumor-inflammation signature (TIS) and PAM50 classification were normalized using a ratio of the expression value to the geometric mean of all housekeeping genes on the panel.

Genes included in TIS and PAM50 are normalized using a ratio of the expression value to the geometric mean of the housekeeper genes used only for TIS or PAM50, respectively^{62,63}. Genes not in the PAM50 signature were additionally normalized using a ratio of the housekeeper-normalized data and a panel standard run on the same cartridge or a panel standard run on the same codeset. Finally, the data was \log_2 transformed. 48 signatures capturing breast cancer biology as defined by NanoString were calculated, including TIS and molecular subtyping. Signature scores were adjusted with constants to express values in a similar range and making scores comparable across assays. The Risk of Recurrence score was \log_2 transformed to obtain values within the range of the other signatures for differential expression analysis. PAM50 subtype calling was performed as described previously^{39,63}. TNBC subtypes⁴⁰ were identified using a calculated weighted average of the luminal A and luminal B PAM50 subtype correlation and AR gene expression and the signature scores for Mammary Stemness and TIS. TNBC subtypes were called based on a set of decision rules on the aforementioned scores by NanoString.

Gene expression analysis independent validation cohort

Gene expression data and clinical characteristics of the validation cohort were obtained directly from the primary investigators⁴¹. Briefly, microarray experiments (GEO accession number GSE34138) or RNA-sequencing (GEO accession number GSE192341) were performed on pre-treatment biopsies from patients with stage I-III HER2-negative breast cancer in the Netherlands Cancer Institute, treated with neo-adjuvant chemotherapy. Data from these experiments were pooled and normalized as previously described⁴¹. There was no overlap between samples of this independent validation cohort and the main cohort studied in this manuscript.

Statistical analysis

Categorical variables were described as proportion of patients within each ER expression group (i.e. ER 0%, 1-9%, 10-50%, 51-99%, 100%) and differences were assessed by Fisher's exact test. Differences between groups for continuous variables were assessed by non-parametric statistical tests: Mann-Whitney-U for differences between two groups and Kruskal-Wallis test for differences between three or more groups. Post-hoc analyses of the Kruskal-Wallis test were performed with a Dunn's test. Differential expression analysis of signatures was performed with QluCore Omics Explorer where the difference in group means between groups (ER 0%, 1-9%, 10-50%, 51-99%, 100%) was tested with t-tests for each variable. Statistical analysis was performed by SPSS statistics (IBM, version 28.0.1.0), GraphPad Prism (version 9.0.1) and QluCore Omics Explorer (version 3.8). P-values are unadjusted unless otherwise reported, all statistical tests were two-sided and a p-value of less than 0.05 was considered statistically significant.

Data availability

All data used for this study are included in Supplementary Table 1 (available with the online version of this article). Data from the validation cohort are available via GEO accession numbers GSE34138 (microarray) and GSE192341 (RNA-sequencing).

Acknowledgements

We thank the Tumor Registry of the Netherlands Cancer Institute for making the data available, in particular Michel Vergouwen and Tony van de Velde. We acknowledge the Core Facility of Molecular Pathology & Biobanking for their support in staining and RNA isolations of the human material, in particular Annegien Broeks and Hans Halfwerk. Research in the Kok group is funded by the Netherlands Organization for Scientific Research (NWO-VIDI 09150172010043) and the Hendrika Roet fund. We thank the Dutch Cancer Society (NKI2015-7542) for supporting (part of) the study.

Author contributions

L.V. collected and analysed the clinical, pathological and transcriptomic data. Together with M.K., LV. conceived the project and wrote the manuscript. J.S. and H.M.H. performed the histological scoring of the pathology slides. M.S.K. collected and curated the clinical data. S.B. was involved in the statistical analysis. S.C. performed RNA isolations and NanoString experiments. M.D. curated the selection of tumor blocks. E.H.L. collected and kindly provided the data of the independent validation cohort. G.S.S. and S.C.L. provided essential input during the study. M.K. supervised the project. All authors edited and approved the manuscript.

Conflicts of interest

L.V., J.S., M.S.K., S.B., S.C., M.D., and E.H.L. declare no competing financial or non-financial interests. G.S.S. reports the following financial interests: research funding to the institute from Agendia, AstraZeneca, Merck, Novartis, Roche and Seagen and the following non-financial interests: consulting role for Biovica and Seagen, outside the submitted work. S.C.L. reports the following financial interests: research funding to the institute from Roche/Genentech, AstraZeneca, BMS, Tesaro, Merck, Immunomedics, Eurocept Pharmaceuticals, Agendia and Novartis and the following non-financial interests: a consulting role and travel grant from Daiichi Sankyo, outside this work. H.M.H. reports support from Roche Diagnostics, outside the submitted work, and no non-financial interests. M.K. reports the following financial interests: research funding to the institute from BMS, Roche, AstraZeneca/MedImmune and the following non-financial interests: an advisory role for BMS, Roche, MSD and Daiichi Sankyo, outside the submitted work.

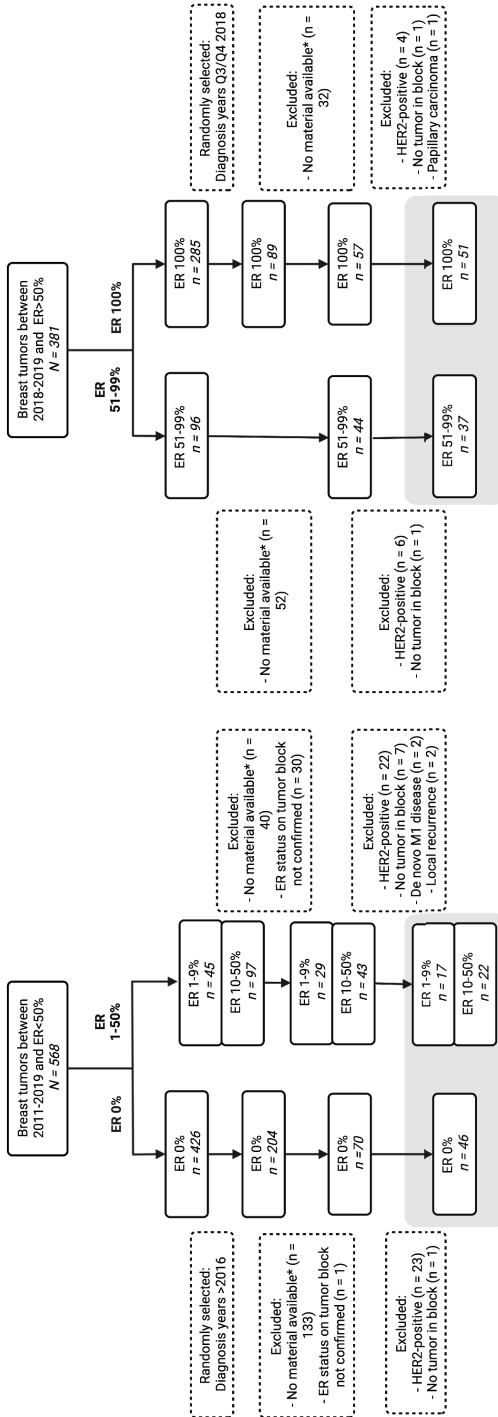
References

1. Cardoso, F. et al. Early breast cancer: ESMO Clinical Practice Guidelines for diagnosis, treatment and follow-up†. *Ann Oncol* 30 (8), 1194-1220, 2019.
2. Allison, K. H. et al. Estrogen and Progesterone Receptor Testing in Breast Cancer: ASCO/CAP Guideline Update. *Journal of Clinical Oncology* 38 (12), 1346-1366, 2020.
3. Harvey, J. M., Clark, G. M., Osborne, C. K. & Allred, D. C. Estrogen receptor status by immunohistochemistry is superior to the ligand-binding assay for predicting response to adjuvant endocrine therapy in breast cancer. *Journal of clinical oncology : official journal of the American Society of Clinical Oncology* 17 (5), 1474-1481, 1999.
4. Davies, C. et al. Relevance of breast cancer hormone receptors and other factors to the efficacy of adjuvant tamoxifen: patient-level meta-analysis of randomised trials. *Lancet (London, England)* 378 (9793), 771-784, 2011.
5. Voorwerk, L. et al. Immune induction strategies in metastatic triple-negative breast cancer to enhance the sensitivity to PD-1 blockade: the TONIC trial. *Nature Medicine*, 2019.
6. Tutt, A. et al. Carboplatin in BRCA1/2-mutated and triple-negative breast cancer BRCAness subgroups: the TNT Trial. *Nat Med* 24 (5), 628-637, 2018.
7. Conte, P. F. et al. Phase III randomized study of adjuvant treatment with the ANTI-PD-L1 antibody avelumab for high-risk triple negative breast cancer patients: The A-BRAVE trial. *Journal of Clinical Oncology* 38 (15_suppl), TPS598-TPS598, 2020.
8. Dieci, M. V. et al. Neoadjuvant Chemotherapy and Immunotherapy in Luminal B-like Breast Cancer: Results of the Phase II GIADA Trial. *Clinical Cancer Research* 28 (2), 308-317, 2022.
9. Specialisten, F. M. Richtlijndatabase Borstkanker. Consulted at 31-03-2022.
10. Schrodi, S. et al. Outcome of breast cancer patients with low hormone receptor positivity: analysis of a 15-year population-based cohort. *Ann Oncol* 32 (11), 1410-1424, 2021.
11. Villegas, S. L. et al. Therapy response and prognosis of patients with early breast cancer with low positivity for hormone receptors - An analysis of 2765 patients from neoadjuvant clinical trials. *European Journal of Cancer* 148, 159-170, 2021.
12. Fujii, T. et al. Revisiting the definition of estrogen receptor positivity in HER2-negative primary breast cancer. *Ann Oncol* 28 (10), 2420-2428, 2017.
13. Dieci, M. V. et al. Impact of estrogen receptor levels on outcome in non-metastatic triple negative breast cancer patients treated with neoadjuvant/adjuvant chemotherapy. *NPJ Breast Cancer* 7 (1), 101, 2021.
14. Paakkola, N. M., Karakatsanis, A., Mauri, D., Foukakis, T. & Valachis, A. The prognostic and predictive impact of low estrogen receptor expression in early breast cancer: a systematic review and meta-analysis. *ESMO Open* 6 (6), 100289, 2021.
15. Ohara, A. M. et al. PAM50 for prediction of response to neoadjuvant chemotherapy for ER-positive breast cancer. *Breast Cancer Res Treat* 173 (3), 533-543, 2019.
16. Park, Y. H. et al. Prevalence, treatment patterns, and prognosis of low estrogen receptor-positive (1% to 10%) breast cancer: a single institution's experience in Korea. *Breast Cancer Res Treat* 189 (3), 653-663, 2021.
17. Iwamoto, T. et al. Estrogen receptor (ER) mRNA and ER-related gene expression in breast cancers that are 1% to 10% ER-positive by immunohistochemistry. *Journal of clinical oncology : official journal of the American Society of Clinical Oncology* 30 (7), 729-734, 2012.
18. Zhang, Z. et al. Pathological features and clinical outcomes of breast cancer according to levels of oestrogen receptor expression. *Histopathology* 65 (4), 508-516, 2014.
19. Ma, H. et al. Quantitative measures of estrogen receptor expression in relation to breast cancer-specific mortality risk among white women and black women. *Breast cancer research : BCR* 15 (5), R90, 2013.
20. Denkert, C. et al. Tumour-infiltrating lymphocytes and prognosis in different subtypes of breast cancer: a pooled analysis of 3771 patients treated with neoadjuvant therapy. *The Lancet. Oncology* 19 (1), 40-50, 2018.
21. Mahmoud, S. M. A. et al. Tumor-Infiltrating CD8+ Lymphocytes Predict Clinical Outcome in Breast Cancer. *Journal of Clinical Oncology* 29 (15), 1949-1955, 2011.
22. Hammerl, D. et al. Clonality, antigen recognition and suppression of CD8+ T cells differentially affect prognosis of breast cancer subtypes. *Clinical Cancer Research*, clincanres.0285.2019, 2019.

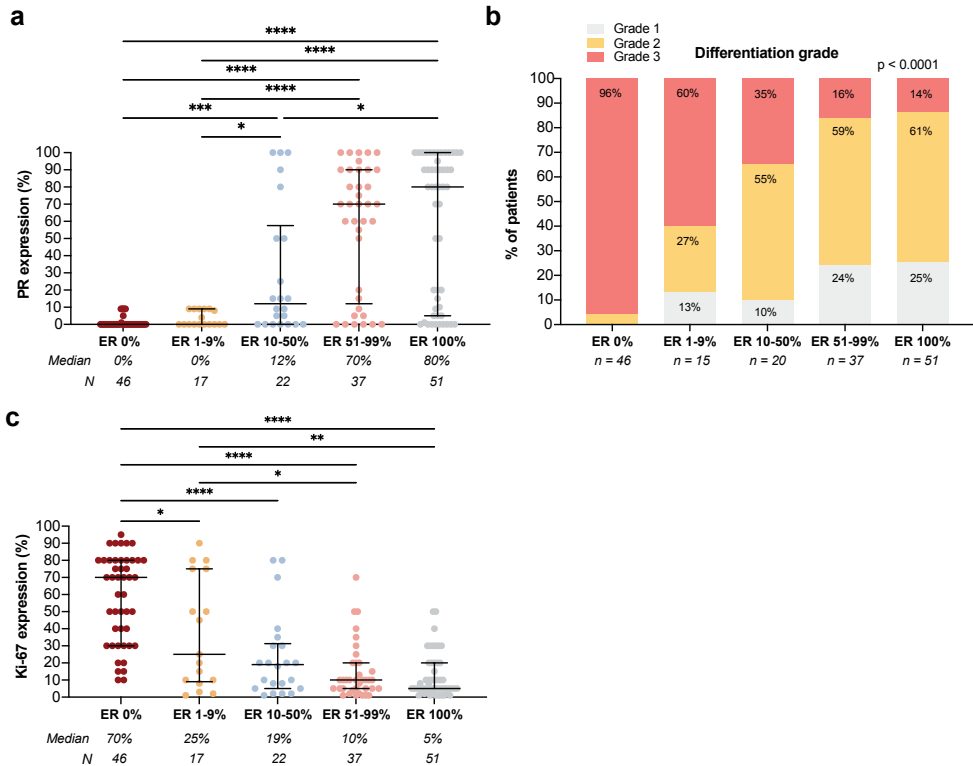
23. Park, J. H. et al. Prognostic value of tumor-infiltrating lymphocytes in patients with early-stage triple-negative breast cancers (TNBC) who did not receive adjuvant chemotherapy. *Annals of Oncology*, 2019.
24. de Jong, V. M. T. et al. Prognostic Value of Stromal Tumor-Infiltrating Lymphocytes in Young, Node-Negative, Triple-Negative Breast Cancer Patients Who Did Not Receive (neo)Adjuvant Systemic Therapy. *Journal of Clinical Oncology*, JCO.21.01536, 2022.
25. Loi, S. et al. Tumor-Infiltrating Lymphocytes and Prognosis: A Pooled Individual Patient Analysis of Early-Stage Triple-Negative Breast Cancers. *Journal of clinical oncology : official journal of the American Society of Clinical Oncology* 37 (7), 559-569, 2019.
26. Adams, S. et al. Prognostic value of tumor-infiltrating lymphocytes in triple-negative breast cancers from two phase III randomized adjuvant breast cancer trials: ECOG 2197 and ECOG 1199. *Journal of clinical oncology : official journal of the American Society of Clinical Oncology* 32 (27), 2959-2966, 2014.
27. Egelston, C. A. et al. Tumor-infiltrating exhausted CD8+ T cells dictate reduced survival in premenopausal estrogen receptor-positive breast cancer. *JCI Insight* 7 (3), 2022.
28. Sobral-Leite, M. et al. Assessment of PD-L1 expression across breast cancer molecular subtypes, in relation to mutation rate, BRCA1-like status, tumor-infiltrating immune cells and survival. *Oncoimmunology*, 1-15, 2018.
29. Esteva, F. J., Hubbard-Lucey, V. M., Tang, J. & Pusztai, L. Immunotherapy and targeted therapy combinations in metastatic breast cancer. *The Lancet. Oncology* 20 (3), e175-e186, 2019.
30. Schmid, P. et al. Pembrolizumab plus chemotherapy as neoadjuvant treatment of high-risk, early-stage triple-negative breast cancer: results from the phase 1b open-label, multicohort KEYNOTE-173 study. *Ann Oncol* 31 (5), 569-581, 2020.
31. Nanda, R. et al. Effect of Pembrolizumab Plus Neoadjuvant Chemotherapy on Pathologic Complete Response in Women With Early-Stage Breast Cancer: An Analysis of the Ongoing Phase 2 Adaptively Randomized I-SPY2 Trial. *JAMA Oncology* 6 (5), 676-684, 2020.
32. Pusztai, L. et al. Durvalumab with olaparib and paclitaxel for high-risk HER2-negative stage II/III breast cancer: Results from the adaptively randomized I-SPY2 trial. *Cancer cell* 39 (7), 989-998. e985, 2021.
33. Bianchini, G. et al. LBA12 Predictive value of gene-expression profiles (GEPs) and their dynamics during therapy in the NeoTRIPaPDL1 trial. *Annals of Oncology* 32, S1283-S1284, 2021.
34. Denkert, C. et al. Biomarkers for response to immunotherapy in triple-negative breast cancer: Differences between survival and pCR biomarkers. *Journal of Clinical Oncology* 40 (16_suppl), 583-583, 2022.
35. Loi, S. et al. Abstract PD5-03: Relationship between tumor-infiltrating lymphocytes (TILs) and outcomes in the KEYNOTE-119 study of pembrolizumab vs chemotherapy for previously treated metastatic triple-negative breast cancer (mTNBC). *Cancer Research* 80 (4_Supplement), PD5-03-PD05-03, 2020.
36. Cortes, J. et al. Pembrolizumab plus chemotherapy versus placebo plus chemotherapy for previously untreated locally recurrent inoperable or metastatic triple-negative breast cancer (KEYNOTE-355): a randomised, placebo-controlled, double-blind, phase 3 clinical trial. *Lancet (London, England)* 396 (10265), 1817-1828, 2020.
37. Leisha A. Emens, L. D. G., Peter Schmid, Hope S. Rugo, Sylvia Adams, Carlos H. Barrios, Andreas Schneeweiss, Veronique Dieras, Hiroji Iwata, Ching-Wei Chang, Hartmut Koeppen, Stephen Y. Chui, Sherene Loi, Luciana Molinero; . The tumor microenvironment (TME) and atezolizumab + nab-paclitaxel (A+nP) activity in metastatic triple-negative breast cancer (mTNBC): IMpassion130. American Society of Clinical Oncology conference 2021; *Journal of Clinical Oncology* 39, 2021 (suppl 15; abstr 1006), 2021.
38. Sorlie, T. et al. Gene expression patterns of breast carcinomas distinguish tumor subclasses with clinical implications. *Proc Natl Acad Sci U S A* 98 (19), 10869-10874, 2001.
39. Wallden, B. et al. Development and verification of the PAM50-based Prosigna breast cancer gene signature assay. *BMC medical genomics* 8, 54-54, 2015.
40. Burstein, M. D. et al. Comprehensive genomic analysis identifies novel subtypes and targets of triple-negative breast cancer. *Clinical cancer research : an official journal of the American Association for Cancer Research* 21 (7), 1688-1698, 2015.
41. Hoogstraat, M. et al. Comprehensive characterization of pre- and post-treatment samples of breast cancer reveal potential mechanisms of chemotherapy resistance. *NPJ Breast Cancer* 8 (1), 60, 2022.

42. Wolf, D. M. et al. Redefining breast cancer subtypes to guide treatment prioritization and maximize response: Predictive biomarkers across 10 cancer therapies. *Cancer cell* 40 (6), 609-623.e606, 2022.
43. Keenan, T. E. et al. Molecular correlates of response to eribulin and pembrolizumab in hormone receptor-positive metastatic breast cancer. *Nat Commun* 12 (1), 5563, 2021.
44. Segovia-Mendoza, M. & Morales-Montor, J. Immune Tumor Microenvironment in Breast Cancer and the Participation of Estrogen and Its Receptors in Cancer Physiopathology. *Frontiers in immunology* 10, 2019.
45. Svoronos, N. et al. Tumor Cell-Independent Estrogen Signaling Drives Disease Progression through Mobilization of Myeloid-Derived Suppressor Cells. *Cancer Discov* 7 (1), 72-85, 2017.
46. Chakraborty, B. et al. Inhibition of estrogen signaling in myeloid cells increases tumor immunity in melanoma. *The Journal of clinical investigation* 131 (23), 2021.
47. Wagner, J. et al. A Single-Cell Atlas of the Tumor and Immune Ecosystem of Human Breast Cancer. *Cell* 177 (5), 1330-1345.e1318, 2019.
48. Aponte-López, A., Fuentes-Panana, E. M., Cortes-Muñoz, D. & Muñoz-Cruz, S. Mast Cell, the Neglected Member of the Tumor Microenvironment: Role in Breast Cancer. *Journal of Immunology Research* 2018, 2584243, 2018.
49. Hou, Y. et al. STAT1 facilitates oestrogen receptor α transcription and stimulates breast cancer cell proliferation. *J Cell Mol Med* 22 (12), 6077-6086, 2018.
50. Glajcar, A. et al. The relationship between breast cancer molecular subtypes and mast cell populations in tumor microenvironment. *Virchows Arch* 470 (5), 505-515, 2017.
51. Li, X. et al. Immune profiling of pre- and post-treatment breast cancer tissues from the SWOG S0800 neoadjuvant trial. *J Immunother Cancer* 7 (1), 88, 2019.
52. Cai, Y. W., Shao, Z. M. & Yu, K. D. De-escalation of five-year adjuvant endocrine therapy in patients with estrogen receptor-low positive (immunohistochemistry staining 1%-10%) breast cancer: Propensity-matched analysis from a prospectively maintained cohort. *Cancer*, 2022.
53. De La Motte Rouge, T. et al. 167MO Association between ER, PR and HER2 levels and outcome under palbociclib (Pal) + aromatase inhibitors (AIs) as first-line therapy for ER+ HER2- metastatic breast cancer (MBC): An exploratory analysis of the PADA-1 trial. *Annals of Oncology* 33, S200, 2022.
54. Adams, S. et al. A Multicenter Phase II Trial of Ipilimumab and Nivolumab in Unresectable or Metastatic Metaplastic Breast Cancer: Cohort 36 of Dual Anti-CTLA-4 and Anti-PD-1 Blockade in Rare Tumors (DART, SWOG S1609). *Clinical cancer research : an official journal of the American Association for Cancer Research* 28 (2), 271-278, 2022.
55. Harbeck, N. et al. Adjuvant abemaciclib combined with endocrine therapy for high-risk early breast cancer: updated efficacy and Ki-67 analysis from the monarchE study. *Ann Oncol* 32 (12), 1571-1581, 2021.
56. Jerusalem, G. et al. 92MO Neoadjuvant nivolumab (NIVO) + palbociclib (PALBO) + anastrozole (ANA) for estrogen receptor-positive (ER+)/human epidermal growth factor receptor 2-negative (HER2-) primary breast cancer (BC): CheckMate 7A8. *Annals of Oncology* 33, S165-S166, 2022.
57. Huppert, L. A. et al. Pathologic complete response (pCR) rates for HR+/HER2- breast cancer by molecular subtype in the I-SPY2 Trial. *Journal of Clinical Oncology* 40 (16_suppl), 504-504, 2022.
58. Caruana, D., Wei, W., Martinez-Morilla, S., Rimm, D. L. & Reisenbichler, E. S. Association between low estrogen receptor positive breast cancer and staining performance. *npj Breast Cancer* 6 (1), 5, 2020.
59. Salgado, R. et al. The evaluation of tumor-infiltrating lymphocytes (TILs) in breast cancer: recommendations by an International TILs Working Group 2014. *Annals of Oncology* 26 (2), 259-271, 2015.
60. Kulangara, K. et al. Clinical Utility of the Combined Positive Score for Programmed Death Ligand-1 Expression and the Approval of Pembrolizumab for Treatment of Gastric Cancer. *Arch Pathol Lab Med* 143 (3), 330-337, 2019.
61. Geiss, G. K. et al. Direct multiplexed measurement of gene expression with color-coded probe pairs. *Nature Biotechnology* 26 (3), 317-325, 2008.
62. Danaheer, P. et al. Pan-cancer adaptive immune resistance as defined by the Tumor Inflammation Signature (TIS): results from The Cancer Genome Atlas (TCGA). *J Immunother Cancer* 6 (1), 63, 2018.
63. Parker, J. S. et al. Supervised Risk Predictor of Breast Cancer Based on Intrinsic Subtypes. *Journal of Clinical Oncology* 27 (8), 1160-1167, 2009.
64. Ayers, M. et al. IFN-gamma-related mRNA profile predicts clinical response to PD-1 blockade. *The Journal of clinical investigation* 127 (8), 2930-2940, 2017.

Supplemental Material

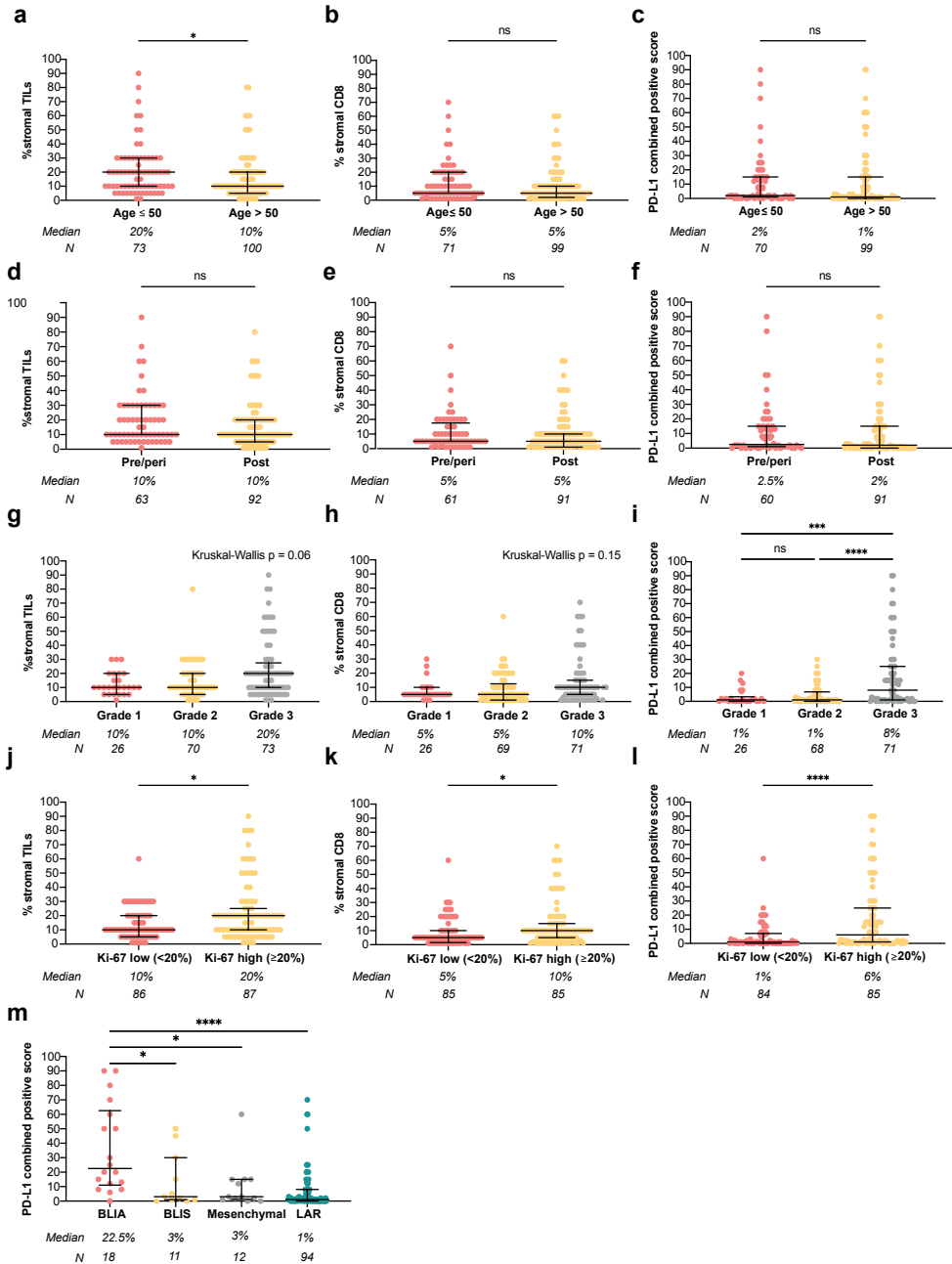


Supplementary Figure 1: Flow chart of selection of tumors with different estrogen receptor (ER) expression levels. All patients diagnosed with breast tumors with ER expression between 1-50% between 2011 and 2019 were selected. For the groups with 0%, 51-99% and 100% ER expression, a random period was taken within these diagnosis years aiming for similar group sizes. Figure was created with Biorender.com. *No tumor block of untreated invasive breast tumor available within the Netherlands Cancer Institute.

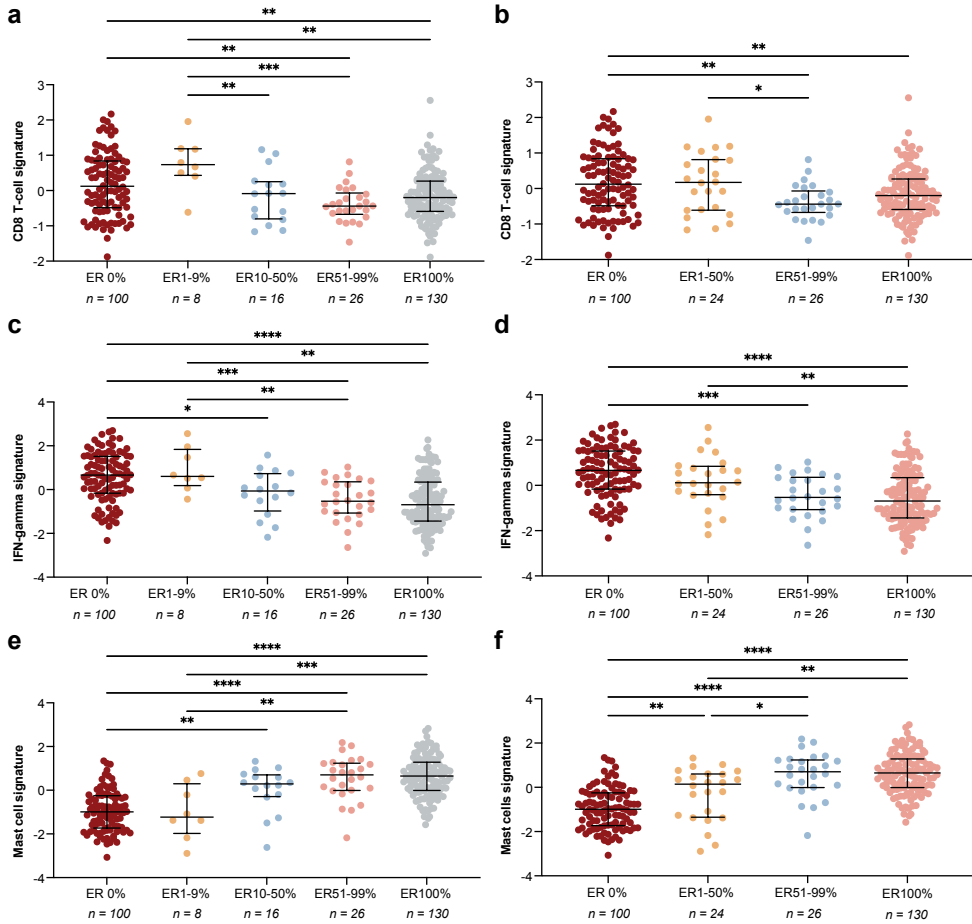


Supplementary Figure 2: Intrinsic features of breast tumors with different levels of ER expression. (a) PR expression in relation to ER expression. Statistics by Kruskal-Wallis with post-hoc Dunn's test. (b) Proportion of patients per tumor grade according to Bloom-Richardson in relation to ER expression. Numbers display percentage per group, statistics by Fisher's exact test. (c) Ki-67 expression in relation to ER expression. Statistics as in (a). (a),(c) Median with interquartile range. Only statistically significant comparisons are shown. * $p < 0.05$, ** $p < 0.01$, *** $p < 0.001$, **** $p < 0.0001$.

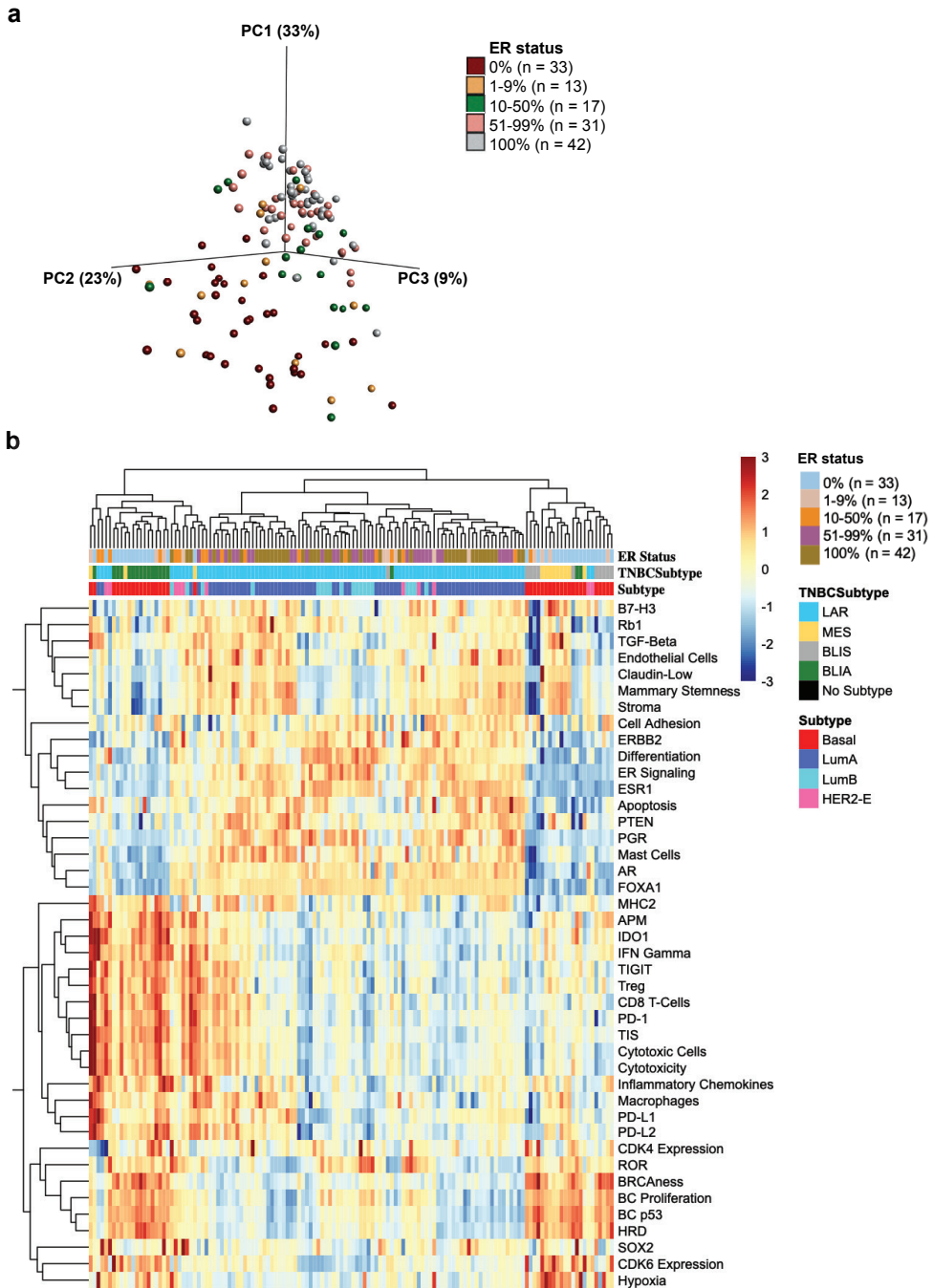
Supplementary Figure 3: (see next page) Immune cell composition and PD-L1 expression per age, menopausal status, tumor grade and Ki-67 expression levels. (a) Levels of stromal tumor infiltrating lymphocytes (sTILs) according to age ≤ 50 or age > 50 . (b) Levels of stromal CD8+ T cells (percentage of CD8+ T cells of the stromal area) according to age ≤ 50 or age > 50 . (c) PD-L1 expression, assessed as the combined positive score (CPS), according to age ≤ 50 or age > 50 . (d) Levels of stromal tumor infiltrating lymphocytes (sTILs) in relation to pre- or perimenopausal status vs. postmenopausal. (e) Levels of stromal CD8+ T cells (percentage of CD8+ T cells of the stromal area) in relation to pre- or perimenopausal status vs. postmenopausal. (f) PD-L1 expression (CPS) in relation to pre- or perimenopausal status vs. postmenopausal. (g) Levels of stromal tumor infiltrating lymphocytes (sTILs) per tumor grade according to Bloom-Richardson. (h) Levels of stromal CD8+ T cells (percentage of CD8+ T cells of the stromal area) per tumor grade according to Bloom-Richardson. (i) PD-L1 expression (CPS) per tumor grade according to Bloom-Richardson. (j) Levels of sTILs in tumors with low Ki-67 expression ($< 20\%$) and high Ki-67 expression ($\geq 20\%$). (k) Levels of stromal CD8+ T cells in tumors with low Ki-67 expression ($< 20\%$) and high Ki-67 expression ($\geq 20\%$). (l) PD-L1 expression (CPS) in tumors with low Ki-67 expression ($< 20\%$) and high Ki-67 expression ($\geq 20\%$). (m) PD-L1 expression (CPS) according to TNBC subtype: basal-like immune activated (BLIA), basal-like immune-suppressed (BLIS), mesenchymal or luminal androgen receptor (LAR) tumors in relation to ER expression. TNBC subtypes were assessed with the NanoString nCounter® Breast Cancer 360™ panel. For (g)-(i), (m) statistics by Kruskal-Wallis with post-hoc Dunn's test; for (a)-(f) and (j)-(l) statistics by Mann-Whitney. Only statistically significant comparisons are shown. ns (non-significant): $p > 0.05$, * $p < 0.05$, ** $p < 0.01$, *** $p < 0.001$, **** $p < 0.0001$.



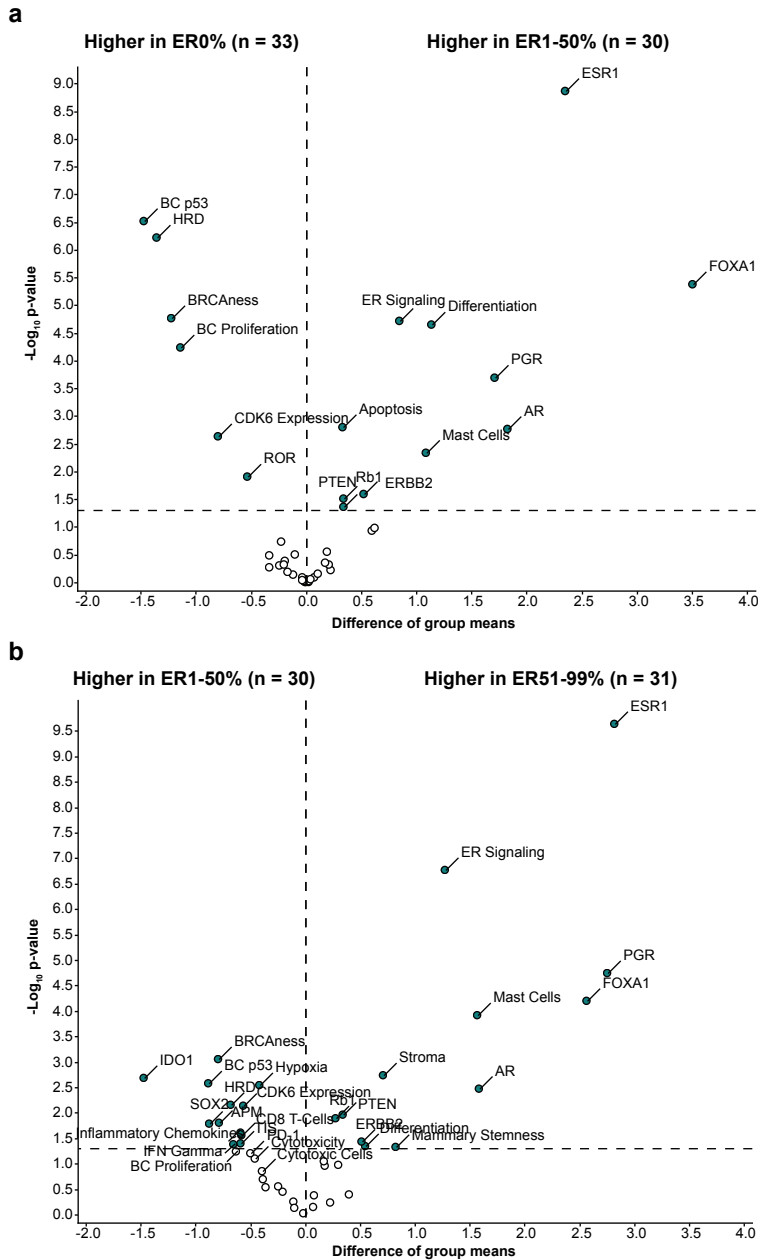
Supplementary Figure 3: Immune cell composition and PD-L1 expression per age, menopausal status, tumor grade and Ki-67 expression levels.



Supplementary Figure 4: Expression of immune signatures in relation to estrogen receptor (ER) expression levels in an independent validation cohort. (a) CD8+ T-cell signature expression in relation to ER expression with separate groups of tumors with ER 1-9% and ER10-50%. Average expression of *CD8A*, *CD8B*. (b) CD8+ T-cell signature expression in relation to ER expression with a pooled group of ER1-50%. Average expression of *CD8A*, *CD8B*. (c) Interferon (IFN)- γ signature expression in relation to ER expression with separate groups of tumors with ER 1-9% and ER10-50%. Average expression of *CXCL9*, *CXCL10*, *STAT1*. (d) Interferon (IFN)- γ signature expression in relation to ER expression with separate groups of tumors with a pooled group of ER1-50%. Average expression of *CXCL9*, *CXCL10*, *STAT1*. (e) Mast cell signature expression in relation to ER expression with ER 1-9% and ER10-50%. Average expression of *MS4A2*, *CPA3*, *HDC*, *TPSAB1*. (f) Mast cell signature expression in relation to ER expression with a pooled group of ER1-50%. Average expression of *MS4A2*, *CPA3*, *HDC*, *TPSAB1*. (a)-(f) Median with interquartile range, statistics by Kruskal-Wallis with post-hoc Dunn's test. Only statistically significant comparisons are shown. * $p < 0.05$, ** $p < 0.01$, *** $p < 0.001$, **** $p < 0.0001$.



Supplementary Figure 5: Unbiased analysis of NanoString Breast Cancer 360™ signatures. (a) Principal component analysis (PCA) of the NanoString nCounter® Breast Cancer 360™ panel signatures in all included tumors (n = 136). Three principal components (PC) are depicted with PC1 explaining 33% of the variance, PC2 explaining 23% of the variance and PC3 explaining 9% of the variance. Tumors are annotated by ER expression level as indicated by the legend. (b) Heatmap of normalized gene signatures across all tumors with hierarchical clustering of scaled gene signatures and samples. Samples are annotated with ER expression level, PAM50 molecular subtype and TNBC subtype.



Supplementary Figure 6: Differential expression of NanoString Breast Cancer 360™ signatures in pooled ER low-positive and intermediate-positive tumors. (a) Difference in gene expression of signatures between the group with 0% ER expression and the pooled group with 1-50% ER expression. **(b)** Difference in gene expression of signatures between the pooled group with 1-50% ER expression and 51-99% ER expression. **(a)-(b)** On the x-axis the difference in group means is displayed, on the y-axis the unadjusted p-value per variable by student t-tests. The vertical line indicates no change, the horizontal line indicates a p-value of 0.05.



Chapter 9

Discussion and future perspectives

Triple-negative breast cancer (TNBC): not so negative anymore

In 2017, at the start of my PhD research, no targeted treatment options were defined for patients with metastatic TNBC. Patients had a median overall survival of 12-18 months once metastasized and were all treated with palliative chemotherapy^{1,2}. At the time of writing this discussion, several new treatment options for patients with metastatic TNBC were available or upcoming: PARP inhibition for patients with germline *BRCA1/2* mutations³; antibody-drug conjugates (ADCs) sacituzumab govitecan (SG)⁴ and trastuzumab deruxtecan (T-DXd)⁵; and PD-(L)1 blockade plus chemotherapy⁶. In 2018, the phase III IMpassion130 trial demonstrated improved survival in patients with PD-L1 positive metastatic TNBC with atezolizumab (PD-L1 blockade) plus nab-paclitaxel⁷. IMpassion131 evaluated the efficacy of atezolizumab plus paclitaxel, powered to detect differences in the PD-L1 positive subgroup⁸; this trial did not demonstrate a benefit of atezolizumab addition over placebo. As we proposed in **chapter 2**, this discrepancy could have several reasons, such as chance and subtle differences in patients' characteristics. Comparison of blood samples from both trials demonstrated reduced proliferation of effector B cells, NK cells and T cells in patients treated with steroid premedication in IMpassion131⁹, suggesting potential interference with PD-(L)1 blockade responses, but this needs to be confirmed. Pembrolizumab (PD-1 blockade) plus chemotherapy has been approved for first-line treatment of patients with PD-L1 positive, metastatic TNBC, based on the KEYNOTE-355 trial⁶. While this milestone for the treatment of TNBC sets the stage for immunotherapy in TNBC, much is unclear about the immunogenic effects of chemotherapy, in-depth characterization of responses to PD-(L)1 blockade and other subgroups potentially benefitting from PD-(L)1 blockade.

Immunomodulatory strategies to improve PD-(L)1 blockade and dissection of responses to PD-(L)1 blockade in metastatic breast cancer

In **chapter 3**, we investigated the clinical and immunological effects of four short-term immune induction treatments, two weeks of cyclophosphamide, doxorubicin, cisplatin or irradiation, or a two-week waiting period, followed by PD-1 blockade, in patients with metastatic TNBC in the TONIC-trial. We show that priming the tumor microenvironment (TME) by low-dose doxorubicin and cisplatin, followed by PD-1 blockade, induced clinically meaningful responses and increased expression of immune-related gene signatures and T-cell infiltration.

In the TONIC trial, as described in **chapter 3**, radiation with 3x 8 Grey to a single metastatic lesion could not induce a more inflamed TME. Metastatic breast cancer generally has an immunosuppressive phenotype with limited T-cell infiltration and substantial heterogeneity between metastatic sites¹⁰. In another trial, a response rate of 18% was seen upon concurrent radiation and PD-1 blockade in metastatic TNBC, including radiological responses in non-irradiated lesions¹¹. Still, it is unclear what the additional effect of radiation is on these responses. In **chapter 3**, we did not observe any radiological responses in non-irradiated lesions, suggesting that

sequential administration of radiation to a single lesion followed by PD-1 blockade might not be sufficient to elicit a systemic immune response directed at each tumor site in most TNBC patients.

Focusing on the three cohorts in the TONIC trial with chemotherapy, we observed that doxorubicin and cisplatin, followed by PD-1 blockade, were most promising in inducing the expression of immune-related genes and T-cell infiltration. In the neoadjuvant NeoTRIP trial¹² with a chemotherapy backbone of platinum and taxanes, the pCR rate in the atezolizumab arm did not differ significantly from the control arm and supported by our data, this confirms a favorable role of anthracyclines in combination with PD-(L)1 blockade. While in **chapter 3**, we described platinum as one of the winners in terms of induction capacity, in **chapter 5**, we observed no apparent immunogenic effects of carboplatin. As cisplatin and carboplatin have comparable DNA-damaging capacity^{13,14}, we don't expect differences in the potency of these agents. However, patients with TNBC are generally more sensitive to platinum than patients with ER-positive disease¹⁵. This matches the findings described in **chapter 5**, in which most responses were observed in triple-negative (TN) lobular breast cancer (ILC). Validation of doxorubicin and platinum as priming strategies for improved responses to PD-(L)1 blockade in TNBC patients is required.

When the trial results were published, the TONIC trial design was based on outdated statistical considerations. Current data on PD-(L)1 blockade monotherapy (**chapter 1**) demonstrates an average response rate of 5-10% in a heavily pre-treated patient population¹⁶⁻¹⁸, instead of the hypothesized 30% of patients free-of-progression at 12 weeks in TONIC. The cisplatin cohort in TONIC was one of the winners based on the translational findings and clinical responses (23% of patients reached an objective response), but this was insufficient to continue accrual in the second stage of Simon's two-stage design. Instead, only the doxorubicin cohort was allowed to continue accrual. A new protocol for an adaptive trial was written with more realistic statistical criteria, TONIC-2 (NCT04159818). The expansion cohort of doxorubicin in TONIC-1 and the new cisplatin cohort in TONIC-2 were accompanied by a control cohort in which only PD-1 blockade was administered (Figure 1). In **chapter 3**, the most considerable immunomodulatory effects in the TME were observed after six weeks of PD-1 blockade, suggesting that PD-1 blockade could prime tumors for further immunotherapy-based treatments. To test this hypothesis, serial biopsies are taken in the PD-1 blockade monotherapy cohorts after one cycle and after three cycles of PD-1 blockade. This allows the study of early changes in the TME and to compare two weeks of PD-1 blockade versus two weeks of induction chemotherapy.

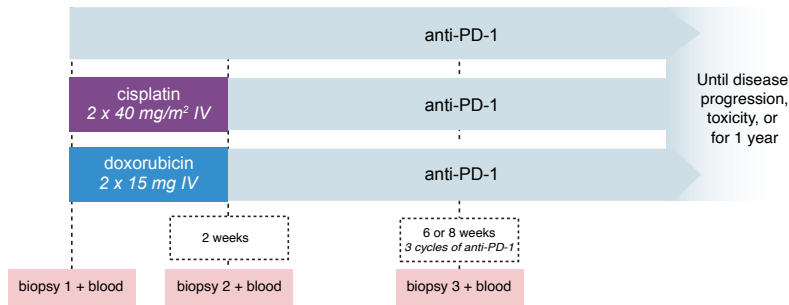


Figure 1: Flow chart design of TONIC expansion cohorts. In the expansion phase (stage II) of TONIC (NCT02499367), patients were randomized between two weeks of doxorubicin followed by PD-1 blockade vs PD-1 blockade monotherapy. In TONIC-2 (NCT04159818), patients were randomized between two weeks of cisplatin followed by PD-1 blockade vs PD-1 blockade monotherapy. Blood and biopsies of a metastatic lesion were taken at baseline, after two weeks (post-induction treatment or after one cycle of anti-PD-1) and three cycles of anti-PD-1.

Adaptive clinical trials, such as the TONIC trial and the ongoing I-SPY2 trial, allow rapid prioritization of promising therapeutic strategies¹⁹. Although this concept should be exploited further, one disadvantage of the TONIC trial is the non-comparative nature, meaning that formally we cannot claim superiority of one cohort over the other. In a commentary by Demaria *et al.*²⁰, it was argued that baseline characteristics of the included patients could have influenced the trial's outcome. While this can pose a problem, this is inevitable in small, randomized trials. As addressed in **chapter 7**, the number of patient categories instigated by stratification factors should not exceed a particular cut point to avoid imbalances in prognostic characteristics^{21,22} and stratification factors should be carefully chosen to avoid any risks involved in the use of such a factor, such as the delayed start of treatment. To tackle this, we implemented sTILs as a stratification factor in the doxorubicin expansion cohort and TONIC-2 trial (**chapter 7**). We focused the translational research in **chapter 3** by studying serial biopsies from the same patient, thereby limiting the influence of interpatient heterogeneity on these results.

Rational combinations for priming the TME of TNBC patients are needed to improve PD(L)1-blockade. Combining ICB with the potent ADCs SG and T-Dxd for rapid tumor control seems like a promising strategy. The first preliminary data on T-Dxd plus PD-L1 blockade in metastatic TNBC indeed demonstrated a high response rate (67%)²³. Other rational combinations such as ICB plus anti-angiogenic agents^{24,25} or ICB plus PARP inhibition, particularly in patients with a germline *BRCA* mutation^{26,27}, also showed promising activity. In patients with inflamed tumors, combinations of immuno-oncology (IO) agents, for example PD-L1 blockade plus inhibition of other checkpoints such as CTLA4 or LAG3, hold promise in other tumor types, such as melanoma^{28,29}. Clinical results of trials investigating anti-LAG3 in breast cancer have yet to be reported³⁰, but CTLA-4 blockade combined with PD-1 blockade seems effective in selected breast cancer groups, such as metaplastic breast

cancer³¹ and breast cancer with high mutational burden³². So far, most clinical trials focus on adding ICB to standard treatment instead of testing a biologically relevant rationale. The adaptive trial design of TONIC is ideal for the exploration of novel combinations. Since PD-(L)1 blockade will be administered standard in either the early-stage or metastatic setting, we can assume that the study landscape will focus on PD-(L)1 refractory patients. Herein, individual patient profiles should be considered, such as IO-IO combinations in patients with inflamed tumors, priming with ADCs or angiogenesis inhibitors followed by ICB for additional tumor control in patients with a high metastatic burden or PARP inhibition plus ICB in patients with germline *BRCA* mutations.

In **chapter 4**, we have characterized the systemic immune responses of the patients with metastatic TNBC treated in the TONIC trial (both the patients described in **chapter 3** and the doxorubicin cohort expansion phase of TONIC-1). We observed a consistent increase in eosinophils both in the blood and in the tumor after six weeks of PD-1 blockade across responders and not in non-responders. We used data from three other clinical cohorts to demonstrate that this increase seems tumor-type independent. *In vivo* experiments in genetically engineered mouse models (GEMMs) for breast cancer showed that eosinophils were crucial for response to ICB and that the systemic eosinophil expansion upon ICB was induced by increased bone marrow production stimulated by IL-5 producing CD4⁺ T cells. Eosinophils migrated to tumors under the influence of IL-33 and were capable of activating CD8⁺ T cells required for an ICB response. In human samples, we demonstrated a clear correlation between intratumoral increases in eosinophils and CD8⁺ T-cell infiltration and IL-33 expression in responders, suggesting a similar mechanism in patients. Finally, we showed that administration of recombinant IL-33 plus ICB improved tumor control and survival *in vivo* compared to ICB alone.

Our data provide a strong rationale for the engagement of eosinophils to improve ICB responses in relatively immunological cold tumors such as breast cancer. As IL-33 is involved in the pathogenesis of many inflammatory diseases, such as asthma, atopic dermatitis and inflammatory bowel diseases, modulation of this axis might lead to serious side effects³³. Since we show that IL-33 is essential to recruit eosinophils to the tumor site, it is tempting to speculate that local administration of IL-33 might be able to induce this effect and avoid the systemic side effects that might be inevitable upon systemic administration.

Since myeloid cells are often overlooked when studying systemic or intratumoral immune responses in cancer³⁴, partly due to their sensitivity to freezing, our study highlights the importance of studying the crosstalk between innate and adaptive immune responses. Our unique pipeline with analysis of fresh blood from trial patients is an excellent example of synergy between clinic and research laboratories and allowed in-depth evaluation of myeloid cells. The comparison of clinical and murine data in our study is hampered by differences in treatment regimens and the lack of heterogeneity between individual mice as compared to individual patients. However, the GEMMs used in this study are relatively close to the clinical

setting, since mice developed spontaneous mammary tumors in a somatic genetic background that is observed in patients as well³⁵. As nicely shown in **chapter 4**, translating preclinical findings to the clinic and back is essential to truly understand the biology of disease and the actual mechanism of the treatment administered. *In vivo* (intervention) experiments and interdepartmental collaborations are crucial herein.

In **chapter 5**, the vital importance of clinical validation of preclinical work is again nicely demonstrated. Based on preclinical and translational data, we hypothesized that carboplatin immune induction plus PD-L1 blockade could be effective in a subset of patients with metastatic ILC. In this chapter, we demonstrate the promising potential of this treatment regimen, particularly in TN-ILC and show that carboplatin plus PD-L1 blockade increased the expression of immune-related genes. One patient of interest with a durable response of at least one year had Estrogen Receptor (ER)+ ILC and had an inflamed TME before the start of carboplatin. This suggests that although rare, a subset of patients with ILC and high T-cell infiltration might benefit from PD-(L)1 blockade.

Most responses (four out of six) were seen in TN-ILC, in which a potential anti-tumor effect of carboplatin could not be excluded and was short-lived, with only one patient truly having a durable response to PD-L1 blockade. It remains to be determined why responses to PD-L1 blockade were limited in patients with advanced classical ER-positive ILC. We hypothesize that this might be due to tumor-associated macrophages, shown in **chapter 5** to be highly abundant in both primary tumors and metastatic lesions based on CIBERSORTx analysis. We also showed increased mast cells in metastatic lesions compared to matched primary tumors. Reducing the numbers of those generally immunosuppressive myeloid cells might be needed for effective T-cell activity required for an ICB response^{36,37}. While we hypothesized that carboplatin could increase type I interferons and MHC class I expression based on preclinical research^{38,39}, we did not observe significant effects of carboplatin alone on intratumoral or systemic T cells or the expression of immune-related gene signatures. This implies that induction with carboplatin is insufficient to overcome intrinsic ICB resistance observed in patients with classical, metastatic ILC and that additional strategies are needed to improve PD-L1 blockade.

As highlighted throughout **chapter 5**, clinical trials in ILC have only been initiated in the last years, with the GELATO trial being the first report of a clinical trial designed explicitly for ILC. Novel combination regimens in classical ILC are currently under evaluation⁴⁰ and include targeting genomic alterations in the *PIK3CA* pathway and *HER2*^{41,42} or targeting of the synthetic lethality between ROS1 and E-cadherin (E-cadherin loss is one of the hallmarks of ILC)⁴³. Results of the GELATO trial and the ongoing clinical trials in ILC are crucial for a better understanding of the disease's biology. This will provide novel ideas for further personalized treatment of classical ILC. Ideally, patients can be treated with different combinations based on their tumor profiles, such as PD-(L)1 blockade for patients with high T-cell infiltration; blockade of the PI3K-Akt pathway in case of activation of this

pathway by for example *PIK3CA* mutations; HER2-targeting ADCs or tyrosine kinase inhibitors in case of *HER2* alterations. International collaborations and in-depth characterization of tumors are crucial herein.

Predictive biomarkers for response to PD-(L)1 blockade in breast cancer

In **chapter 6**, we summarized the state-of-the-art biomarkers emerging for response to PD-(L)1 blockade in breast cancer. Unsurprisingly, the field rapidly evolved and there is currently more data on potential predictive biomarkers for ICB response. As described in **chapter 6**, mismatch repair deficiency (MMRd) is one of the significant determinants of response to ICB. One patient included in the TONIC trial (**chapter 3**) had an MMRd tumor and had a durable, ongoing response to PD-1 blockade⁴⁴. While rare in breast cancer⁴⁵, MMRd patients are very likely to respond to PD-(L)1 blockade⁴⁶ and, therefore, might pose ideal candidates for de-escalation of chemotherapy.

PD-L1 expression is currently the only biomarker for response to PD-(L)1 blockade in metastatic breast cancer used in the clinic. As described in **chapters 3, 5 and 6**, the presence of PD-L1 on immune cells is associated with response to PD-(L)1 blockade in metastatic breast cancer patients. However, technical limitations of PD-L1 assessments, such as differences in staining patterns based on the sample's age, different scoring methods for each antibody, high interrater variability, and costs, hamper its use in the clinic^{47,48}. Based on the KEYNOTE-355 results⁶, PD-L1 expression in metastatic TNBC should currently be assessed with antibody clone 22C3 and is scored as a combined positive score with a cut-off of 10%. Comparison between PD-L1 antibody clones in samples from IMpassion130 demonstrated higher sensitivity of 22C3, but PD-L1 positivity largely overlapped in patients benefitting from PD-(L)1 blockade independent of antibody clone⁴⁹. Limitations of the PD-L1 staining should be addressed in future research.

As elaborated in **chapter 7**, several risks are involved in using a biomarker in clinical trials or daily practice. Stromal tumor-infiltrating lymphocytes (sTILs) are a basic read-out for immune infiltration and can be assessed from a Hematoxylin & Eosin (H&E) slide⁵⁰. There is evidence that sTILs hold solid prognostic value in early TNBC⁵¹⁻⁵⁴ making sTILs an attractive biomarker in TNBC. In **chapter 7**, we describe the use of sTILs as a stratification factor in the doxorubicin expansion cohort of the TONIC trial. We demonstrate that incorporating digital slides, a novel bioinformatics platform, oversight by a central manager, and digital scoring of trained pathologists can be used to efficiently and reliably obtain sTILs scores. Data from IMpassion130 showed that high sTILs (cut-off 10%) were predictive of outcome after atezolizumab plus nab-paclitaxel⁵⁵, but as of now, no data on sTILs have been presented from the KEYNOTE-355. sTILs might also be predictive for PD-(L)1 blockade monotherapy in metastatic TNBC, as described in **chapter 3**. sTIL levels were higher in responders as compared to non-responders, which was

also observed in the KEYNOTE-86 cohorts⁵⁶. Patients with high sTILs ($\geq 5\%$) treated in the KEYNOTE-119 had a better outcome upon pembrolizumab monotherapy as compared to chemotherapy, while patients with low sTILs ($< 5\%$) had a better outcome after chemotherapy⁵⁷. These data indicate that sTILs might aid in the de-escalation of chemotherapy in favor of PD-(L)1 blockade in patients with metastatic TNBC. Future trials are needed to confirm these findings and demonstrate whether sTILs can be superior for predicting PD-(L)1 blockade response in breast cancer over PD-L1 expression.

In **chapter 3**, we found that the presence of CD8+ T cells was associated with response to PD-1 blockade in patients with metastatic TNBC, which was also seen by others^{55,58}. It is generally assumed that exhausted CD8+ T cells, characterized by high expression of PD-1 and other immune checkpoints, such as LAG3 and tumor residency markers (e.g. CXCL13), are one of the most critical cell types required for PD-(L)1 blockade response and therefore a valuable biomarker for response⁵⁹. In breast cancer, several studies investigated this T-cell subset⁶⁰⁻⁶². Still, its association with PD-(L)1 blockade response in breast cancer is not known yet and assessment of exhausted CD8+ T cells in clinical trial samples of IMpassion130, KEYNOTE-119 and KEYNOTE-355 are therefore eagerly awaited. An inflamed spatial pattern of T cells in the tumor area seems to be associated with PD-(L)1 blockade response in metastatic TNBC, as shown by Hammerl *et al.*⁶³ using the data from the TONIC-trial (**chapter 3**) and in the IMpassion130 study⁶⁴. In ER-positive breast cancer, less is known about potential biomarkers for response. One study demonstrated the predictive value of exhausted CD8+ T-cells in a small group of patients with metastatic ER-positive breast cancer⁶⁵. Additionally, data from the I-SPY2 trial implied a potential predictive role for immune-related genes in neoadjuvant pembrolizumab response in both patients with early-stage TNBC and ER-positive breast cancer⁶⁶.

Tumor mutational burden (TMB) has been associated with ICB response in other cancer types^{67,68}, but this is less clear in breast cancer⁶⁹. Using data from the TONIC-trial (**chapter 3**), McGrail *et al.* demonstrated that there was no clear cut-off for TMB that was predictive for PD-(L)1 blockade response in TNBC and other cancers in which TMB did not correlate with CD8+ T-cell infiltration⁷⁰. Interestingly, the TAPUR trial demonstrated a relatively high response rate (20%) to pembrolizumab in patients with advanced breast cancer and high TMB⁷¹. It remains to be determined, however, if these findings truly reflect a predictive role of TMB to pembrolizumab in breast cancer or if the high ORR is merely due to the inclusion of patients with a favorable prognosis. It is also unclear if other factors, such as PD-L1 expression or sTILs, had an impact on the high ORR.

Finally, host factors are important in PD-(L)1 blockade response. Lactate dehydrogenase (LDH) has been shown to correlate with rapid progression during PD-(L)1 blockade in breast cancer^{58,72}. The patients that were included in the TONIC trial (**chapter 3**) and GELATO trial (**chapter 5**) all had an LDH below two times the upper limit standard, possibly also causing a slightly higher response rate of 20%

in the TONIC trial (**chapter 3**) as compared to other cohorts. Additionally, a high tumor load has been described as negatively associated with PD-(L)1 blockade response in other cancer types^{73,74}. In this thesis, we show that this is also the case for breast cancer, with in **chapter 3** a strong association with low levels of circulating tumor marker CA15-3 in responding patients and in **chapter 5** a lower clinical benefit rate in patients with three or more metastatic sites.

Additionally, liver metastasis might be a strong indicator of intrinsic resistance to PD-(L)1 blockade. As shown in **chapter 5**, a higher clinical benefit rate was seen in ILC patients with no liver metastasis. Also, in the TONIC trial, we observed a strong correlation with a low clinical benefit rate in TNBC patients with liver metastasis (Figure 2A), which was also seen in other trials with PD-(L)1 blockade monotherapy in metastatic TNBC^{17,58}. This can be due to the strongly immunosuppressive environment induced by liver metastasis, in which tumor-associated macrophages induce apoptosis of activated CD8+ T-cells and thereby diminishing systemic CD8+ T-cell levels⁷⁵. No association was found with liver metastasis or a high number of metastatic sites and poor outcome after chemotherapy plus PD(L)1-blockade in the IMpassion130 and KEYNOTE-355, assuming that for these patients, chemotherapy as a partner for PD(L)1-blockade is needed^{6,7}. Other potential strategies in patients with liver metastasis might be the inhibition of macrophage activity by colony-stimulating receptor one receptor (CSF1R) inhibition⁷⁶.

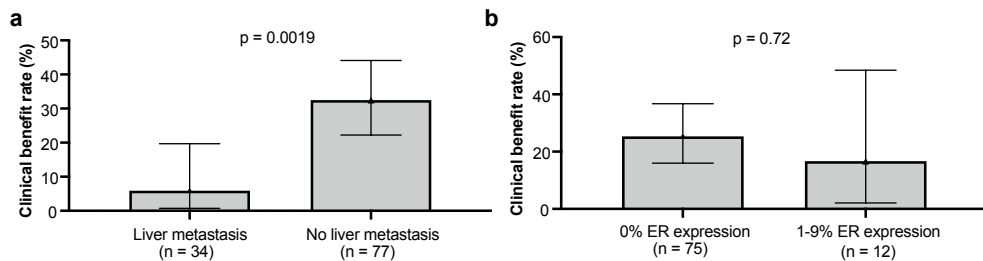


Figure 2: clinical benefit rate (CBR) in TONIC-1 (**chapter 3** plus patients included in doxorubicin expansion phase) in patients with metastatic TNBC treated with PD-1 blockade with or without liver metastasis (**a**) and with 0% vs low-positive ER expression (1-9%) assessed on a metastatic lesion (**b**). Unavailable continuous receptor status (<10%) for 24 patients. CBR consists of complete response, partial response and stable disease for 24 weeks. Error bars represent 95% confidence intervals. Statistics by Fisher's exact test.

Based on this data and the concept of the cancer immunogram⁷⁷, in which it is described that several aspects of a patient determine an effective immune response, this can also be used for de-escalation of treatment. In patients with MMRd tumors or low tumor load, no liver metastasis and high sTILs or PD-L1 expression, PD-(L)1 blockade alone can induce substantial responses without the toxicity of chemotherapy or other combinations. It must be noted that PD-(L)1 blockade generally induces only low-grade adverse events but can induce impactful and sometimes life-threatening immune-related toxicity in a minority of patients,

which as compared to chemotherapy-related toxicity might have a delayed onset⁷⁸. Especially in breast cancer patients, a substantial fraction of patients develops endocrine toxicity, such as adrenal insufficiency or thyroid dysfunction, which requires lifelong supplementation⁷⁸. However, multiple studies focusing on health-related quality-of-life (QoL) in breast cancer patients demonstrate that the addition of PD-1 blockade to chemotherapy in patients with early-stage TNBC (KEYNOTE-522)⁷⁹ or metastatic TNBC (KEYNOTE-355)⁸⁰ did not have a negative impact on QoL, as compared to patients treated with chemotherapy alone. Additionally, QoL in patients with metastatic TNBC treated with PD-1 blockade monotherapy in the KEYNOTE-119 was generally better as compared to patients treated with physician's choice chemotherapy⁸¹. These findings consolidate the role of PD(L)1-blockade in the treatment of TNBC, but future research is needed to dissect which patients experience severe side effects of PD(L)1-blockade and to develop biomarkers not only for treatment response but also for treatment toxicity.

Estrogen receptor expression and response to PD(L)1-blockade in breast cancer

This thesis highlights that responses to PD(L)1-blockade are more frequently observed in patients with TNBC than patients with ER-positive breast cancer. While the current indication for PD-(L)1 blockade is limited to TNBC, in this thesis, we demonstrate that a potential specific subgroup of ER-positive patients might benefit from PD-(L)1-blockade. In **chapter 8**, we show that patients with low and intermediate ER expression (1-50%) have a comparable immune landscape to patients with TNBC (ER 0%) in terms of TILs, CD8 T cells, PD-L1 expression and immune-related gene expression. This implies that these patients might benefit from PD(L)1-blockade. Since TONIC had a cut-off of <10% for ER-negativity, as is common practice in the Netherlands⁸², patients with low-positive ER expression (1-9%) on metastases were included. We observed no difference in clinical benefit in patients with low-positive ER expression compared to patients with 0% ER expression (Figure 2B). Exploratory analysis of the I-SPY2 trial demonstrated that in ER-positive patients, lower expression of *ESR1* and *PGR* correlated with higher pCR rates after the addition of neo-adjuvant durvalumab plus olaparib or pembrolizumab^{66,83} and in patients with metastatic ER-positive breast cancer low ER signaling associated with response to pembrolizumab plus eribulin⁸⁴. Assuming that others will confirm that patients with low and intermediate ER expression potentially benefit from PD-(L)1 blockade, novel trials or baskets within existing clinical trials could accelerate and potentially prioritize PD-(L)1 blockade for patients with low or intermediate ER expression in combination with endocrine treatment. Since severe toxicity of ICB with the current standard therapy in metastatic ER-positive breast cancer, CDK4/6 inhibitors, is seen, this combination will not be feasible⁸⁵.

In **chapter 8**, we observed a correlation between mast cell presence and higher ER expression. In contrast, in **chapter 5**, we saw higher levels of mast cells in metastatic lesions compared to primary tumors. In the durvalumab-olaparib and

pembrolizumab arm of the I-SPY2 trial, mast cells were significantly associated with non-pCR in the ER-positive subgroup^{66,83} and mast cells have been implied in residual disease after neo-adjuvant chemotherapy⁸⁶. Immune cells, particularly myeloid cells such as macrophages and mast cells, express ER and are therefore sensitive to estrogen signaling and inherently to estrogen deprivation treatments³⁷. While the complex crosstalk between estrogen signaling and the immune system needs to be fully elucidated, an essential relationship between immunosuppressive myeloid cells and ER signaling with potentially detrimental effects on effector T-cell functioning and ICB response is implied⁸⁷. However, a subgroup of patients with ER-positive breast cancer responds to PD-(L)1 blockade, particularly in the early-stage setting^{83,88,89}, implying that some breast tumors are sensitive to T-cell killing regardless of the potential presence of myeloid cells and ER signaling in immune cells. Therefore, we want to challenge the traditional paradigm of dividing HER2-negative breast cancer into ER-positive and TNBC in light of their potential to respond to PD-(L)1 blockade. As nicely proposed by Wolf and colleagues⁶⁶, novel treatment options require a new definition of breast cancer subtypes, with immune-enriched breast cancer being the subtype most likely to benefit from PD-(L)1 blockade. Based on the data described in this thesis, this HER2-negative immune-enriched subgroup will mainly consist of patients with MMRd breast cancers, TNBC, breast tumors with low and intermediate ER expression and potentially a subset of ILC patients.

Future perspectives

Leveraging translational research of clinical trial samples described in this thesis is essential to better understand disease biology and treatment response. On-treatment samples allow for in-depth characterization of treatment responses important for rational combination therapy. For example, as we show in **chapter 4** of this thesis, the dynamic changes in eosinophil levels in the blood and tumors observed in patients with a clinical response to PD-1 blockade were an important piece of the puzzle on how eosinophils are a crucial mediator in CD8+ T-cell activation. Additionally, biopsies from a progressive lesion after an initial response to PD-1 blockade are crucial to better understand acquired resistance to immunotherapy, such as potentially targetable acquired mutations⁹⁰. Novel techniques now allow the high-dimensional investigation of the TME of breast cancer. Using techniques for in situ profiling of tumors, for example, multi-parameter immunohistochemistry⁹¹, mass cytometry⁹² or multibeam ion imaging (MIBI)⁹³, provides information on the distance between tumor cells and effector immune cells, abundance, and function of immune cells, including myeloid cells. Additionally, single-cell RNA sequencing of tumor digests might aid in understanding cell states to further clarify the mechanisms of PD-(L)1 blockade^{62,94}. Using computer-based algorithms for scoring of this complex characterization of the immune microenvironment and a simple read-out such as sTILs⁹⁵ will help to avoid interrater variability common in pathology-based assessments.

Future research on IO in breast cancer should focus on rational biomarkers and combination treatments. Essential questions to answer are: 1) for which early-stage breast cancer patients is PD-1 blockade monotherapy sufficient for curation; 2) how can we rationally combine or sequence PD-1 blockade with other agents in those patients not likely to benefit from PD-1 blockade, such as CTLA-4 blockade, ADC's, angiogenesis inhibition or PARP inhibition; 3) which predictive biomarkers are associated with response to PD-1 blockade in early-stage and/or metastatic TNBC and which patients are likely to develop immune-related toxicity; 4) which IO agents, such as anti-CTLA4 or anti-LAG3, synergize with PD-1 blockade clinically and immunologically and is this sufficient to overcome resistance after previous treatment with PD-1 blockade; 5) can we further exploit the translational findings from this thesis into (pre)clinical trials by for example: engaging eosinophils via local stimulation of IL-33; targeting macrophages in breast cancer patients with liver metastasis or inhibiting mast cells in patients with ER-positive breast cancer. I am optimistic that by further extensive translational research and (international) collaboration between preclinical and clinical researchers, we will rapidly gain a better understanding of PD-(L)1 blockade in breast cancer and clinical trials with novel rational (combination) treatments will inevitably emerge.

References

1. Kassam, F. et al. Survival outcomes for patients with metastatic triple-negative breast cancer: implications for clinical practice and trial design. *Clinical breast cancer* 9 (1), 29-33, 2009.
2. den Brok, W. D. et al. Survival with metastatic breast cancer based on initial presentation, *de novo* versus relapsed. *Breast Cancer Res Treat* 161 (3), 549-556, 2017.
3. Robson, M. et al. Olaparib for Metastatic Breast Cancer in Patients with a Germline BRCA Mutation. *New England Journal of Medicine* 377 (6), 523-533, 2017.
4. Bardia, A. et al. Sacituzumab Govitecan in Metastatic Triple-Negative Breast Cancer. *New England Journal of Medicine* 384 (16), 1529-1541, 2021.
5. Modi, S. et al. Trastuzumab Deruxtecan in Previously Treated HER2-Low Advanced Breast Cancer. *New England Journal of Medicine*, 2022.
6. Cortes, J. et al. Pembrolizumab plus chemotherapy versus placebo plus chemotherapy for previously untreated locally recurrent inoperable or metastatic triple-negative breast cancer (KEYNOTE-355): a randomised, placebo-controlled, double-blind, phase 3 clinical trial. *Lancet (London, England)* 396 (10265), 1817-1828, 2020.
7. Schmid, P. et al. Atezolizumab and Nab-Paclitaxel in Advanced Triple-Negative Breast Cancer. *N Engl J Med*, 2018.
8. Miles, D. et al. Primary results from IMpassion131, a double-blind, placebo-controlled, randomised phase III trial of first-line paclitaxel with or without atezolizumab for unresectable locally advanced/metastatic triple-negative breast cancer. *Annals of Oncology* 32 (8), 994-1004, 2021.
9. Molinero, L. et al. Impact of steroid premedication on atezolizumab (atezo)-induced immune cell activation: A comparative analysis of IMpassion130 and IMpassion131 peripheral blood mononuclear cells (PBMCs). *Journal of Clinical Oncology* 40 (16_suppl), 1083-1083, 2022.
10. Szekely, B. et al. Immunological differences between primary and metastatic breast cancer. *Ann Oncol* 29 (11), 2232-2239, 2018.
11. Ho, A. Y. et al. A phase 2 clinical trial assessing the efficacy and safety of pembrolizumab and radiotherapy in patients with metastatic triple-negative breast cancer. *Cancer* 126 (4), 850-860, 2020.
12. Gianni, L. et al. Pathologic complete response (pCR) to neoadjuvant treatment with or without atezolizumab in triple-negative, early high-risk and locally advanced breast cancer: NeoTRIP Michelangelo randomized study. *Annals of Oncology* 33 (5), 534-543, 2022.
13. Unger, F. T., Klasen, H. A., Tchartchian, G., de Wilde, R. L. & Witte, I. DNA damage induced by cis- and carboplatin as indicator for *in vitro* sensitivity of ovarian carcinoma cells. *BMC cancer* 9 (1), 359, 2009.
14. Dasari, S. & Tchounwou, P. B. Cisplatin in cancer therapy: molecular mechanisms of action. *Eur J Pharmacol* 740, 364-378, 2014.
15. Iwase, M. et al. Long-term survival analysis of addition of carboplatin to neoadjuvant chemotherapy in HER2-negative breast cancer. *Breast Cancer Res Treat* 180 (3), 687-694, 2020.
16. Dirix, L. Y. et al. Avelumab, an anti-PD-L1 antibody, in patients with locally advanced or metastatic breast cancer: a phase 1b JAVELIN Solid Tumor study. *Breast Cancer Res Treat* 167 (3), 671-686, 2018.
17. Adams, S. et al. Phase 2 study of pembrolizumab (pembro) monotherapy for previously treated metastatic triple-negative breast cancer (mTNBC): KEYNOTE-086 cohort A. *Journal of Clinical Oncology* 35 (15_suppl), 1008-1008, 2017.
18. Winer, E. P. et al. Pembrolizumab versus investigator-choice chemotherapy for metastatic triple-negative breast cancer (KEYNOTE-119): a randomised, open-label, phase 3 trial. *The Lancet. Oncology* 22 (4), 499-511, 2021.
19. Berry, D. A. Adaptive clinical trials in oncology. *Nature Reviews Clinical Oncology* 9 (4), 199-207, 2012.
20. Demaria, S., Romano, E., Brackstone, M. & Formenti, S. C. Immune induction strategies to enhance responses to PD-1 blockade: lessons from the TONIC trial. *Journal for ImmunoTherapy of Cancer* 7 (1), 318, 2019.
21. Therneau, T. M. How many stratification factors are “too many” to use in a randomization plan? *Control Clin Trials* 14 (2), 98-108, 1993.
22. Silcocks, P. How many strata in an RCT? A flexible approach. *British journal of cancer* 106 (7), 1259-1261, 2012.

23. Schmid, P. et al. BEGONIA: Phase 1b/2 study of durvalumab (D) combinations in locally advanced/metastatic triple-negative breast cancer (TNBC)—Initial results from arm 1, d+paclitaxel (P), and arm 6, d+trastuzumab deruxtecan (T-DXd). *Journal of Clinical Oncology* 39 (15_suppl), 1023-1023, 2021.
24. Lwin, Z. et al. LBA41 LEAP-005: Phase II study of lenvatinib (len) plus pembrolizumab (pembro) in patients (pts) with previously treated advanced solid tumours. *Annals of Oncology* 31, S1170, 2020.
25. Chen, L. et al. Combination of famitinib with camrelizumab plus nab-paclitaxel as first-line treatment for patients with immunomodulatory advanced triple-negative breast cancer (FUTURE-C-PLUS): A prospective, single-arm, phase 2 study. *American Society of Clinical Oncology conference* 2021; *J Clin Oncol* 39, 2021.
26. Domchek, S. M. et al. Olaparib and durvalumab in patients with germline BRCA-mutated metastatic breast cancer (MEDIOLA): an open-label, multicentre, phase 1/2, basket study. *The Lancet Oncology* 21 (9), 1155-1164, 2020.
27. Vinayak, S. et al. Open-label Clinical Trial of Niraparib Combined With Pembrolizumab for Treatment of Advanced or Metastatic Triple-Negative Breast Cancer. *JAMA Oncol* 5 (8), 1132-1140, 2019.
28. Larkin, J. et al. Five-Year Survival with Combined Nivolumab and Ipilimumab in Advanced Melanoma. *New England Journal of Medicine* 381 (16), 1535-1546, 2019.
29. Tawbi, H. A. et al. Relatlimab and Nivolumab versus Nivolumab in Untreated Advanced Melanoma. *New England Journal of Medicine* 386 (1), 24-34, 2022.
30. Bianchini, G., De Angelis, C., Licata, L. & Gianni, L. Treatment landscape of triple-negative breast cancer - expanded options, evolving needs. *Nature reviews. Clinical oncology* 19 (2), 91-113, 2022.
31. Adams, S. et al. A Multicenter Phase II Trial of Ipilimumab and Nivolumab in Unresectable or Metastatic Metaplastic Breast Cancer: Cohort 36 of Dual Anti-CTLA-4 and Anti-PD-1 Blockade in Rare Tumors (DART, SWOG S1609). *Clinical cancer research : an official journal of the American Association for Cancer Research* 28 (2), 271-278, 2022.
32. Barroso-Sousa, R. et al. Abstract GS2-10: Nimbus: A phase 2 trial of nivolumab plus ipilimumab for patients with hypermutated her2-negative metastatic breast cancer (MBC). *Cancer research* 82 (4_Supplement), GS2-10-GS12-10, 2022.
33. Liew, F. Y., Girard, J.-P. & Turnquist, H. R. Interleukin-33 in health and disease. *Nature Reviews Immunology* 16 (11), 676-689, 2016.
34. Demaria, O. et al. Harnessing innate immunity in cancer therapy. *Nature* 574 (7776), 45-56, 2019.
35. Sflomos, G. et al. Atlas of Lobular Breast Cancer Models: Challenges and Strategic Directions. *Cancers* 13 (21), 5396, 2021.
36. Mehta, A. K., Kadel, S., Townsend, M. G., Oliwa, M. & Guerriero, J. L. Macrophage Biology and Mechanisms of Immune Suppression in Breast Cancer. *Frontiers in immunology* 12, 2021.
37. Chakraborty, B. et al. Inhibition of estrogen signaling in myeloid cells increases tumor immunity in melanoma. *The Journal of clinical investigation* 131 (23), 2021.
38. Schadt, L. et al. Cancer-Cell-Intrinsic cGAS Expression Mediates Tumor Immunogenicity. *Cell Rep* 29 (5), 1236-1248.e1237, 2019.
39. Wan, S. et al. Chemotherapeutics and radiation stimulate MHC class I expression through elevated interferon-beta signaling in breast cancer cells. *PloS one* 7 (3), e32542, 2012.
40. Van Baelen, K. et al. Current and future diagnostic and treatment strategies for patients with invasive lobular breast cancer. *Annals of Oncology*, 2022.
41. Ciriello, G. et al. Comprehensive Molecular Portraits of Invasive Lobular Breast Cancer. *Cell* 163 (2), 506-519, 2015.
42. Michaut, M. et al. Integration of genomic, transcriptomic and proteomic data identifies two biologically distinct subtypes of invasive lobular breast cancer. *Sci Rep* 6, 18517-18517, 2016.
43. Bajrami, I. et al. E-Cadherin/ROS1 Inhibitor Synthetic Lethality in Breast Cancer. *Cancer Discovery* 8 (4), 498-515, 2018.
44. Kok, M. et al. Profound Immunotherapy Response in Mismatch Repair-Deficient Breast Cancer. *JCO Precision Oncology* 1 (1), 1-3, 2017.
45. Davies, H. et al. Whole-Genome Sequencing Reveals Breast Cancers with Mismatch Repair Deficiency. *Cancer research*, 2017.
46. Le, D. T. et al. Mismatch repair deficiency predicts response of solid tumors to PD-1 blockade. *Science* 357 (6349), 409-413, 2017.

47. Gonzalez-Ericsson, P. I. et al. The path to a better biomarker: application of a risk management framework for the implementation of PD-L1 and TILs as immuno-oncology biomarkers in breast cancer clinical trials and daily practice. *J Pathol* 250 (5), 667-684, 2020.
48. Badve, S. S. et al. Determining PD-L1 Status in Patients With Triple-Negative Breast Cancer: Lessons Learned From IMpassion130. *JNCI: Journal of the National Cancer Institute* 114 (5), 664-675, 2021.
49. Rugo, H. S. et al. PD-L1 Immunohistochemistry Assay Comparison in Atezolizumab plus nab-Paclitaxel-Treated Advanced Triple-Negative Breast Cancer. *J Natl Cancer Inst* 113 (12), 1733-1743, 2021.
50. Salgado, R. et al. The evaluation of tumor-infiltrating lymphocytes (TILs) in breast cancer: recommendations by an International TILs Working Group 2014. *Annals of Oncology* 26 (2), 259-271, 2015.
51. Loi, S. et al. Tumor infiltrating lymphocyte stratification of prognostic staging of early-stage triple negative breast cancer. *npj Breast Cancer* 8 (1), 3, 2022.
52. Loi, S. et al. Tumor-Infiltrating Lymphocytes and Prognosis: A Pooled Individual Patient Analysis of Early-Stage Triple-Negative Breast Cancers. *Journal of clinical oncology : official journal of the American Society of Clinical Oncology* 37 (7), 559-569, 2019.
53. Park, J. H. et al. Prognostic value of tumor-infiltrating lymphocytes in patients with early-stage triple-negative breast cancers (TNBC) who did not receive adjuvant chemotherapy. *Annals of Oncology*, 2019.
54. de Jong, V. M. T. et al. Prognostic Value of Stromal Tumor-Infiltrating Lymphocytes in Young, Node-Negative, Triple-Negative Breast Cancer Patients Who Did Not Receive (neo)Adjuvant Systemic Therapy. *Journal of Clinical Oncology*, JCO.21.01536, 2022.
55. Emens, L. A. et al. Atezolizumab and nab-Paclitaxel in Advanced Triple-Negative Breast Cancer: Biomarker Evaluation of the IMpassion130 Study. *JNCI: Journal of the National Cancer Institute*, 2021.
56. Loi, S. et al. LBA13 - Relationship between tumor infiltrating lymphocyte (TIL) levels and response to pembrolizumab (pembro) in metastatic triple-negative breast cancer (mTNBC): Results from KEYNOTE-086. *European Society of Medical Oncology conference 2017; Ann Oncol* 28 (suppl_5), v605-v649, 2017.
57. Loi, S. et al. Abstract PD5-03: Relationship between tumor-infiltrating lymphocytes (TILs) and outcomes in the KEYNOTE-119 study of pembrolizumab vs chemotherapy for previously treated metastatic triple-negative breast cancer (mTNBC). *Cancer research* 80 (4_Supplement), PD5-03-PD05-03, 2020.
58. Emens, L. A. et al. Long-term Clinical Outcomes and Biomarker Analyses of Atezolizumab Therapy for Patients With Metastatic Triple-Negative Breast Cancer: A Phase 1 Study. *JAMA Oncol*, 2018.
59. Thommen, D. S. et al. A transcriptionally and functionally distinct PD-1(+) CD8(+) T cell pool with predictive potential in non-small-cell lung cancer treated with PD-1 blockade. *Nat Med* 24 (7), 994-1004, 2018.
60. Bassez, A. et al. A single-cell map of intratumoral changes during anti-PD1 treatment of patients with breast cancer. *Nature Medicine* 27 (5), 820-832, 2021.
61. Savas, P. et al. Single-cell profiling of breast cancer T cells reveals a tissue-resident memory subset associated with improved prognosis. *Nat Med* 24 (7), 986-993, 2018.
62. Zhang, Y. et al. Single-cell analyses reveal key immune cell subsets associated with response to PD-L1 blockade in triple-negative breast cancer. *Cancer cell* 39 (12), 1578-1593.e1578, 2021.
63. Hammerl, D. et al. Spatial immunophenotypes predict response to anti-PD1 treatment and capture distinct paths of T cell evasion in triple negative breast cancer. *Nature Communications* 12 (1), 5668, 2021.
64. Emens, L. A. et al. The tumor microenvironment (TME) and atezolizumab + nab-paclitaxel (A+nP) activity in metastatic triple-negative breast cancer (mTNBC): IMpassion130. *Journal of Clinical Oncology* 39 (15_suppl), 1006-1006, 2021.
65. Terranova-Barberio, M. et al. Exhausted T cell signature predicts immunotherapy response in ER-positive breast cancer. *Nat Commun* 11 (1), 3584, 2020.
66. Wolf, D. M. et al. Redefining breast cancer subtypes to guide treatment prioritization and maximize response: Predictive biomarkers across 10 cancer therapies. *Cancer cell* 40 (6), 609-623.e606, 2022.
67. Marabelle, A. et al. Association of tumour mutational burden with outcomes in patients with advanced solid tumours treated with pembrolizumab: prospective biomarker analysis of the multicohort, open-label, phase 2 KEYNOTE-158 study. *The Lancet. Oncology* 21 (10), 1353-1365, 2020.

68. Yarchoan, M., Hopkins, A. & Jaffee, E. M. Tumor Mutational Burden and Response Rate to PD-1 Inhibition. *N Engl J Med* 377 (25), 2500-2501, 2017.
69. Samstein, R. M. et al. Tumor mutational load predicts survival after immunotherapy across multiple cancer types. *Nat Genet* 51 (2), 202-206, 2019.
70. McGrail, D. J. et al. High tumor mutation burden fails to predict immune checkpoint blockade response across all cancer types. *Annals of Oncology* 32 (5), 661-672, 2021.
71. Alva, A. S. et al. Pembrolizumab in Patients With Metastatic Breast Cancer With High Tumor Mutational Burden: Results From the Targeted Agent and Profiling Utilization Registry (TAPUR) Study. *Journal of clinical oncology : official journal of the American Society of Clinical Oncology* 39 (22), 2443-2451, 2021.
72. Nanda, R. et al. Pembrolizumab in Patients With Advanced Triple-Negative Breast Cancer: Phase Ib KEYNOTE-012 Study. *Journal of clinical oncology : official journal of the American Society of Clinical Oncology* 34 (21), 2460-2467, 2016.
73. Chardin, D. et al. Baseline metabolic tumor volume as a strong predictive and prognostic biomarker in patients with non-small cell lung cancer treated with PD1 inhibitors: a prospective study. *J Immunother Cancer* 8 (2), 2020.
74. Joseph, R. W. et al. Baseline Tumor Size Is an Independent Prognostic Factor for Overall Survival in Patients With Melanoma Treated With Pembrolizumab. *Clinical Cancer Research*, 2018.
75. Yu, J. et al. Liver metastasis restrains immunotherapy efficacy via macrophage-mediated T cell elimination. *Nat Med* 27 (1), 152-164, 2021.
76. Salvagno, C. et al. Therapeutic targeting of macrophages enhances chemotherapy efficacy by unleashing type I interferon response. *Nat Cell Biol* 21 (4), 511-521, 2019.
77. Blank, C. U., Haanen, J. B., Ribas, A. & Schumacher, T. N. CANCER IMMUNOLOGY. The “cancer immunogram”. *Science* 352 (6286), 658-660, 2016.
78. Gumusay, O., Callan, J. & Rugo, H. S. Immunotherapy toxicity: identification and management. *Breast Cancer Res Treat* 192 (1), 1-17, 2022.
79. Dent, R. A. et al. 135MO HRQoL with neoadjuvant pembrolizumab + chemotherapy vs placebo + chemotherapy, followed by adjuvant pembrolizumab vs placebo for early-stage TNBC: Results from KEYNOTE-522. *Annals of Oncology* 33, S600-S601, 2022.
80. Cescon, D. W. et al. 164O Health-related quality of life (HRQoL) with pembrolizumab (pembro) + chemotherapy (chemo) vs placebo (pbo) + chemo as 1L treatment for advanced triple-negative breast cancer (TNBC): Results from KEYNOTE-355. *Annals of Oncology* 33, S197-S198, 2022.
81. Schmid, P. et al. 141P Impact of pembrolizumab versus chemotherapy on health-related quality of life in patients with metastatic triple negative breast cancer. *Annals of Oncology* 31, S65-S66, 2020.
82. Specialisten, F. M. Richtlijndatabase Borstkanker. Consulted at 31-03-2022.
83. Pusztai, L. et al. Durvalumab with olaparib and paclitaxel for high-risk HER2-negative stage II/III breast cancer: Results from the adaptively randomized I-SPY2 trial. *Cancer cell* 39 (7), 989-998. e985, 2021.
84. Keenan, T. E. et al. Molecular correlates of response to eribulin and pembrolizumab in hormone receptor-positive metastatic breast cancer. *Nat Commun* 12 (1), 5563, 2021.
85. Jerusalem, G. et al. 92MO Neoadjuvant nivolumab (NIVO) + palbociclib (PALBO) + anastrozole (ANA) for estrogen receptor-positive (ER+)/human epidermal growth factor receptor 2-negative (HER2-) primary breast cancer (BC): CheckMate 7A8. *Annals of Oncology* 33, S165-S166, 2022.
86. Li, X. et al. Immune profiling of pre- and post-treatment breast cancer tissues from the SWOG S0800 neoadjuvant trial. *J Immunother Cancer* 7 (1), 88, 2019.
87. Segovia-Mendoza, M. & Morales-Montor, J. Immune Tumor Microenvironment in Breast Cancer and the Participation of Estrogen and Its Receptors in Cancer Physiopathology. *Frontiers in immunology* 10, 2019.
88. Dieci, M. V. et al. Neoadjuvant Chemotherapy and Immunotherapy in Luminal B-like Breast Cancer: Results of the Phase II GIADA Trial. *Clinical Cancer Research* 28 (2), 308-317, 2022.
89. Nanda, R. et al. Effect of Pembrolizumab Plus Neoadjuvant Chemotherapy on Pathologic Complete Response in Women With Early-Stage Breast Cancer: An Analysis of the Ongoing Phase 2 Adaptively Randomized I-SPY2 Trial. *JAMA Oncology* 6 (5), 676-684, 2020.
90. Zaretsky, J. M. et al. Mutations Associated with Acquired Resistance to PD-1 Blockade in Melanoma. *New England Journal of Medicine* 375 (9), 819-829, 2016.
91. Tsujikawa, T. et al. Quantitative Multiplex Immunohistochemistry Reveals Myeloid-Inflamed Tumor-Immune Complexity Associated with Poor Prognosis. *Cell Rep* 19 (1), 203-217, 2017.

92. Bianchini, G. et al. Abstract GS1-00: Single-cell spatial analysis by imaging mass cytometry and immunotherapy response in triple-negative breast cancer (TNBC) in the NeoTRIPaPDL1 trial. *Cancer research* 82 (4_Supplement), GS1-00-GS01-00, 2022.
93. Keren, L. et al. A Structured Tumor-Immune Microenvironment in Triple Negative Breast Cancer Revealed by Multiplexed Ion Beam Imaging. *Cell* 174 (6), 1373-1387.e1319, 2018.
94. Bassez, A. et al. A single-cell map of intratumoral changes during anti-PD1 treatment of patients with breast cancer. *Nat Med* 27 (5), 820-832, 2021.
95. Amgad, M. et al. Report on computational assessment of Tumor Infiltrating Lymphocytes from the International Immuno-Oncology Biomarker Working Group. *npj Breast Cancer* 6 (1), 16, 2020.

Appendix

Nederlandse samenvatting
List of publications
Curriculum Vitae
Acknowledgements/dankwoord

Nederlandse samenvatting

In de laatste jaren wordt steeds duidelijker dat borstkanker meer omvat dan alleen de tumorcellen zelf. Het disfunctionerende immuunsysteem speelt een belangrijke rol in de ontwikkeling van borstkanker en eventuele uitzaaiingen hiervan. Uit onderzoek is gebleken dat het aantal immuuncellen dat aanwezig is in borsttumoren voorspellend is voor de uitkomst van patiënten met een vorm van borstkanker die lastig te behandelen is, namelijk triple-negatieve borstkanker (TNBC). Bij deze vorm van borstkanker, gekarakteriseerd door de afwezigheid van hormoonreceptoren en de HER2 groeifactor receptor (vlag op de tumorcellen), was er tot voor kort geen behandeling mogelijk specifiek gericht op dit subtype. Hierbij was chemotherapie de enige optie met veel bijwerkingen tot gevolg. Echter, sinds de start van mijn promotie 5 jaar geleden is er een enorme sprong gemaakt in de manier waarop we tegen TNBC aankijken. Omdat is gebleken dat het aantal immuuncellen en het aantal DNA-fouten die potentieel een aanwakkerend effect hebben op het immuunsysteem relatief hoog is in TNBC, bleek immuuntherapie effectief te zijn in een substantiële groep patiënten. Deze vorm van therapie, zogenoemde checkpoint blokkade, blokkeert de rem die tumorcellen aan het immuunsysteem doorgeven (de interactie tussen PD-L1 en PD-1), waardoor immuuncellen, zoals T cellen, de tumorcellen beter herkennen en kunnen opruimen. In het eerste deel van dit proefschrift wordt onderzocht hoe de werking van immuuntherapie optimaal kan worden benut om de uitkomsten hiervan te verbeteren voor patiënten met uitgezaaide borstkanker. In het tweede deel van dit proefschrift wordt onderzocht hoe we patiënten beter kunnen selecteren die een grotere kans hebben op een goede respons op immuuntherapie.

In **hoofdstuk 2** bediscussiëren we een vergelijking tussen twee grote fase III studies met tegenstrijdige resultaten. In deze studies werd onderzocht of immuuntherapie (PD-L1 blokkade) in combinatie met chemotherapie beter werkte dan chemotherapie met placebo bij patiënten met uitgezaaide TNBC. Uit de IMpassion130 studie bleek dat PD-L1 blokkade in combinatie met nab-paclitaxel effectief was in patiënten met expressie van PD-L1. Echter, uit IMpassion131, waarin paclitaxel met PD-L1 blokkade of placebo werd gegeven, werd dit verschil niet gevonden. Dit kan deels verklaard worden door subtiele verschillen in patiënt karakteristieken en toeval, maar heeft mogelijk ook te maken met verschillende effecten op het immuunsysteem tussen paclitaxel en nab-paclitaxel en het gebruik van immunosuppressiva in de IMpassion131. Hoewel de IMpassion130 resultaten veelbelovend waren, is immuuntherapie met chemotherapie voor patiënten met uitgezaaide PD-L1 positieve TNBC pas definitief goedgekeurd op basis van de resultaten van de KEYNOTE-355 studie. In deze studie werd tevens aangetoond dat immuuntherapie (PD-1 blokkade) in combinatie met chemotherapie effectief is in patiënten met uitgezaaide PD-L1 positieve TNBC. Omdat deze studie wel was opgezet om de effectiviteit aan te tonen in deze subgroep, in tegenstelling tot de IMpassion130, werd pas op basis van de KEYNOTE-355 de behandeling goedgekeurd.

In de bovengenoemde fase III studies werd immuuntherapie gecombineerd met chemotherapie. Dit leidt echter tot veel bijwerkingen voor patiënten en in potentie een vernietigend effect van de chemotherapie op circulerende en tumor-specifieke immuuncellen. Deze effecten lijken echter afhankelijk van de dosering van de chemotherapie, waarbij uit eerder onderzoek is gebleken dat lage dosis chemotherapie juist een positief effect op het immuunsysteem kan hebben. Om te testen of lage dosis chemotherapie of bestraling het immuunsysteem kan stimuleren om de werking van immuuntherapie te verbeteren werd de TONIC-trial opgezet, waarvan de resultaten beschreven worden in **hoofdstuk 3**. In deze studie werden 67 patiënten met uitgezaaide TNBC behandeld met een kortdurende voorbehandeling van twee weken, met ofwel: 1) adriamycine; 2) cisplatin; 3) cyclofosamide; 4) bestraling van een uitzaaiing; 5) een wachtperiode, gevolgd door tweewekelijks PD-1 blokkade (nivolumab). Er werd bloed en tumormateriaal afgenomen voor de start van de behandeling, na de twee weken voorbehandeling en na 6 weken immuuntherapie. De belangrijkste bevinding was dat de meeste patiënten die goed reageerden op de immuuntherapie een voorbehandeling hadden gehad met ofwel adriamycine of cisplatin. Tevens zagen we dat behandeling met adriamycine of cisplatin gevolgd door immuuntherapie zorgde voor verhoogde expressie van immuun-gerelateerde genen en meer T-cel infiltratie. Hoewel de verschillende armen in de studie niet direct met elkaar vergeleken kunnen worden, duiden deze resultaten erop dat adriamycine en cisplatin een mogelijk stimulerend effect hebben op het immuunsysteem bij patiënten met TNBC met als gevolg een betere respons op immuuntherapie. Om dit verder te onderzoeken en de resultaten te valideren zijn er in deze twee behandelarmen meer patiënten geïnccludeerd (tweede deel van de TONIC-1 studie en in de TONIC-2 studie).

Translatieel onderzoek van patiënten samples zoals bloed en het tumormateriaal, is essentieel om een beter begrip te krijgen van hoe immuuntherapie bij borstkanker werkt. In **hoofdstuk 4** wordt beschreven dat eosinofielen, een type immuun cel welke normaliter betrokken is bij het opruimen van parasieten maar ook bij astma en allergieën, noodzakelijk zijn voor een effectieve respons op immuuntherapie. We vonden dat in patiënten met uitgezaaide TNBC (geïnccludeerd in de TONIC-studie, beschreven in **hoofdstuk 3**) die goed reageerden op PD-1 blokkade er een stijging was van het aantal eosinofielen in het bloed en in de tumoren. Dit was echter niet te zien in patiënten die geen respons hadden op de immuuntherapie. Ook zagen we dat de stijging van de eosinofielen samenging met een stijging van CD8+ T cellen in de tumoren, waarbij deze killer immuuncellen zorgen voor het uiteindelijke opruimen van de tumorcellen. Om te bekijken wat de precieze rol is van de eosinofielen hebben we gebruikt gemaakt van muismodellen welke veel overeenkomsten hebben met hoe borstkanker zich gedraagt in patiënten. In deze muizen zagen we hetzelfde patroon als bij de patiënten, eosinofielen stegen in het bloed en in de tumoren in de muizen die behandeld waren met PD-1 blokkade met chemotherapie. Belangrijker nog, bij het blokkeren van de eosinofielen bleek er geen respons meer op te treden op de behandeling. Dit bleek te berusten op activatie van CD4+ T cellen na behandeling met immuuntherapie, waarbij deze helper immuuncellen IL-5 produceren. Dit stofje zorgt voor verhoogde aanmaak in het beenmerg van eosinofielen welke vervolgens in de circulatie terecht komen. Eosinofielen komen onder invloed van IL-33 in de

tumoren waar ze CD8+ T cellen kunnen activeren om uiteindelijk de effectiviteit van immuuntherapie te verbeteren. Het onderzoek beschreven in **hoofdstuk 4** maakt duidelijk dat deze cascade in zowel patiënten met kanker als muismodellen essentieel is voor een effectieve respons op immuuntherapie. Vervolgonderzoek in studies waarin deze cascade gestimuleerd kan worden, kan mogelijk leiden tot nieuwe doorbraken om immuuntherapie voor kankerpatiënten te verbeteren.

In **hoofdstuk 5** beschrijven we de resultaten van de GELATO-studie, waarin patiënten met uitgezaaide lobulaire borstkanker werden behandeld met PDL1-blokkade (atezolizumab) in combinatie met chemotherapie (carboplatin). Lobulaire borstkanker ontstaat vanuit de melkklieren en gedraagt zich opmerkelijk anders dan borstkanker uitgaande van de melkgangen. Patiënten met uitgezaaide lobulaire borstkanker hebben een kortere overlevingsduur en vaker uitzaaiingen in de botten en in het maag-darm kanaal. Uit eerder onderzoek is gebleken dat een gedeelte van de lobulaire borsttumoren hoge expressie heeft van immuun-gerelateerde genen en dat immuuntherapie daardoor mogelijk een grotere kans heeft om aan te slaan in deze groep. Omdat lage dosis chemotherapie een positief effect kan hebben op het immuunsysteem (zie **hoofdstuk 2**) werd lage dosis carboplatin voor 12 weken met immuuntherapie gecombineerd waarna de immuuntherapie alleen verder gegeven werd. Zes van de 23 patiënten hadden enige respons op de behandeling, waarvan vier patiënten langer dan een halfjaar en een patiënt zelfs langer dan een jaar. Vier patiënten van de zes met een respons hadden borstkanker zonder expressie van de hormoonreceptor, TNBC. In tumormateriaal afgenomen van een uitzaaiing zagen we een stijging van CD8+ T cellen en hogere genexpressie van verschillende markers voor een effectieve immuunrespons na 6 weken combinatiebehandeling. Deze studie toont dat PD-L1 blokkade met chemotherapie effectief is in met name patiënten met TNBC, wat aansluit bij de reeds bestaande goedkeuring van deze behandeling voor deze patiëntengroep.

In het tweede deel van dit proefschrift wordt de focus verschoven naar de identificatie en toepassing van potentiële markers om eventuele respons op immuuntherapie te voorspellen. In **hoofdstuk 6** beschrijven we de bestaande literatuur van deze biomarkers met aandacht voor onderzoeksdata in andere tumortypen en potentiële biomarkers voor immuuntherapie respons in borstkanker. Op basis van de toen bestaande literatuur vonden we dat PD-L1 expressie op immuuncellen bij de tumor en de aanwezigheid van T cellen bij de tumor (tumor-infiltrerende lymfocyten, TILs) voorspellend kunnen zijn voor de respons op immuuntherapie. Dit hebben we kunnen bevestigen door onze eigen patiënten te onderzoeken en de resultaten hiervan zijn beschreven in **hoofdstuk 2**.

Aangezien de bepaling van TILs technisch makkelijk is doordat er weinig bewerking van het tumormateriaal nodig is, is dit een zeer praktische biomarker. Uit verschillende onderzoeken bleek dat TILs een potentieel sterk voorspellende waarde voor immuuntherapie respons hadden (zie **hoofdstuk 2** en **hoofdstuk 6**). Hierom hebben we TILs gebruikt in de opzet van het vervolg van de TONIC-studie. Echter aan de implementatie van biomarkers in klinische studies kleven vaak uitdagingen en risico's, zoals vertraging in inclusie. In **hoofdstuk 7** beschrijven we onze workflow om

TILs effectief en efficiënt als biomarker te kunnen gebruiken. Door vlak na het biopt hier een hoog-resolutie scan van te maken, deze vervolgens online en anoniem te uploaden in SlideScore konden we een panel van expert pathologen in verschillende centra TILs laten scoren. Door hier tijdsdoelen aan te geven, waren we in staat om bij 96% van de geïnccludeerde patiënten binnen 72 uur een definitieve TIL score te hebben. Dit konden we vervolgens gebruiken om patiënten te stratificeren in de twee behandelarmen van de studie. Ons beschreven stappenplan kan als een blauwdruk gebruikt worden om de risico's te verkleinen die horen bij de implementatie van een biomarker voor de inclusie van patiënten in een klinische trial.

Tot slot beschrijven we in **hoofdstuk 8** dat een potentiële nieuwe groep van borstkanker patiënten baat kan hebben van immuuntherapie. Immuuntherapie is met name effectief in TNBC, waarbij de meeste onderzoeken verricht zijn bij patiënten met volledige afwezigheid van de oestrogeen (hormoon)receptor. Echter uit eerder onderzoek is gebleken dat karakteristieken van borsttumoren met lage expressie van de oestrogeen receptor (met minder dan 10% expressie) lijken op die van tumoren met geen enkele expressie van deze receptor. In **hoofdstuk 8** hebben we gekeken of dit ook geldt voor de aanwezigheid van immuuncellen en expressie van immuun-gerelateerde genen. We vonden dat het immuunprofiel van de groep borsttumoren met oestrogeenreceptor expressie tussen de 1 en 9%, maar ook tussen de 10 en 50%, gelijkenissen vertoont met borsttumoren zonder enige expressie van de oestrogeenreceptor. Borsttumoren met meer dan 50% expressie van de oestrogeenreceptor hadden veel minder T cellen rondom de tumor en lagere PD-L1 expressie in vergelijking met tumoren met minder dan 50% expressie. Alleen mestcellen, een type immuuncel dat een remmende werking kan hebben op T cellen, waren hoger in tumoren met hoge oestrogeenreceptor expressie. Deze bevindingen wijzen erop dat patiënten met borsttumoren met lage expressie van de oestrogeenreceptor (<50%) mogelijk baat kunnen hebben van immuuntherapie. Dit moet echter verder onderzocht worden in analyses binnen klinische studies.

In dit proefschrift wordt aangetoond dat immuuntherapie effectief is in een selecte groep van patiënten met uitgezaaide borstkanker en dat immuuntherapie met lage dosis chemotherapie een stimulerend effect kan hebben in deze groep. Het in detail onderzoeken van patiëntmaterialen is essentieel voor een beter begrip van de respons op immuuntherapie bij borstkanker patiënten. In dit proefschrift wordt hiermee onder andere aangetoond dat eosinofielen noodzakelijk zijn voor een effectieve respons op immuuntherapie en dat TILs veilig en efficiënt gebruikt kunnen worden als potentiële biomarker voor immuuntherapie respons. Ook kan op basis van dit werk verder onderzocht worden of patiënten met borsttumoren met een lage expressie van de hormoonreceptor daadwerkelijk baat kunnen hebben bij immuuntherapie en worden aanknopingspunten geïdentificeerd hoe immuuntherapie verder verbeterd kan worden bij patiënten met borstkanker. Toekomstig onderzoek zal moeten uitwijzen welke patiënten met een nieuwe immuuntherapie combinatie behandeld kunnen worden, welke patiënten voldoende hebben aan alleen immuuntherapie en of de biomarkers genoemd in dit proefschrift ingezet kunnen worden in de klinische praktijk.

List of publications

Thesis related:

L. Voorwerk, J. Sanders, M.S. Keusters, S. Balduzzi, S. Cornelissen, M. Duijst, E.H. Lips, G.S. Sonke, S.C. Linn, H.M. Horlings, M. Kok. **Immune landscape of breast tumors with low and intermediate estrogen receptor expression.** *Npj Breast Cancer*. In revision.

L. Voorwerk*, O.I. Isaeva*, H.M. Horlings, S. Balduzzi, M. Chelushkin, N.A.M. Bakker, E. Champanhet, H. Garner, K. Sikorska, C.E. Loo, I. Kemper, I.A.M. Mandjes, M. de Maaker, J. J.L. van Geel, J. Boers, M. de Boer, R. Salgado, M.G.J. van Dongen, G.S. Sonke, K.E. de Visser, T.N. Schumacher, C.U. Blank, L.F.A. Wessels, A. Jager, V.C.G. Tjan-Heijnen, C.P. Schröder, S.C. Linn, M. Kok. **PD-L1 blockade in combination with carboplatin as immune induction in metastatic lobular breast cancer: the GELATO-trial.** *Nature Cancer*. In revision.

O.S. Blomberg*, L. Spagnuolo*, H. Garner*, L.Voorwerk*, O.I. Isaeva**, E. v. Dyk**, N.A.M. Bakker**, M. Chalabi, C. Klaver, M. Duijst, K. Kersten, M. Brüggemann, D. Pastoors, C.-S. Hau, K. Vrijland, E.A.M. Raeven, D. Kaldenbach, K. Kos, I.S. Afonina, P. Kaptein, L. Hoes, W.S.M.E. Theelen, P. Baas, E.E. Voest, R. Beyaert, D.S. Thommen, L.F.A. Wessels, K.E. d. Visser***, M. Kok***. **IL-5-producing CD4⁺ T cells and eosinophils cooperate to enhance response to immune checkpoint blockade in breast cancer.** *Cancer Cell*. 2023; 41 (1): 106-123.e10.

L. Voorwerk, M. Kok. **“IMpassionate conflicts” in immunotherapy trials for metastatic triple-negative breast cancer.** *Annals of Oncology*. 2021; 32 (8): 947-949

J. Hudeček*, L. Voorwerk*, M. van Seijen, I. Nederlof, M. de Maaker, J. van den Berg, K.K. van de Vijver, K. Sikorska, ..., R. Salgado, M. Kok, H.M. Horlings and the International Immuno-Oncology Biomarker Working Group. **Application of a risk-management framework for integration of stromal tumor-infiltrating lymphocytes in clinical trials.** *npj Breast Cancer*. 2020; 6 (15).

L. Voorwerk*, M. Slagter*, H.M. Horlings, K. Sikorska, K.K. van de Vijver, M. de Maaker, I. Nederlof, R.J.C. Kluin, S. Warren, S.F. Ong, T.G. Wiersma, N.S. Russell, F. Lalezari, P.C. Schouten, N.A.M. Bakker, S.L.C. Ketelaars, D. Peters, C.A.H. Lange, E. van Werkhoven, H. van Tinteren, I.A.M. Mandjes, I. Kemper, S. Onderwater, M. Chalabi, S. Wilgenhof, J.B.A.G. Haanen, R. Salgado, K.E. de Visser, G.S. Sonke, L.F.A. Wessels, S.C. Linn, T.N. Schumacher, C.U. Blank, M. Kok. **Immune induction strategies in metastatic triple-negative breast cancer to enhance the sensitivity to PD-1 blockade: the TONIC-trial.** *Nature Medicine*. 2019 ;25(6):920-928.

L. Voorwerk, M. Kat, M. Kok. **Towards predictive biomarkers for Immunotherapy response in breast cancer patients.** *Breast cancer management*. 2018; 7(1), bmt-2017-0014.

Other publications:

I. Nederlof*, L. Voorwerk*, M. Kok. **Facts and hopes in immunotherapy for early-stage triple-negative breast cancer.** *Clinical Cancer Research*. 2023; CCR-22-0701.

D.J. McGrail, P.G. Pilié, N.U. Rashid, L. Voorwerk, M. Slagter, M. Kok, E. Jonasch, M. Khasraw, A.B. Heimerger, N.T. Ueno, R. Ferrarotto, J.T. Chang, S.-Y. Lin. **Validation of cancer-type-dependent benefit from immune checkpoint blockade in TMB-H tumors identified by the FoundationOne CDx assay.** *Annals of Oncology*. 2022; 33(11): 1204-1206

K. van Baelen, T. Geukens, M. Maetens, V. Tjan-Heijnen, C.J. Lord, S.C. Linn, F.-C. Bidard, F. Richard, W.W. Yang, R.E. Steele, S.J. Pettitt, C. van Ongeval, M. De Schepper, E. Isnaldi, I. Nevelsteen, A. Smeets, K. Punie, L. Voorwerk, H. Wildiers, G. Floris, A. Vincent-Salomon, P.W.B. Derksen, P. Neven, E. Senkus, E. Sawyer, M. Kok, C. Desmedt. **Current and future diagnostic and treatment strategies for patients with invasive lobular breast cancer.** *Annals of Oncology*. 2022; 33(8): 769-785

I. Pérez-Núñez, C. Rozalén, J.A. Palomeque, I. Sangrador, M. Dalmau, L. Comerma, A. Hernández-Prat, D. Casadevall, S. Menendez, D.D. Liu, M. Shen, J. Berenguer, I.R. Ruiz, R. Pena, J.C. Montañés, M. Mar Albà, S. Bonnin, J. Ponomarenko, R.R. Gomis, J.M. Cejalvo, S. Servitja, D.M. Marzese, L. Morey, L. Voorwerk, J. Arribas, B. Bermejo, M. Kok, L. Pusztai, Y. Kang, J. Albanell, T. Celià-Terrassa. **LCOR mediates interferon-independent tumor immunogenicity and responsiveness to immune checkpoint blockade in triple-negative breast cancer.** *Nature Cancer*. 2022; 3(3): 355-370

D.J. McGrail, P.G. Pilié, H. Dai, T. Nguyen Anh Lam, Y. Liang, L. Voorwerk, M. Kok, X.H.-F. Zhang, J.M. Rosen, A.B. Heimerger, C.B. Peterson, E. Jonasch, S.-Y. Lin. **Replication stress response defects are associated with response to immune checkpoint blockade in non-hypermutated cancer.** *Science Translational Medicine*. 2021; 13 (617): eabe6201

D. Hammerl, J.W.M. Martens, M. Timmermans, M. Smid, A.M. Trapman-Jansen, R. Foekens, O.I. Isaeva. L. Voorwerk, H.E. Balcioglu, R. Wijers, I. Nederlof, R. Salgado, H.M. Horlings, M. Kok, R. Debets. **Spatial immunophenotypes predict response to anti-PD1 treatment and capture distinct paths of T cell evasion in triple-negative breast cancer.** *Nature Communications*. 2021; 12 (1): 5668

P. Llinàs-Arias, S. Íñiguez-Muñoz, K. McCann, L. Voorwerk, J.I.J. Orozco, M. Ensenyat-Mendez, B. Sesé, M.L. DiNome, D.M. Marzese. **Epigenetic regulation of immunotherapy response in triple-negative breast cancer.** *Cancers*. 2021; 13 (16): 4139

D.J. McGrail, P.G. Pilié, N.U. Rashid, L. Voorwerk, M. Slagter, M. Kok, E. Jonasch, M. Khasraw, A.B. Heimberger, B. Lim, N.T. Ueno, J.K. Litton, R. Ferrarotto, J.T. Chang, S.L. Moulder, S.-Y. Lin. **High tumor mutation burden fails to predict immune checkpoint blockade response across all cancer types.** *Annals of Oncology*. 2021; 32 (5): 661-672

Z. Kos, E. Roblin, ..., M. Kok, H.M. Horlings, ..., J. Hudeček, L. Voorwerk, ..., R. Salgado and the International Immuno-Oncology Biomarker Working Group. **Pitfalls in assessing stromal tumor infiltrating lymphocytes (sTILs) in breast cancer.** *npj Breast Cancer*. 2020; 6 (17).

M. Amgad, E. Specht Stovgaard, ..., L. Voorwerk, ..., H.M. Horlings, J. Hudeček, ..., M. Kok, ..., R, Salgado, L.A.D. Cooper and the International Immuno-Oncology Biomarker Working Group. **Report on computational assessment of Tumor Infiltrating Lymphocytes from the International Immuno-Oncology Biomarker Working Group.** *npj Breast Cancer*. 2020; 6 (16).

V.C.M. Geurts, L.A. van den Hoven, L. Voorwerk, M. Kok. **MIMOSA-trial: effectiviteit en veiligheid van monalizumab gecombineerd met trastuzumab bij patiënten met gemetastaseerde HER2 positieve borstkanker.** *Nederlands Tijdschrift voor Oncologie*. 2021; 18:62-5.

D.T. Kruger, X. Alexi, M. Opdam, K. Schuurman, L. Voorwerk, J. Sanders, V. van der Noort, E. Boven, W. Zwart, S.C. Linn. **IGF-1R pathway activation as putative biomarker for linsitinib therapy to revert tamoxifen resistance in ER-positive breast cancer.** *International Journal of Cancer*. 2020; 146 (8):2348-2359

L. Voorwerk, M. Kok. **Effectiviteit van atezolizumab en carboplatin in patiënten met gemetastaseerd lobulaire borstkanker: GELATO-studie.** *Nederlands Tijdschrift voor Oncologie*. 2018; 15:64-7.

*These authors contributed equally

** These authors contributed equally

*** These authors contributed equally, co-corresponding authors

Curriculum Vitae

Leonie Voorwerk was born on 18th of May 1991 in Purmerend. After obtaining her high school degree in 2009, Leonie started her Bachelor studies Biomedical Sciences at the VU University in Amsterdam. She performed her bachelor's internship at the lab of prof. dr. R.D.M. Steenbergen at the Cancer Centre Amsterdam. After obtaining her bachelor's degree in 2012, Leonie completed the pre-master program of Medicine at the University of Amsterdam in 2013. In 2016 she obtained her master's degree in Medicine at the University of Amsterdam. Her scientific internship was performed in the lab of prof. dr. W. Zwart in the Netherlands Cancer Institute (NKI) on a shared project with the lab of prof. dr. S.C. Linn. From January 2017, Leonie worked as a medical doctor (resident not in training) at the Medical Oncology department in the Antoni van Leeuwenhoek hospital. She started her PhD in the lab of dr. M. Kok at the NKI in July 2017. During her PhD, apart from the work described in this thesis, Leonie was involved in the protocol writing and initiation of the MIMOSA-trial (NCT04307329) and the initiation of a new institute wide biobanking initiative for breast cancer patients. From July 2022 onwards, Leonie works as a resident not in training at the Internal Medicine department at the Spaarne Gasthuis.

Acknowledgements/dankwoord

Veel dank aan iedereen die een bijdrage heeft geleverd aan dit proefschrift of die mij op een andere manier gesteund heeft in de afgelopen jaren. Mijn dank gaat uit naar de stichting Hendrika Roet voor jullie bijdrage aan het onderzoek in Marleen's lab. Ik heb jullie oprechte interesse in ons werk enorm gewaardeerd. Bovenal wil ik de patiënten en hun families bedanken die ons in een van de meest kwetsbare periodes van hun leven het vertrouwen geven om mee te doen in de studies beschreven in dit proefschrift.

Dank aan prof. dr. Linde Meyaard, prof. dr. Jacco van Rheenen, prof. dr. Marjanka Schmidt, prof. dr. Helena Verkooijen en prof. dr. Elske van der Wall om zitting nemen in mijn beoordelingscommissie. Daarnaast veel dank aan mijn promotiecommissie. **Karin**, de twinning constructie met het lab van Marleen is goud waard zoals eens te meer is gebleken. Dank voor je kritische blik op mijn werk maar ook het vertrouwen wat jij mij hebt gegeven tijdens mijn PhD.

Hugo, ik heb ontzettend veel van je geleerd over borstkanker pathologie, maar ook van jouw visie op de wetenschap en je oprechte interesse in de mensen om je heen. Dank voor je begeleiding tijdens mijn promotie! **Sabine**, jij durfde het aan om mij aan te nemen als master student op een lastig gedeeld project met Wilbert Zwart. Dank voor je vertrouwen en je altijd creatieve en originele inbreng tijdens werkbesprekingen. Heel bijzonder dat je na het begeleiden van de promotie van Marleen ook mijn promotor bent! **Marleen**, ik vond het een eer om samen met jou je lab te mogen opbouwen. Als vreemde eenden in de bijt op B6, bleken we al snel een goed team. Dank voor je mentorschap, aandacht voor mijn persoonlijke ontwikkeling en leerdoelen, voor je inspiratie en vooral veel dank voor de prachtige kansen die je me geboden hebt. Ik kijk uit naar wat de toekomst zal brengen voor jou en je lab!

Tijdens mijn PhD heb ik met vele mensen mogen samenwerken. Veel dank aan alle co-auteurs. Dank aan **Lydia, Michiel, Lidwina** en **Theresa** van de Wetenschappelijke Administratie. **Karolina** en **Sara**, thank you both for your patience and detailed explanations. **Els, Mandy** en **Tiny**, dank voor jullie hulp in de organisatie van onze veel te ingewikkelde labcodes. Dank aan **Dennis, Sten, Ingrid** en **Annegien** en de rest van de **CFMPB** voor jullie ondersteuning rondom het verwerken van de patiëntmaterialen. Geen vraag of verzoek was te veel en ik heb het altijd gewaardeerd hoe laagdrempelig jullie te bereiken zijn. **Jan**, thanks for your help with setting up the many many (many!) SlideScore studies. **Michiel**, dank voor je hulp in de eindeloze DNA/RNA isolaties, inscannen van coupes, opsturen van samples en het zijn van een heel fijne collega! Dank aan alle internist-oncologen en fellows die patiënten hebben geïnccludeerd in de studies, met name **Carolien Schröder, Carolien Smorenburg, Gabe, Jacqueline, Marloes, Martin, Marcel, Vincent** en **Vivianne**. Heel veel dank aan verpleegkundig specialisten, **Inge, Marjo, Margaret**,

Suzanne, Marjolein, en het secretariaat, met name **Kim**, voor de poliklinische ondersteuning van de studie patiënten. Zonder jullie zou ons onderzoeksleven een stuk lastiger zijn! **Ingrid**, jij bent goud waard voor de klinisch onderzoekers! De hoeveelheid administratief werk die jij doet om de trials in het gareel te houden is ongelooflijk. Dank voor je steun in deze, maar vooral ook voor de gezelligheid en de gesprekken tussen de meetings door. **Nicolien**, dank voor het me wegwijs maken in de wonderde wereld van het darm microbioom. Many thanks to the following PIs from the NKI for their input on my work: **Christian, Daniel, Daniela, Hein, Heinz, John, Karin, Leila, Lodewyk, Lotje, Michiel** en **Ton**. Veel dank aan alle pathologen die onze studies mede mogelijk hebben gemaakt, met name **Joyce, Jose** en **Koen. Roberto**, mijn speciale dank gaat uit naar jou. Bedankt voor je support, je input en je passie om uiteindelijk TILs naar de kliniek te brengen.

Zonder gezelligheid geen PhD! Ik heb genoten van de borrels en praatjes bij de Medische Oncologie en op zowel B6 als B3! Dank hiervoor aan, o.a. **Lisanne, Paulien, Daisy, Kelly, Steven, Pia, Rhianne, Chiara, Feline, Mirjam, Anne, Jos, Meike, Mireille, Wouter, Lorenzo, Georgi, Myriam, Ronak, Aldo, Wietske, Elselien, Marnix, Christel, Kim, Tisee, Antoinette, Claudia, Kevin, Danique, Karin, Tessa, Lisette, Judith, Irene, Maartje, Vincent, Marte, Anna** en **Merel. Serena**, thanks for being the best roomie during COVID times! **Olga** en **Lorenzo**, thanks for introducing me in the wondrous world of *in vivo* studies, super proud of our work together. **Annemiek** en **Leonora**, dank voor de gezelligheid tijdens ASCO! **Noor**, ik heb genoten van onze samenwerking op B3 en je humor/gezelligheid. Dat wordt echt een heel mooi boekje! **Maarten**, veel dank voor onze discussies over wetenschap en de gezelligheid van de borrels en etentjes binnen en buiten het NKI! **Hannah**, you were a great teacher in the curious world of myeloid cells. Thank you for the great collaboration over the years and your continuous guidance during my PhD. **Anastasia**, who would've thought that when we were put together in an office, we would become good friends. Many thanks for your friendship over the years, your great company in- and outside the NKI and of course for being my paranymp!

To all former and present labmembers (Kokkies), **Marieke, Elisa, Maksim, Mi, Robbert-Jan, Olga, Manon**, many thanks for being great colleagues. We all have different skills and knowledge, but really synergize when it comes to our projects! **Milou**, dank voor je hulp en het in korte tijd verzetten van veel werk voor je stageproject! **Chris** en **Maxime**, jullie zorgden voor zonneshijn in het lab, dank dat ik altijd bij jullie terecht kon om even te klagen, te ventileren of gewoon te zijn! **Iris**, jij kan alles interessant en begrijpelijk maken! Dank voor de brainstorms, je input, je collegialiteit en de gezelligheid. **Veerle**, dank voor je hulp in het oppakken van de vele lopende projecten en studies en het aanhoren van mijn frustraties. Ik weet zeker dat de projecten tot een goed einde komen onder jouw bezielende leiding en wens je heel veel plezier in de komende jaren met het afronden van je PhD!

Veel dank aan mijn collega's van het Spaarne Gasthuis en aan alle vrienden en familie die het leven buiten het NKI een stuk leuker maken! **Jacques** en **Sonja**, dank voor jullie enthousiasme bij elke (kleine) mijlpaal! **Iris K.**, **Iris C.** en **Josephine**, dank voor de gezelligheid tijdens al onze post-Bali etentjes. Op naar nog vele leuke avonden en nieuwe trips! **Manon**, **Silvia** en **Huda**, al tijdens onze AVL-tijd in 2017 waren jullie mijn steun en toeverlaat en nog steeds blijft onze band hecht, dank hiervoor. **Huda**, op nog vele sportmiddagen, lunches, etentjes en trips! Epsteinbar groep, **Emma**, **Jorn**, **Ted**, **Corina**, **Dianne**, **Isabelle**, **Patricia**, dank voor de altijd gezellige tijd als we bij elkaar zijn. **Corina**, het was een plezier om je huisgenootje te zijn en heerlijk om onze gedeelde frustraties af en toe te kunnen uiten! **Dianne**, het is altijd leuk met jou, dank voor alle gezelligheid en steun in het NKI en daarbuiten! **Anne**, **Stephanie**, **Tristan**, **Lesley** en **Marlies**, hoe bijzonder het is dat we elkaar na al die jaren nog in het oog hebben! Lieve **Lesley**, dank je wel voor je luisterende oor en begrip, onze heerlijke gesprekken over werk, politiek, showbizz en van alles en nog wat. Lieve **Marlies**, dank je wel voor al je steun tijdens onze lange telefoongesprekken, je luisterende oor, je begrip en het altijd bij me checken of het echt wel goed gaat. Jullie zijn geweldig!

Lieve **Tim**, ik had me geen leukere zwager kunnen wensen. Dank voor je relativeringsvermogen, je steun en enthousiasme voor mijn werk. Lieve **Iris**, ik geniet ervan dat we de laatste jaren zo hecht zijn geworden als zussen. Veel dank voor al je steun, je luisterende oor en je humor. Ik had me geen betere paranimf kunnen wensen!

Papa en mama, deze paar zinnen zijn natuurlijk veel te weinig om jullie te bedanken voor alles wat jullie voor me doen en hebben gedaan. Jullie hebben mij en **Iris** altijd onze eigen weg laten kiezen, ook al was dat onbekend terrein voor jullie. Jullie trots tijdens mijn PhD was altijd voelbaar en dat geeft vleugels! Dank jullie wel voor jullie steun en het er altijd voor me zijn voor zowel de kleine als de grote dingen.

